ELECTROCHEMICAL RESPONSE AND CHLORIDE THRESHOLD OF STEEL IN HIGHLY RESISTIVE CONCRETE SYSTEMS

A THESIS

submitted by

SRIPRIYA RENGARAJU

for the award of the degree

of

DOCTOR OF PHILOSOPHY

BUILDING TECHNOLOGY AND CONSTRUCTION MANAGEMENT DIVISION

DEPARTMENT OF CIVIL ENGINEERING
INDIAN INSTITUTE OF TECHNOLOGY MADRAS
CHENNAI 600 036
JULY 2019

THESIS CERTIFICATE

This is to certify that the thesis titled, **ELECTROCHEMICAL RESPONSE AND CHLORIDE THRESHOLD OF STEEL IN HIGHLY RESISTIVE CONCRETE SYSTEMS**, submitted by **Ms. SRIPRIYA RENGARAJU (Roll No.: CE14D024)** to the Indian Institute of Technology Madras, Chennai, for the award of the degree of Doctor of Philosophy, is a bona fide record of the research work done by her under my supervision. The contents of this thesis, in full or in parts, have not been submitted to any other Institute or University for the award of any degree or diploma.

Dr. Radhakrishna G. Pillai

Research Guide & Associate Professor

Building Technology and Construction Management Division

Department of Civil Engineering

Indian Institute of Technology Madras

Chennai - 600 036, India

Chennai, India

Date: 31st July 2019

Dedicated to

my father-in-law, Shri. P. Natarajan and

my parents, Shri. K. Rengaraju and Smt. N. Kamalavalli

ACKNOWLEDGEMENTS

I praise the Almighty for making me dream and work towards achieving the same. I am indebted forever to all the teachers who imparted knowledge and values to me in various stages of my life. I would, first of all, thank my guide, Dr. Radhakrishna G. Pillai, who helped me to realize my strengths and weaknesses. His passion to mould students and his strive for perfectionism are exceptional. He always knocks at a place, where there is darkness and shows light on it.

My doctoral committee members' constant review in my research work has made my thesis to this shape. I would like to special mention Prof. Ravindra Gettu for his constant inputs to improve my thesis. I remember that research methodology class even today where he mentioned: "The transformation of oneself in the journey is more important than earning a degree". I would like to express my gratitude to Prof. Manu Santhanam, from whom I learnt concrete technology. His deep understanding of concepts and belief in the idea "A good research is that, which contradicts your earlier research hypothesis" are commendable. I would like to thank Dr. Lakshman Neelakantan, for his valuable suggestions in electrochemical testing throughout the research period. In spite of having a different background, his patience to listen to my problems and suggestions are exceptional. His positive approach and encouragement gave me so much strength. I express my sincere gratitude to Prof. K. Ramamurthy, Head of Department of Civil Engineering, and former Heads, Prof. A. Meher Prasad and Prof. S.R. Gandhi, for facilitating excellent research facility and other academic related requirements during my stay in the department ─ with a special mention to Prof. K. Ramamurthy for his constant motivation and support.

ABSTRACT

Nowadays, concretes containing supplementary cementitious materials (SCMs) and having moderate to high resistivity are used to delay the onset of corrosion and enhance service life. To estimate service life, the chloride threshold (Cl_{th}) of the steel-cementitious binder (denoted as "S-B" herein) system is required and defined as the chloride concentration required at the S-B interface to initiate corrosion. The hardened S-B interface is a metal-sol-gel system, which poses different challenges in acquiring and interpreting electrochemical/corrosion test data as compared to a metal-aqueous system. These challenges lead to difficulties in using existing test methods to estimate corrosion resistance and Cl_{th} and hence, the service life of HR S-B systems. In particular, some of the existing test methods to determine Cl_{th} are not suitable for the cementitious binder systems with high resistivity. Examples of such highly resistive (HR) systems are concrete with SCMs (such as fly ash, limestone calcined clay cement) and/or low water-cement ratio. Because of these, the designers and engineers are often facing challenges in estimating the effect of various steel and SCMs available in the market on the service life of structures. Enabling designers and engineers in selecting suitable S-B systems is the focus of this thesis.

This thesis evaluated existing corrosion test methods, developed procedures to acquire and interpret electrochemical response from HR S-B systems, developed an accelerated test method to estimate Cl_{th} of HR S-B systems (named as "hr-ACT" test method), and then developed a computer program (named as "SL-Chlor") and nomograms to estimate probabilistic corrosion-free service life (say, corrosion initiation time) of various S-B systems. The experiments were conducted on thermomechanically treated steel embedded in systems containing (a) OPC - Ordinary Portland Cement (OPC), (b) PFA - Pulverized Fuel Ash (or fly ash) based cement and (c) LC3 – Limestone calcined clay cement.

First, this thesis evaluated the ability of the following test methods to assess corrosion performance of HR S-B systems: (i) half-cell potential (HCP), (ii) macrocell corrosion (MCC), (iii) impressed current corrosion (ICC), and (iv) linear polarization resistance (LPR) technique. It was found that the HCP measurements from HR S-B systems are greatly influenced by the high resistivity of the cover concrete and makes it difficult to interpret the data and estimate the probability of corrosion. The MCC tests (ASTM G109) indicated that the resistivity of concrete influences the type of macrocell corrosion circuits and the measured current could mislead and fail to detect the initiation of corrosion in HR S-B systems (some PFA and all LC3 specimens studied). The ICC tests took a significantly long time to assess corrosion in LC3 systems as compared to OPC and PFA systems. Raman spectra on these specimens indicated that the prolonged application of impressed current could change the type/nature of corrosion products. Hence, the use of ICC tests with long duration should not be adopted for evaluating HR S-B systems. Then, LPR tests were conducted and found not effective in detecting corrosion initiation in HR S-B systems due to the difficulty in decoupling the cover resistance and polarization resistance of steel. The technique of IR-compensation was not successful in the adapted corrosion test specimen design.

Due to the limitations found in the HCP, ICC, MCC, and LPR test methods, the factors affecting the electrochemical response were evaluated and then, a suitable short-term test method to determine the Cl_{th} of steel in HR systems was developed using EIS technique. First, a suitable 3-electrode corrosion cell (annular system) for the metal-sol-gel system was designed. A lollipop type specimen with single steel rebar embedded in cylindrical mortar cover was designed to facilitate the Circuit 2 type corrosion (both anode and cathode on the same rebar) observed in HR systems. Using this test specimen, the effect of various test parameters (i.e., scan rate, scan range, AC amplitude, AC frequency, spacing between the electrodes, etc.) affecting the electrochemical response from HR systems was evaluated. Based

on the test results, it was found that LPR technique may not always detect corrosion initiation in moderate to highly resistive systems; whereas electrochemical impedance spectroscopy (EIS) technique could always detect corrosion initiation in HR systems. Also, experiments were conducted using a relative humidity (RH) sensor and it was determined that a wet-dry exposure cycle of 2 days wet followed by 5 days dry is suitable and performing all the repeated EIS measurements at the end of 2 days of wetting can ensure similar microclimate (about 95% RH) at the S-B interface – a worst-case scenario for early corrosion initiation with least amount of chlorides. Combining all these learnings, a suitable test method using EIS was developed to determine the Cl_{th} of steel in HR systems and named as 'hr-ACT' test.

Existing software programs have limitations in using probabilistic estimates of Cl_{th}, chloride diffusion coefficient (D_{Cl}), cover depth (d) and the ageing coefficient (m) for HR S-B systems. Hence, a computer program (named as 'SL-Chlor') was developed (using Fick's 2nd law of diffusion) to accommodate user-defined probabilistic estimates of these parameters and estimate the probabilistic, the corrosion-free service life of HR S-B systems. The estimated service life of OPC, PFA and LC3 systems demonstrated the synergistic effects of m, D_{Cl}, and Cl_{th} in enhancing the service life. For example, it was found that an S-B system with low Cl_{th} could exhibit longer service life if the D_{Cl} is low. This thesis emphasizes that Cl_{th} is a function of both steel and cementitious binder used and to select steel and concrete materials and cover depth based on the estimates of corrosion-free service life of the S-B system under consideration (rather than either Cl_{th} alone or D_{Cl} alone). Using SL-Chlor, nomograms for various coastal exposure conditions were made to facilitate easy use of these concepts during the design stage and choose the steel/concrete materials and cover depth to achieve durability.

Keywords: Steel, concrete, chloride, corrosion, highly resistive, fly ash, limestone calcined clay, polarization resistance, electrochemical impedance spectroscopy, service life, nomogram.

TABLE OF CONTENTS

LIST OF FIGURES

LIST OF TABLES

NOTATIONS AND ABBREVIATIONS

%bwob	Percentage by weight of binder
%bwoc	Percentage by weight of concrete
CE	Counter electrode
CIA	Corrosion inhibiting admixture
Cl_s	Surface chloride concentration [%bwoc]
Cl_{th}	Chloride threshold [%bwoc]
d	Cover depth [mm]
D_{365d}	Diffusion coefficient determined at the age of 365 days [m^2/s]
D_{cl}	Chloride diffusion coefficient [m^2/s]
D_{ref}	Chloride diffusion coefficient at t_{ref} [m^2/s]
E_{corr}	Corrosion Potential
EIS	Electrochemical impedance spectroscopy
EoT	End of exposure/testing
FA	Fly Ash
GGBS	Ground granulated blast furnace slag
HCP	Half-cell potential
$I_{corr,avg}$	total average corrosion current [coulombs]
$I_{corr,avg,raw}$	total average corrosion current calculated from modified data [coulombs]
$I_{corr,avg,raw}$	total average corrosion current calculated from raw data [coulombs]
i_{corr}	Corrosion current density
i_j	macrocell current at time t_j [amps]
LC3	Limestone calcined clay cement
LPR	Linear polarization resistance

m	Ageing coefficient for the chloride diffusion coefficient
M35	Concrete with characteristic cube compressive strength of 35 MPa at 28 days
M50	Concrete with characteristic cube compressive strength of 50 MPa at 28 days
n	Number of time steps
N_f	Number of instances of failure
OPC	Ordinary portland cement
P_f	Probability of failure
PFA	Blend of 70% OPC and 30% PFA
PPC	Portland pozzolana cement
PSC	Portland slag cement
QST	Quenched and self tempered;
	Also known as Thermo-mechanically treated (TMT) in India
RC	Reinforced concrete
RE	Reference electrode
R_p	Polarization resistance
S-B	Steel-cementitious binder; For brevity, it is referred as steel-binder
SCE	Saturated calomel electrode
SCMs	Supplementary cementitious materials
SF	Silica fume
SPS	Simulated pore solution
t	Age of the structure [years]
t_j	time at which the measurement of the macrocell current is carried out
TC_j	total average corrosion current from ASTM G109 equation [coulombs]
T_{crack}	time-to-crack
TMT	Thermo-mechanically treated

t_{ref}	Reference time [years]
w/b	water-to-binder ratio
WE	Working electrode
Z'	real part of impedance
Z"	imaginary part of impedance
$\sigma_{(t)}$	Electrical conductivity of concrete at time t [mS/m]
σ_{ref}	Electrical conductivity of concrete at t_{ref} [mS/m]

CHAPTER 1

INTRODUCTION

1.1 PROBLEM STATEMENT

Developing countries like India are investing heavily in infrastructure projects. The design life of major infrastructure projects is more than fifty years. However, many of them are facing premature corrosion - significantly contributing to India's corrosion cost of about 4-5% of GDP (Duggal, 2016). Lieser and Xu (2010) reported that "…rapidly developing nations can avoid repeating the costly infrastructure repair and replacement cycle of industrialized nations by adopting advanced materials and construction methods…". These advanced materials (say, steel-cementitious binder (S-B) systems) include (i) highly resistive concrete, (ii) corrosion inhibitors, and (iii) steel rebars with metallic coating. For brevity, steel-cementitious binder is referred as steel-binder hereafter. Engineers need to assess the critical service life parameters of advanced S-B systems in the short term (few months) – to judge if they are truly 'advanced' and can enhance the service life. One of the critical service life parameters is the chloride threshold (Cl_{th}), which is the amount of chlorides required at the steel-concrete interface to initiate corrosion. The estimation of Cl_{th} is very challenging because of its dependency on various factors such as (i) material properties of cover concrete, (ii) properties of steel reinforcement, and (iii) microclimate at the S-B interface. The suitability of the existing electrochemical techniques and Cl_{th} test methods (for conventional S-B systems) to the advanced S-B systems needs to be assessed.

1.2 MOTIVATION FOR THE STUDY

The production of portland cement consumes mineral resources and releases a large amount of CO_2, causing ecological impact and global warming. To reduce the impact and enhance the durability, supplementary cementitious materials (SCMs), such as fly ash, slag, limestone calcined clay, that exhibit high ionic resistivity when added to ordinary portland cement (OPC) are being introduced in the cement industry. The service life of reinforced concrete structures with such systems depends on both transport properties and corrosion performance. Significant research is available on the microstructure and transport properties of these cementitious systems. However, information on the corrosion performance of these systems is not available and hence, estimating the service life becomes very challenging. This research is aimed at a holistic assessment of the suitability of new cement alternatives in reinforced concrete structures by assessing corrosion performance as well as service life against chloride-induced corrosion, which may lead to the widespread use of such alternatives.

1.3 DEFINITIONS

Definitions of some key terms used in this study are as follows:

1. Ageing coefficient (m): Factor accounted for reduced chloride diffusion coefficient (D_{cl}) due to ageing (hydration)

2. Annular geometry: Arrangement of electrodes in a concentric circular form

3. Anode: The portion which is corroding (loss of electrons)

4. Artefacts: Unusual electrochemical responses, which cannot be analysed with the equivalent electrical circuits.

5. Cathode: The portion which consumes electrons and supports the corrosion process; no loss of metal

6. Chloride diffusion coefficient (D_{cl}): The rate of chloride ingress across a unit area of a cementitious system.

7. Chloride threshold (Cl_{th}): The minimum amount of chlorides at the steel reinforcement level required to initiate active corrosion.

8. Corrosion cell: Formation of anode, cathode and electrolyte, which results in active corrosion; A combination of working electrode; counter electrode and reference electrode for measurement of corrosion

9. Electrolyte: The medium, which supports the transfer of ions

10. Macrocell corrosion: Distinguishable anode and cathode, which could be located on the same rebar or on different rebars

11. Ohmic drop: Voltage drop between the reference and working electrode

12. Passive film: A protective film formed on the steel surface, which resists corrosion

13. Pitting corrosion: Corrosion in the form of pit and distinguishable anode and cathode

14. Planar geometry: Arrangement of electrodes in the same plane

15. Polarization resistance: Resistance of the material to change from equilibrium potential

16. Premature corrosion: Corrosion initiation and lose of service life before the design life period of structures

17. Resistivity of concrete: Measure of resistance offered by concrete on the application of potential; indirect measurement of porosity, pore solution conductivity and moisture content.

18. Service life (SL): The time required to initiate corrosion of the embedded steel reinforcement.

19. Solution resistance: Inherent resistance of the electrolyte for the current to pass through

20. Steel-binder (S-B) systems: Any system with steel embedded in concrete/mortar

21. Surface chloride concentration (Cl_s): The chloride content at the external surface of concrete cover; Depends on the exposure conditions

22. T_{crack} : The duration required for the appearance of visual crack due to corrosion in S-B systems

23. Uniform corrosion: Uniform throughout and non-distinguishable anode and cathode; can be called as microcell

1.4 RESEARCH QUESTIONS

1. All the existing test methods were developed for low resistive OPC systems. Can the currently available techniques be directly applied to assess the Cl_{th} of steel embedded in highly resistive cementitious systems (HRCS)? What are the associated challenges?

2. The ohmic drop due to the presence of cover is negligible in case of low resistive systems. When HRCS is used, what will be influence of ohmic drop in the electrocehmical response? How should the ohmic drop be accounted in HRCS?

3. The thickness of the cementitious cover influences the microclimate (availability of moisture, oxygen, temperature) at the steel-binder interface. If the specimens are subjected to wet-dry cyclic regime, what will be ideal day for taking the the repeated electrochemical measurements in laboratory testing?

4. The configuration of the corrosion cell and the choice of the input parameters in the advanced techniques like linear polarisation resistance affect the electrochemical

response. What are the influences of the electrode configuration (cell design) and the electrical input parameters on the electrochemical response from HRCS?

5. What should be the corrosion initiation criteria? How to define the initiation of corrosion in terms of electrochemcial rsponse?

6. Can OPC Cl_{th} be used for other binder systems?

7. How does the choice of materials affect service life?

   i) Which is the most influencing parameter of service life? Is it only the Cl_{th} or is the coefficient of diffusion?

   ii) How to choose materials effectively at the site?

1.5 OBJECTIVES AND SCOPE

Following are the objectives of this research work. The sub-bullet points following each objective indicate its scope.

(i) To evaluate the suitability of the existing techniques for assessing corrosion characteristics of highly resistive steel-binder (S-B) systems

   - Evaluation of half-cell potential (HCP) and macrocell corrosion (MCC)

   - Evaluation of impressed current corrosion (ICC)

   - Evaluation of polarization resistance using wet-dry corrosion (WDC) test

(ii) To assess the effect of the properties of cement mortar and configuration of electrodes on the electrochemical response from the highly resistive steel-binder systems

   - Linear polarization resistance (LPR)

   - Electrochemical impedance spectroscopy (EIS)

   - Mortar cover thickness: 10 mm

   - Exposure: 2 days wet and 5 days dry in simulated pore solution with 3.5% NaCl

(iii)   To develop a short-term test method for determining the chloride threshold of highly

resistive steel-binder systems (to be named as hr-ACT test method)

- Mortar with OPC, PFA, and LC3

- LPR and EIS techniques

(iv)   To develop a computer program (to be named as SL-Chlor) and nomograms to estimate

deterministic/probabilistic corrosion-free service life of various steel-binder systems

- Probability of corrosion initiation (P_{ci}), cover depth (d), chloride threshold (Cl_{th}),

ageing coefficient (m), chloride diffusion coefficient (D_{cl}), and surface chloride

concentration (Cl_s).

Overall, the scope of this work is restricted to study of corrosion of steel (Quenched and Self

tempered (QST), also known as Thermo-mechanically treated (TMT)) embedded in three

binders, namely ordinary portland cement (OPC), OPC with 30% replacement of fly ash (PFA),

and limestone calcined clay cement (LC3 - 50% clinker, 30% calcined clay, 15% crushed

limestone and 5% gypsum from industrial trial production).

1.6 RESEARCH SIGNIFICANCE

Major infrastructure projects are designed for 100+ years. Many materials come in the market

claiming for low cost, constructability, sustainability and durability. To ensure the claimed

performance, there is a need to assess the material behaviour, especially Cl_{th}. Traditional test

methods available for S-B systems were developed for concretes with low-to-moderate

resistivity. Nowadays, highly resistive binder systems are available for which no clear

guidelines for data acquisition and interpretation are available.

The exposure condition adopted during the experiments can influence the microclimate

and hence, the estimates of Cl_{th}.can have huge scatter. However, literature does not clearly state

what exposure should be adopted in the laboratory to mimic a particular microclimate at the

6

S-B interface (to mimic real-life scenarios with various climatic and chloride conditions); and more importantly, when to measure the repeated electrochemical responses of the S-B system to determine chloride threshold. Also, the electrochemical response from the S-B system is affected by the electrode configuration, which influences the ohmic drop. Because of these reasons and lack of understanding of the correlations, at present, the failure criteria adopted in one type of experiment cannot be directly adopted in another type of experiment. The present work establishes the resistivity range for which the existing test methods are suitable and presents a short term test method that considers various electrochemical and test parameters to estimate Cl_{th} of S-B systems, especially with highly resistive binders.

Even though many models are available for the estimation of the service life of structures against chloride-induced corrosion, they are very complex and not user-friendly. Due to unavailability of user-friendly tools, design engineers find it difficult to implement the research findings while selecting new materials for enhancing the service life of structures. The user-friendly nomograms developed as part of this work help to predict the service life of structures when different materials are exposed to various environmental conditions. This can help engineers in design office to choose materials effectively for achieving the desired durability.

1.7 RESEARCH METHODOLOGY

Figure 1.1 shows the methodology adopted in detail. First the existing methods for corrosion assessment were evaluated for its suitability. From the outcome of this first experimental program, a number of parameters affecting electrochemical testing were found. The effect of various input parameters and corrosion cell geometry on the electrochemical response were studied. A test method (hr-ACT) was developed for determining the Cl_{th} of highly resistive (HR), S-B systems. This method was verified for OPC and then tested for HR, S-B systems

and Cl_{th} was determined. A MATLAB® code was developed to estimate the service life (SL-Chlor). A set of nomograms were developed with the code for various chloride conditions.
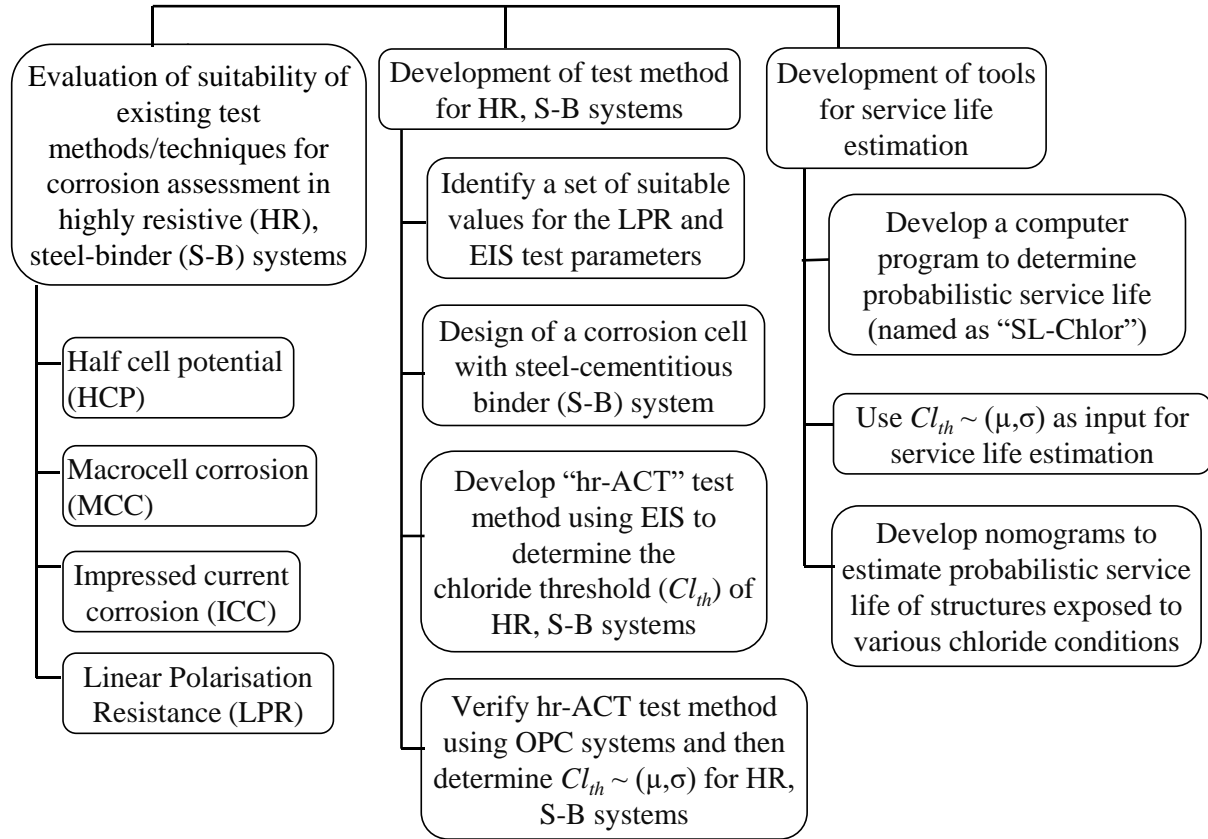
Figure 1.1 Experimental program and methodology

1.8 ORGANISATION OF THE THESIS

This thesis is organized using a Chapter-subsection format. There are eight Chapters (first level heading) and several subsections within each chapter. The outline of the chapters are as follows.

- Chapter 1 (the current chapter) introduces the problem statement, motivation for the study and the research questions, which led to the formulation of research objectives. Research significance and the methodology carried out for the research objectives are also provided.

- Chapter 2 provides a review of the literature in detail. This section starts with the service life and critical parameters, codal requirements of Cl_{th} and variation of Cl_{th} followed by testing techniques. The effect of microclimate and electrochemical cell geometry on the electrochemical measurements are also discussed. A detailed discussion of service life estimation, input parameters needed, and the need for the simplified tool are presented. A summary of the literature review is provided at the end.

- Chapter 3 covers the experimental program. The materials used are described first followed by the methods adopted in this research work. The test details are also included.

- Chapter 4 covers the experimental results of ASTM G109 test method, impressed current corrosion (ICC) test method, and linear polarization resistance (LPR) technique and discusses the suitability of these test methods for evaluating corrosion in highly resistive concrete in detail.

- Chapter 5 covers the results of the research work carried out to understand the effect of test parameters on the electrochemical response, which plays a crucial role in determining the Cl_{th}.

- Chapter 6 includes the step-by-step procedure carried out to determine the Cl_{th} of three cementitious systems, namely OPC, PFA and LC3.

- Chapter 7 describes the service life estimation of a reinforced concrete structure with Ficks' second law of diffusion. Case studies demonstrating the synergistic effect of various parameters are presented. A set of nomograms for estimating the service life for different exposure conditions are also given.

- Chapter 8 presents the conclusions of this research along with the recommendations for future work.

- Appendix A provides the comprehensive experimental program in detail, which led to the modification of impressed current corrosion test specimen.

- Appendix B gives the details of the experiment carried out with the premixed chlorides for corrosion rate assessment.

- Appendix C explains the study of microclimate at the S-B interface using temperature and humidity sensors

- Appendix D presents the details of the preliminary study conducted using ASTM G109 specimens for corrosion assessment in highly resistive concrete systems

- Appendix E describes the step-by-step procedure to fit the equivalent electrical circuit to determine the polarization resistance of steel

CHAPTER 2

LITERATURE REVIEW

2.1 INTRODUCTION

This chapter presents a review of literature relevant to the chloride-induced corrosion of steel in binder systems and service life estimation of structures exposed to chlorides. Further, the chapter sets forth the various phases of service life and critical parameters needed for its estimation. Then, the influence of materials followed by the exposure conditions and the microclimate in the S-B interface on the Cl_{th} are discussed in detail. The measurement techniques and their effect on the measurement of Cl_{th} are then reviewed. Following this, the corrosion cell design and its influence on Cl_{th} estimation are surveyed with a summary of standard test methods. Then, various service life estimation models and the input parameters required are put forward with the need for simplified tools for engineers.

2.2 SERVICE LIFE OF REINFORCED CONCRETE STRUCTURES

Figure 2.1 shows the various phases of the service life of concrete structures. During the initiation phase, the chlorides from the outside environment (Cl_s) can pass through the cover concrete (d) and reach the steel surface by diffusion and other mechanisms, which depends on chloride diffusion coefficient (D_{cl}) and ageing coefficient (m) of concrete. The chlorides start building up at the steel-binder (S-B) interface, reaching a threshold level known as Cl_{th}, at which the corrosion of steel initiates (Angst et al., 2009). The time taken to initiate corrosion is called the initiation period, which is the focus of this work. To delay the onset of corrosion, highly resistive binder types with SCMs, which can resist the ingress of chlorides, are being used.

11

$$fn\left[D_{Chloride}, m, Cl_{threshold}, d, Cl_{surface}\right]$$
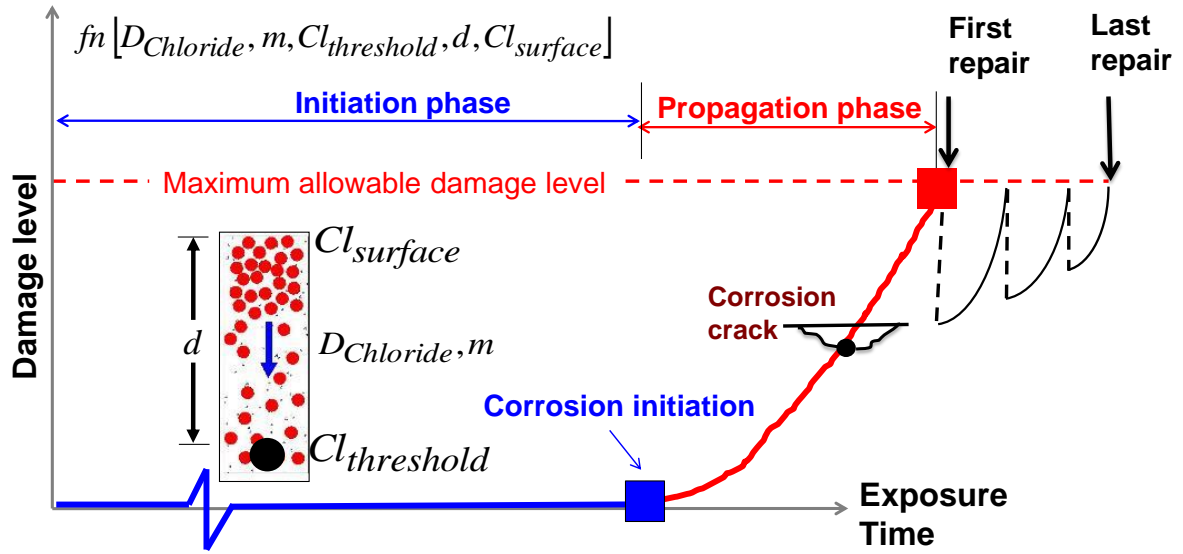
Figure 2.1 Schematic showing various phases and factors affecting the service life

2.2.1 Effect of binder types on service life

Nowadays, a variety of cementitious binders with various SCMs are available, the use of which affects the corrosion initiation of steel in concrete in four ways. First, SCMs can enhance the pore size distribution of the hardened cement matrix by either the filler effect or secondary hydration reactions. A reduction in the mean pore diameter can reduce the chloride ingress rate, which in turn can delay the onset of corrosion. Second, SCMs consume OH^- ions during the secondary hydration reactions and increase the ionic resistivity. Table 2.1 shows the classification of concretes showing the relationship between the resistivity and chloride ion permeability. Figure 2.2 shows the range of resistivity exhibited by various concretes with SCMs (Dhandapani and Santhanam, 2017; Dhanya, 2015; Dotto et al., 2004; Malakooti, 2017). Higher the concrete resistivity, the less will be the ionic flow between anodic and cathodic regions and hence, less corrosion (Alonso et al., 1988; Hornbostel et al., 2013). Third, SCMs enhance the chloride binding capacity of concrete, which in turn restricts the chloride ions from reaching the steel to a great extent. One of the complexes that help in binding the chlorides is Friedel's salt, the formation of which is dependent on the alumina content in the OPC and SCM

12

(Talero et al., 2011). Fourth, SCMs can lead to a reduction in the pH and the pH buffer capacity of concrete, which in turn can reduce the Cl_{th} (Bentur et al., 1997).

Table 2.1 Resistivity classification based on chloride ion permeability (AASHTO T 358 (2017))

Chloride ion permeability, k	Surface Resistivity, ρ (kΩ.cm)
High	< 12 (Negligible)
Moderate	12 - 21 (Low)
Low	21 - 37 (Moderate)
Very low	37 – 254 (High)
Negligible	> 254 (Very High)
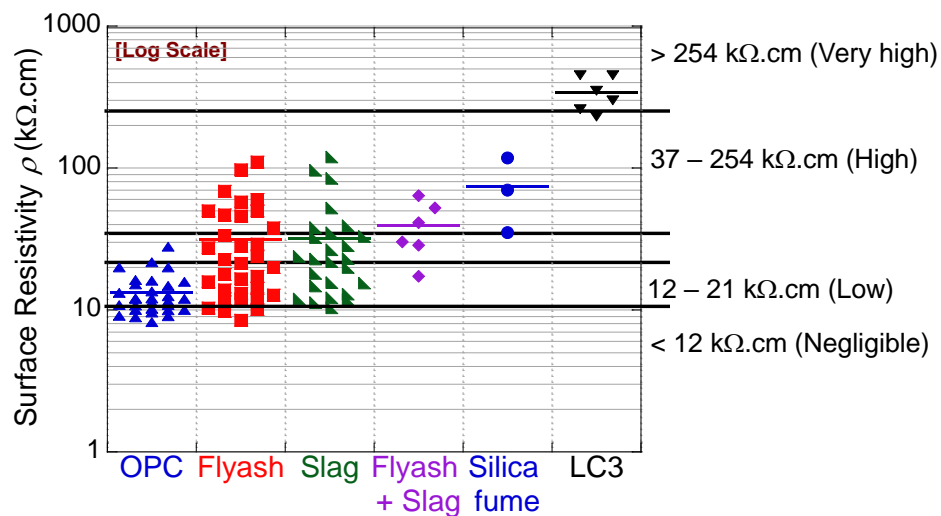
Figure 2.2 Surface resistivity of concretes made with various binders [categories are as per AASHTO T 358 (2017)]

2.2.2   Estimation of service life

Quantitative estimation of two parameters, namely the chloride diffusion coefficient (D_{cl}) of cementitious/binder cover and the Cl_{th} of the S-B system is crucial for estimating the service life. There are different standard test methods available to determine the D_{cl} of concrete. Determination of Cl_{th} of the S-B system is challenging as there are no standard test methods

13

available. Engineers need to do educated guess of Cl_{th} value for meaningful estimation of service life. The scope of this research is restricted to the estimation of Cl_{th} of the S-B system and service life of structures exposed to chlorides.

2.2.3 Definition of chloride threshold *(Cl_{th})*

Researchers define Cl_{th} as the amount of chlorides required to de-passivate the steel, whereas engineers define Cl_{th} as the amount of chlorides required to initiate visible corrosion. "So far not even the definition of the term 'chloride threshold' is clear and no generally accepted test method exists" (RILEM TC 235-CTC). The allowable chloride content is restricted in the new construction by different standards in lieu of a clear definition of Cl_{th}. Some engineers use 0.4% by weight of binder (bwob) as acceptable Cl_{th} for new construction, based on their experience with OPC (Moreno et al., 2004). However, when OPC is partially replaced with SCMs, these alternative binder systems are reported to have lower Cl_{th} than 0.4% bwob (Angst et al., 2009; Pillai et al., 2018). Andrade (2016) reported that "…tests considering partial saturation or de-icing salts are not standardized..." So Cl_{th} of steel was determined by various approaches, which is discussed next.

2.3 EVALUATION OF CHLORIDE THRESHOLD TEST METHODS

The test methods to determine the Cl_{th} of steel has evolved over years. Initially, the steel was immersed in chloride solution and the half-cell potential or polarization resistance were monitored over a period of time and an absolute failure criteria was fixed (Diamond, 1986, Li and Sagues, 1999). When the criteria is met, the amount of chloride in the solution was reported as $Cl_{th.}$ Then, Cl_{th} of steel in concrete was found by prolonged exposure and comparison of weight loss (Thomas, 1996). To shorten the duration, half-cell potential was monitored (ASTM C876). Then, macrocell specimens were widely used to find the chloride threshold (ASTM G109). This took longer time duration (in years), especially in binders containing SCMs. To

shorten the time required for testing, admixed chlorides at different levels were introduced and the corrosion rate was monitored in OPC mortar (Alonso et al., 1996). A new method was introduced by Trejo and Pillai (2003), where the chlorides were migrated towards the steel embedded in mortar by application of voltage. This reduced the time required for the determination of Cl_{th} to a greater extent. However, the test methods involving admixed chlorides and migration of chlorides have limitations when highly resistive binders and corrosion inhibiting admixtures are used. With time, techniques for assessing corrosion also evolved. From Galvanostatic control to potentiostatic control, instruments with fine-tuned precisions are now available at a cheaper price. Hence, corrosion testing is possible in smaller labs. Also, techniques such as electrochemical noise, acoustic emission are being used for corrosion assessment. It is therefore necessary to establish standard test methods and guidelines to utilize the technology available to its best potential in lab as well as field conditions.

2.3.1 Chloride threshold in aqueous systems

Traditionally, Cl_{th} is found by testing the bare metal in solution. This was done to shorten the time taken for the experiment and reduce the variation due to the binder properties, concrete mix proportions, moisture content, and temperature (Diamond, 1986; Li and Sagues, 1999; Saremi and Mahallati, 2002; Yu et al., 2012; Liu et al., 2016; Figueira et al., 2017; Ogunsanya and Hansson, 2019). However, Mammoliti et al. (1999) tested the effectiveness of corrosion inhibitors in synthetic pore solution and mortar and found that the S-B interface plays a major role in the initiation of corrosion as it buffers alkalinity by the dissolution of calcium hydroxide. The nature of the S-B interface (porosity, resistivity and pH) depends on the type of binder and water/binder (w/b) used in the S-B systems (Alexander et al., 2013). Therefore, the estimation of Cl_{th} should be done using S-B systems for realistic results.

2.3.2 Chloride threshold in steel-binder (S-B) systems

Cl_{th} of steel embedded in cementitious systems is different from the Cl_{th} in solution due to physical and chemical variation in the S-B interface. The duration of testing spans from several weeks to years as the chloride ingress to the steel surface in the concrete is slow. In addition, the pore structure, pH, pH buffering capacity, presence of voids and cracks induce spatial variability in the chloride ingress. This could affect the reproducibility of results even if the material and exposure conditions are the same. Attempts are made to develop a standard test method for determining the Cl_{th}, which can yield reproducible results.

2.3.3 Electrochemical testing – traditional approach

Electrochemical measurement techniques are widely adopted in the laboratory to detect the corrosion initiation and then determine Cl_{th}. The advantages and disadvantages of various techniques are discussed in the following subsections.

2.3.3.1 Half-cell potential (HCP)

The half-cell potential is a thermodynamic parameter and indicates only the probability of the occurrence of corrosion. It cannot give information on corrosion kinetics (Ohtsu and Yamamoto 1997). Figure 2.3 shows the arrangement for half-cell potential (HCP) measurement. The potential difference measured between the reference electrode and the steel embedded in concrete is known as half-cell potential. This method requires a reference electrode and a multi-meter. The standard ASTM C876 can be used for data interpretation of conventional S-B systems. However, the absolute limits given in ASTM C876 cannot be used for all the advanced S-B systems, especially those with coated rebars. The half-cell potential measured in S-B systems is not related to the inherent potential of steel alone. It is a function of the S-B interface and the ease with which the metal transfers its electrons to the concrete pore solution (Hansson 1984). The half-cell potential measurement can fluctuate due to

16

moisture content, the resistivity of the cementitious matrix, cover thickness, the coating on steel and the ASTM C876 cannot be adopted for all the exposure conditions (Gulikers et al., 2003; Elsener 2001; Pour-Ghaz et al., 2010; RILEM TC 154-EMC).
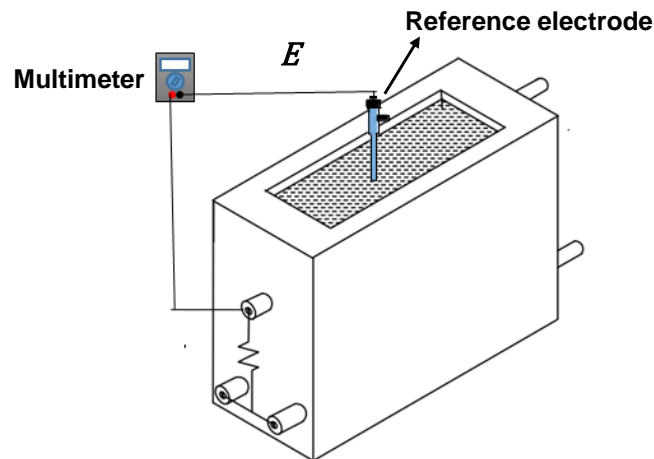
Figure 2.3 Arrangement for half-cell potential measurement forASTM C876 tests

Another use of this test method is to detect corrosion initiation. A significant reduction in potential (say, by about 150 mV) is used by many researchers as a criterion for corrosion initiation and the corresponding chloride concentration has been reported as Cl_{th}. Though perceived as a simple method, this possesses several challenges in practice. It can detect only when significant corrosion has occurred (to be able to see with visible eyes); and not as soon as the corrosion is initiated. Because of this time lag, the half potential techniques for detecting corrosion initiation may lead to erroneous — Cl_{th} values, especially when accelerated test methods are adopted. Hence, the half-cell potential test is not recommended to detect localized corrosion.

2.3.3.2 Macrocell corrosion (MCC)

The ASTM G109 test method was developed based on the work by Berke et al. (1990). This method monitors the possible macrocell corrosion mechanisms in conventional S-B systems.

Figure 2.4 shows the schematic of the ASTM G109 specimen. The top rebar acts as an anode and the two bottom rebars act as a cathode. The macrocell voltage drop across a 100 Ω resistor is measured and the Cumulative Macrocell Current (CMC) is calculated. When the CMC is greater than 150 C, the specimen is considered to be initiated and chloride present at the S-B interface is reported as the Cl_{th}.
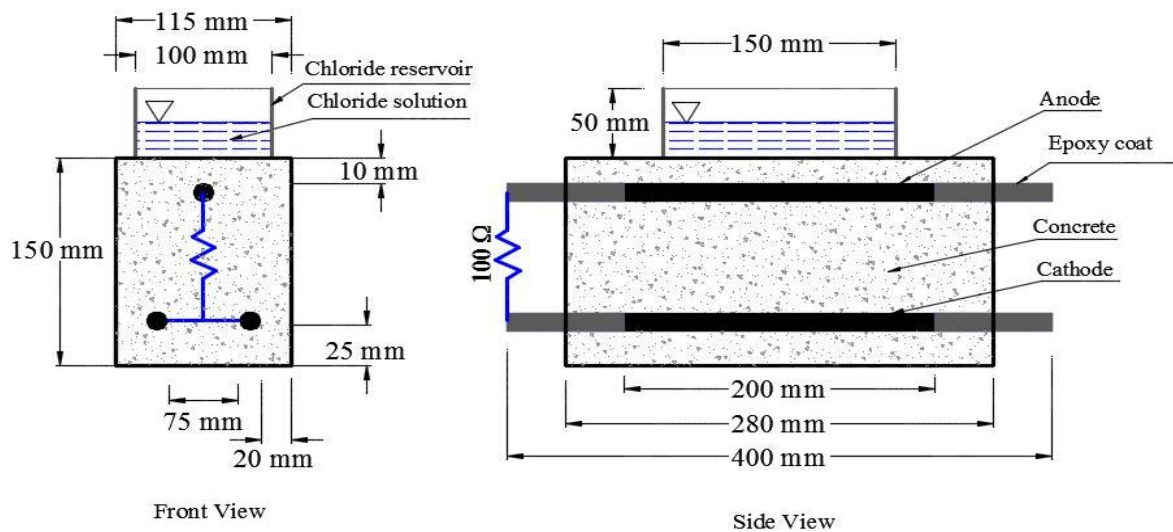
Figure 2.4 Schematic of ASTM G109 specimen (Pillai, 2009)

This method is advantageous due to its simplicity in casting and exposure. However, the following limitations do exist while adopting this test method for S-B systems, which are summarized as follows:

1. The ingress of chlorides through the cover concrete takes several years to reach the steel surface.. Hence, the corrosion assessment of good quality concrete in short term is difficult.

2. The ohmic drop is very high due to the presence of thick cover, especially in highly resistive concrete. Hence, the HCP of the steel measured in this type of specimen may not indicate the ongoing corrosion.

18

3. The macrocell corrosion technique indicates corrosion activity, but severely underestimates corrosion rates (Berke et al., 1990).

4. When both the top and bottom bars (anode and cathode, respectively) start corroding, the macrocell corrosion current indicates lesser corrosion, which is not representative of the cumulative corrosion (Berke et al., 1990).

5. When the corrosion rates are small, the macrocell current cannot be indicative of true corrosion, unless a sophisticated voltmeter is used (Berke et al., 1990). Sophisticated voltmeter (say, minimum 5.5 digits) is essential for extending this test for Cl_{th} estimation.

6. Ionic resistance of the concrete could inhibit the current flow between the top and bottom bars (Berke et al., 1990). The cover depth and concrete resistivity play an important role in the initiation of corrosion. The concrete resistivity controls the macrocell current ─ denser the concrete, the less will be the macrocell corrosion current (Arya and Vassie, 1995; Elsener, 2002).

2.3.4 Electrochemical testing - advanced methods

Most of the advanced electrochemical test methods rely on instantaneous electrochemical response and give useful information on corrosion kinetics. Hence, these methods can be used to obtain repeated measurements on the same specimen until the corrosion is initiated. The linear polarization resistance (LPR) and electrochemical impedance spectroscopy (EIS) techniques are widely used for detecting corrosion initiation. However, these methods are affected by the characteristics of S-B systems such as resistivity, steel type, coatings, and microclimate. Hence, the design of corrosion cell and various input parameters (scan rate, etc.) should be chosen appropriately so that the electrochemical response is not affected

significantly. The working principles, the advantages and disadvantages of these techniques are discussed next.

2.3.4.1 <u>Linear polarization resistance (LPR)</u>

Figure 2.5 shows the experimental set-up needed for conducting an LPR experiment and the typical response. At first, the Open Circuit Potential (OCP) is measured between the reference electrode and the working electrode. The working electrode is perturbed or polarized from this measured OCP by the application of small voltage over a range (say, OCP Vs ±10mV) and the current response is measured. A polarization curve (E vs. Log I) is obtained. The potential sweep is linear over a small range near the corrosion potential or equilibrium potential, E_{corr}, in the polarization curve, and the slope (over the zero current axes) is taken as polarization resistance (R_p) of the working electrode.

The input parameters such as scan rate and scan range should be selected carefully for S-B systems. Scan rate should be slow enough to fully charge the double layer capacitance (S-B interface). However, scan rate such as 0.1667 mVs^{-1}, which is used for aqueous systems is being used for S-B systems. Also, the maximum scan rate (0.05 mVs^{-1}) that can be used for polarization resistance is reported by Poursaee (2010) for steel in different states of corrosion, such as passive and active. However, the implications of using different scan rates are not known. The scan range should be just enough to get the linear region and should not disturb the corrosion potential. Generally, LPR is done over a small range (say, OCP Vs ±10mV). However, the sweep is considered to be in the linear range till OCP Vs ±50mV. The effect of scan range and scan rate are not clearly understood, especially for the steel in a passive state.
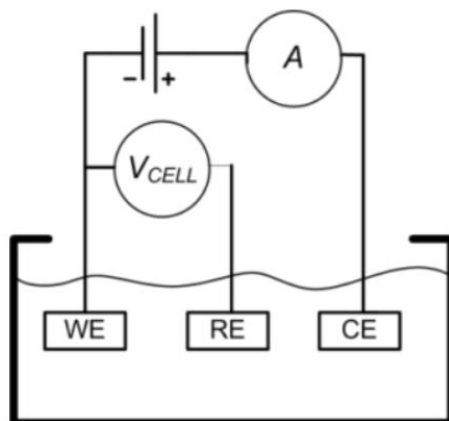
(a) Experimental set-up for LPR testing (Jaime et al., 2013)
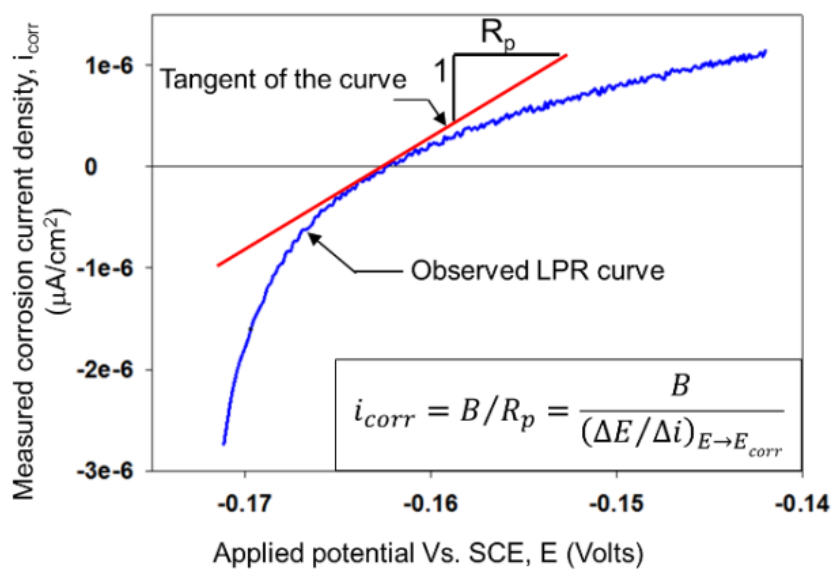
(b) Typical LPR curve

Figure 2.5 Experimental set-up and LPR curve

The following are the advantages and disadvantages of the LPR technique.

a) Advantages

1. A relatively simple method to determine the polarization value (R_p) when $R_p \gg R_\Omega$, the electrolyte resistance (Kelly et al., 2003; Mansfeld, 1976).

2. Repeated measurements are possible (non-destructive in nature) and it takes a few minutes for corrosion measurement

3. Data analysis is simpler when compared to other advanced methods

b) Disadvantages

1. Assumes that the corrosion is uniform and does not distinguish between resistance polarization and diffusion polarization (Walter and Centre 1977).

2. For highly resistive cementitious systems, electrolyte resistance (ohmic drop) is not negligible. The ohmic drop can distort the polarization curve as well as the input scan rate, which could influence the measured R_p. Current interruption technique is essential to overcome this effect (Mansfeld 1982).

3. LPR is dependent on temperature and moisture conditions during measurement. Millard et al. (2001) studied S-B systems and showed that R_p is dependent on temperature and RH at the S-B interface and also reported that the cyclic wet-dry regime could influence the cover resistance, which in turn could change the corrosion rate

4. LPR gives the total R_P of S-B systems. Therefore, the interpretation of the response obtained from LPR tests on advanced S-B systems (with highly resistive electrolyte, corrosion inhibitors, coating etc.) is challenging and needs to be studied as no guidelines are available to interpret the data and understand the performance of individual components.

2.3.5 Electrochemical impedance spectroscopy (EIS)

EIS is one of the widely used techniques for measuring the corrosion of steel in concrete, especially for advanced S-B systems. Figure 2.6 shows the typical response spectra and a typical equivalent electrical circuit of the S-B system. In this test, the AC signal (~10 mV amplitude) is perturbed over a range of frequency (10^6 Hz to 10^{-2} Hz) along with the DC voltage (say, OCP) and the response spectrum is analyzed with the help of equivalent circuits. EIS technique can yield more information than LPR about the reaction kinetics at the S-B interface. It is possible to understand the performance of the individual component in an advanced S-B system. However, a deep understanding of the system and the relevant electrical parameters are required for analysis and serious challenges do exist in formulating a suitable equivalent circuit, especially for advanced S-B systems (Ribeiro and Abrantes 2016).
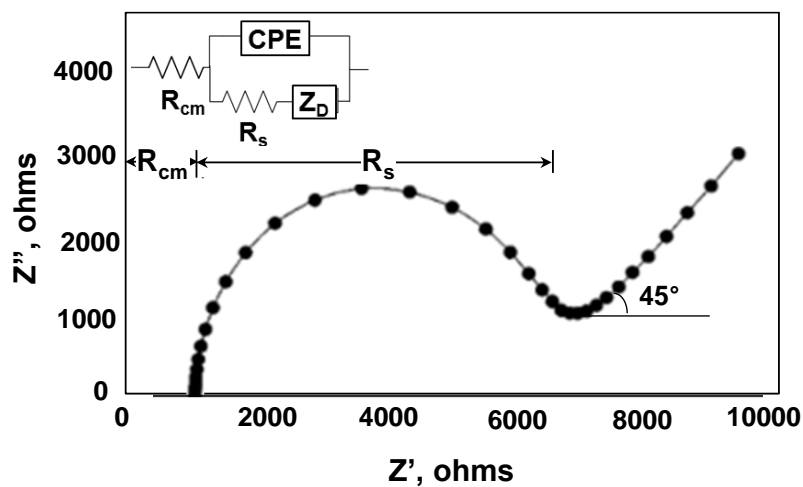
Figure 2.6 Typical EIS spectra and equivalent circuit

a) Advantages

1. ElS is an effective tool for investigating electrochemical mechanisms involving dielectric and transport properties of materials, passive surfaces, and porous electrodes (Feliu et al., 1998, Song 2000, Dhouibi et al., 2002, Chechirlian et al.,1993, Jain and Neithalath, 2011).

2. The electrochemical response of each component of the system, namely concrete, coating, double layer, steel etc. can be identified from the EIS spectra.

3. The technique is capable of differentiating closely related mechanisms occurring in the cover concrete and the S-B interface.

b) Disadvantages

1. Formulating and fitting an equivalent circuit requires an in-depth understanding of the physical S-B system. The elements in the equivalent circuit should have some representation of the physical components.

2. Determination of kinetic parameters requires in-depth knowledge of the reaction mechanism that can happen in the system.

3. EIS gives the electrochemical measurements averaged for the entire surface of the steel specimen, even though pitting occurs locally.

2.3.6 Usability of standardized test methods in S-B systems

The test methods adopted include different electrochemical techniques, exposure conditions and corrosion initiation criteria. Table 2.2 shows the summary of test methods and their usefulness in testing the S-B systems. ASTM standards (C876, G109) are useful for conventional S-B systems of low-moderate resistivity. They may not work well for corrosion detection and Cl_{th} of advanced S-B systems. Advanced electrochemical techniques (LPR and EIS) enable capturing of the instantaneous electrochemical response of advanced S-B systems. However, such response depends on the exposure condition, properties and thickness of cover concrete, corrosion cell geometry, and input test parameters adopted for testing. There is a lack of guidelines for data interpretation with the fundamental understanding of the electrochemical response from the different S-B systems. Japanese Industrial Standards (JIS) A 6205 standard does not address the corrosion process simulating the natural condition and is not suitable for

detecting corrosion initiation and estimating the Cl_{th} in S-B systems. The failure criteria for different exposure conditions should be established for a realistic estimation of Cl_{th} in S-B systems. The challenges in adopting different electrochemical techniques and the adoption of failure criteria are discussed in detail in Subsections 2.3.3, 2.3.4 and 2.3.7.

Table 2.2 Summary of standard test methods available for testing

Methods	Electrolyte	Exposure Condition	Remarks
ASTM C876 - 2015 (Half-cell Potential)	Concrete	Laboratory/ Field conditions	• Only for uncoated steel reinforcement • Failure criteria: Half-cell potential < -350 mV vs CSE – 90% probability of corrosion
ASTM G109 - 2009 (Macrocell corrosion)	Concrete	Wet-dry cycle (14w – 14 d)	• Only for uncoated steel reinforcement • Failure criteria: Cumulative Current >150 C
ASTM G59 ASTM G5, ASTM G180, ASTM G102 (Polarization curves)	NA	Immersion	• Cannot be used for electrolyte resistance of significant value • Cannot distinguish the corrosion mechanism of different steel types
ASTM STP 1506 (EIS)	NA	Varied temperature	Can be used for performance evaluation of coated steels in aqueous systems
ASTM STP 1188 (EIS)	NA	NA	Can be used for performance evaluation of coated steels in high resistive media
JIS A 6205	Concrete	180ºC, 1 Pa, Saturated water vapour	For evaluating corrosion inhibiting admixtures in concrete

2.3.7 RILEM TC 235-CTC

RILEM TC 235-CTC committee tried to develop a test method to determine Cl_{th} of steel embedded in concrete. Figure 2.7 shows the schematic of the specimen adopted.
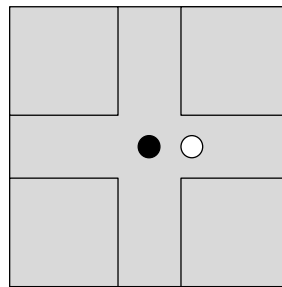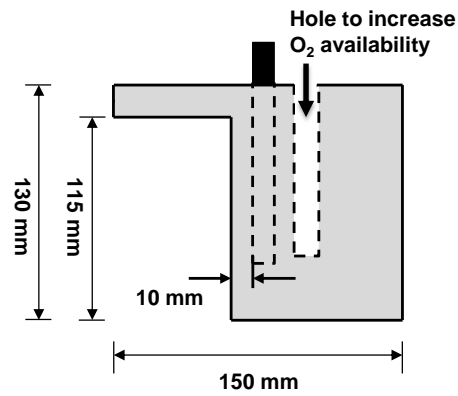
(a)

(b)

Figure 2.7 RILEM TC 235 specimens (a) Schematic with dimensions and (b) in mist room

The specimen had a hole near the steel to increase the availability of oxygen. The sudden drop in potential was considered as the indicator for corrosion initiation point. In spite of very low concrete cover (10 mm) and specimen geometry adopted, corrosion initiation did not happen for most of the specimens after testing for more than 2.5 years. The committee could not develop a short-term method to find the Cl_{th} of the S-B system. This emphasizes the complexity of the phenomenon and challenges involved in developing such a test method for S-B systems.

2.4 VARIATIONS IN MEASURED CHLORIDE THRESHOLD

Figure 2.8 summarizes the Cl_{th} values reported in the literature. The number on the top of each bar represents the frequency of occurrence, i.e. the number of papers published with the test parameters or techniques. The vertical line indicates the range of scattering in the values reported. The second and third bar shows the variation in Cl_{th} reported depending on the type of cover material used (mortar/concrete). It has been reported that the Cl_{th} can be similar in both mortar and concrete, with similar microclimate at the S-B interface (Hussain and Ishida (2011). Moreover, the electrochemical response of the S-B interface will be more uniform when the cover is made of mortar instead of concrete (because mortar is more homogenous than concrete). Hence, the present study adopts mortar for electrochemical cell design and assessment of Cl_{th}.

Figure 2.8 Variation in Cl_{th} reported in literature (Angst et al., 2009)

The Cl_{th} of concrete depends on the type of binders being used. For example, Cl_{th} of concretes with SCMs (Silica fume (SF), Flyash (FA), and GGBS) are low when compared to OPC. The reduction of Cl_{th} depends on the amount of reactive silica/ amorphous content of the SCM. This reduction is attributed to the consumption of $Ca(OH)_2$ due to the pozzolanic reaction, which in turn leads to reduced pH buffering capacity at the interface. However, the time to reach the Cl_{th} at the interface is always longer due to lower ionic conductivity. The refined pore structure helps to restrict the ionic movement and thus the chlorides from reaching the steel surface.

The exposure condition such as the wet-dry cycle, premixed chlorides, migration might influence the Cl_{th} in addition to the materials used. It is to be noted that the values used for each bar in Figure 2.8 contain different S-B systems, exposure conditions, and test methods. The detection techniques such as half-cell potential, potentiostatic control/polarization led to

28

different Cl_{th} due to data interpretation and failure criteria adopted. The techniques widely used for determining Cl_{th} are discussed in detail in Subsection 2.3.

It is not appropriate to combine all such data of Cl_{th} and use that for service life estimation. In other words, the Cl_{th} values cannot be generalized - it must be reported for different conditions prevailing at the S-B interface for the specific material used. Such Cl_{th} values can ensure more realistic service life estimation. To achieve this, the factors affecting the chloride conditions at the S-B interface, microclimate at the S-B interface, electrochemical response and data interpretation, etc. to arrive at the Cl_{th} need to be studied in further detail.

In summary, the Cl_{th} value reported in the S-B system is affected by three major parameters namely (i) ingredients of S-B system such as binder type, type of steel, inhibitors, (ii) exposure conditions which include techniques used to accelerate chloride ingress and corrosion initiation, and microclimate at interface such as relative humidity, oxygen, temperature, and pH, and (iii) electrochemical testing techniques such as half-cell potential, impressed current and their input parameters. In addition, cracked concrete and stressed steel lead to a variation of chloride threshold, which is beyond the scope of this research.

2.4.1 Effect of materials on chloride threshold

The Cl_{th} of the S-B systems depends on the type of materials being used. Three main types are discussed in detail. First, the effect of binders on Cl_{th} is discussed followed by steel and admixtures.

2.4.1.1 Effect of binder types

As explained earlier in Subsection 2.2.1, the type of binders influence the pH and pH buffering capacity at the S-B interface. In addition to the type of binder, the replacement level also plays a vital role in the chloride threshold as the availability of $Ca(OH)_2$ at the S-B interface depends on both the reactivity of SCM and replacement level of OPC (Wild et al., 1996, Heikal et al.,

2000 and Meddah et al., 2014). Also, the type of binder can influence the formation of passive film, which in turn can affect the chloride threshold.

2.4.1.2 <u>Effect of steel types and surface finish</u>

Highly polished steel surface can provide better resistance compared to the non-polished surface (Mammoliti et al., 1996). Alonso et al. (2000) reported that the Cl_{th} of ribbed bars did not change much when compared to smooth bars even though the corrosion rate did. Angst et al. (2011) found that rebar corrosion always started at the back side of the casting face (also the chloride ingress direction) of the specimen at a lower chloride threshold in comparison with the top face. This was attributed to poor bonding between concrete and steel due to plastic settlement, bleed water collection and high porosity of interfacial zone due to high w/b. To increase the longevity of structures exposed to chlorides, stainless steel rebars, galvanized rebars, coated rebars (epoxy coated, cement polymer coated etc.) are being used. Several controversies in performance of these rebars have been observed. For example, the de-bonding of the coating and crevice corrosion were observed in most cases of coated rebars with slight damage whereas galvanized coating is too active to provide long-term corrosion resistance (Manning, 1996; Dong at al., 2012). In general, the Cl_{th} of the as-received rebars are less than the smooth finished and coated rebars (Erdogdu et al., 2001). Also, stressed rebars and prestressed strands have less Cl_{th} than the unstressed steel, which is beyond the scope of this work.

2.4.1.3 <u>Effect of corrosion-inhibiting admixtures</u>

Corrosion-inhibiting admixtures (CIAs) have a direct influence on Cl_{th}, by acting as a barrier against the chloride attack on the passive layer of steel and are very effective for delaying the initiation of corrosion (Mammoliti et al., 1999). There are mainly two types of CIAs, namely anodic inhibitors and bi-polar inhibitors. Significant research has been done on different types

of CIAs (anodic, bipolar,etc.) and there are mixed opinions on their corrosion performance (Berke and Hicks, 2004; Jamil et al., 2004; Kessler et al.,2003; Nmai, 2004; Saricimen et al., 2002; Söylev and Richardson, 2008). In general, it is believed that Cl_{th} can be enhanced by adding CIAs. However, the addition of CIAs can adversely affect the microstructure and resistivity of concrete, which in turn can accelerate the chloride ingress rate (Li et al., 2000; Paredes et al., 2010). Also, in order to be effective in corrosion resistance, CIAs should be added in the recommended dosage (Rengaraju et al., 2015). The study of the influence of inhibitors on Cl_{th} is beyond the scope of this work.

2.4.2 Effect of exposure conditions on the chloride threshold

Natural corrosion in reinforced concrete structures is typically a slow process, say decades. However, engineers need information on corrosion resistance in the short term, say a few months for selecting materials. For obtaining corrosion results in short term, various techniques are used to accelerate the access to chlorides at the S-B interface and/or corrosion process. The effect of these techniques followed by the microclimate at the S-B interface and the effect of chlorides on the formation of corrosion products are discussed in detail.

2.4.2.1 <u>Effect of accelerated ingress of chlorides</u>

Techniques for accelerating the access to chlorides at the S-B interface include (i) immersion in chloride solution, (ii) cyclic wet-dry exposure using chloride solution, (iii) premixing the concrete with chlorides (say, admixed chlorides), and (iv) impressed current or potential gradient.

2.4.2.2 <u>Immersion and wet-dry cycle</u>

When immersed in a chloride solution or when subjected to cyclic wet-dry exposure, the Cl⁻ ions accumulate at the S-B interface due to diffusion and/or capillary suction. This condition mimics the real field structures and hence, the form of corrosion and the corrosion products are

31

close to the realistic corrosion process (Angst et al., 2009). However, this type of exposure takes a long time to initiate corrosion in good quality concretes. For example, ASTM G109 test using cyclic wet-dry exposure could take several years to initiate corrosion (Hansson et al., 2006) – the more the corrosion resistance of the system, the more will be the test duration. Hence, researchers started assessing the corrosion performance of steel by embedding it in mortar instead of concrete. Even then, it takes several months to initiate corrosion when pozzolans are used (Fajardo et al., 2009). The test duration would be longer if the w/b is low. Hence, to bypass or shorten the test duration required for natural chloride ingress in good quality concrete specimens, researchers have either used admixed chlorides or impressed current to assess the corrosion performance.

2.4.2.3 Admixed chlorides

Admixed chlorides in fresh concrete can accelerate the cement hydration and change the morphological structure of C-S-H gel (Koleva et al., 2007). The presence of chlorides in the fresh concrete leads to the formation of the non-uniform and weak passive film on the steel surface, which in turn leads to corrosion in the areas, where chlorides are present. Hence, the passive film in such specimens with admixed chlorides do not represent that of a concrete structure with natural exposure conditions and the corrosion rate and corrosion products may differ leading to erroneous conclusions (Poursaee and Hansson, 2009). Li et al. (2011) monitored the corrosion rate for admixed chloride specimens for one year and found that the corrosion rate decreases over a period of time. They attributed it to the sufficient availability of mixing water during the initial period, which was consumed at the later stages. The exposure condition required for sustained corrosion is not well-reported. Hence, it is not recommended to adopt admixed chloride technique to assess chloride threshold and corrosion initiation, except for testing the chloride contaminated raw materials (Poursaee and Hansson, 2007).

2.4.2.4 <u>Impressed current</u>

It is common to adopt impressed current technique (by applying a constant potential gradient) to assess corrosion performance in short term (Austin et al., 2004). Some believed that impressed current would not induce significant changes in the corrosion process. The impressed current technique can be used for two purposes. First, it can be applied directly onto the steel to accelerate the corrosion process. For example, Care and Raharinaivo (2007) reported that an impressed current of 100 µA/cm^2 did not induce any changes in the nature of corrosion products formed on the steel and properties of the interface when embedded in OPC mortar with and without chlorides. Based on this belief, the impressed current technique has been widely used to assess the effect of SCMs on corrosion rate and corrosion-induced cracking (Sharkawi and Seyam, 2018; Narasimulu et al., 2014; Abosrra et al., 2011; Sangoju et al., 2011; Austin et al., 2004). However, the more the current and time of application, the more could be the effect on the concrete cover and corrosion products. Microstructural changes can happen in concrete cover when a potential gradient of 20 V is applied for an extended period (say, more than 300 hours). This is due to the migration of chloride ions and hydroxyl ions towards the steel and Ca^{2+} and other cations away from the steel (Marcotte et al., 1999; Care and Raharinaivo, 2007). In such cases, the porosity and interconnectivity of pores increase and lead to oozing of corrosion products, which in turn lead to lack of expansive stresses and cracking of concrete cover – although significant corrosion could have occurred. Poursaee and Hansson (2009) reported that chloride exposure with and without impressed current would lead to different types of corrosion and corrosion products. Second, the impressed current technique can be used to drive the chlorides to the steel surface, which bypasses the time required for Cl_{th} testing (Trejo and Pillai, 2003). However, the nature of the S-B interface can vary due to the application of the potential, especially for inhibitors systems with complex ions (Karuppanasamy and Pillai, 2015) and is not suitable for finding the Cl_{th} in such systems.

33

In sum, the technique adopted to accelerate the chloride ingress could significantly alter the nature of the S-B interface and should be used depending on the nature of the S-B systems.

2.4.3   Effect of micro-climate at the S-B interface

Corrosion initiation of steel depends on the physical and microclimate conditions of the S-B interface. Major factors influencing the microclimate at the S-B interface are (i) moisture, (ii) oxygen, (iii) temperature, and (iv) pH conditions. The microclimate depends heavily on the bulk properties and thickness of cover concrete and ambient exposure conditions. The formation of the passive film and the amount of chlorides needed for de-passivation depends on the microclimate. Also, the relationship between the cover and exposure condition can be used to determine when to take electrochemical measurements. This timing for measurement is very important for performing Cl_{th} studies using wet-dry exposure conditions.

2.4.3.1 <u>Effect of moisture at the S-B interface on chloride threshold</u>

Figure 2.9 shows the effect of relative humidity on Cl_{th} due to the changes in exposure conditions (Pettersson, 1996). When the RH is 90%, the amount of chlorides required to initiate corrosion is less and thus considered as critical chloride threshold. When the RH is less than 45% or greater than 90%, corrosion cannot occur due to the deficit of either moisture or oxygen, respectively, at the S-B interface (Hussain et al., 2012; Enevoldsen et al., 1994). There could be a lag between the wet-dry cycle at the S-B interface and the wet-dry cycle at the concrete surface (Hong and Hooton 1999; Ryu et al., 2011; Zhang et al., 2012; Jaśniok and Jaśniok, 2015). This lag is mainly because of the material properties and thickness of the cover concrete. Hence, the wet-dry cycle (at the concrete surface) to be adopted for achieving a particular wet-dry condition or relative humidity (RH) at the S-B interface is important to be known. Also, electrochemical measurements are affected significantly by RH at the interface (Law et al., 2004). As the Cl_{th} study heavily depends on the RH at the S-B interface, the timing of

electrochemical measurement is also crucial. There is a need to understand the relationship between the wet-dry regime, and the material properties and thickness of cover on the RH at the S-B interface - to develop guidelines to mimic real-life scenarios in the laboratory.
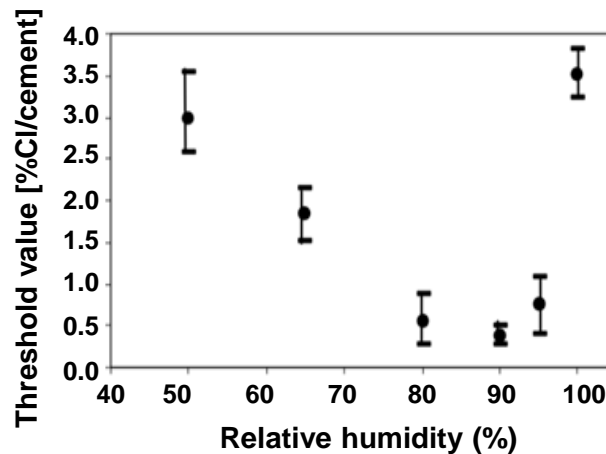
Figure 2.9 Effect of relative humidity on Cl_{th} of steel in mortar (Pettersson, 1996)

2.4.3.2 Effect of oxygen at S-B interface on corrosion process

Oxygen at the interface plays a key role in the nature of the passive layer formed at the steel surface (Kim and Young 2013). Oxygen is essential for the corrosion process to occur. In submerged conditions, the corrosion rate can be very low due to the deficit of oxygen. However, in highly humid surface conditions, the corrosion rate could depend on the quality and thickness of cover concrete. In particular, higher porosity will lead to higher concentrations of oxygen at the S-B interface, which in turn could lead to higher corrosion rate (Hussain et al., 2012). Also, notice that when sufficient chlorides and high humid conditions are present, hydrogen evolution in the crevices can sustain the corrosion rate, even in the absence of oxygen (Gonzalez et al., 2010). Therefore, electrochemical testing should be conducted at oxygen levels that mimic real-life scenarios (Alexander, 2016). As in the case of moisture conditions, the wet-dry regime can influence the oxygen availability at the S-B interface. However, limited information is available on the effect of oxygen concentrations at the S-B interface on Cl_{th}.

2.4.3.3 <u>Effect of temperature at S-B interface on corrosion process</u>

Temperature plays a key role in the stability and composition of the passive film and the corrosion potential could change with the change in temperature (Deus et al., 2012). An increase in temperature could lead to an increase in the corrosion rate. However, this effect cannot be directly related to the Arrhenius equation as the corrosion rate in concrete decreases beyond 50 °C due to the reduced oxygen solubility in the pore solution. Blockage of pores could happen in high temperature when concrete is in high humid conditions (Al-Khaja, 1997; Yuan et al., 2009; Alhozaimy et al., 2012). Also, the ambient temperature and the temperature at the S-B interface will become similar within a few hours (Liu et al., 2015). This lag could vary as a function of specific heat capacity and thermal conductivity of concrete. The electrochemical response (say, corrosion rate) can be greatly affected by a few degree Celsius change in temperature. Therefore, maintaining a known and constant temperature throughout the duration of testing is essential. Also, the author could not find literature on the effect of temperature at the S-B interface on the Cl_{th} measurement.

2.4.3.4 <u>Effect of pH at S-B interface on chloride threshold</u>

Ordinary Portland cement concrete systems are highly alkaline. In systems with SCMs, the pH at the S-B interface could be slightly low (say, around 12) because of the consumption of $[OH]^{-}$ ions for secondary hydration process or pozzolanic reactions (Angst et al., 2009; Thomas 1996; Alexander et al., 2013). Figure 2.8 shows the effect of pH on Cl_{th}. The lower the pH at the S-B interface, the lower will be the Cl_{th} (Bentur et al., 1997; Kim and Young, 2013).
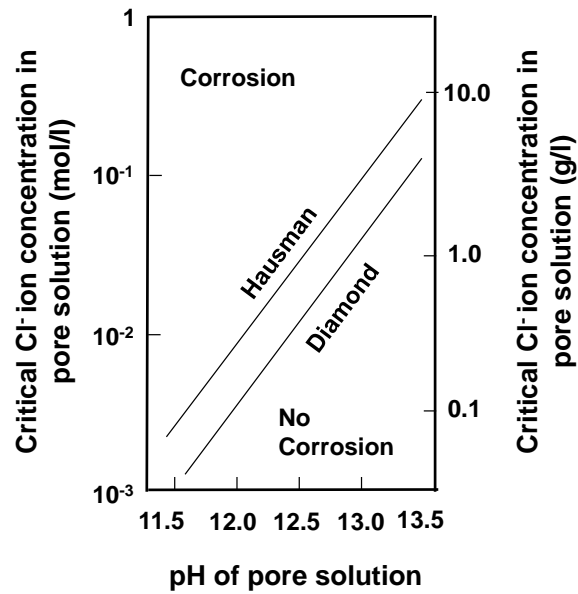
Figure 2.10 Effect of pH on Cl_{th} (Bentur et al., 1997)

In summary, the passive film and Cl_{th} depends on the microclimate at the S-B interface. The rate of change of microclimate at the S-B interface is a function of the external environment. However, literature does not clearly state what exposure condition should be adopted in the laboratory to mimic a particular microclimate at the S-B interface (to mimic real-life scenarios with various climatic and chloride conditions); and more importantly, when to measure the electrochemical response of the S-B system.

2.4.3.5 <u>Embedded sensors for assessing micro-climate in concrete</u>

Sensors can be used in the S-B interface to understand the microclimate, which is of primary concern in corrosion initiation. Norris et al. (2008) used micro-electromechanical systems (MEMS) sensor to monitor RH inside the concrete, the application of which was difficult for long-term data acquisition. Duffó and Farina (2009) developed embedded sensors to monitor corrosion in new and existing structures in field conditions. The half-cell potential, oxygen, temperature, corrosion rate, and resistivity of concrete were measured using those sensors. However, it is difficult to adopt the sensor to the laboratory specimen design. McCarter et al.

(2010) used a multi-electrode sensor to capture the change in resistivity at different cover depths of two different concretes when subjected to wet-dry cycles and the temperature changes. They found that the convection zone in concrete is 30 mm, beyond which there is no change in resistivity due to the external environment. But, note that the thickness of this zone could also be dependent on the other properties of concrete. Martínez and Andrade (2009) developed in-house sensors to monitor the parameters such as resistivity and oxygen availability inside concrete in field conditions. The major problem with many of the sensors is associated with their suitability for embedment in an alkaline environment for long-term. SHT1X series sensor with rubber encapsulation inside the mortar was used by Chang and Hung (2012). However, the data measured could be questionable due to the effect of encapsulation. This limitation could be overcome by using a system with a sensor and a filter cap. Such systems can be used to monitor the RH and temperature inside the mortar for several months (Barroca et al., 2013). In this study, SHTnX series sensor with a filter cap is used to monitor the effect of wet-dry cycles on the RH and temperature at the S-B interface. Such data will be used to choose an appropriate wet-dry cycle for further experiments on Cl_{th}.

2.4.4 Effect of microclimate on the formation of corrosion products

The formation of different phases of iron and its hydroxides/oxides (say, α-, β-, γ-, and δ-FeOOH, and γ-Fe$_2$O$_3$) depends on the microclimate at the S-B interface (Misawa et al., 1974). Figure 2.11 shows the typical phases of iron oxides in the chloride-rich environment and its relative magnitude of expansion (Hansson et al., 2012). Corrosion-induced cracking of concrete cover is highly dependent on the expansive stresses generated by the unit volume of corrosion products.
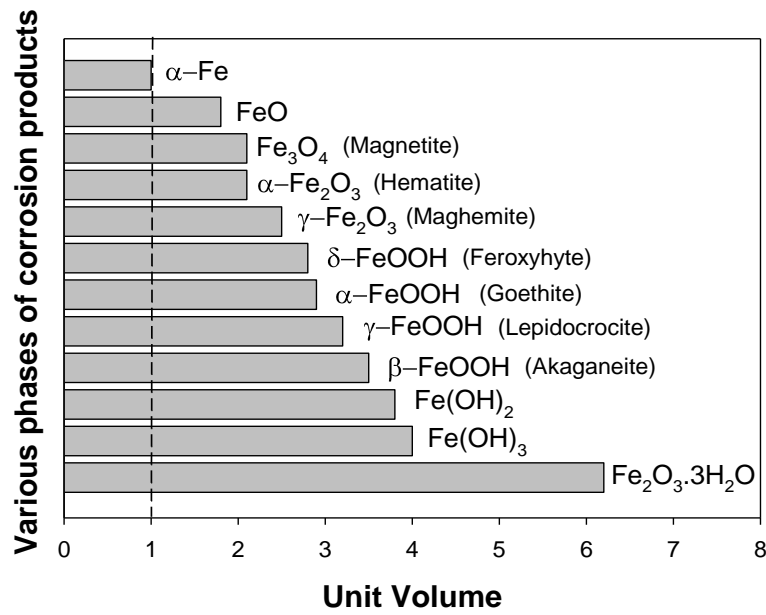
Figure 2.11 Phases of iron oxides with their expansion (Hansson et al., 2012)

The formation of different corrosion products in S-B systems subjected to chlorides is summarized in Table 2.3. Care et al. (2008) found that the corrosion-induced cracking and the time-to-crack, $T_{crack,}$ depend on the ability of corrosion products to ingress the surrounding concrete pores. This is dependent on the composition and density of corrosion products and the porosity of the S-B interface and surrounding concrete, which is affected by the incorporation of SCMs. For example, the presence of limestone could lead to a more porous passive film at the S-B interface (Batic et al., 2013), whereas the presence of metakaolin could lead to less porous S-B interface (Frías and Cabrera, 2000). Hence, the formation of the passive layer and the corrosion products should be investigated to assess the effect on electrochemical response.

Table 2.3 Formation of corrosion products in the presence of chlorides

Initial product	Later products formed	Nature of the product	Reference
Passive layer	Magnetite (Fe_3O_4) / Hematite (α-Fe_2O_3)	During the initial phase of curing, an inner layer composed of magnetite and outer layer with oxygen availability composed of hematite is formed. Presence of hematite gives the orange color to the rust. Formation of hematite or magnetite does not induce cracking as these oxides occupy only twice volume of steel and displace readily	Marcotte et al., 2007
Green rust I	Hematite	Green rust can dissolve in pore solution and ooze out through the pore spaces in concrete and on exposure to atmosphere forms hematite.	
	Feroxyhyte (δ FeOOH)	If the concentration of chloride is low, then Feroxyhyte is formed. 3 times increase in volume is observed.	Sagoe-Cretsil and Glasser, 1993
	Akagenite (β-FeOOH)	If the concentration of chloride is very high, then Akagenite is formed. 3.5 times increase in volume is observed.	
	Lepidocrocite (γ-FeOOH)	If the electrochemical potential is high, then Lepidocrocite is formed. 3.1 times increase in volume is observed.	
Lepidocrocite	Amorphous ferric oxyhydroxide	Lepidocrocite converts to an intermediate unstable product when the surrounding pH reduces	Criado et al., 2015
Amorphous ferric oxyhydroxide	Goethite (α - FeOOH)	2.9 times increase in volume	

2.4.4.1 <u>Characterization of corrosion products</u>

For characterizing the corrosion products, various techniques such as XRD, scanning electron microscopy (SEM), Mössbauer spectroscopy, Raman spectroscopy, and Electron micro probe analyzer (EMPA) are employed by researchers (Koleva et al., 2006; Suda et al., 1993; de la Fuente et al., 2011). Out of these, Raman spectroscopy is adopted widely due to its simplicity of data analysis and no sophisticated specimen preparation. All other techniques need specimen preparation before acquiring the data. Like every method of analysis, Raman spectroscopy also has its disadvantages. Raman spectrum is acquired at a particular spot and hence, it does not give the idea of an overall layer of corrosion products. Prolonged exposure and laser heat can transform one corrosion product to another (Criado et al., 2015). Hence, precautions should be taken to avoid such exposures while characterizing corrosion products.

2.4.5 Cell geometry

Figure 2.12 shows the corrosion cell with Working Electrode (WE) (specimen being tested), Counter Electrode (CE) and Reference Electrode (RE). The reliability of the response data from the advanced electrochemical test methods depends on the configuration of the specimen and electrodes and the specific properties of S-B systems.
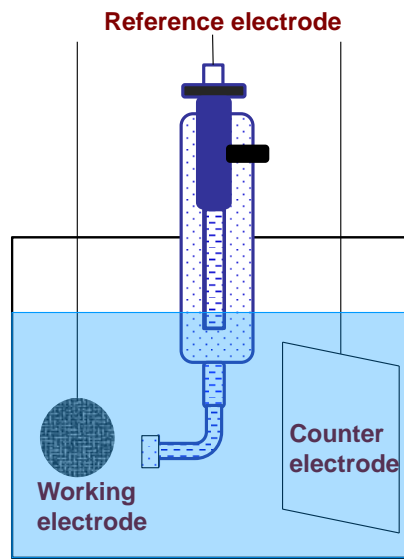
Figure 2.12 Schematic of a typical 3-electrode corrosion cell

2.4.5.1 The positioning of electrodes and electrolyte resistance

The corrosion cell geometry can influence the electrochemical measurements in S-B systems due to the current distribution (Andrade et al., 1995; Myland and Oldham 2000). The positioning of RE in the solid electrolyte is not as flexible as the liquid electrolyte (Rutman and Riess, 2008). The position of RE between CE and WE (steel rebar) will affect the value of the solution resistance measured in the specimen. RE outside the current path will give low solution resistance. If localized corrosion is happening on one side of the steel rebar, then low-frequency spectra will be different (Pech-Canul et al., 1998). The S-B specimen with CE embedded in concrete can have a different impedance spectrum when compared to that of an S-B system with CE kept outside the concrete. Zhang et al. (2014) also found that RE-WE-CE planar arrangement lowered the solution resistance in bio-anodes. The current distribution will not be the same in all geometries and the effect of the relative position of electrodes affect the electrochemical data. Hence, the cell design should ensure minimum ohmic drop and uniform current distribution to have reliable electrochemical measurements. As there are no guidelines for the test set-up in S-B systems, different researchers have adopted different geometry, which

could affect the electrochemical data - making these data questionable and difficult to compare with results from other laboratories. The Cl_{th} values reported in the literature varies irrespective of the similar S-B system and electrochemical parameters adopted for testing (Angst et al., 2009). This variation arises due to the electrode configuration and geometry of the specimen adopted for testing. Hence, there is a need to understand the effect of specimen and electrode configuration on electrochemical response ─ to enable the appropriate detection of corrosion initiation and corresponding Cl_{th} in advanced S-B systems.

2.4.5.2 <u>Effect of thickness and resistance of electrolyte (cover depth)</u>

The 3-electrode cell measurements are very sensitive to the electrode configuration. Symmetric configuration can accurately measure the impedance of an electrode; however, it was found, based on studies in aqueous media, that the electrolyte resistance is not linearly related to the distance between the RE and WE (Hsieh et al., 1997). The electrolyte resistance is dependent on three factors, namely (i) the arrangement of electrodes in the corrosion cell, especially the distance between WE and RE, (ii) the conductivity of the electrolyte, and (iii) the polarization resistance of the WE (Hack et al., 1990). The conductivity of electrolyte can change with time and distance (Ehrhardt, 1990). A similar change in conductivity occurs in S-B systems as the cementitious system is a poor electrolyte with high resistivity. Different S-B systems can have different resistivity. Hence, the solution resistance at the same depth in different S-B systems need not be similar. Resistivity at any point in the S-B systems could depend on the exposure conditions, type of binder, material packing, w/b, etc. Also, the cover depth could affect the microclimate in the S-B interface as discussed in Section 2.4.5.2.

Figure 2.13 shows the ohmic drop occurring in the corrosion cell due to the electrolyte resistance. Due to the high resistivity of concrete, the potential measured at the tip of RE and true potential at the WE is not the same and the measured potential at the concrete surface is

always less than the actual potential at the S-B interface. This phenomenon is called ohmic drop. Due to this, the electrochemical measurements are subjected to distortions. To reduce the ohmic drop, the RE should be kept as close as possible to the WE. However, to achieve this in S-B system, a complex cell design (with embedded luggin probe etc.) has to be adopted, a specimen of such kind is difficult to cast. Furthermore, in sol-gel electrolytes (S-B systems), non-uniform current distribution occurs due to poor corrosion cell design, which further distorts the corrosion measurements. The ohmic drop is an important factor to be considered in the modern electrochemical measurement techniques like LPR and EIS. The study of the effect of cover depth on ohmic drop and microclimate is needed.
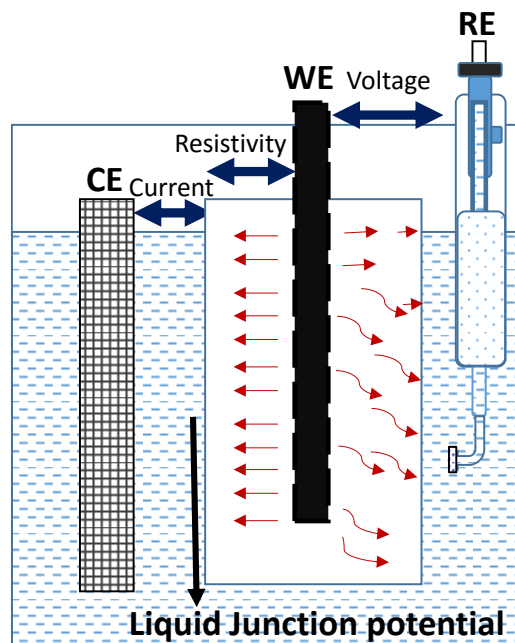
Figure 2.13 Illustration of ohmic drop in S-B systems

2.4.5.3 <u>Effect of size of the specimen</u>

Chloride-induced pitting corrosion is stochastic in nature and dependent on specimen size as more flaws may be expected in bulk (Takeyama and Shibata, 1977). Typical specimen size adopted in aqueous electrochemistry is 1 sq.cm. The smaller the specimen size lesser the ohmic

drop. Li and Sagüés (2002) found that smaller laboratory specimens were overestimating the realistic Cl_{th} value of S-B systems in structures. It was also reported that the Cl_{th} is dependent on specimen size and followed a probabilistic distribution. Angst et al. (2011) found that corrosion initiation followed the spatial variation in the presence of chlorides. The presence of weak spots such as voids, bleed water accumulation, and other flaws in the S-B interface was found to be more in larger specimens than the smaller specimens – hence, larger the specimen, the larger will be the probability of corrosion initiation. It was also reported that there could be a characteristic length, which should be adopted if one needs to scale up to the real structures. However, no quantitative estimates on this characteristic length are reported in the literature.

2.4.5.4 <u>Effect of size of the counter electrode (CE)</u>

In aqueous electrochemistry, to avoid the rate-limiting step due to CE surface area, the area of CE is kept higher (Metrohm, 2011). Typically, the surface area of CE is kept as at least twice the area of WE (ASTM G61, 2014; ASTM G109). Ideally, the size of the counter electrode should be 100 times as that of the working electrode (Bockris et al., 2000). The size of CE can influence the electrochemical measurement and it should be chosen in such a way to avoid the rate-limiting step.

In summary, the electrode configuration (corrosion cell geometry) and the effect of various cell geometries need to be studied to understand the current distribution, which affects the ohmic drop. Because of these reasons and lack of understanding of the correlations, at present, the failure criteria adopted in one experiment in one lab cannot be directly adopted to another experiment in another lab. Therefore, there is a need to standardize the corrosion cell configuration and exposure conditions that can be used to mimic the field conditions and then, estimate Cl_{th} of advanced S-B systems.

2.4.6 Corrosion initiation criteria

Table 2.4 summarizes various approaches to corrosion initiation criteria adopted by researchers for determining Cl_{th} in various exposure conditions. The approaches used for initiation criteria can be classified into four categories, namely (i) fixed exposure time, (ii) fixed corrosion parameter (open circuit potential (OCP), charge passed, polarisation resistance (R_p), Corrosion current density (i_{corr}), etc.), (iii) sudden increase/decrease in corrosion parameter, and (iv) statistically significant change in the corrosion parameter. These criteria were adopted based on the researchers experience and understanding of the definition of Cl_{th}.

Table 2.4 Review of approaches detecting corrosion initiation from literature

Initiation Criteria	Author
Significant weight loss from certain exposure time	Thomas, 1996
Fixed OCP ($E_{corr} < -350$ mV Vs. CSE)	ASTM C876; Song et al., 2008; Izquierdo et al., 2004; Pacheco and Polder, 2016
Fixed charge passed (Q > 150 Coulombs)	ASTM G109
Fixed polarisation resistance ($R_p < 10,000$ $\Omega.cm^2$)	Law et al. (2004)
Fixed current density ($i_{corr} > 0.1$ $\mu A/cm^2$)	Soleymani and Ismail, 2004; Andrade and Alonso, 1996; RILEM TC 154-EMC
Sudden increase/decrease in corrosion parameter (OCP, R_p/i_{corr}, Current required for maintaining potentiostatic control)	RILEM TC-235; Angst et al., 2011; Lollini et al., 2016; Boubitsas and Tang, 2013
Statistically significant change in the corrosion parameter	Trejo and Pillai, 2003; Karuppanasamy and Pillai, 2017

Figure 2.14 shows the different initiation points adopted in literature and their possible influences on Cl_{th} estimation. The initiation time (t_1) indicates the specimen achieving corrosion current density of 0.1 μA/cm^2. The time (t_2) corresponds to the statistically significant increase in R_p compared to prior readings. The time (t_3) corresponds to the fixed R_p of 10,000 Ω.cm^2. Clearly, the time taken for each initiation criteria and Cl_{th} values in each case differ leading to wide variability in the reported Cl_{th} values. These different initiation criteria were based on visible corrosion spot observed by the authors in OPC specimens. These criteria may be good for finding the Cl_{th} in concrete with low and moderate resistivity. Nowadays, concretes with high and very high resistivity are being used. Table 2.1 shows the AASHTO T 358 (2017) classification of resistivity based on the chloride ion permeability. In such cases of very high resistivity, the electrochemical response may be different and may not comply with the traditional systems. There are no guidelines to acquire and interpret data from such highly resistive systems, which the present study is focused upon.
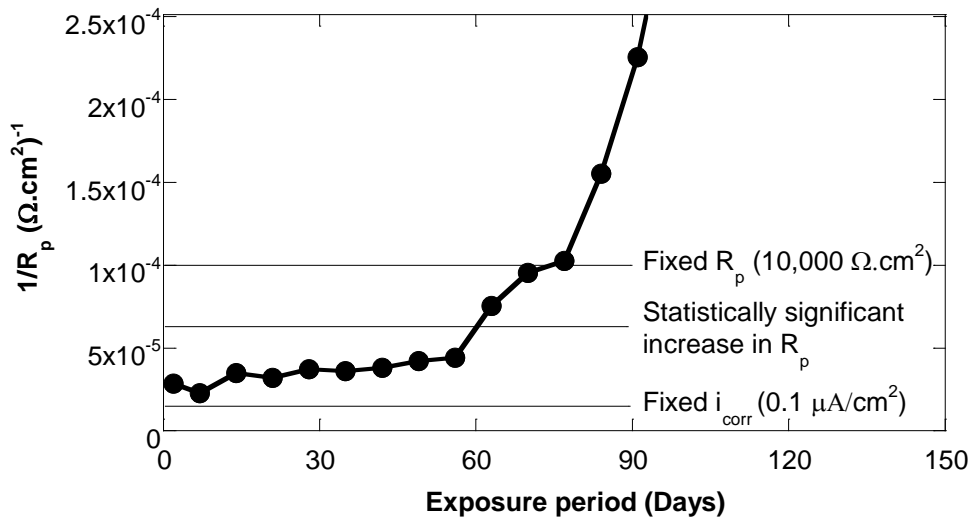
Figure 2.14 Effect of corrosion initiation criteria on Cl_{th}

2.5 SERVICE LIFE ESTIMATION

The service life of any structure depends on the interaction of many factors, which can be broadly categorized into three categories (i) structural, (ii) material, and (iii) environmental aspects. The engineer can manipulate the first two parameters to combat the effects of the third one. Most of the codal provisions emphasize the material specifications such as Cl_{th} and structural specifications such as cover, the grade of concrete etc. for a given exposure condition. However, many failure instances of premature corrosion are reported even though these codes are being followed. To overcome such issues and enhance the service life, various materials such as highly resistive cement/binder, corrosion inhibitors, and coatings for steel and concrete surfaces can be adopted. However, the engineer needs to know the most influencing parameters that affect the service life to choose the preventive measures as well as to cope with the site conditions. For this to happen, the service life estimation tools should be user-friendly and parameters should be easy to evaluate.

2.5.1 Chloride ingress equations

To estimate the service life of structures against chloride-induced corrosion, the ingress of chlorides can be modelled as either pure diffusion or multi-ionic transport (convection, wicking, diffusion etc.) by considering Fick's first law or second law (Marchand and Samson, 2009). Fick's first law is based on diffusion through flux, i.e. concentration gradient and the equation is as follows

$$J = D_{cl} \cdot \frac{\partial \varphi_{cl}}{\partial x} \qquad\qquad 2.1$$

where, J is the flux, D_{cl} is the diffusion coefficient of chlorides in concrete, ϕ_{cl} is the chloride concentration, and x is the depth of penetration. Fick's second law is based on diffusion and is based on a change in concentration with time and is expressed as follows

$$\frac{\partial Cl(x,t)}{\partial t} = D_{cl} \cdot \frac{\partial Cl^2(x,t)}{\partial x^2} \qquad\qquad 2.2$$

where, Cl is the chloride concentration, D_{cl} and x are as in Equation. 2.1 and t is the exposure time or age of the structure.

2.5.2 Available models for chloride ingress

Many software programs and mathematical models are available for calculating the service life of concrete structures. Table 2.5 summarizes the models available and their underlying equations. The chloride ingress is estimated in these models by either simple one-dimensional ingress or two-dimensional using finite difference approach or finite element approach. The definition of chloride concentration calculated from these models varies from one to another. For example, chloride estimation from the error function gives the total chloride content at any given instant at a particular depth whereas ClinConc gives the free chloride concentration. As the models incorporate more and more parameters to achieve realistic results, it becomes very difficult to estimate the service life.

Table 2.5 Available models to predict the chloride ingress

Model Name	Equations
Sqrt-time (de Vera et al., 2017)	$x = D_{cl} \sqrt{t}$; where x-concrete cover; D_{cl} – diffusion co-efficeint; t -time
Error function (de Vera et al., 2017); DuraPGulf (Shekarchi et al., 2008)	$$C(x,t) = C_i + (C_s - C_i).erfc\left(\frac{x}{\sqrt{4D_{cl}t}}\right)$$ where, C_i = initial chloride concentration; C_s-surface chloride concentration; *erfc*- complementary error function
Constant flux (de Vera et al., 2017)	$$C(x,t) = C_i + 2J\sqrt{\frac{t}{\pi D_{cl}}}\exp\left(-\frac{x^2}{4D_{cl}t}\right) - \frac{Jx}{D_{cl}}erfc\left(\frac{x}{\sqrt{(4D_{cl}t)}}\right)$$ where, J- flux;
CHLODIFF (Oslakovic et al., 2010)	$$C(x,t) = [C_i + k(t-1)].erfc\left(\frac{x}{2\sqrt{\tau}}\right) + k\left[(1 + \frac{x^2}{2\tau}).erfc\left(\frac{x}{2\sqrt{\tau}}\right)\right.$$ $$\left. - \frac{x}{\sqrt{\pi\tau}}e^{-\frac{x^2}{4\tau}}\right]$$ where, k- coefficient for accounting linear increase in C_i; $\tau = \int_0^t D_{cl}(s)ds$; factor for temporal variation of D_{cl}
Duracrete (Duracrete, 2000)	$$g = C_{cr}^d - C_{s,cl}^d\, erfc\left(\frac{x^d}{2\sqrt{\frac{t}{R_{cl}^d(t)}}}\right)$$ where, $R_{cl}^d = (D_{cl})^{-1}$; C_{cr}^d-chloride at steel surface; $C_{s,cl}^d$- surface chloride concentration; x^d- concrete cover
ClinConc (Tang, 2008)	$$\frac{C - C_i}{C_s - C_i} = erf\left(\frac{x}{2\sqrt{\frac{K_D D_{cl}}{1-m}.\left(\frac{t_{ref}}{t}\right)^m.\left[\left(1 + \frac{t_{ref}}{t}\right)^{1-m} - \left(\frac{t_{ref}}{t}\right)^{1-m}\right].t}}\right)$$
LightCon (Sun et al., 2010)	$$t_{SL} = t_{ref}\left(\frac{x}{2.erfc^{-1}\left(\frac{C_{cr} - C_i}{C_s - C_i}\right).\sqrt{t_{ref}\, D_{cl,ref}}}\right)^{\left(\frac{2}{1-\ln\left(\frac{D_{cl}/D_{cl,ref}}{t_{ref}/t}\right)}\right)}$$ where, t_{SL}- estimated service life; $C_{cr} - Cl_{th}$

Table 2.6 shows some of the models with their features and limitations. The suitability of the service life models depends on the location and the condition of the structures. Even after developing so many models, there exists uncertainty between the laboratory and the field

exposure conditions. This uncertainty is due to challenges in obtaining realistic input parameters, poor understanding of the corrosion mechanisms, and not considering the local microclimatic conditions of the steel and size effect (Angst, 2019). Unless these challenges are addressed, refining the models based on the input parameters affect the prediction marginally and may not reflect the service life of structures in the field conditions.

Table 2.6 Comparison of the models/tools available for estimation of service life

Models/Tools	Features	Limitations
Square root of time	Simple and easy to calculate	Many influencing parameters are not considered
Life 365[TM]	• Simple and easy to use • Finite difference approach	• Limitations in the value of certain input parameters (m) • No probabilistic consideration of input parameters • The effect of chloride binding is not considered • Deterministic approach
Duracrete	Probabilistic performance based durability design of concrete structures	• The effect of chloride binding is not considered • The effect of corrosion inhibitor is not considered • Higher complexity due to many input parameters • Empirical model
Clinconc	• Finite difference approach • Multi-ionic transport • Chloride binding is considered • The corrosion initiation is mainly due to the free chlorides • Treats materials and environment separately	Modeled for submerged structures
Chlodiff	Developed for new structures for which no data is available	Unrealistic longer estimation of service life

2.5.3   Input parameters

All the service life models from simple models like SQRT (time), error function, constant flux to more complex models like Life-365^{TM}, CHLODIFF, Duracrete, ClinConc, etc. consider diffusion coefficient (D_{cl}), chloride threshold (Cl_{th}), and cover depth (d). The secondary parameters such as ageing coefficient (m), surface chloride concentration (Cl_s) also influence the estimation of service life.

2.5.3.1 Cover depth (*d*)

Cover depth is one of the most influencing parameters, which governs the service life irrespective of the models used. Standards such as IS 456(2000) recommend minimum cover depth, w/b, and strength class depending on the exposure conditions of the structure for ensuring durability. Increasing the cover is not recommended beyond certain limits due to the structural aspects and cracking tendency. The quality of concrete cover should be ensured at the site by proper compaction during placement and adequate curing.
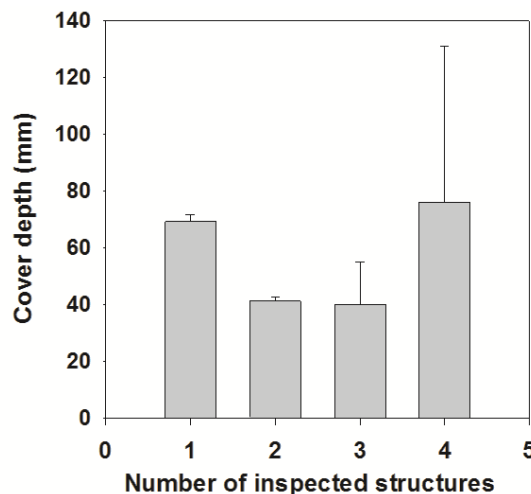
Figure 2.15 Variation of cover depth observed in field structures

Figure 2.15 shows the variation observed in the cover depth of field structures (Polder and Rooij, 2005, Sagues et al., 2001). This illustrates that the variation in cover depth can range from zero to 100% from the design cover depth depending on the quality control at site.

Therefore, cover depth should be considered with standard deviation instead of a single value. Also, it is not enough to have physical cover to ensure the durability of the structure. To get the advantage of the cover, major emphasis is in terms of the choice of the binder and w/b that influences the D_{cl}.

2.5.3.2 Diffusion coefficient (D_{cl})

The rate at which the chloride ingress occurs through the cover concrete by means of diffusion is denoted as D_{cl}. The service life models use D_{cl} to estimate the duration at which the corrosion initiation occurs i.e. the end of the corrosion-free service life. Figure 2.16 shows the spread of D_{cl} obtained from various concrete (Note: 70 references for 100 data points in Figure 2.16 are given as a list at the end of the REFERENCES section). The D_{cl} depends on the type of binder, w/b, compaction and curing. For practical purposes, D_{cl} can be considered to be in range between 1×10^{-12} and 1×10^{-10} for estimation of service life.
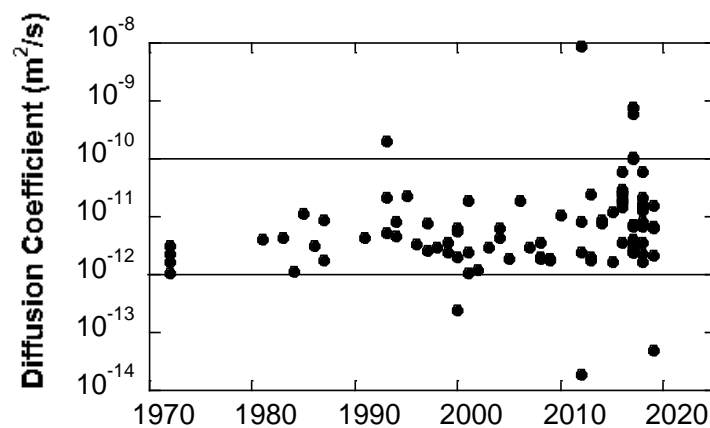
Figure 2.16 Chloride diffusion coefficient values reported in literature.
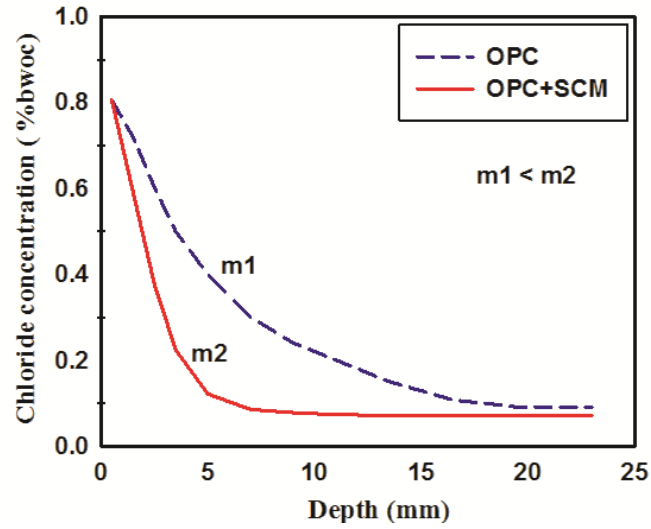
Figure 2.17 Change in diffusion coefficient profile of concretes with and without SCM

Figure 2.17 shows the typical diffusion coefficient profile of concrete with and without SCMs. It is well established that D_{cl} decreases with the age of concrete. It is evident from Figure 2.17 that the addition of SCM in concrete can decrease the D_{cl}. Table 2.7 summarizes the equations used in different models for the calculation of D_{cl}. For example, Life-365^{TM} considers D_{cl} as a function of time and temperature. CHLODIFF considers D_{cl} as a function of w/c, admixtures, temperature, the presence of a crack, curing condition, and wind direction. ClinConc considers D_{cl} as a function of time, temperature, chloride binding, alkalinity, factor compensating for field condition, leaching etc. Since D_{cl} based on bulk diffusion tests are time-consuming, Duracrete offers equation which converts the migration coefficient (based on NT BUILD 492) to diffusion coefficient. These equations of D_{cl} are based on either empirical formulations or physical phenomena. As the sophistication of models increases, the calculation of D_{cl} becomes close to reality but more complex to calculate. The present work uses the simple calculation of D_{cl} based on time alone.

54

Table 2.7 Summary of different approaches for calculation of D_{cl}

Models	Equations for diffusion coefficient
Time dependent (de Vera et al., 2017)	$$D_{cl}(t) = D_{ref} \left(\frac{t_{ref}}{t}\right)^m$$
	where, D_{ref} - D_{cl} at reference time; t_{ref} (usually, 28 days); $D_{cl}(t)$ – D_{cl} at any time instant, t
Life-365™ (Life–365, 2012).	$$D_{cl}(t,T) = D_{ref} \left(\frac{t_{ref}}{t}\right)^m e^{\frac{U}{R}\left(\frac{1}{T_{ref}} - \frac{1}{T}\right)}$$
	$$D_{ref} = 10^{-12.06 + 2.4(w/c)} \cdot e^{-0.165 \cdot SF}$$
	where, U- activation energy of the diffusion process; R-gas constant; $T_{ref} = 293K$; T-absolute temperature; w/c- water to cement ratio; SF - % of silica fume (valid upto 15%)
ClinConc (Tang, 2008)	$$D_{cl} = \frac{(0.8a_t^2 - 2a_t + 2.5)\left(1 + 0.59K_{b,ref}\right) \cdot k_{TD}}{1 + k_{OH,ref} \cdot K_{b,ref} \cdot k_{Tb} \cdot f_b \cdot \beta_b \cdot \left(\frac{C_s}{35.45}\right)^{\beta_b - 1}} \cdot D_{ref}$$
	where, a_t - time–dependent factor for chloride binding; $K_{b,ref}$ – binding factor found at t_{ref}; f_b and β_b – chloride binding constants; k_{OH} - factor for alkalinity; k_{TD} and k_{Tb} are the temperature factors for D_{cl} and chloride binding
CHLODIF (Oslakovic et al., 2010)	$$D_{cl} = D_{\frac{w}{c}} \cdot f_{int}(CIAs, SCMs, SPs, curing, crack) \cdot f_{ext}(t, T, RH, W_s, C_s)$$
	$$D_{cl} = 5 \times 10^{-13} \cdot e^{4.8708(w/c)} \cdot f_{int} \cdot \left[1 + 256\left(1 - \frac{RH}{100}\right)^4\right]^{-1} \cdot t^{-m}$$
	where, CIA – Corrosion inhibiting admixtures, SCMs- supplementary cementitious materials; SPs- Super plasticizers, RH- relative humidity; W_s- wing influence
DuraPGulf (Shekarchi et al., 2008)	$$D_{cl} = D_{cl,ref}\left(\frac{t_{ref}}{t}\right)^m \cdot \exp\left[\frac{U}{R} \times \left(\frac{1}{T_{ref}} - \frac{1}{T}\right)\right] \cdot \left[1 + 256\left(1 - \frac{RH}{100}\right)^4\right]^{-1}$$
Duracrete (Duracrete, 2000)	$$D_{cl} = k_e \cdot k_c \cdot D_{RCM} \cdot \left(\frac{t_{ref}}{t}\right)^m$$
	where, k_e – environmental factor; k_c – curing factor; D_{RCM} - D_{cl} from migration tests

2.5.3.3 Ageing coefficient (*m*)

D_{cl} decreases over a period of time due to the prolonged hydration and such effect is more prominent in the cases of blended cement and in structures where moisture is continuously available. (Al-Alaily and Hassan, 2016). Life-365™ estimates *m* based on the Equation 2.3

$$m = 0.2 + 0.4 \left(\frac{\%FA}{50} + \frac{\%SG}{70} \right) \leq 0.6 \qquad\qquad 2.3$$

where FA and SG are fly ash and slag respectively. Here ageing factor for other SCMs is not considered. Also, experimental values of *m* based on electrical resistivity were reported to be higher than the estimated value of *m* from Life-365™. Clinconc defines *m* as follows

$$m = -0.45a_t^2 + 0.66a_t + 0.02 \qquad\qquad 2.4$$

To find m experimentally, two approaches are proposed. In the first approach, the determination of D_{cl} from specimens subjected to prolonged exposure is done. Then, regression analysis is done to determine *m*. In the second approach, indirect methods based on electrical conductivity of concrete are used. Andrade et al. (2011) proposed the following equation to find the electrical conductivity of concrete

$$\sigma_t = \sigma_{ref} \left(\frac{t_{ref}}{t} \right)^m \qquad\qquad 2.5$$

where, σ_t and σ_{ref} are the electrical conductivities at exposure time t, and reference time t_{ref} (e.g., 28 days). Values of m-for concrete vary depending on the type of binder and w/b, which is summarized in Table 2.8.

Table 2.8 Ageing coefficient of different binders reported in the literature

Binder	m	Reference
OPC	0.2-0.4	Stanish and Thomas, 2003; Ferreira et al., 2016
OPC+10-20% Fly ash (FA)	0.40	Markeset and Skjølsvold, 2010
OPC+30% FA	0.55	Pillai et al., 2018
OPC+35% FA	0.52	Markeset and Skjølsvold, 2010
OPC+>50% FA	0.7	Stanish and Thomas, 2003
OPC+ Upto 10% Silica fume (SF) +20 % FA	0.46	Markeset and Skjølsvold, 2010
OPC+8-10% SF	0.38	
OPC+20% SF	0.43	
OPC+20% Slag	0.32	Park et al, 2016
OPC+40% Slag	0.52	
OPC+60% Slag	0.7	
OPC+70% Slag	1.2	Markeset and Skjølsvold, 2010
OPC+25% Metakaolin (MK)	0.55	Ferreira et al., 2016
LC3	0.5	Pillai et al., 2018
Sulphate resisting portland cement (SRPC)	0.3	Tang and Gullikers, 2007
SRPC+20% FA	0.69	

2.5.3.4 Chloride threshold (Cl_{th})

As reported earlier in Subsection 2.3, since there are no standard test methods and guidelines available, huge scatter in the reported Cl_{th} values is observed. The service life estimation depends on this Cl_{th} value and hence, the estimated number of years also is subjected to

variation. Realistic estimation of Cl_{th} is crucial for service life estimation, which is the focus of this work.

2.5.3.5 Surface chloride concentration (Cl_s)

Since chloride ingress is based on the concentration gradient, the chloride concentration at the outer surface of the cover (Cl_s) is an important parameter to consider apart from d, D_{cl} and Cl_{th}. This concentration depends mainly on the location of the structure and quality of the concrete mix (binder, w/c). Figure 2.18 gives the maximum surface chloride concentration and its build-up rate based on the exposure conditions given by Life-365^{TM}. This classification is very helpful to the engineer to account for the surface chlorides, which other models lack to consider and prior knowledge is required for the input values. Alternatively, this value can also be found from field structures considering the age and exposure conditions of the structure.

k = Buildup rate of chlorides on the concrete surface
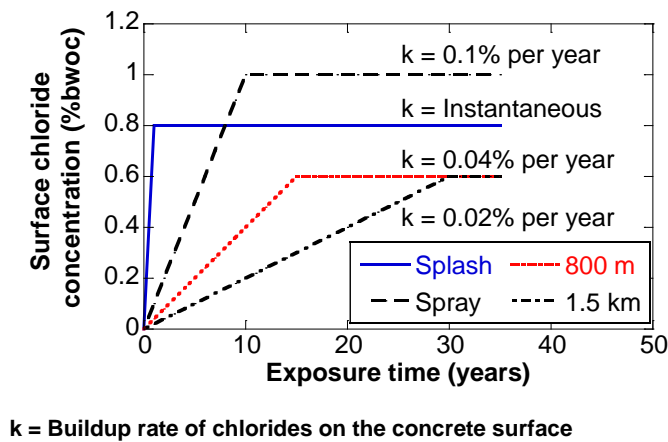
Figure 2.18 Surface chloride concentration profile (Life-365^{TM})

Other factors such as cross-section, the location of the structure (windward side/ leeward side) also influence the service life. In summary, when the models consider more sophisticated equations for estimating the chloride ingress, it becomes more complex and is not user-friendly. Also, as number of parameters exist, there arises the question of influencing parameters and discrepancy among the researchers.

2.5.4 Sensitivity analysis

Since the initiation phase is dependent on the amount of chlorides available at the interface, this phase is modelled using different chloride ingress models by various researchers. This leads to so many input parameters and how to get those parameters and their importance are not clear. In addition, the sensitivity analysis of the input parameters leads to more confusion due to ambiguity in the order of influence reported. Table 2.9 shows the result of the sensitivity analyses of influencing parameters on service life showing significant discrepancies. The evolution of material characteristics with time is not considered in many of the models while doing sensitivity analysis. Also, the interaction of these variables in the service life is not discussed much in literature. There is a need to understand the parameters, its interaction, and its impact on the estimated service life.

Table 2.9 Ranking of parameters influencing service life

Ranking of parameters	Reference
$d > Cl_{th} > Cl_s > t$	Prezzi et al., 1996
$m > d > D_{cl} > Cl_{th} > Cl_s$ (w/b = 0.5)	Pettersson and Norberg, 2000
$d > m > D_{cl} > Cl_{th} > Cl_s$ (w/b = 0.7)	
$D_{cl} > d$	Kirkpatrick et al., 2002
$d > D_{cl}$ & $Cl_{th} > Cl_s$	Khatri and Sirivivatnanon, 2004
$d > m > D_{cl} > t_i > Cl_{th} > Cl_s$	Ferreira, 2007
$d > D_{cl} > Cl_{th}$	Trejo and Reinschmidt, 2007
$Cl_{th} > Cl_s > D_{cl}$	Zhang et al., 2011

Note: a > b indicates "a" influences more than "b".

SUMMARY OF THE KNOWLEDGE GAP

In sum, the reliability of service life estimation lies in the input parameters used for its calculation. Literature reports a wide range of Cl_{th} and it is often difficult to choose one for service life estimation. This is mainly because of the lack of demarcation of Cl_{th} based on the materials and exposure conditions. In addition to the materials and the exposure conditions, the testing methods play a significant role in the determination of the Cl_{th}. The testing methods which are prevalent in practice are designed based on the assumption that the concrete is of low resistivity and its resistance is neglected. However, with the usage of SCMs, the resistivity can be significant enough to mask the ongoing active corrosion. Also, the electrochemical measurements obtained from a testing method depends on the corrosion cell configuration. Hence, the corrosion cell, testing technique, and its input parameters should be chosen effectively to account for the resistivity of the concrete in order to obtain realistic values of chloride threshold. There is a need for a test method to determine the Cl_{th} of steel in short term when highly resistive binders are used. The present work focuses on the development of a test method to determine the Cl_{th} of steel in highly resistive binder systems.

The Cl_{th} of highly resistive concretes with SCMs is lower due to reduced pH and pH buffering capacity. Several codes restrict the materials based on their Cl_{th} value. It is to be noted that SCMs in concrete can impart very high resistance against the ingress of chloride ions and delay the onset of corrosion in spite of lower Cl_{th}. Therefore, to choose the materials for durable concrete structures, engineers need to estimate the service life of structures with these material properties. However, the service life estimation is more complicated due to the number of parameters involved. There are no clear guidelines of material parameters based on their sensitivity towards enhancing the service life of structures. There are no readymade user-friendly tools available for them to have a quick estimation for materials selection. Thus, this

work focuses on developing a user-friendly nomogram for service life estimation with a study of the sensitivity of input parameters.

CHAPTER 3

EXPERIMENTAL PROGRAM

3.1 INTRODUCTION

This chapter explains the materials and methodology adopted. The materials are discussed in detail first followed by methodology. The methodology section is explained in four sub-sections with one objective each in detail.

3.2 MATERIALS

The various materials used for the specimen preparation and data acquisition are described in detail in this section.

3.2.1 Binder

Three types of binders namely, ordinary portland cement of 53 grade (OPC) confirming to IS 269: 2015, PFA (70%, OPC and 30% Class F fly ash), and Limestone Calcined Clay Cement (LC3) [50% clinker, 30% calcined clay, 15% limestone and 5% gypsum] were used for the study. Class F fly ash sourced from North Chennai thermal plant (as received) was used for the study. Industrial trial production of LC3 cement, which is yet to be commercialized was used for this study. Table 3.1 gives the physical properties of the binders used and Table 3.2 gives their oxide composition

Table 3.1 Physical properties of binders

Binders and mineral admixtures	Specific Gravity	Specific surface area (m^2/kg)
OPC	3.18	320
LC3	3.01	520
Class F fly ash	2.49	330

Table 3.2 Oxide composition of the binders used

Oxides	Concentration (%)				
	OPC	LC3			Class F fly ash
		Clinker	Calcined Clay	Limestone	
Al_2O_3	4.17	5.24	24.95	1.74	29.95
CaO	64.59	63.81	0.09	48.54	1.28
Fe_2O_3	3.89	3.41	5.08	1.62	4.32
K_2O	0.59	0.19	0.21	0.13	1.44
MgO	0.88	3.06	0.19	0.467	0.61
Na_2O	0.16	0.32	0.05	-	0.16
SiO_2	19.01	21.12	58.43	10.07	59.32
SO_3	1.7	0.63	-	0.01	0.16
TiO_2	0.23	-	0.10	1.41	0.206
LOI	1.4	0.98	9.58	37.09	-

3.2.2 Steel

The property of steel specimens plays a key role in the initiation time for corrosion. Hence, the TMT steel specimens were tested for proper martensitic ring formation using Nital solution (Nair, 2017). Tata tiscon brand was found to be good for smaller and bigger diameter and the same brand was used throughout this study. An 8 mm steel rebar for mortar specimens and 16 mm rebar for concrete specimens were used. The steel rebar was cleaned in ultrasonic cleaner using ethanol reagent before using it in concrete/mortar.

3.2.3 Aggregate

To have the repeatability in the procedure, all mortar samples were cast with standard IS 650 sand (Fine aggregate). Grade 2 (500 µ – 1 mm size) and Grade 3 sand (90 – 500 µ size) were used for mortar study. These grades were fixed in equal proportion after trying with different w/b for uniform flow without segregation in the flow table test. The cement to sand ratio was 1:2.75 as per ASTM C109. River sand (passing through 4.75 mm) confirming to (IS: 383 -

1970) was used for concrete studies. Coarse aggregate (Granite) of 10 mm and 20 mm confirming to (IS: 383 - 1970) was used for concrete studies.

3.2.4 Water and Superplasticizer

Distilled water was used for mortar specimens and tap water was used for concrete specimens. In addition to water, to achieve the desired workability, Polycarboxylate ether (PCE) based superplasticizer (Master-Gelenium Sky 8223) was used for the study wherever required. It had a solid content of 33% and density 1080 kg/m^3. The pH and specific gravity were 6.0 and 1.08, respectively.

3.2.5 Electrodes

For all the experiments involving counter electrode (CE), Nichrome mesh was chosen as CE. It had good corrosion resistance properties and was stable in the alkaline chloride rich environment. All the experiments made use of Saturated Calomel Electrode (SCE) as the reference electrode. The reference electrode was stored in the bottle of saturated KCl at constant room temperature (25 °C) to avoid fluctutations during the repeated experiments.

3.3 METHODOLOGY

The main focus of this study is to acquire and interpret the electrochemical response of highly resistive systems to estimate the Cl_{th} and service life. Based on this, the experimental program has been designed, which is given in Figure 3.1 [Note: Figure 3.1 is the reproduction of Figure 1.1 for the convenience of the reader].
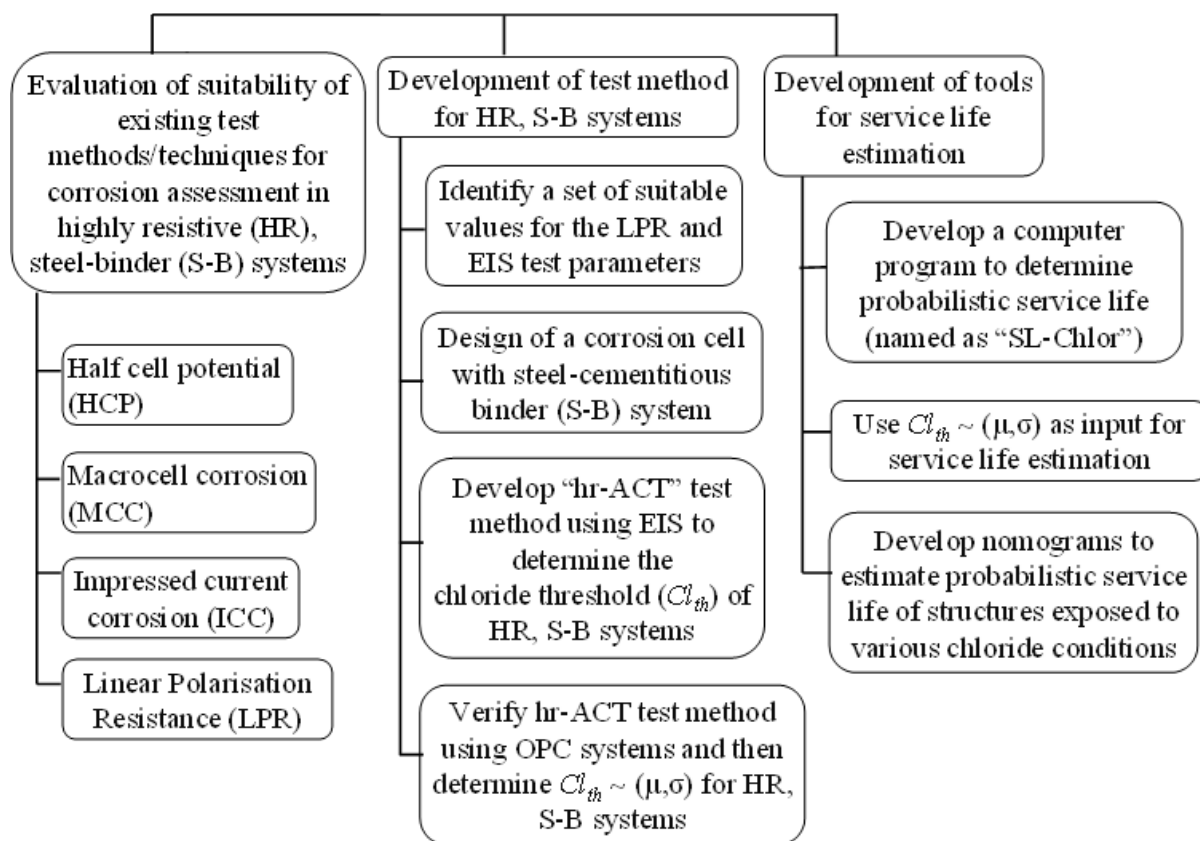
Figure 3.1 Experimental program (reproduced from Figure 1.1)

3.4 PROGRAM 1 ─ EVALUATION OF THE SUITABILITY OF EXISTING TECHNIQUES FOR HIGHLY RESISTIVE SYSTEMS

This objective focuses on widely used existing test methods and evaluates their suitability for testing highly resistive S-B systems. First, a standard test method ASTM G109 was evaluated to understand its suitability for acquiring data from advanced S-B systems. Since the time taken for G109 test method was longer, to quickly assess the corrosion performance of LC3, impressed current corrosion test was also conducted. Then, a short-term test method based on LPR technique was also evaluated for its feasibility to assess the corrosion rate in highly resistive systems. The methodology adopted and materials used are discussed in detail for each test.

3.4.1 Macrocell corrosion

The suitability of the test method for evaluating the performance of solid steel rebars in the highly resistive cementitious matrix is assessed. The comparison of open circuit potential and cumulative current in low resistive and the high resistive cementitious matrix is done.

3.4.1.1 Specimen preparation

Figure 3.2 shows the specimen design adopted as per the standard ASTM G109. Three binders, namely OPC, PFA and LC3 and 16 mm TMT steel were taken for study. The M25 concrete mix was taken for the study. Table 3.3 shows the mix design of the concrete used. The size of the coarse aggregate was restricted to 10 mm to have a reduced cover depth of 19 mm as per the standard. Six specimens were cast for each combination.
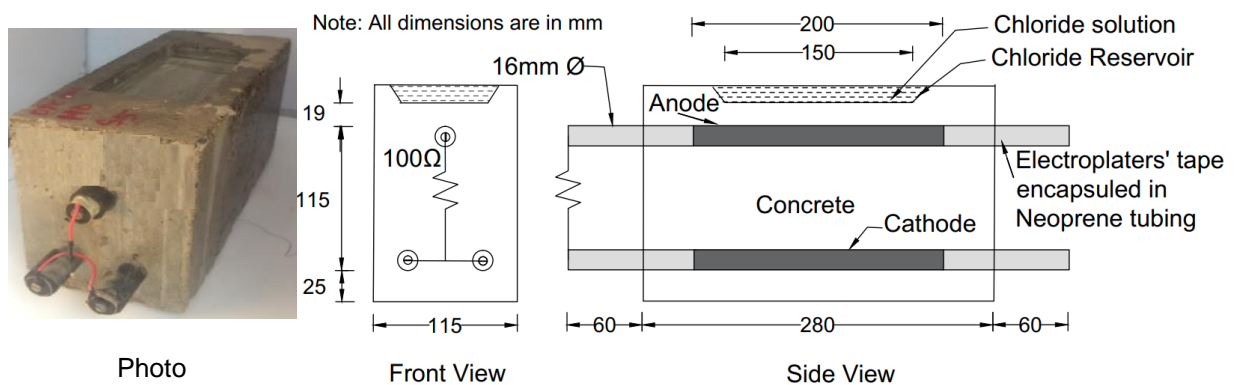
Figure 3.2 Macrocell corrosion test specimen and its schematic diagram

Table 3.3 Mix design used for ASTM G109 specimen

Ingredients	Quantity (kg/m³ of concrete)
Binder	360
w/b	0.5
Fine aggregate	877
Coarse aggregate	954

As shown in Figure 3.3, TMT/QST steel pieces of 16 mm diameter were used for this study. The steel pieces of 360 mm length were cut using a chop saw with an abrasive cutting blade. The surface of the rebar was cleaned using ethanol in an ultrasonic cleaner as shown in the Figure 3.3 and wiped clean using a cloth. The 200 mm long portion at the center of the steel rebar piece was exposed and the rest were covered with electroplaters tape and neoprene tubing. The ASTM G109 specimens were cast using the prepared steel rebar pieces and cured for 28 days after casting. A 100 Ω resistor is connected between the top and bottom bar with the help of a 4 mm screw.

(a) Cleaning in ultrasonic cleaner

(b) Cleaned specimens

(c) Ends wrapped with electroplaters tape

(d) Neoprene tubing protection over the tape
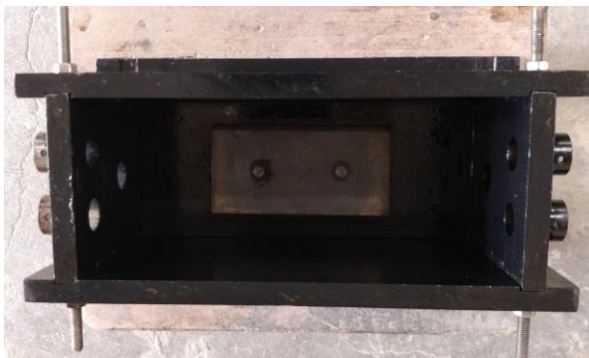
(e) Mould with provisions for dam
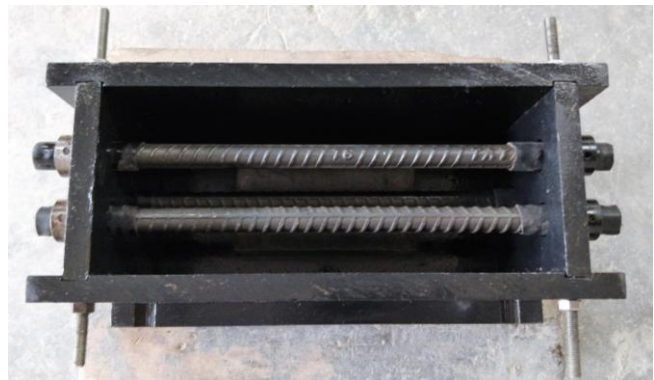
(f) Mould with steel rebars ready for casting

Figure 3.3 Step-by-step procedure shown for casting ASTM G109 test specimen

3.4.1.2 Chloride exposure and corrosion monitoring

The specimens were subjected to cyclic wet-dry exposure (14 days of ponding followed by 14 days of drying) using 3% sodium chloride solution. Figure 3.4 shows the arrangement for measurement of HCP and I_{corr} in ASTM G109 specimens. The voltage across the 100 Ω resistor (i.e., in Circuit 1 - between the top and bottom rebars) was measured using a 5.5 digit precision multimeter at the 7th day of wetting in each cycle. This was used to calculate the I_{corr}, average in Circuit 1. The End of Testing (EoT) was defined as the time when I_{corr}, average attains 150 Coulombs (as per the ASTM G109). In addition, half-cell potential of the top rebar was monitored as per ASTM C876 with respect to saturated calomel electrode (SCE). The time to corrosion was calculated as per ASTM G109 standard. At the end of exposure/testing, all the specimens were autopsied and the anode rebars were visually observed for corrosion spots.
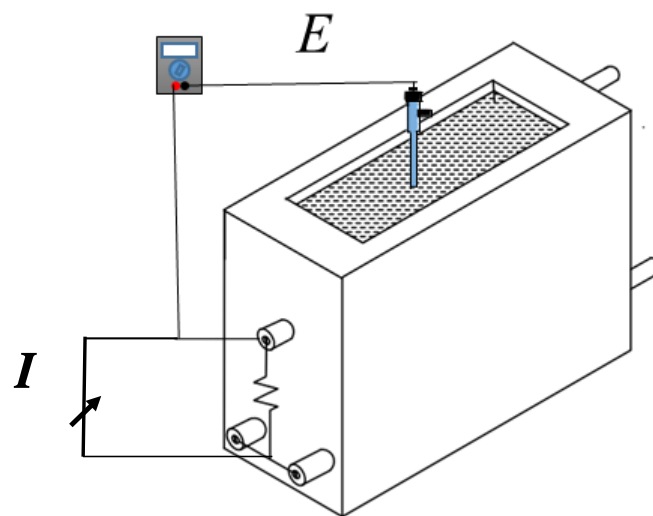
Figure 3.4 Set-up for HCP and I_{corr} tests in ASTM G109 specimen

3.4.2   Impressed current corrosion test method

The experimental design evaluates the ability of this test method to assess the corrosion rate of steel embedded in three binder types (OPC, PFA, and LC3 systems) in severe corrosive exposure conditions simulating the field conditions. Table 3.4 provides the mix design adopted

for this study. The slump during concreting was maintained between 80 and 120 mm. Two grades of concrete M35 and M50 were designed for each binder type. 100 mm cubes were used for determining the compressive strength and 150 x 300 mm cylinder was used for split tensile strength for each grade of concrete. The specimens were categorized into three groups (T1, T2 and T3) as shown in Table 3.4. A total of 60 specimens with five replicas for each combination of binder and concrete grade were cast. In the first group T1, all the three types of binders, namely OPC, PFA, and LC3 systems in two grades M35 and M50 were studied. When the OPC specimen cracked, the companion specimens of PFA and LC3 were also taken out from testing. In the second group T2, only the PFA and LC3 specimens of M35 and M50 grade were taken for testing. When the PFA specimen cracked, the LC3 companion specimen was taken out from testing. For the third group, T3, the LC3 specimens were tested till the specimen cracked or 500 hours of potential application, whichever was earlier.

Table 3.4 Mix design and experimental program of ICC test method

Materials		**M35**			**M50**		
Binder type		OPC	PFA	LC^3	OPC	PFA	LC^3
Binder content (kg/m^3)		310	360	310	360	380	440
Fine aggregate (kg/m^3)		695	721	770	703	699	711
Coarse aggregate (kg/m^3)	10 mm	496	463	501	477	475	462
	20 mm	744	694	751	716	713	694
w/b		0.5	0.45	0.45	0.4	0.35	0.35
Number of ICC specimens	T1 group	5	5	5	5	5	5
	T2 group	-	5	5	-	5	5
	T3 group	-	-	5	-	-	5

3.4.2.1 <u>Specimen design</u>

Figure 3.5 shows the schematic diagram and the actual photograph of the impressed current corrosion (ICC) test set-up. Each ICC test specimen consisted of a concrete cylinder (200 mm long x 100 mm diameter) with a 16 mm diameter TMT rebar (100 mm long) embedded at the centre. The end cover of 50 mm was maintained, which ensured the failure (crack) through the sides (42 mm side cover). The rebar was cleaned in an ultrasonic cleaner with ethanol as a reagent. A 4 mm stainless steel rod was inserted in the thread given at the centre of the rebar. To avoid the connection edge from galvanic corrosion, a heat shrink tube was put till 50 mm of stainless steel rod as shown in Figure 3.5(a). From the preliminary study (Appendix A), it was found that the longer application of voltage led to corrosion of stainless steel and heating of the specimen, which resulted in loss of connection to the specimen. To ensure the isolation of the stainless steel rod, the epoxy coating was also done on top of the heat shrink tube and the edge of the steel rebar facing the heat shrink tube. For more details, see Appendix A. Hence the specimen was redesigned for cover and application of potential. Specimens were cured for 28 days before testing.
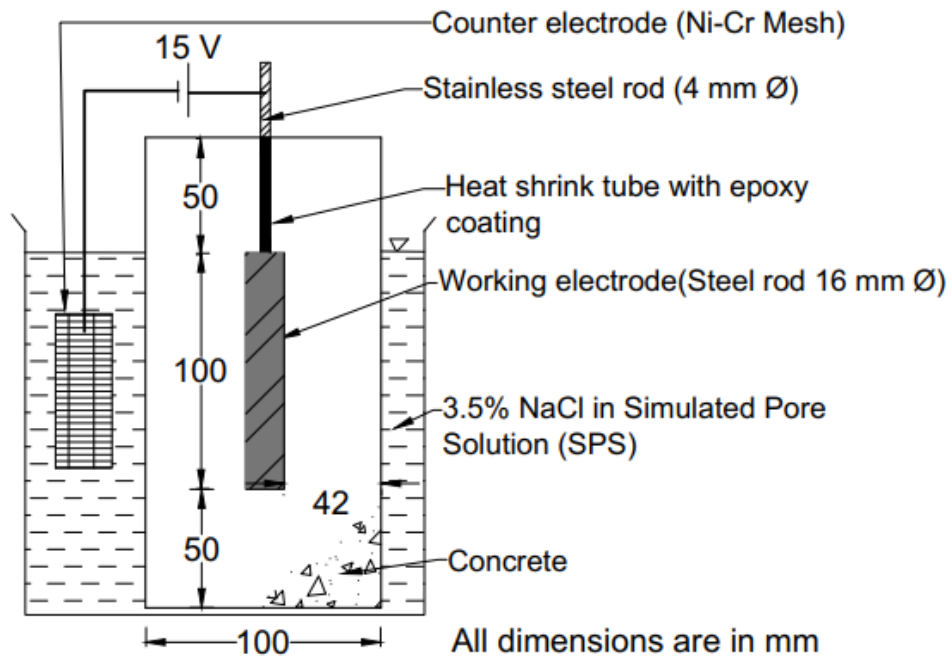
(a)

(b)

Figure 3.5 Test set-up of ICC specimen (a) Schematic and (b) photo

3.4.2.2 <u>Testing methodology</u>

Specimens were submerged in Simulated Pore Solution (SPS) (One litre of SPS composed of 10.4 g of NaOH, 23.2 g of KOH, 0.3 g of $Ca(OH)_2$ and 966 g of distilled water (Alapati, 2014)) with 3.5% NaCl after curing. The rebar in the specimen was connected to the positive terminal of the DC power supply system. A nickel chromium mesh placed in the electrolyte was connected to the negative terminal. An external potential gradient of 15 V was applied for 10 hours a day until failure (visible crack) occurred. The potential application was restricted to 10 hours to avoid the microstructural changes that can occur due to prolonged exposure (heating of concrete) in high resistive concrete as described in Appendix B. The corrosion current was measured (across a shunt) every 4 hours during the application of the potential. The T_{crack} is defined as the duration, at which visible (using naked eyes) crack was observed. The T1 specimens with OPC, PFA and LC3 binders were autopsied to study the microstructural characterisation of their interface.

3.4.2.3 <u>Microstructure characterisation of S-B interface</u>

a) Visual observation

The visual observation of rust was done for all the specimens just after splitting. In the case of the ICC test method, the cracked concrete specimens were split into halves by the split tensile strength test method and the steel rebars were taken out. The visual observation was followed by the oxide composition analysis within ten minutes of the autopsy.

b) Composition of corrosion products

After the potential application, the oxide composition of the rust in three different types of concrete was characterised by Raman spectra. Raman spectroscopy is very popular due to the acquisition of data by non-contact and non-destructive methodology. T_{crack}. Monochromatic light with a wavelength of 488 nm^{-1} and 600 gratings was used to acquire the spectra using Horiba Jobin Yvon HR 800 UV instrument. This spectrum serves as a fingerprint for the

particular substance. Raman spectra are based on the vibrational spectroscopic technique in which the sample scatters the incident light depending on the molecular vibration and crystal structure. Before taking the spectrum, the instrument was calibrated with silicon. The spectra obtained was compared with literature for the specific peaks to identify the oxide phases. The spots of severe rust at the concrete interface were identified for each of the binder types. The laser was focused on the rust spots by keeping the specimen on the platform directly below the lens to generate the spectra. In the case of LC3 specimens, since there was no visible rust accumulation at the concrete surface due to low corrosion rate, the rusted steel specimen was taken directly for oxide analysis immediately after splitting. These results were compared with the results obtained from specimens subjected to chlorides in a wet-dry cycle. All the ICC steel specimens were cleaned in ASTM G1 solution and visually observed for corrosion pits.

c) Porosity at the steel-binder interface

As severe corrosion was expected for the ICC specimens, the porosity at the S-B interface was studied to understand the porosity induced due to buffering of $Ca(OH)_2$. The porosity was characterised with the help of mercury intrusion porosimetry (MIP). MIP was done using Thermo Scientific, Pascal 140–440 porosimeter instrument. This instrument can measure pore sizes ranging from 100 to 0.003 μm. The portion of the broken specimen, which had the impression of the steel was taken. The concrete chunks without larger aggregates from three different locations of the 100 mm long S-B interface (i.e. top, middle and bottom) were collected. The mass of the sample was maintained constant for all the three classes of concrete, namely OPC, PFA and LC3. The M35 grade of concrete was studied to understand the porosity of the interface using MIP.

3.4.3 Linear polarisation resistance (LPR)

Based on the learnings from sub-objective 1 and 2, the specimen design was modified as follows

1. A lollipop type specimen with a single rebar was designed to assess the Cl_{th}

2. Since Cl_{th} is an S-B interface property, which is not significantly influenced by aggregate, mortar instead of concrete was used so that the results could be obtained in a few months.

3.4.3.1 <u>Determination of corrosion rate</u>

The corrosion rate of the TMT rebar embedded in three binders, namely OPC, PFA and LC3 was assessed with three levels of admixed chlorides (0%, 5% and 10% NaCl). The lollipop specimen was prepared using 8 mm diameter and 250 mm long TMT bar. The bars were cleaned using isopropanol to remove any rust on the surface. The bars were exposed 50 mm near the bottom and the rest were coated with two thin layers of low viscosity epoxy (Sikadur-52 UF). The prepared steel pieces were embedded in 110 mm long cylindrical mortar (water: cement: sand ratio - 0.5:1:2.75) and 10 mm cover. Due to alkalinity of the system and ageing of epoxy, crevice corrosion occurred in the non-exposure regions. This led to noise in the LPR data and the testing was discarded. The details of the test method and the results are discussed in the Appendix B. Due to the failure of the lollipop specimen, for determination of Cl_{th}, the lollipop was redesigned, which is explained in the next section.

3.4.3.2 <u>Determination of Cl_{th}</u>

A comprehensive experimental program was designed to estimate the Cl_{th} of TMT rebar embedded in three binders, namely OPC, PFA and LC3. The specimen was modified as shown in Figure 3.6 to eliminate the crevice corrosion due to epoxy degradation. The steel specimens were prepared using 8 mm diameter and 70 mm long TMT bar. The bars were cleaned using ethanol to remove any rust on the surface. The prepared steel pieces were embedded in 110

mm long cylindrical mortar (water: binder: sand ratio - 0.5:1:2.75) and 10 mm cover. The test specimens were cured in a laboratory environment (25°C and 65% RH approximately) for 24±1 hours. After this, the specimens were immersed/cured in simulated pore solution (SPS) for 7 days. Then, each specimen was coated with epoxy in the outer mortar surface leaving 50 mm in the middle. When the specimen was dried on the surface, it was immersed in SPS+3.5% NaCl solution till 28 days.

(a)   (b)
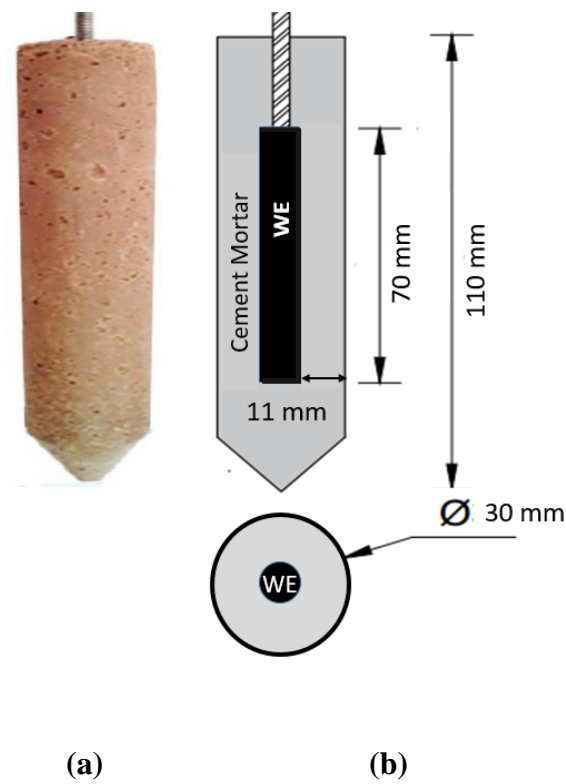
Figure 3.6 Photo and Schematic of the lollipop test specimen

a) Corrosion test set-up

Figure 3.7 shows the test set-up used to conduct the Linear Polarization Resistance (LPR) test consisting of the Solartron 1287 potentiostat, a 3 electrode Corrosion cell set-up (see) with a working electrode (WE), a counter electrode (CE), and a reference electrode (RE). The steel embedded in the lollipop specimen was treated as WE. A 90 mm diameter pipe made of Nichrome wire mesh was used as the CE. The test specimen was placed inside this CE. The saturated calomel electrode (SCE) was used as the RE and placed close to the surface of the mortar with the help of the luggin probe. All the electrodes were placed in a glass beaker with a simulated pore solution (SPS) mixed with 3.5% NaCl. This formed the corrosion cell as shown in Figure 3.7. This corrosion cell set-up was then connected to a potentiostat and computer for recording the readings.

b) Corrosion measurement method

The specimens were subjected to wet-dry cycle (2 days wet and 5 days dry) and electrochemical readings were taken at the end of the wet cycle. At first, the Open Circuit Potential (OCP) of the steel specimen was measured. Immediately after measuring the OCP, the LPR test was conducted using a scan range of ±15 mV with respect to the measured OCP of each specimen. A scan rate of 0.1667 mV/s was used. Failure of the specimen was considered when the polarization resistance value reached 10,000 Ω or a visible corrosion spot (Law et al., 2004).

(a)

(b)

Figure 3.7 (a) LPR test set-up and (b) Corrosion cell

3.5 PROGRAM 2 ─ FACTORS AFFECTING ELECTROCHEMICAL RESPONSE FROM STEEL-BINDER SYSTEMS

Based on the observations in experimental program 1, the lollipop specimen design was slightly changed to ensure uniform cover throughout the length of the rebar. The exposure conditions such as temperature (25°C) and exposure solution (SPS + 3.5% NaCl) and length of the WE (100 mm) were kept constant throughout the test. Standard mortar mix proportion (0.5:1:2.75) with Grade-2 and Grade-3 IS sand in 50:50 was used. Figure 3.8 shows the modified test specimen and the corrosion cell set-up for LPR testing. It was decided to investigate the effect of various input parameters on the electrochemical response of S-B systems. First, factors affecting LPR technique such as scan rate, scan range, and IR-compensation were investigated.

3.5.1 LPR ─ Scan range and scan rate

The effect of scan rates of 0.05, 0.1, and 0.1667 mVs^{-1} and scan ranges of ±10, ±15, and ±30 mV versus OCP were investigated. Various LPR tests with IR compensation ON was conducted. However, significant noise was observed in all the tests with IR compensation ON. Various attempts were made to troubleshoot this; however, a suitable solution was not obtained. Hence, the suitability of EIS for determining R_p was investigated.
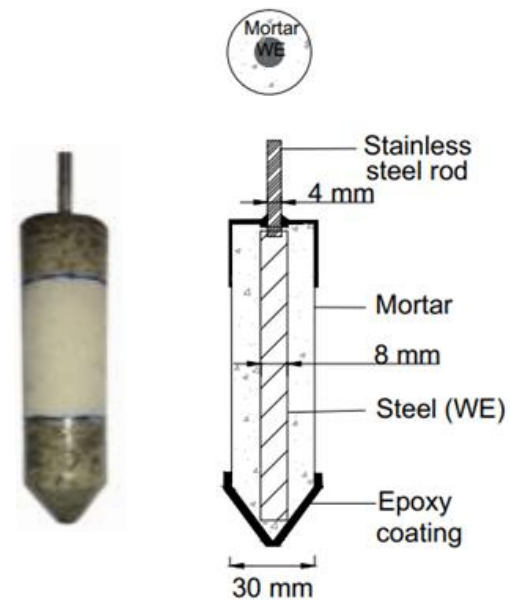
(a) Test specimen
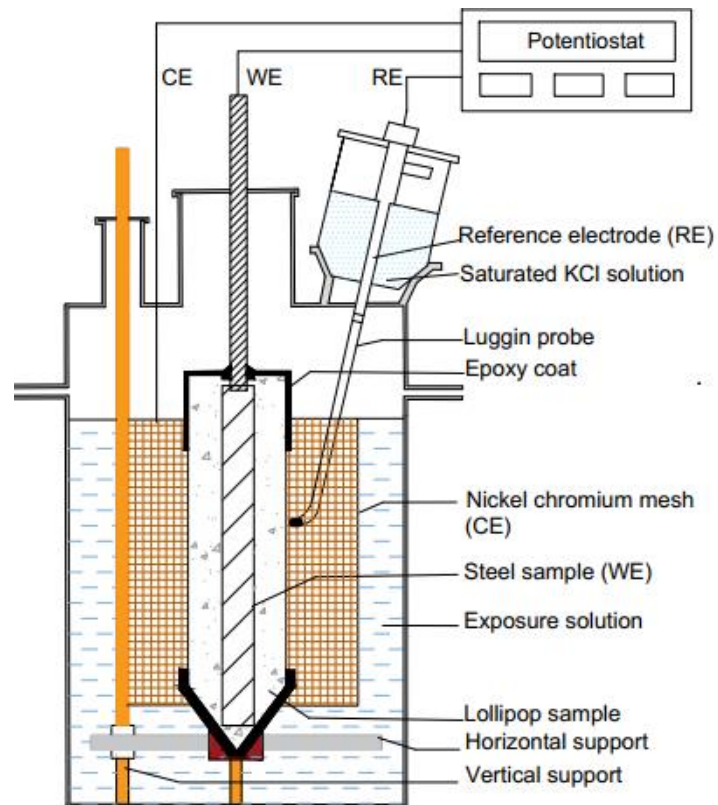
(b) Test set-up

Figure 3.8 Modified LPR test specimen and set-up

3.5.2 EIS – Amplitude and frequency range of AC signal

For determining R_p using EIS, same corrosion cell set-up was used. Based on the challenges faced during the preliminary tests, the effects of positioning of RE with respect to WE were found critical and studied. Then, the effect of two different AC perturbation signal amplitudes (±10 and ±50 mV peak-to-peak value) were studied and an amplitude suitable for highly resistive systems was decided. Then, the electrochemical response obtained at the suitable amplitude and in a frequency range of 1 MHz to 0.01 Hz was studied and a frequency range suitable for the highly resistive system was determined. In all these studies, the DC potential was maintained at OCP and data was collected at 10 points per decade.

3.5.3 Microclimate at the S-B interface

To maintain the microclimate at the S-B interface during the electrochemical testing and avoid changes in the $Cl_{th,}$ temperature and humidity sensors were embedded at various cover depths in three binders, namely OPC, PFA and LC3. This study was aimed to understand the effect of cyclic wet-dry regime as well as binder types at various cover depths. The sensors at 50 mm depth failed due to 100% saturation for a longer period. Corrosion of wire connecting the breakout board led to loss of data in some specimens. The details of the sensor and its installation are given in Appendix C. The outcome of this testing is that 100% saturation occurred at the end of 2nd day of wetting and hence, for hr-ACT test, the cyclic wet-dry regime was kept at 2 days wet and 5 days dry.

3.5.4 Design of corrosion cell

3.5.4.1 Effect of size of the counter electrode

Three sizes of the counter electrode ─ 2, 8, 20 times the size of the working electrode were taken for the study. Nichrome mesh in annular form was used for the study.

3.5.4.2 <u>Effect of electrode configuration</u>

Two different geometries are taken for consideration for electrode configuration as shown in Figure 3.9. The R_p of the same lollipop specimen will be measured in both annular and planar geometries to better understand the EC response.

(a) **Annular**	**(b)** **Planar**
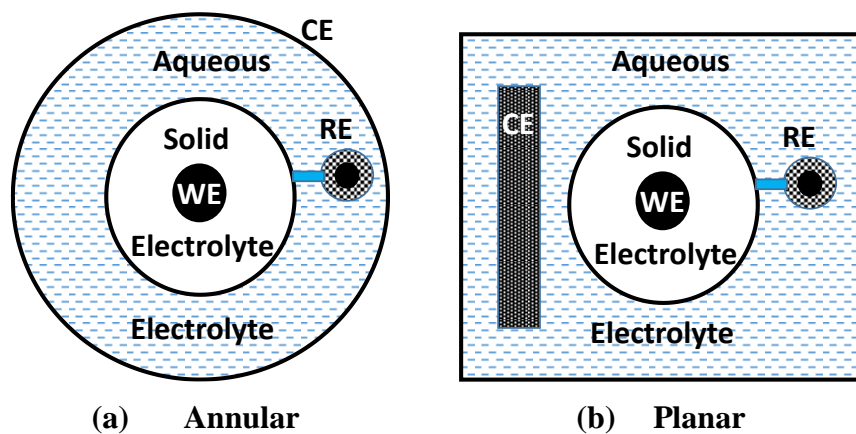
Figure 3.9 Electrode configuration showing annular and planar arrangement

PROGRAM 3 ─ "HR-ACT" TEST METHOD FOR ESTIMATION OF CHLORIDE THRESHOLD

For determining R_p of the steel embedded in mortar, both LPR and EIS were monitored. Lollipop mortar specimens were used for the study. The specimens were subjected to cyclic wet-dry regime following 2 days wet in 3.5 % NaCl +SPS solution and 5 days dry at 25 °C and 65 ± 5 % RH, after 14 days of curing to avoid the longer duration of testing. For conducting LPR experiments, the scan range adopted was ±10 mV and the scan rate was 0.05 mVs^{-1}. For EIS, a frequency range of 100 kHz to 0.01 Hz was studied for an AC amplitude of 10 mV. In EIS studies, the DC potential was maintained at OCP and data was collected at 10 points per decade.

3.5.5 Failure criteria

A statistical corrosion initiation criterion was adopted as shown in Figure 3.10. First, a stable data of five consecutive readings of $1/R_p$ were identified, in which each of the reading falls within mean ± 1.5 times the standard deviation ($\mu_{st} \pm 1.5\sigma_{st}$). Once the stable data was identified, the specimens were continued with the monitoring till $1/R_p$ crosses the value mean + 3 times the standard deviation ($\mu_{st} + 3\sigma_{st}$), the specimen was considered to be initiated.
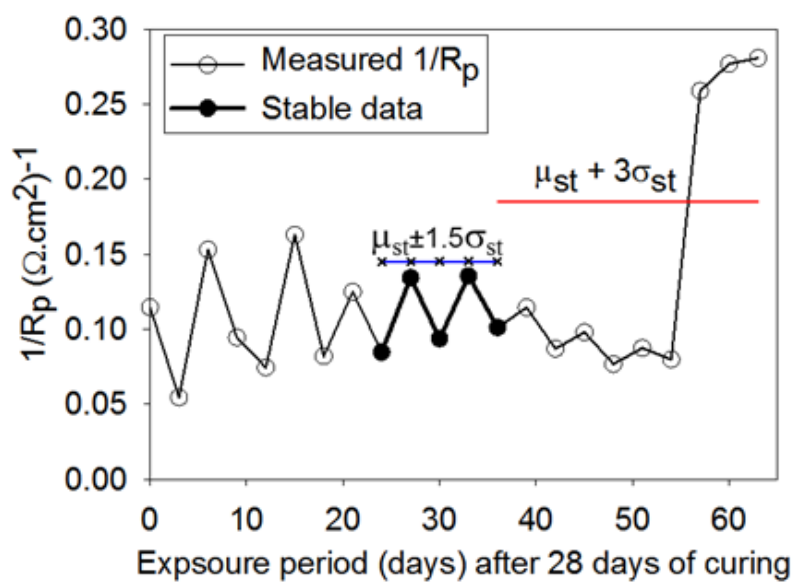
Figure 3.10 Corrosion initiation criteria

Table 3.5 Test parameters used for Cl_{th} determination

Test Variable	Level 1	Level 2	Level 3
Binder	OPC	PFA	LC^3
w/b	0.5	0.5	0.4
Steel	Uncoated TMT		
Total Number of specimens	15 (5 specimens in each case)		

3.5.6 Determination of chloride content

The mortar powder from the S-B interface is collected with the help of the Dremel tool. Then, the powder sample of 1.5 g is digested using 10 ml of digestion solution, (a mixture of 60 g of acetic acid, 50 g of isopropyl alcohol, and 940 g of distilled water) and stabilized by the addition of 40 ml of stabilizing solution. The stabilizing solution is prepared by the combination of 40 ml of the mixture containing 0.1545 grams of NaCl and 1 liter of distilled water with 960 ml of distilled water. The chloride specific ion probe is calibrated for millivolt readings with known chloride concentrations. Then, the millivolt readings for the final solution are converted mathematically into equivalent total percent chloride content.

3.6 PROGRAM 4 – SYNERGISTIC EFFECT OF VARIOUS PARAMETERS ON SERVICE LIFE OF S-B SYSTEMS

To understand the effect of binders on service life of structures, a user-friendly tool was developed using MATLAB®. This was written mainly to incorporate the realistic values of ageing coefficient *m*, and coefficient of variation of input parameters, which are not readily available.

3.6.1 Development of service life estimation tool (SL-Chlor)

A MATLAB® code has been written to estimate the service life using error function solution (Equation 3.1) (Nilsson, 2001) of Fick's second law of diffusion considering one-dimensional chloride ingress.

$$C(x,t) = C_i + (C_s - C_i).erfc\left(\frac{x}{\sqrt{4D_{cl}t}}\right)$$
$$\text{3.1}$$

where, *C(x,t)* is the chloride concentration at depth x, from the exposed surface at exposure time t, Cl_i is the initial chloride concentration, Cl_s is the surface chloride concentration, D_{cl} is

the apparent chloride diffusion coefficient in m²/s, and erf() is the mathematical error function. The probabilistic service life of the structure is considered as the time period at which the chloride accumulation at the steel surface is greater than the chloride threshold. The model assumes the structural element as crack-free. The step by step procedure for obtaining the service life is explained next.

Step 1: Obtain all the input parameters needed for the computation of chloride content at the surface of the steel.

  Sub-step 1: Obtain the following input parameters from the user.

  - o Mean and standard deviation values of d, D_{cl} (28 days) and Cl_{th}

  - o Aging coefficient, m

  - o Maximum surface chloride concentration

  - o Exposure condition

All the user input variables are taken in an excel file.

  Sub-step 2: Hard code the following input variables

  - o Service life = 200 years

  - o Duration of complete hydration of concrete = 2 years

  - o Chloride build-up rate - according to the exposure condition given by the user [Figure 2.18 gives the chloride build-up rate according to the exposure condition].

For probabilistic estimation of service life, 1000 number of simulations are considered.

Table 3.6 gives the input parameters that are needed for the program and the test methods to arrive at the input parameters.

Sub-step 2: Hard code the following input variables

- o Service life = 200 years

- o Duration of complete hydration of concrete = 2 years

- o Chloride build-up rate - according to the exposure condition given by the user [Figure 2.18 gives the chloride build-up rate according to the exposure condition].

For probabilistic estimation of service life, 1000 number of simulations are considered.

Table 3.6 Input parameters for service life estimation

Input parameters	Standard values for the input parameters(mean)	Is standard deviation considered?	Test methods to arrive at the parameter
Cover depth (d)	10 - 100 mm	Yes (User Input)	Fixed by the designer
Ageing coefficient (m)	0.2 - 1	NA	ASTM C1556-11a at 28, 90, 180 days
Diffusion coefficient (D_{cl})	1E-12 to 1E-10 m^2/s	Yes (User Input)	ASTM C1556-11a
Time for complete hydration	2 years	NA	Depending on the type of concrete
Chloride threshold (Cl_{th})	0 - 0.3%bwoc	Yes (User Input)	hr-ACT (Rengaraju and Pillai, 2019)
Max. Surface chloride concentration (Cl_s)	0.6 - 1%bwoc	NA	ASTM C1556-11a / NT BUILD 443
Build up rate (% per year)	Instantaneous – 0.04	NA	Location of the structure
%Probability of failure	10 - 90%	NA	Fixed by the designer

%bwoc – by weight of concrete; NA – not applicable

Step 2: Generate random numbers (count = 1000) between μ ± σ given by the user for the three variables namely d, D_{cl} (28 days) and Cl_{th}.

Step 3: Calculate the surface chloride concentration Cl_s

Cl_s is calculated for each year with the chloride build-up rate for the given exposure condition until it attains the maximum surface chloride concentration, $Cl_{s,max}$. Once $Cl_{s,max}$ is attained, the surface chloride concentration remains unchanged.

Step 4: Calculate the diffusion coefficient D_{cl}

For each of the 1000 simulations, D_{cl} profiles are generated considering the Equation 3.2 (Nilsson, 2001). It is assumed that the D_{cl} remains constant after the age of concrete reaches the time for complete hydration (2 years).

$$D_{cl}(t) = D_{ref} \left(\frac{t_{ref}}{t} \right)^m \qquad\qquad 3.2$$

where, $D_{cl,\, t}$ and $D_{cl,\, ref}$ are the diffusion coefficients at exposure time, t, and reference time, t_{ref} (e.g., 28 days) respectively.

Step 5: Calculate the chloride content at the steel surface

For each time step (every year), the amount of chloride at the steel surface is calculated using the error function (Equation 3.1) considering the 1000 random numbers generated for cover depth and diffusion coefficient calculated in Step 4.

Step 6: Compare the chloride content at the steel surface with Cl_{th}

The chloride content for each time step is compared against 1000 random numbers generated for Cl_{th} values.

Step 7: Calculate the probability of corrosion initiation

The number of instances of failure (i.e., $C_x \geq Cl_{th}$) is used to calculate the probability of corrosion initiation for each time step.

Step 8: Compute the cumulative distribution function (CDF)

The service life is taken as the time period at which the probability of corrosion initiation exceeds the probability of failure desired by the user.

3.6.2 Development of nomograms

With the influencing parameters, namely d, D_{cl}, and binder properties (m, and Cl_{th}), a nomogram has been developed for the ease of the site engineers using the model explained earlier. An example has been demonstrated to show the steps needed to arrive at the service life from the nomogram. For a given probability of failure and the chosen cover, concrete properties and type can be varied to a great extent to achieve the desired service life.

3.7 SUMMARY

This chapter presented the materials used and the methodology adopted for the experimental program to achieve the set forth objectives. Further, the methodology adopted for the analytical program to estimate the service life of structures were discussed in detail.

CHAPTER 4

SUITABILITY OF EXISTING TECHNIQUES FOR TESTING HIGHLY RESISTIVE SYSTEMS

4.1 INTRODUCTION

This chapter presents the results obtained from the experimental investigations to achieve Objective 1, which addressed the evaluation of suitability of existing test methods in three sub-objectives. In the sub-objective 1, the efficiency of MCC technique to assess corrosion of steel in highly resistive binders is discussed. The challenges associated with the data interpretation and the possibility of two different electrical circuits are discussed. In the sub-objective 2, the effect of ICC technique on the form of corrosion and the corrosion products formed on the steel surface is presented. A comparison of these with the steel embedded in mortar subjected to corrosion due to diffusion of chlorides is also presented followed by the pore structure analysis. In the sub-objective 3, the suitability of LPR technique for corrosion assessment in highly resistive binders is evaluated.

4.2 SUITABILITY OF EXISTING TECHNIQUES

This section presents the results of the experimental program mentioned in Subsection 3.4. Results of the three test methods evaluated are discussed in detail.

4.2.1 Macrocell corrosion

First, a preliminary study was conducted for a year with ASTM G109 specimens with three different types of cement, namely OPC, Portland pozzolana cement (PPC), and Portland slag cement (PSC) with TMT steel. Figure 4.1 shows the ASTM specimens being exposed for a preliminary study.

Figure 4.1 ASTM G109 specimens being exposed

It was found that a number of challenges exist in data acquisition and interpretation when ASTM G109 specimens are used for corrosion assessment, which are summarized as follows.

(i)   When the bulk resistivity of the concrete is higher (>50 kΩ.cm), the macrocell current measured as per the standard was less and did not indicate the ongoing corrosion, which indicated a possibility of different electrical circuit.

(ii)   A number of reversals in the sign of macrocell current occurred during the testing, and there are no guidelines available to account for the same in the calculation of total average corrosion current $I_{corr,\ average}$.

(iii)   A modified equation for the calculation of $I_{corr,\ average}$ was proposed in case of reversal of current as in Equation 4.1.

$$TC_j = TC_{j-1} + [(t_j - t_{j-1}) \times \frac{i_j + i_{j-1}}{2}]$$

4.1

where, TC = Total corrosion (Coulombs); t_j = Time (seconds) at which the measurement of the macrocell current is carried out; and i_j = Macrocell current (Amps) at time, t_j. If $i_j > 0$, then i_j is considered as zero. Note that the parameter TC_j in ASTM G109 is same as I$_{corr, average}$. For more details regarding the macrocell corrosion in the highly resistive binder types, see Appendix D.

4.2.1.1 <u>Test results</u>

Figure 4.2 shows the half-cell potential (HCP) and macrocell current (Circuit 1) exhibited by the ASTM G109 type specimens with OPC, PFA, and LC3 concrete, respectively. The HCP of low resistive concrete (OPC) dropped suddenly and at early age of exposure whereas in highly resistive concrete (LC3), the reduction of potential was gradual. Also, it is to be noted that the HCP was maintained well above -100 mV (with respect to SCE) in all the LC3 specimens. This range of values were maintained for about 800 days for most of the specimens. The cumulative current was calculated as per the modified Equation 4.1. The cumulative current of 150 C was observed early in OPC when compared to the corresponding PFA and LC3 specimens with higher resistivity. LC3 system shows significantly less macrocell current compared to OPC and PFA systems. The macrocell voltage was nearly zero for all the LC3 specimens. The high resistive systems show very less macrocell voltage between the top and bottom rebar due to ionic resistance (Berke et al., 1990; Arya and Vassie, 1995; Elsener, 2002). All the LC3 specimens did not show any indication of corrosion in the electrochemical response. The refined pore structure and high ionic resistance due to the pozzolanic reaction in early age enhance the corrosion resistance in LC3 specimens.
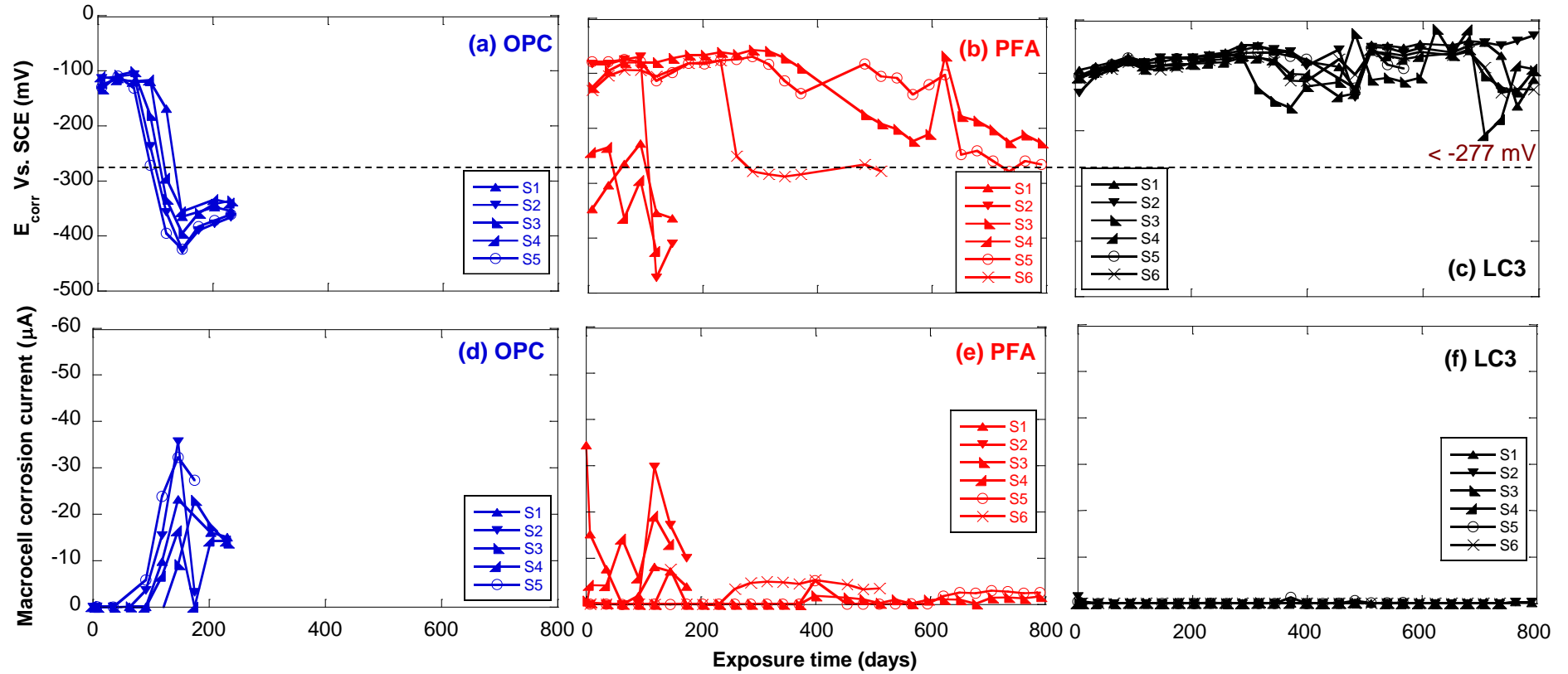
Figure 4.2 ASTM G109 results (a), (b), (c) Half-cell potential (d), (e), (f) Macrocell current observed in OPC, PFA, and LC3 specimens

4.2.1.2 Mechanism of corrosion in highly resistive systems

Due to higher resistivity in LC3, the Circuit 2 type of macrocell corrosion (Figure 4.3(a)) may be predominant, as observed by Hansson et al. (2006). To investigate this further, a LC3 specimen was autopsied. Figure 4.3 shows the rust spots on the steel surface of LC3 specimen. Hence, it can be concluded that measuring Circuit 1 as in ASTM G109 standard may not represent the ongoing corrosion in highly resistive cementitious systems ($\rho > 37$ kΩ.cm). This clearly indicates that the ASTM G109 test method is not suitable for corrosion assessment in highly resistive systems like LC3.

(a)

(b)
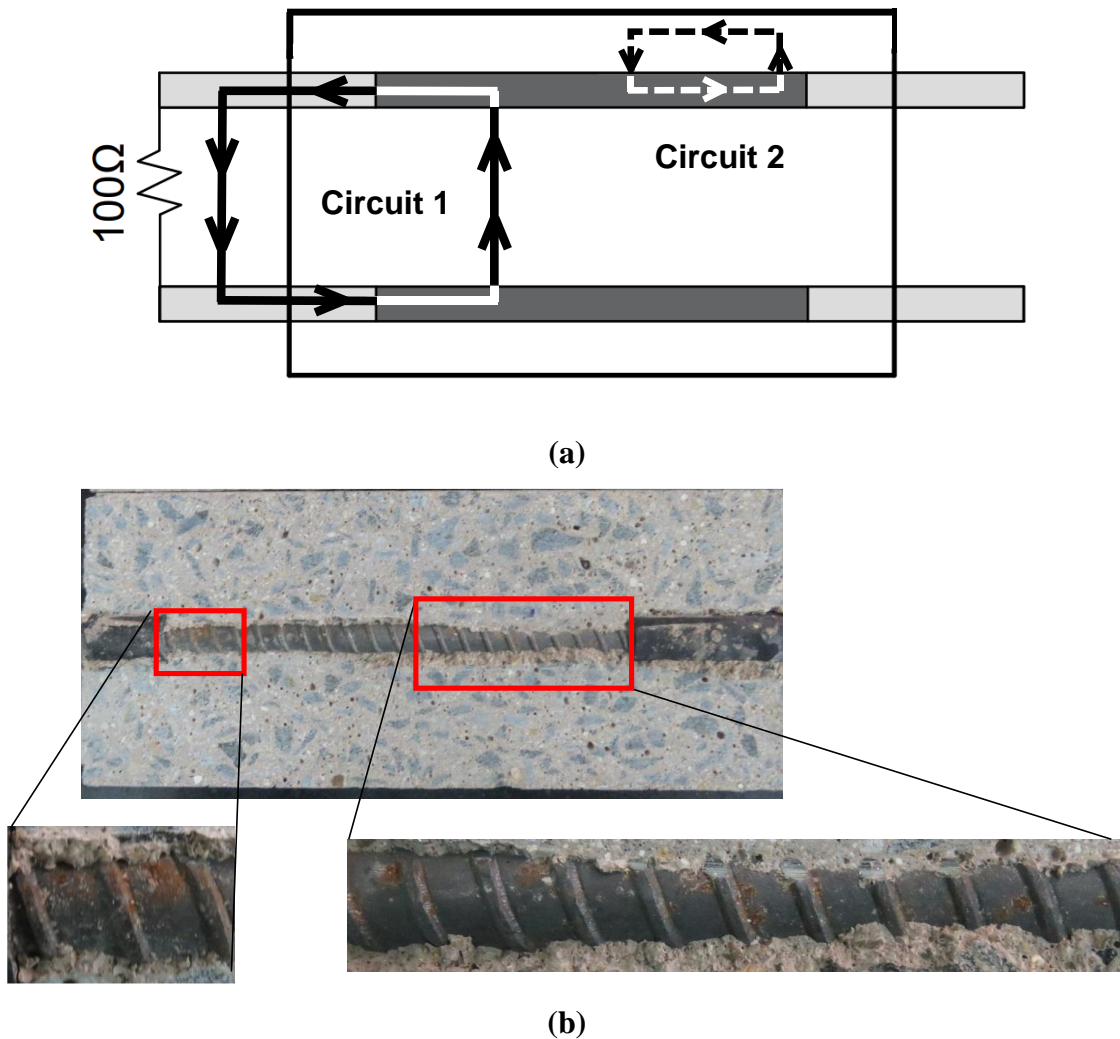
Figure 4.3 (a) Possible corrosion circuits and (b) LC3 specimen showing rust spots as a result of Circuit 2 corrosion

4.2.1.3 <u>Learnings from ASTM G109 testing in highly resistive S-B Systems</u>

There are four major outcomes from this testing

1. In highly resistive S-B systems, macrocell happens within the same rebar and hence chloride threshold specimens can be designed in such a way that it can have a single rebar.

2. The HCP and macrocell corrosion were not indicative of ongoing corrosion. So advanced testing techniques need to be used.

3. The resistivity range of concrete in which ASTM G109 can be used is $\rho < 37$ kΩ.cm, where ρ is the surface resistivity of concrete at 28 days measured using Wenner probe.

4. ASTM G109 test method reveals that the determination of Cl_{th} of steel embedded in concrete would take years. There is a need to develop a test method to determine the Cl_{th} of S-B systems in short term.

4.2.2 Impressed current corrosion test method

Table 4.1 shows the mechanical properties of M35 and M50 concrete with three types of binders, namely OPC, PFA and LC3, which were assessed for corrosion-induced cracking. Keeping the same cover-to-bar-diameter in all the specimens, the specimens were subjected to uniform voltage application to assess the T_{crack} as a function of binder alone. The T_{crack} did not depend on the tensile strength of concrete in this case. The specimens were tested till the visible appearance of crack/500 hours in each group T1, T2 and T3 respectively.

Table 4.1 Mechanical properties of concrete

Properties		M35			M50		
		OPC	PFA	LC^3	OPC	PFA	LC^3
28-day compressive strength (MPa)	mean	45.7	45	44.6	62.8	53.01	54.02
	cov	0.08	0.1	0.03	0.03	0.04	0.03
28-day split tensile strength (MPa)	mean	7.19	6.74	6.89	7.75	8.18	7.72
	cov	0.05	0.06	0.03	0.05	0.1	0.09

4.2.2.1 Effect of resistivity of concrete cover on corrosion current and T_{crack}

Figure 4.4 (a) shows the effect of three different types of binder after the application of voltage in the first group of specimens (T1). Three distinct ranges were observed in the instantaneous corrosion current measured. OPC concrete have lesser resistivity and hence higher instantaneous corrosion current in the range of (40 to 80 mA) was observed. In PFA, the corrosion current observed was lower (10 to 30 mA) whereas LC3 has the lowest in the range of (0 to 2 mA). In the case of T1, the voltage application was done till all the OPC specimens cracked and it was maximum of 160 hours for M35 concrete. Higher the concrete grade, better will be resistivity towards corrosion cracking. An M50 grade of concrete showed better resistance towards cracking than M35 irrespective of binder type. Please note that the variation in instantaneous corrosion current was also minimum in M50 grade than that in M35. Figure 4.4(d) shows that the average time taken for the occurrence of corrosion crack in OPC M50 grade is 380 hours. Figure 4.5(b) shows the typical crack pattern observed in OPC specimens in the T1 group. Since the same cover-to-bar-diameter was maintained for all the concrete and split tensile strength measured for all the three concrete didn't vary significantly, the difference in corrosion current between concrete and time taken for cracking of concrete depend on the resistivity alone in this case.
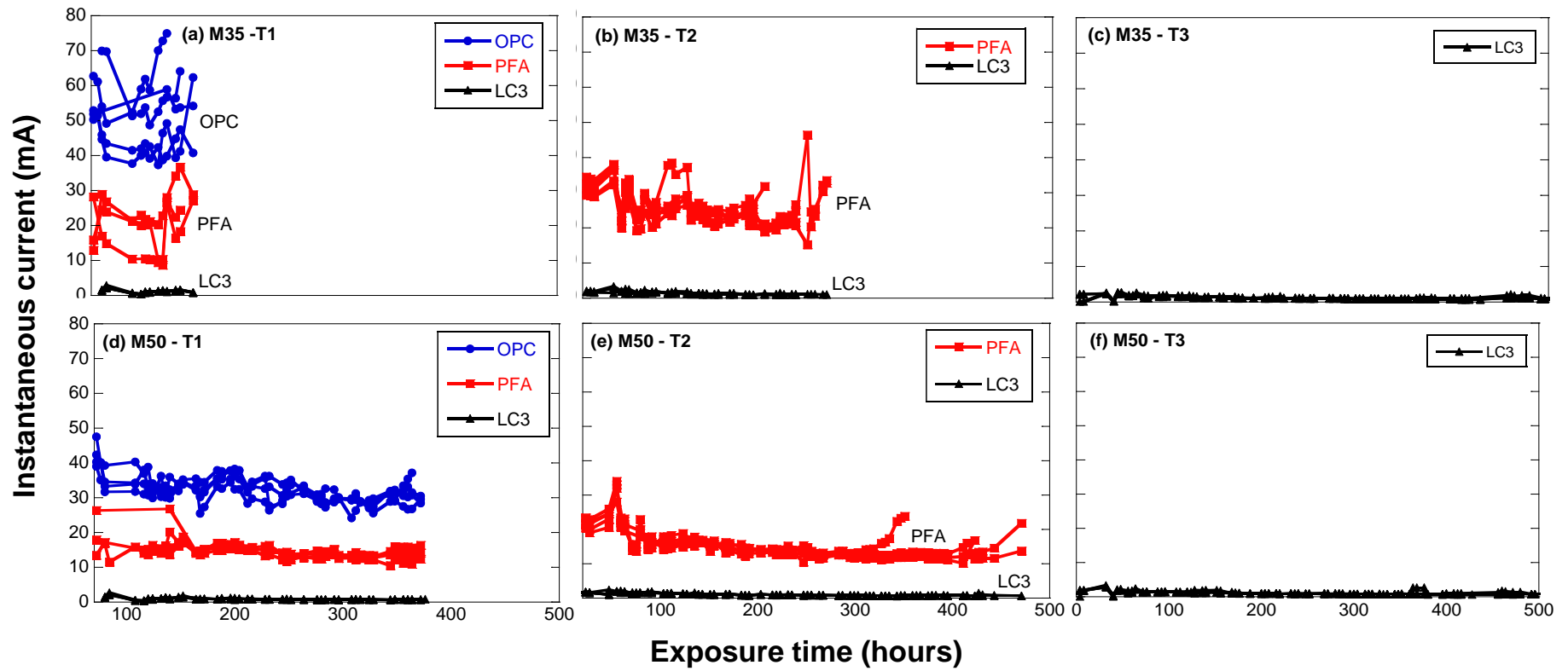
Figure 4.4 Effect of voltage application in three sets T1, T2 and T3

Figure 4.4(b) shows the second group T2, where a comparison of instantaneous corrosion current of PFA and LC3 specimens. PFA specimens cracked at time duration of more than 200 hours of voltage application for M35 and 430 hours for an M50 grade (Figure 4.4 (e). Since strength grade at 28 days was compared, the pozzolanic reaction, which enhances resistivity at 56 days of curing could not be realized for PFA specimens. Nevertheless, the corrosion crack formed on PFA specimens were hairline cracks, and oozing of corrosion products did not occur (Figure 4.5 (c)). The corrosion current in T2 specimens did not increase dramatically even though the hours of voltage application increased nearly 50 hours.

Figure 4.4 (c) and (f) show the corrosion current measured in the third group T3, which consisted of LC3 specimens, where none of the specimens cracked even after 500 hours of voltage application. This phenomenon can be attributed to the early hydration and high resistivity of LC3 compared to OPC and PFA. The resistivity in LC3 is one order higher than PFA and OPC at 28 days of curing (Dhandapani and Santhanam, 2017). LC3 helps in developing the necessary resistance against the ingress of moisture and oxygen, which are very essential for corrosion reaction. When compared to OPC and PFA, LC3 has superior performance in restricting the corrosion current and hence corrosion crack propagation in severe exposure conditions. .Figure 4.5 shows the typical crack pattern in each of the three binders where OPC and PFA specimens showed cracks and LC3 did not show any crack.
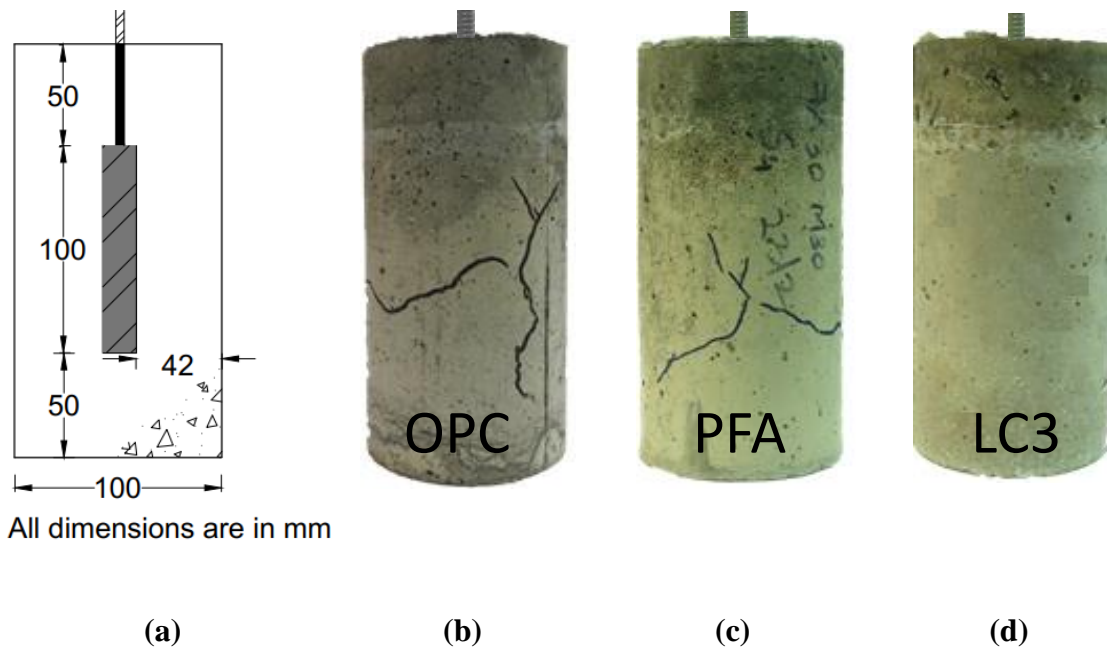
Figure 4.5 (a) Scheamtic of the test specimen and (b), (c), and (d) the typical crack pattern observed after voltage application in OPC, PFA, and LC3 specimens

The calcined clay reacts with portlandite (pozzolanic reaction) to form secondary C-S-H, which is negatively charged (Si/Ca < 0.8) and is capable of adsorbing Na^+ and K^+. Also, C-A-S-H formed due to the substitution of Si^{4+} by Al^{3+} tends to attract the negative ions in the pore solution to neutralize the charge imbalance. The adsorption of ions by C-S-H and C-A-S-H makes the pore solution less conductive. (San Nicolas et al., 2014). LC3 has Si/Ca < 0.8 and hence, lower conductivity (Dhandapani et al., 2018). This proves that the pozzolanic reaction mechanism in supplementary cementitious materials changes the resistivity of the binder resulting in a lower corrosion rate. Thus, LC3 helps in developing the necessary resistance against the ingress of moisture, oxygen, and chlorides, which are very essential for corrosion reaction. LC3 has superior corrosion performance in severe exposure conditions to OPC and PFA.

4.2.2.2 <u>Microstructure characterization of steel-binder interface</u>

The T_{crack} depends on the resistivity, form of corrosion and corrosion products and the porosity of the S-B interface. Since LC3 had very high resistivity, investigation of the other two factors were done to understand their effect on T_{crack}.

a) Nature of corrosion products – visual observation

Figure 4.6 (left photo of (a), (b) and (c)) shows the typical observation of steel embedded in OPC, PFA and LC3 concrete after voltage application. The specimens were corroded uniformly throughout the length of the rebar. The colour of the rust on the embedded steel was black or dark brown and was heavily oxidised in both OPC and PFA specimens. The S-B interface also showed accumulation and displacement of rust in these specimens. LC3 specimens had adherent orange-brown colour rust on the steel surface. No accumulation or radial displacement of rust was observed at the S-B interface in case of LC3. The visual observation of steel after ICC test was compared with steel extracted from specimens subjected to the natural diffusion of chlorides. Figure 4.6 (right photo of (a), (b) and (c)) shows the typical corrosion pattern observed on the steel embedded in OPC, PFA and LC3 mortar specimens after the natural diffusion of chlorides. The corrosion was localised forming pits at specific locations mostly at the centre where the chlorides diffuse faster due to the shortest possible route. This clearly indicates that the form of corrosion (uniform corrosion in ICC specimens and pitting corrosion in chloride diffusion) is different in both the test methods.
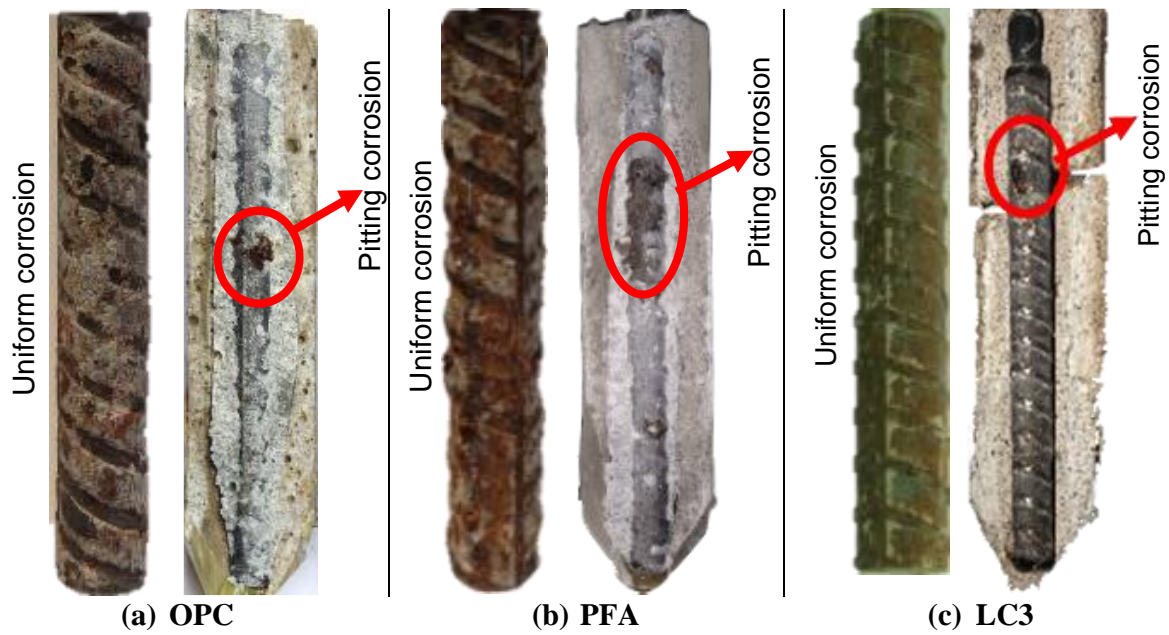
Figure 4.6 Uniform corrosion (ICC) and pitting corrosion (WDC) observed

Figure 4.7 shows the typical observation of steel specimens embedded in OPC, PFA and LC3 concrete after cleaning it in ASTM G1 solution. Small pits and striations were observed on the steel embedded in OPC indicating the higher corrosion rate and mass loss. PFA specimens had pits at distinct locations whereas no corrosion pits were observed in LC3. The formation of cracks in OPC and PFA could have caused the macrocell formation and initiation of pits. The diffusion of chlorides or formation of macrocell was very limited in LC3 specimens due to its higher resistance against the ionic movement and the crack formation. This was the reason for the lower corrosion rate and mass loss.

(a)

(b)
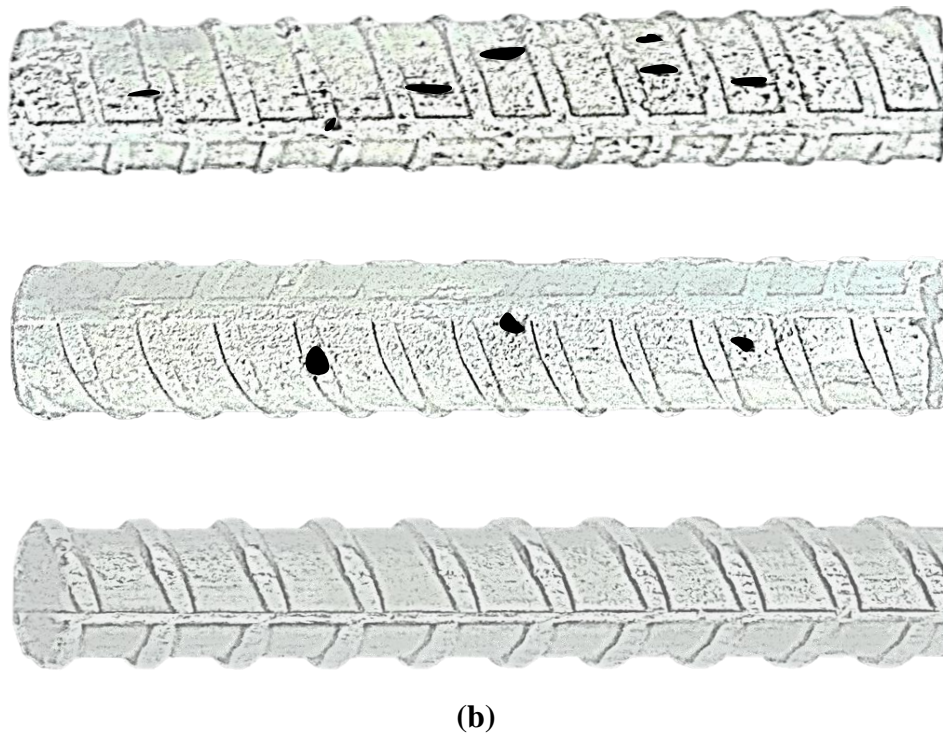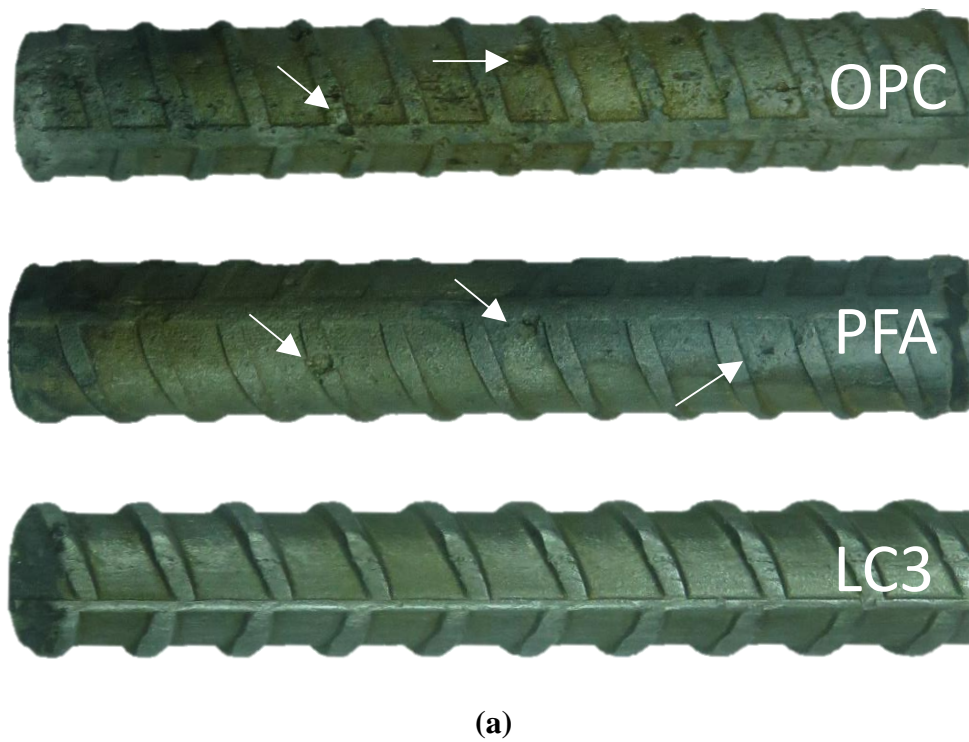
Figure 4.7 Steel pieces after cleaning (a) actual photo and (b) photo marked for pits

b) Nature of corrosion products – Raman Spectroscopy

Figure 4.8 shows the Raman spectra obtained from the corrosion products of steel in three types of concrete namely OPC, PFA and LC3. The pH, pore solution, and resistivity for the ingress of Cl⁻ ions and moisture of the three concrete types vary significantly. Therefore, the peaks obtained from the corrosion products in OPC, PFA and LC3 were very different from one another. It is to be noted that a tolerance of (±10) in the Raman shift (cm^{-1}) is considered in all these plots as the spectra is obtained from steel-concrete interface, which is non-homogeneous and porous and the peak positions were taken from Oh et al., 1998.

Figure 4.8(a) shows the peaks obtained from the rust at S-B interface in OPC concrete with α-FeOOH and γ-FeOOH rust products. The precipitation of γ-FeOOH shows the initial high pH in the OPC system. These iron oxide phases are amorphous in nature and are converted to a more stable phase depending upon the environment. The expansive nature of the products formed and the higher corrosion rate leads to early cracking in OPC concrete.

Figure 4.8(b) shows the peaks obtained from the corrosion products of PFA concrete with δ-FeOOH (peaks at 297, 392, 666 cm^{-1}) and Fe_3O_4 (peaks at 532 and 667 cm^{-1}). The formation of δ-FeOOH could be due to the presence of chlorides in low concentrations. The generation of corrosion products might have taken place due to the application of a potential from the beginning of the test. Due to the application of a positive potential to the steel, Cl⁻ ions also might have migrated towards the steel. Depending on the resistivity of the system, the time taken for the corrosion initiation crack may vary. PFA did not show much improvement over OPC as the pozzolanic reaction is not fully realised at 28 days, which is the start of the test. The nature of the corrosion products formed in both OPC and PFA are similar to the oxide layers reported in the literature (Neff et al., 2011). This shows that both OPC and PFA did not have significant variation

101

in terms of pH. As mentioned earlier, the resistivity of PFA concrete did not play a significant role as the hydration process was ongoing.

Figure 4.8(c) shows the corrosion products formed on the surface of steel embedded in LC3 concrete. Since the corrosion rate was very low, the Raman spectrum was obtained directly from the steel itself. LC3 shows peaks for α-Fe_2O_3 and Fe_3O_4. Hematite is characterised by two strong peaks at 226 and 292 cm^{-1}. Magnetite is characterised by peaks at 532 and 667 cm^{1}. Hematite can form due to atmospheric exposure of green rust I, which could have migrated through the interconnected pores or dehydration/oxygenation of goethite (Marcotte et al., 2007). The hematite is a stable phase with less surface area and has much-compacted structure due to evaporation of water molecule. The expansive pressure is much less when compared to other stable oxides and hydroxides (Care et al., 2008). The presence of hematite shows that LC3 has lower moisture content and lower pH at the interface. The corrosion rate was very much lower with an adherent orange-brown oxide layer on the steel. No visible rust accumulation was found in the S-B interface in LC3. Also, the presence of hematite is accompanied with magnetite, which is similar to the passive layer. Whether the presence of hematite is the indication of an intact passive layer or absence of moisture in the phase transformations, the volumetric expansion is very less.

Figure 4.8(d), (e), (f) shows the Raman spectra obtained from steel embedded in OPC, PFA and LC3 mortar specimens after the natural diffusion of chlorides. Irrespective of the binder, the Raman spectra showed α-FeOOH and β-FeOOH corrosion products at the pit location. The formation of β-FeOOH indicates the presence of chlorides. From the corrosion products, it is clear that the test method influence the nature of corrosion products and type of corrosion. Also, this suggests that the nature of corrosion products plays a key role in exerting the radial stress and hence in the formation of corrosion crack.
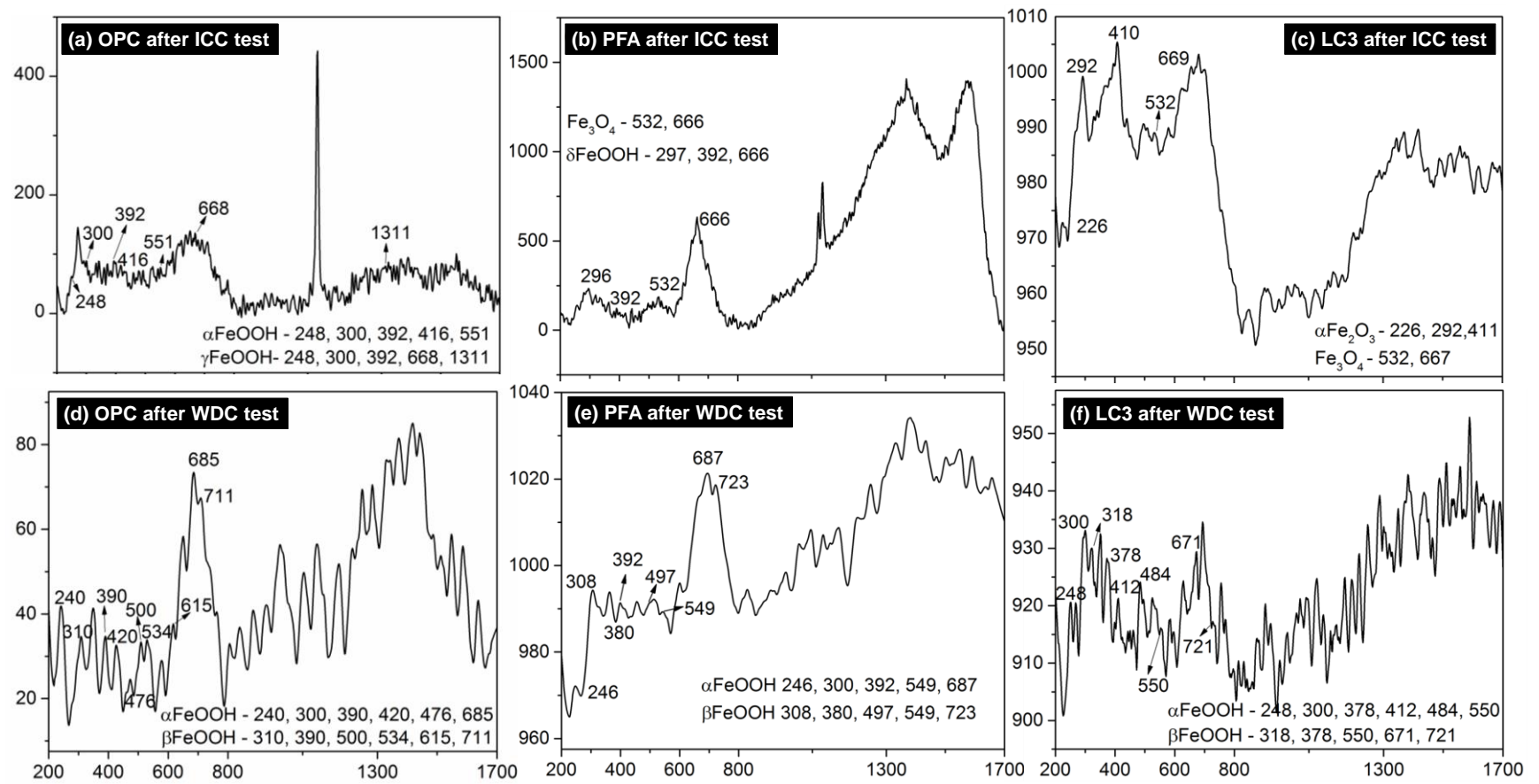
Figure 4.8 Raman spectroscopy showing corrosion products (a), (b), (c) after ICC test, (d), (e), and (f) after WDC test in OPC, PFA, and LC3 specimens

c) Porosity at the steel-binder interface

The porosity of the interface plays a key role in the time needed for crack initiation. The rust products can be accommodated in the interface region and radial pressure build-up may be delayed as rust can move away from the S-B interface to the surrounding through interconnected pores. Figure 4.9(a) and (b) show the specific pore volume (threshold diameter) and the differential intrusion volume (critical pore size) at the interface of the M35 concrete with three binders. In LC3, the threshold diameter was smaller, in the range of 0.1 μm with the critical pore size as 0.025μm. Apart from that two major pore diameters were identified (0.01 and 0.025 μm). This shows that in LC3, a well-refined interface region is formed. The threshold diameter in PFA concrete was in the range 0.4 μm and the critical pore size was 0.07μm. PFA concrete also had multiple prominent pore diameters (0.01 and 0.07 μm). The fine pores measured by MIP may be finer capillary pores or gel pores within CSH in PFA and LC3. In OPC, much larger threshold diameter (0.8 μm) and critical pore diameter of size 0.04 μm were observed.

Restructuring and coarsening of pores could have taken place in OPC due to buffering of calcium hydroxide from the surrounding interface, before severe corrosion and cracking. Small refined pores in PFA and LC3 systems show that the resistivity of the interface is very high for ionic movement, which may prevent the chloride ingress. However, in PFA concretes, as hydration was progressing during testing, the refinement of pores might have exhibited greater pressure for the rust in the interface from moving away leading to hairline cracks.
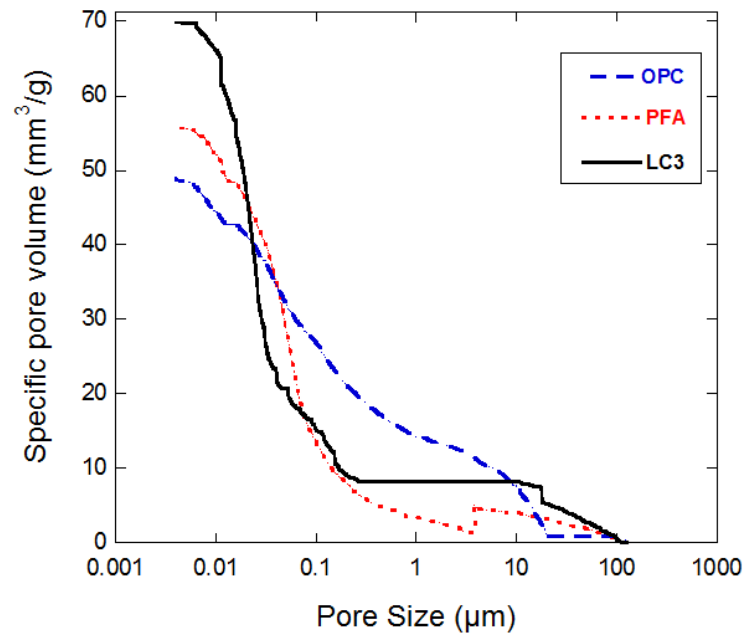
Cumulative intrusion curve
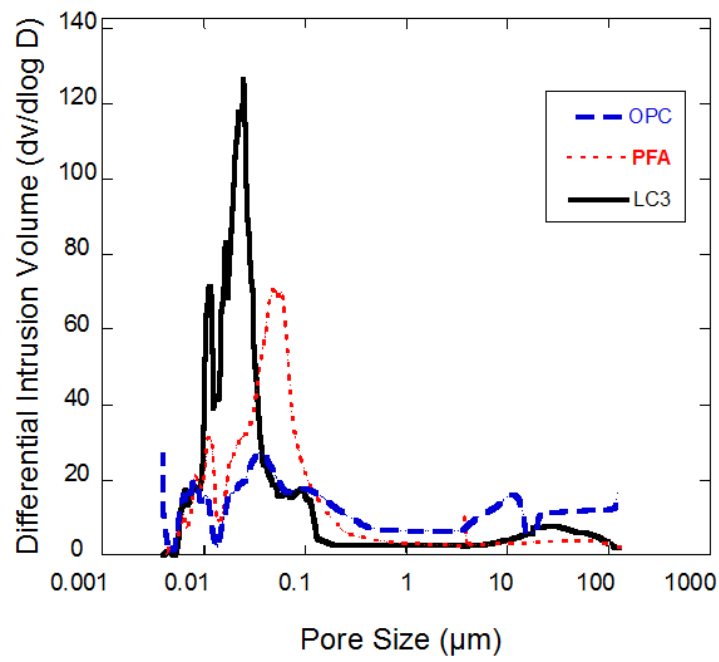
Differential intrusion curve

Figure 4.9 Porosity at the S-B interface measured using MIP

4.2.3 Linear polarisation resistance (LPR)

Figure 4.10 shows the inverse R_p of the lollipop mortar specimens as a function of exposure period and a typical photograph of the corroded S-B interface of the OPC, PFA, and LC3 test specimens. As shown in Figure 4.10 (a) and (b), the onset of corrosion was correctly detected by the electrochemical response of all the OPC and some PFA specimens. Some PFA specimens, even with low $1/R_p$ exhibited corrosion stains on the mortar surface and were found to have significant corrosion upon autopsy. This can be attributed to the significant increase in the resistivity of the mortar cover with age in those specimens. Hence, it can be concluded that the LPR technique (with adopted input parameters) is not always reliable in detecting corrosion initiation.

In the case of LC3 specimens, the $1/R_p$ exhibited no significant increase until about 80 days. However, corrosion stains were observed on the surface of the mortar and visible corrosion was observed on the embedded steel surface when autopsied, as shown in Figure 4.10 (c). This indicates that the LPR technique was not successful in accurately determining R_p and detecting corrosion initiation of any of the LC3 systems with very high resistivity. Hence, the factors affecting the LPR response in highly resistive S-B systems were investigated.
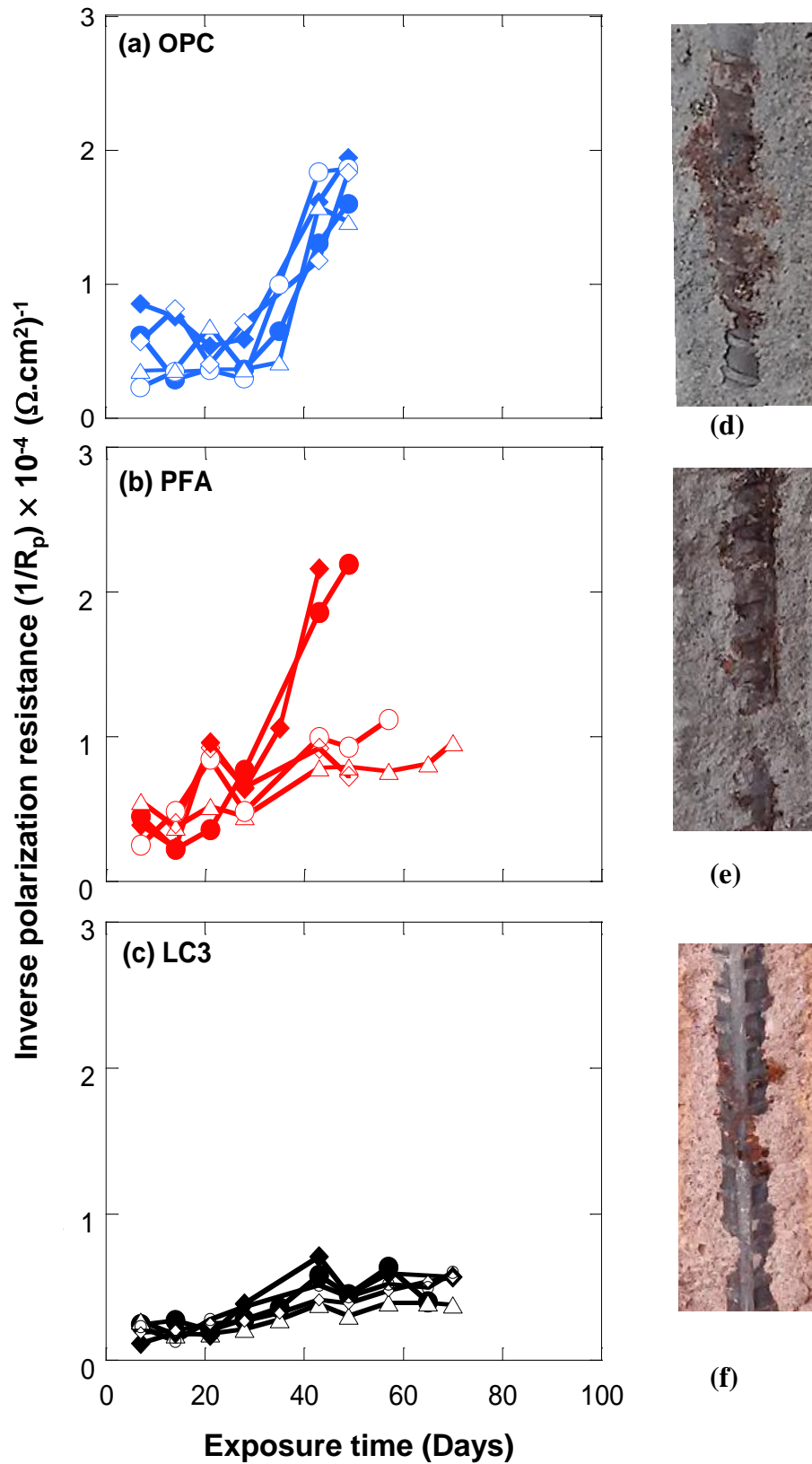
Figure 4.10 (a), (b), (c) Observed inverse polarization resistance and (d), (e), (f) Typical visual observations of OPC, PFA, and LC3 specimens on prolonged exposure to chlorides

107

4.2.3.1 Determination of chloride threshold

Figure 4.11 shows the Cl_{th} values obtained for the OPC, PFA and LC3 binders. The lollipop specimens were autopsied and the mortar powder was collected from the S-B interface. The acid soluble chloride content was found using SHRP 330 method as described in Section 0. The highest mean value of Cl_{th} is obtained for OPC (i.e., 0.4% by weight of binder), which reflects the high alkalinity at the interface. In the blended systems, the alkalinity is lower due to the consumption of $Ca(OH)_2$ in the pozzolanic reactions and consequently, the Cl_{th} values obtained for PFA and LC3 systems are less, which is in agreement with the literature (Bentur et al., 1997). The pozzolanic reactions appear to decrease the Cl_{th} while they increase the ionic resistance and decrease chloride transport. It should be noted that the Cl_{th} found here may not reflect the actual value due to the error in the data acquisition and interpretation as explained earlier. From view point of obtained chloride threshold, OPC performed better as compared to PFA and LC3, as it requires more amount of chloride ions for depassivation/initiation of corrosion of steel reinforcement as compared to PFA and LC3.

%bwob - percent by weight of binder
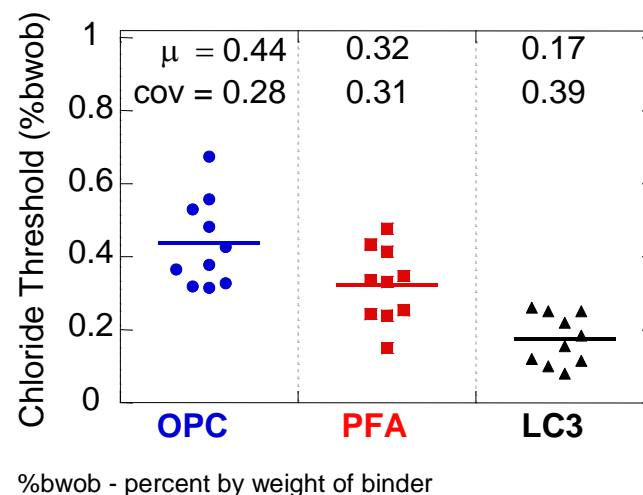
Figure 4.11 Chloride threshold of OPC, PFA, and LC3 determined using LPR technique

4.3 SUMMARY

In Subsection 4.2, the effect of resistivity of the concrete cover due to the nature of the binder being used on the electrochemical response and the challenges in data acquisition and interpretation were demonstrated. This chapter presented the results obtained from ASTM G109 specimens and suitability of this test for the range of resistivity. The possibility of different circuits and the non-identification of ongoing corrosion in highly resistive binders are also investigated. The nature of the corrosion products and the form of corrosion in the ICC test method and the pore structure analysis were examined to find its suitability to assess the corrosion of steel in highly resistive binder systems. Further, the electrochemical response using LPR technique in detecting the corrosion initiation was investigated.

CHAPTER 5

FACTORS AFFECTING ELECTROCHEMICAL RESPONSE FROM STEEL-BINDER SYSTEMS

5.1 INTRODUCTION

This chapter presents the effect of various input parameters on the electrochemical response when LPR and EIS techniques were used. The factors affecting the electrochemical response such as corrosion cell configuration and input parameters were addressed and the results of this section were utilized to choose the test parameters for development of test method for determining the chloride threshold.

5.2 FACTORS AFFECTING ELECTROCHEMICAL RESPONSE IN S-B SYSTEMS

The effect of various parameters obtained from two advanced electrochemical techniques and effect of electrode configuration on the electrochemical response were investigated as per the experimental program described in Subsection 3.5.

5.2.1 Linear polarisation resistance (LPR)

The electrochemical response acquired using LPR technique is affected by three parameters, namely (i) scan range, (ii) scan rate, and (iii) electrolyte resistance. The effects of these three parameters on R_p is investigated in detail.

5.2.1.1 Scan range and Scan rate

Literature recommends a scan rate of 0.05 mVs^{-1} for LPR studies on S-B systems (Poursaee, 2010). This particular scan rate is sufficient to charge the capacitance of double layer (C_{dl}) in S-B systems with low resistivity (say, OPC systems).
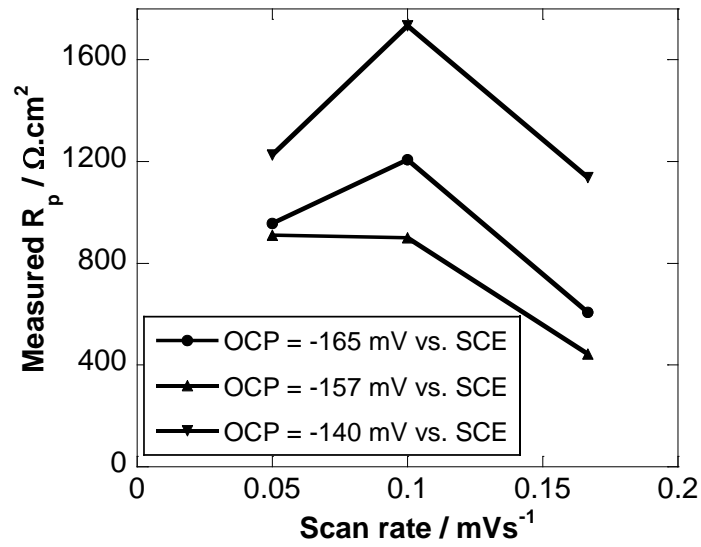
(a)
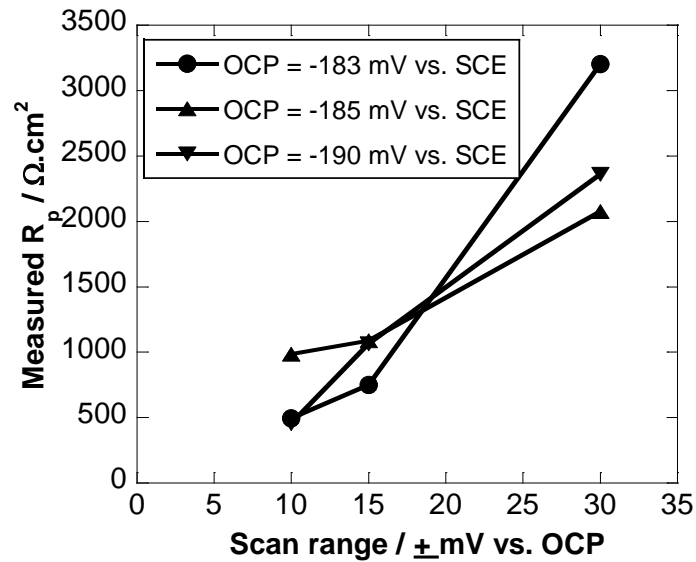
(b)

Figure 5.1 Effect of (a) Scan rate and (b) Scan range on measured R_p

Figure 5.1(a) shows the effect of scan rate on electrochemical response of specimens with moderate resistivity and in a passive state (negligible corrosion). It is shown that as the scan rate increases from 0.05 to 0.1667 mVs^{-1}, the R_p decreases. This is due to the increase in the current across the double layer (C_{dl}) (Ameer et al., 2004). Figure 5.1 (b) shows the effect of scan range on passive specimens. Increase in scan range (i.e., the difference between the

111

starting point of scanning and original OCP) can disturb the OCP of the system resulting in higher R_p and the specimen takes a longer time to return to its original OCP. Also, higher scan range may lead the response to the non-linear region; hence, the induced perturbation should be as minimum as possible. Considering this, a scan range of ±10 mV versus OCP is recommended for LPR tests in S-B systems. Although a different scan rate and scan range had been adopted in Objective 1, the effect of these parameters on R_p was found less than that due to the resistivity of the cementitious system (i.e., porous, sol-gel electrolyte).

5.2.1.2 Effect of electrolyte resistance

The LPR technique gives the combined polarization resistance exhibited by the S-B system, which includes both the resistance of mortar cover (R_m) and polarization resistance of steel (R_p). This technique has the assumption that the R_m is negligible when compared to the R_p of the specimen (Fontana, 1987) – as in the case of a metal-aqueous system. In the case of S-B systems with highly resistive cementitious cover, the R_m is significant and comparable to R_p and hence, this assumption becomes invalid. Due to high resistivity (say, $R_m > 0.5$ R_p), the significant ohmic drop can occur in such systems (Mansfeld, 1976). Such uncompensated ohmic drop can lead to a significant distortion of the input scan rate, which in turn lead to large error in the measured R_p. When the ohmic drop is significant, LPR with positive feedback/current interrupt options is recommended to compensate the same. LPR with positive feedback involves a trial and error approach, where the solution resistance measured is potential dependent and can lead to partial compensation or overcompensation of the ohmic drop (Mansfeld, 1982). Hence, in such cases, LPR with the current interrupt method is suggested. However, this technique for highly resistive S-B systems could not be verified due to significant noise and distortion of the polarization curve. Also, the technique is based on Randle's circuit, where the electrolyte is considered to have only resistance. As the cementitious system is a sol-gel structure with pores partially filled with

the liquid, it has both resistance and capacitance. This might have led to noise when the instrument was set for IR-compensation. Therefore, it can be concluded that the acquisition and interpretation of reliable LPR response from highly resistive S-B systems are challenging. There is a need to understand the performance of individual components to interpret the data. Hence, the EIS technique was adopted for assessing the R_p of steel embedded in S-B systems.

5.2.2 Electrochemical impedance spectroscopy (EIS)

It was attempted to assess the R_p of the lollipop specimen using the same corrosion cell set-up and EIS technique. However, a number of artefacts were observed in the Nyquist plot. The study gives the details of the measures taken to mitigate the artefacts and effect of input parameters on the EIS response.

5.2.2.1 Effect of passive film

Figure 5.2 shows the effect of the presence of mortar cover on the EIS response from a steel specimen with passive film. The inset gives details in the high frequency region. Three EIS spectra are obtained from the (i) S-B system, (ii) S-S system with 2 minutes of immersion, and (iii) S-S system with 10 minutes of immersion. The inset provides the complete spectra of the S-B system (curve closest to the origin). The cover mortar exhibits both resistive and capacitive nature and give rise to a semicircle in the high frequency region in the S-B system. The starting point of the low frequency tail is indicative of the resistance of the mortar cover (say, about 25000 Hz). The two curves of the S-S system with passive film shows difference in the high frequency region as the immersion time increases, whereas the low frequency tail coincides at about 2500 Hz, which represents the resistance of the passive film. This coincidence indicates that the resistance of the passive film is not affected by the immersion time. The deviation exhibited by the two S-S curves

(near the 0.01 Hz region) is negligible. From these results, it can be concluded that the data

interpretation in the S-B system and S-S system should be handled differently.
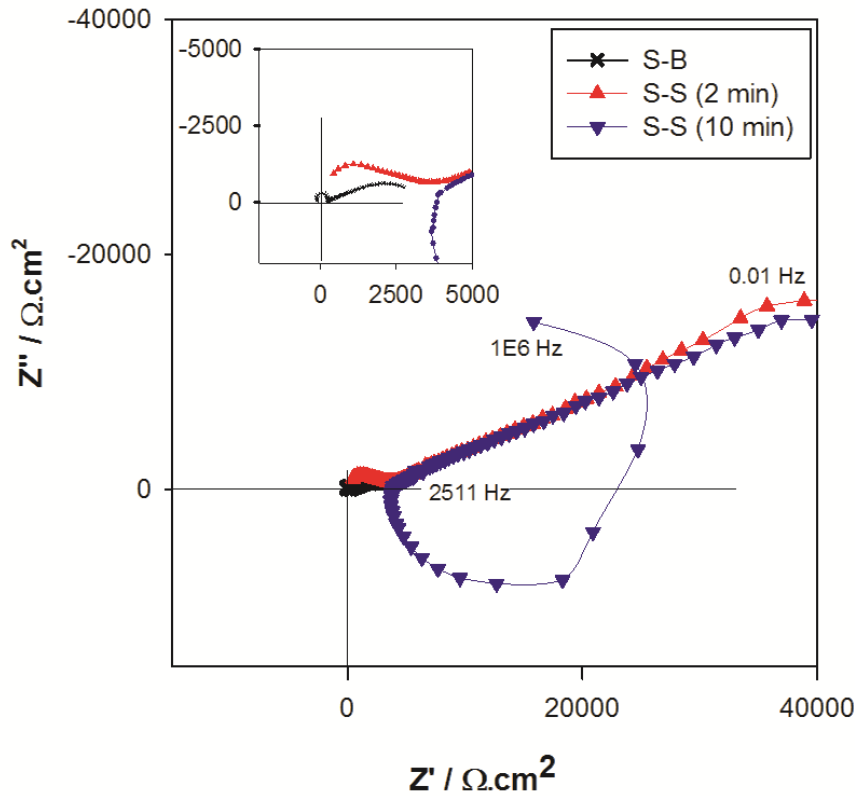
Figure 5.2 Effect of passive film on the Nyquist plot

5.2.2.2 <u>Effect of the position of reference electrode (RE)</u>

Figure 5.3 shows the effect of the position of RE with respect to WE. When RE was kept

at 2 mm away from the mortar surface of the lollipop specimen as shown in Figure 5.4, the

obtained Nyquist plot had severe distortion (artefact) in the high frequency region. When

the EIS response has such kind of artefacts, the curve cannot be analysed with the help of

equivalent electrical circuit. So the reasoning for such artefacts needs investigation to avoid

the same.

From the literature, it was found that this artefact could be either due to the shielding

effect or short-circuiting. The shielding effect causes a redistribution of current lines as the

Luggin probe physically hinders the direct current flow; whereas the close packing of

current lines at the Luggin tip leads to a current cut-off and short-circuiting due to the high impedance of the liquid in the connecting bridge (narrow tubing) of RE (Oldham and Stevens, 2000). Shielding is an issue when the WE is very small (≤ 1 cm^2), which is not the case in the present study. Hence, it can be concluded that short-circuiting is the reason for the distortion in the present case. This distortion was avoided by keeping the RE at a distance of at least twice the diameter of the Luggin probe tip and inserting a platinum wire at the tip (connecting the solution inside the narrow tubing and the solution in the beaker) as shown in Figure 5.5 (a) and (b).
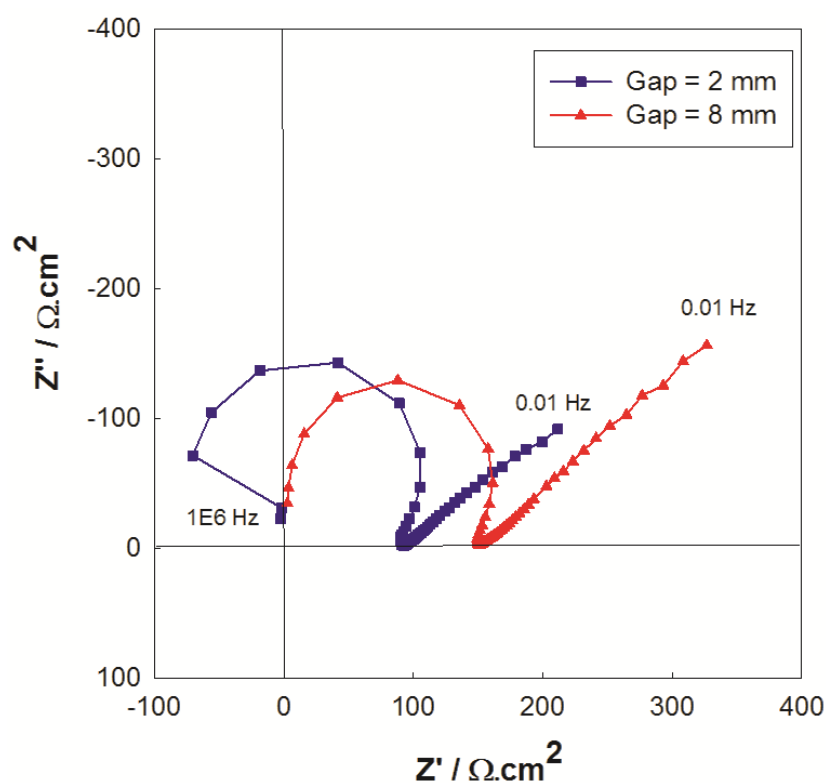
Figure 5.3 Effect of positioning of reference electrode on the Nyquist plot
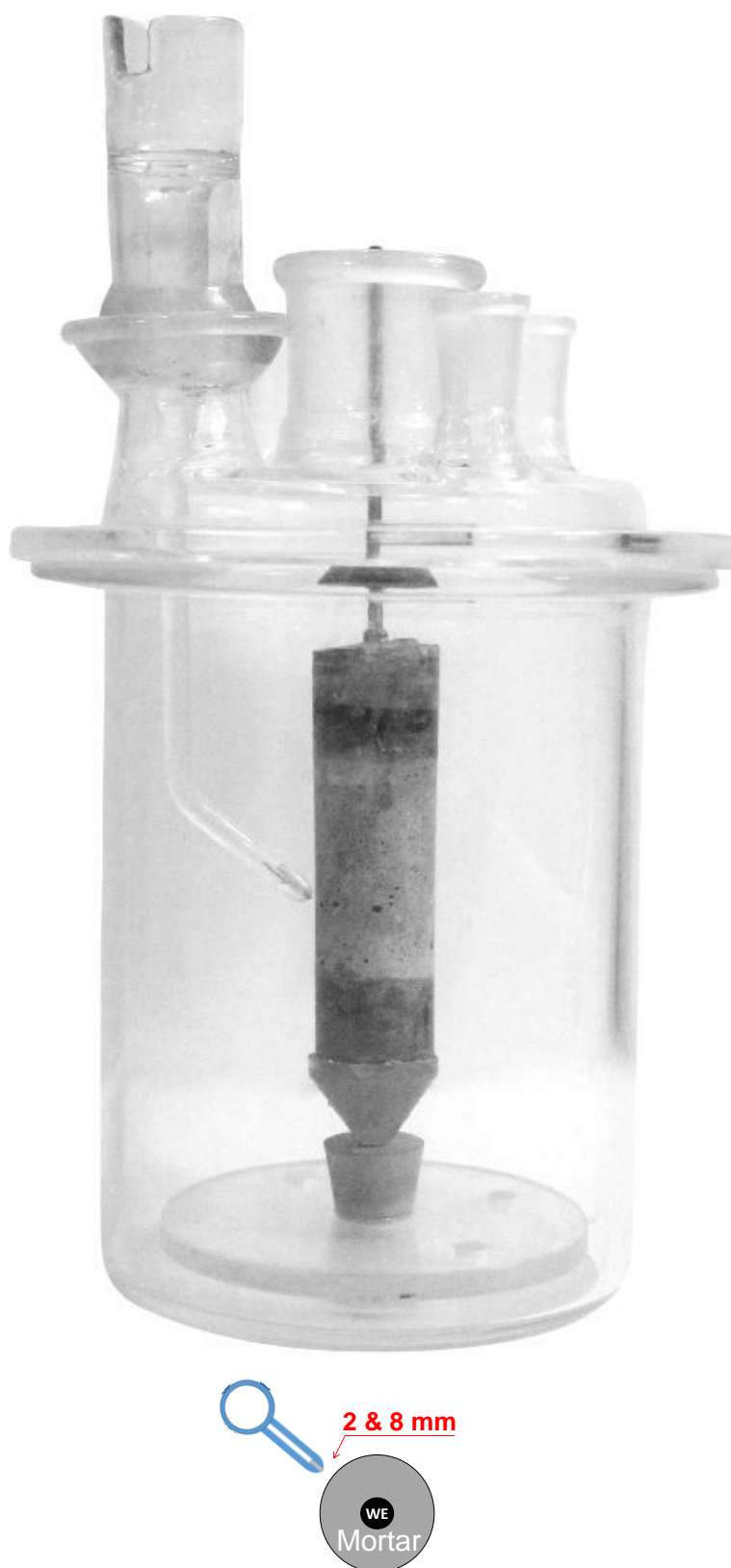
Figure 5.4 Positioning of luggin probe in the test beaker (counter electrode is not shown for clarity)
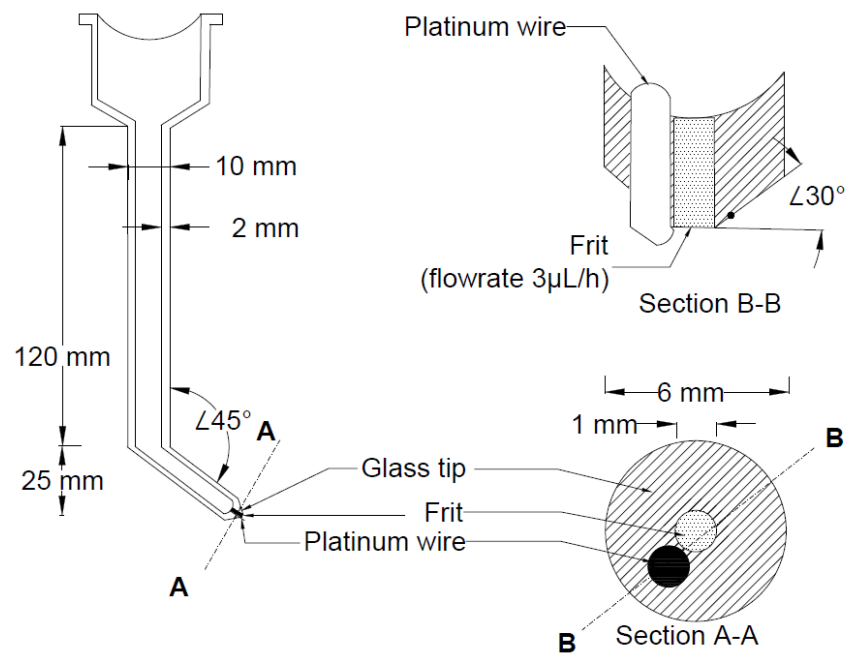
(a)
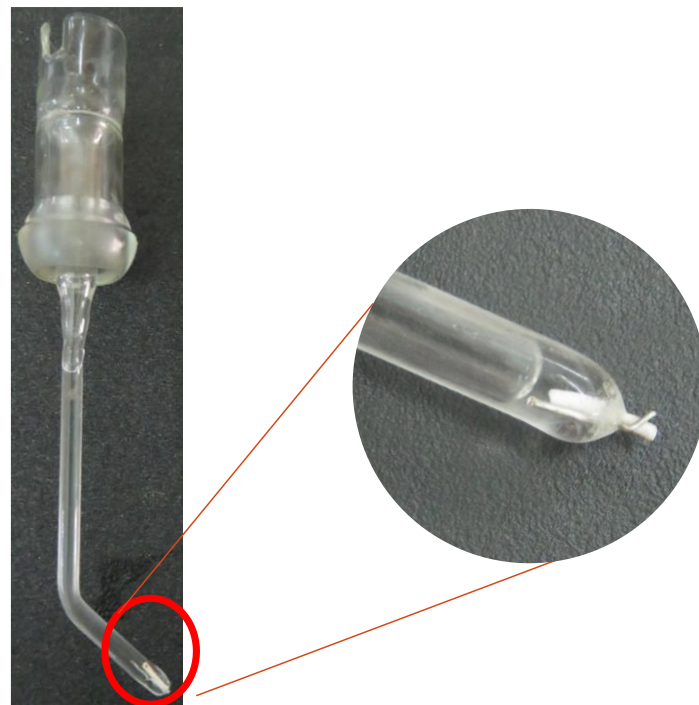
(b)

Figure 5.5 Luggin probe with platinum tip (a) Schematic and (b) Photo

5.2.2.3 <u>Effect of AC amplitude and frequency range</u>

Figure 5.6 (a) and (b) shows that as the AC amplitude increases from 10 to 50 mV, the radius of the semi-circular region (in high frequency region) decreases in both S-S and S-B systems. This electrochemical shift to non-linear region is in agreement with the literature (Victoria and Ramanathan, 2011). However, the low frequency tails of the EIS spectra from the S-S (about 1000 Hz) and S-B systems (about 10 kHz) coincide and do not change with amplitude. This coincidence is due to the high resistance of the passive film against the diffusion of species from solution in S-S systems.

In the case of S-B systems, this resistance is mainly offered by the highly resistive mortar surrounding the steel. This ohmic resistance is unaffected by change in amplitude (Szymczewska et al., 2015). Also, when the passive film is present, the instantaneous corrosion rate do not change rapidly during the EIS test. The steel immersed in acidic solutions may not have passive film and may experience rapid change in instantaneous corrosion rate during the EIS tests, leading to a shift in the starting point of the low-frequency tail. Hence, in this study, the AC amplitude was kept at ±10 mV (peak-to-peak).
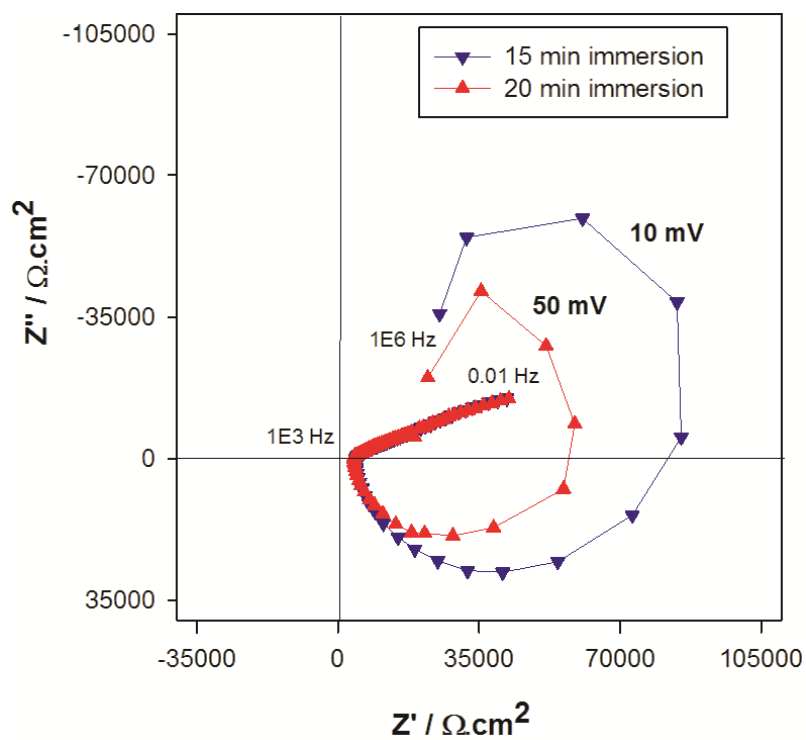
(a) Effect of AC amplitude in Steel-solution system
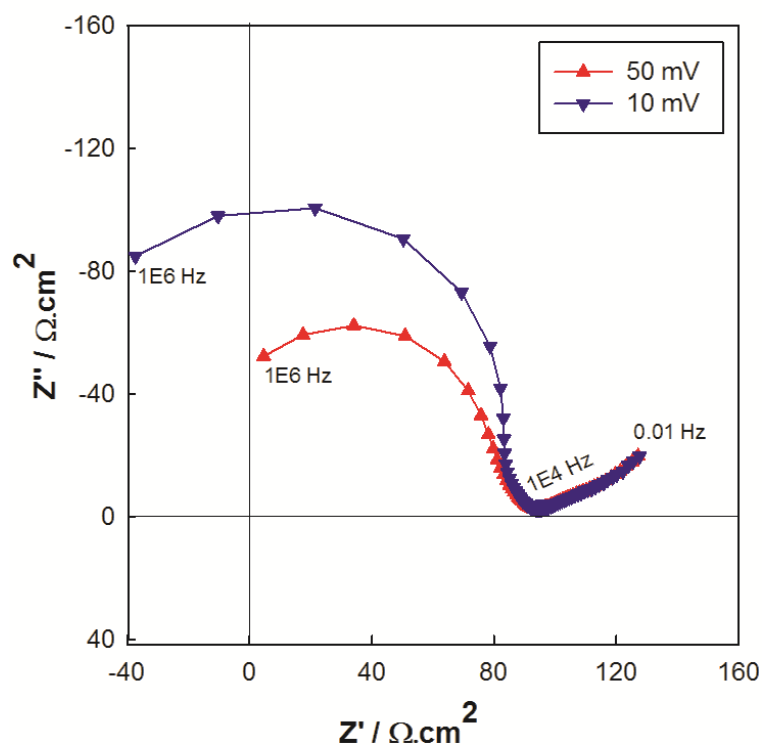
(b) Effect of AC amplitude in S-B system

Figure 5.6 Effect of various systems on the EIS response

119
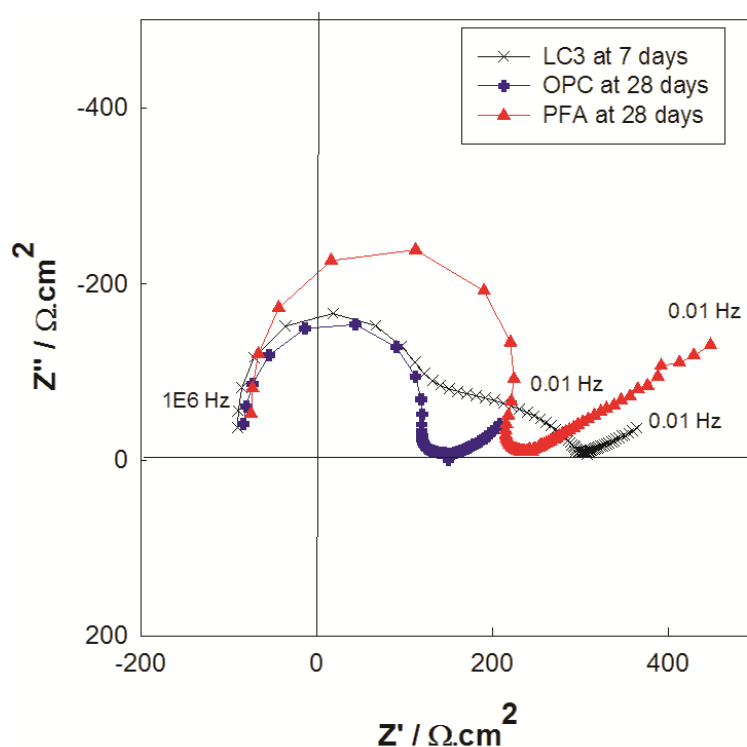
Figure 5.7 Effect of AC frequency on the Nyquist plot

5.2.3 Effect of the corrosion cell configuration

The effect of counter electrode size and annular and planar electrode configuration on the measured polarization resistance of PFA specimens are discussed next.

5.2.3.1 Effect of counter electrode size

Effect of anode-to-cathode ratio (size effect) on electrochemical measurements in S-B system were analyzed for multiple ratios. The size of the counter electrode (CE) were taken as two, eight and twenty times the size (surface area) of the working electrode for this study. Figure 5.8 shows the R_p measured when different CE sizes were used. The R_p reduces as the CE size increases. However, change in the R_p value is not significant enough with the increase in size of CE in all the specimens. Hence, no conclusions can be made out of this test. In order to avoid the rate limiting step due to the CE size, it is recommended that the CE should be at least twice the area of the surface of the working electrode.

120
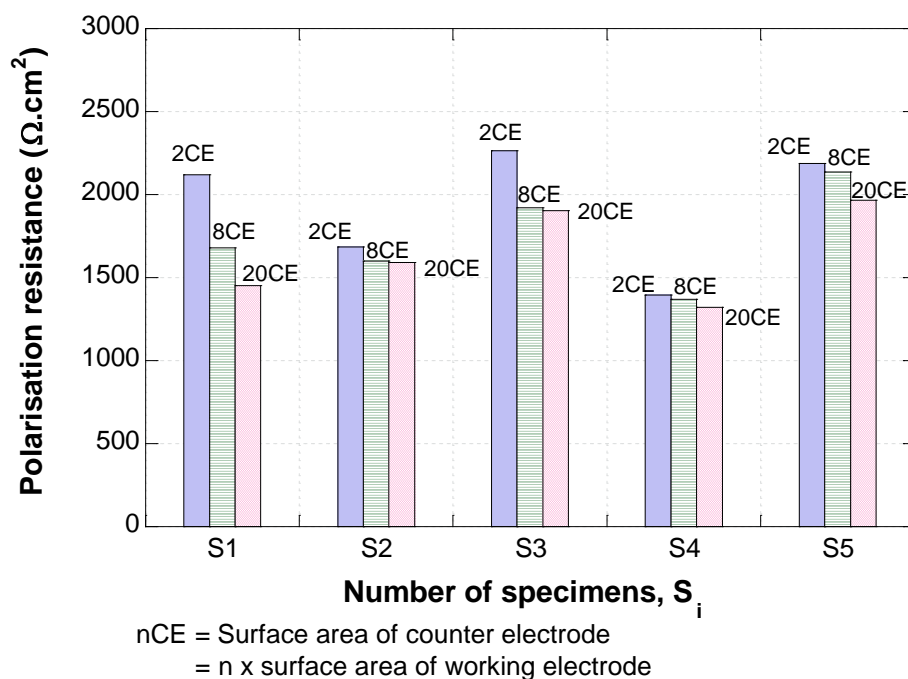
Figure 5.8 Effect of counter electrode size on polarisation resistance

5.2.3.2 Electrode configuration

The effect of positioning of CE on electrochemical measurements in S-B system were analyzed for planar and annular geometry using EIS. Figure 5.9 shows the effect of geometry when the same specimen (lollipop) was kept in annular and planar geometry. The trend in all the specimens is not the same when the electrode configuration was changed from annular to planar. In general, there was a slight increase in R_p when the same CE size was changed from annular to planar geometry. However, literature suggests to have symmetrical arrangement in order to have uniform distribution of current and acquisition of electrochemical response due to pitting as in case of chloride induced corrosion.
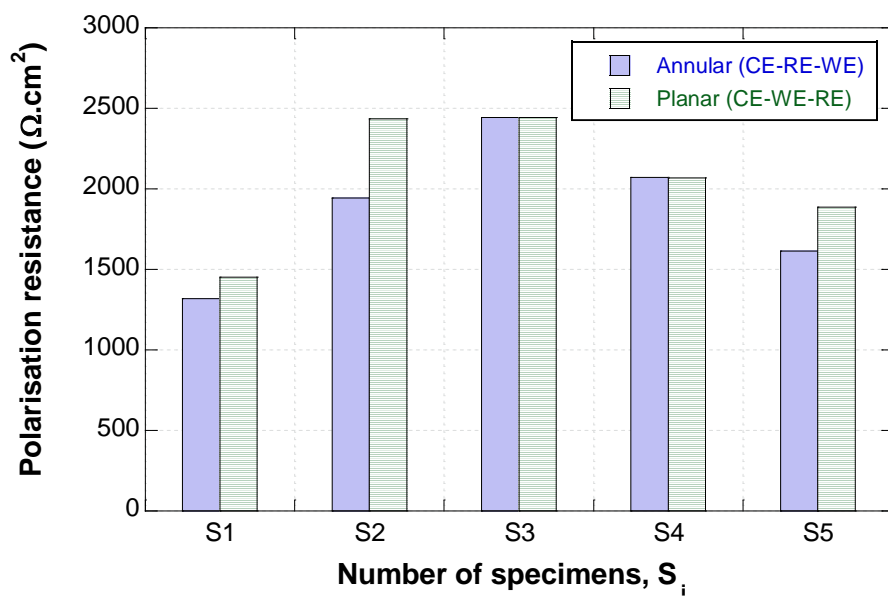
Figure 5.9 Effect of counter electrode position on polarisation resistance

5.3 SUMMARY

This chapter presented the effect of various input parameters of the LPR and EIS techniques on the polarization measurements. The effect of cell configuration on the polarization value was also provided. From this study, the input parameters and electrode configuration for Cl_{th} testing were chosen to minimize the errors due to high resistivity and positioning of electrodes in the corrosion cell.

CHAPTER 6

'hr-ACT' TEST METHOD AND CHLORIDE THRESHOLD OF

STEEL-BINDER SYSTEMS

6.1 INTRODUCTION

This chapter presents the results of the experimental program to determine the Cl_{th} of steel embedded in highly resistive binders. This chapter also presents the role of resistivity of binders in the electrochemical response while determining the Cl_{th}. Then, the EIS response and equivalent electrical circuit used to determine R_p are explained in detail. The Cl_{th} obtained after the testing is also presented. Then, the detailed procedures of the developed 'hr-ACT' test is presented.

6.2 CHLORIDE THRESHOLD TESTING USING "HR-ACT" TEST METHOD

This section provides the results of the experimental program as described in the Subsection 3.6. The input parameters were chosen and the corrosion cell parameters were optimized based on the results of the Objective 2. The specimens were tested using EIS by over siding a perturbation signal of ±10 mV (peak-to-peak) amplitude at OCP and by sweeping the frequency from 100 kHz to 0.01 Hz. The data was collected at 10 points per decade.

6.2.1 EIS response

Figure 6.1 shows the typical Nyquist plots in OPC and PFA1 (low resistivity with w/b 0.5), PFA2 (moderate resistivity with w/b 0.4), and LC3 (very high resistivity with w/b 0.5) specimens. For better clarity, the Nyquist plots in OPC, PFA1 and PFA2 specimens are shown separately as an inset in Figure 6.1. There is a huge variation in the measured R_m in these systems due to their resistivity. This remarkable difference in resistivity, especially in LC3 could have led to a distortion of the electrochemical response from LPR tests. The

summation of high resistance from cover (R_m) and the polarization resistance of steel (R_p) in LC3 systems results in high measured values for combined (R_m+R_p) response, irrespective of ongoing corrosion. Note that LPR technique cannot differentiate the R_p and R_m from the combined (R_m+R_p) response. Because of these, the reduction in R_p due to the initiation of corrosion could not be detected adequately. In the case of EIS technique, the contribution of resistance from each component can be obtained with the help of a suitable equivalent circuit and fitting – helps in separately monitoring the reduction in R_p and detecting corrosion initiation. Another advantage of EIS technique is that the correctness of the electrochemical response can be verified using Kramer-Kraig Transform (KKT). Once verified with KKT, the R_p can be obtained by extracting the value from the equivalent electrical circuit fit.
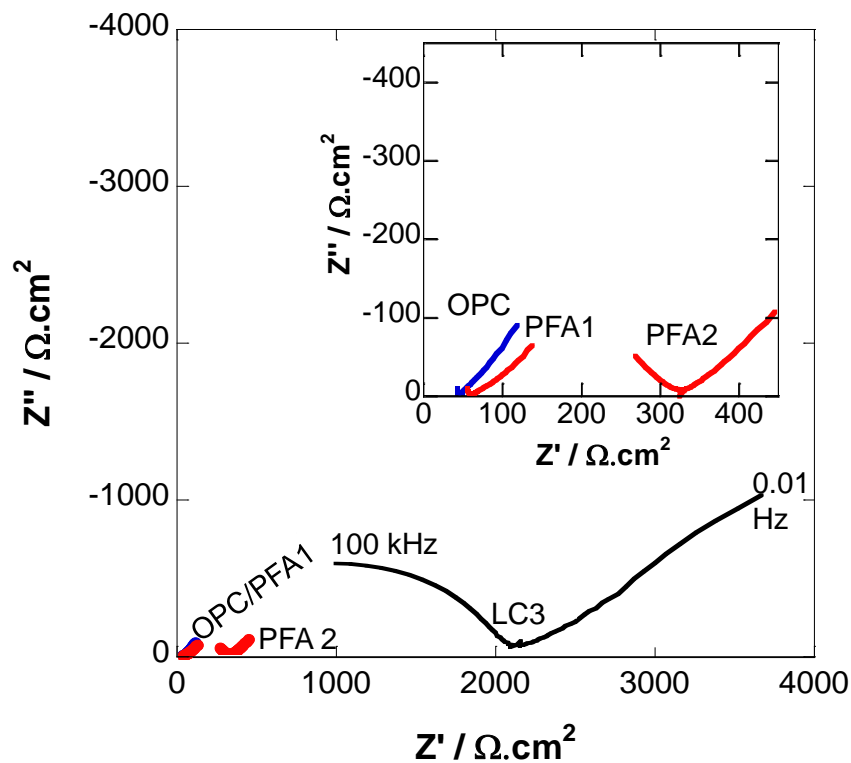
Figure 6.1 Typical Nyquist plot of OPC, PFA, and LC3 specimens

6.2.2 Equivalent electrical circuit

Figure 6.2 (a) shows the typical equivalent electrical circuit used for EIS analysis for obtaining the value of R_p. Typical response and fit of EIS data from steel embedded in LC3 system are shown in Figure 6.2 (b) and (c).

where R_m = Resistance of mortar
$R_{interface}$ = Resistance of double layer
R_p = Polarisation resistance of steel
C_m = Non-ideal capacitance of mortar
C_{dl} = Non-ideal capacitance of double layer
C_{pf} = Non-ideal capacitance of passive film

(a) Equivalent circuit

(b) Nyquist plot

(c) Bode plot
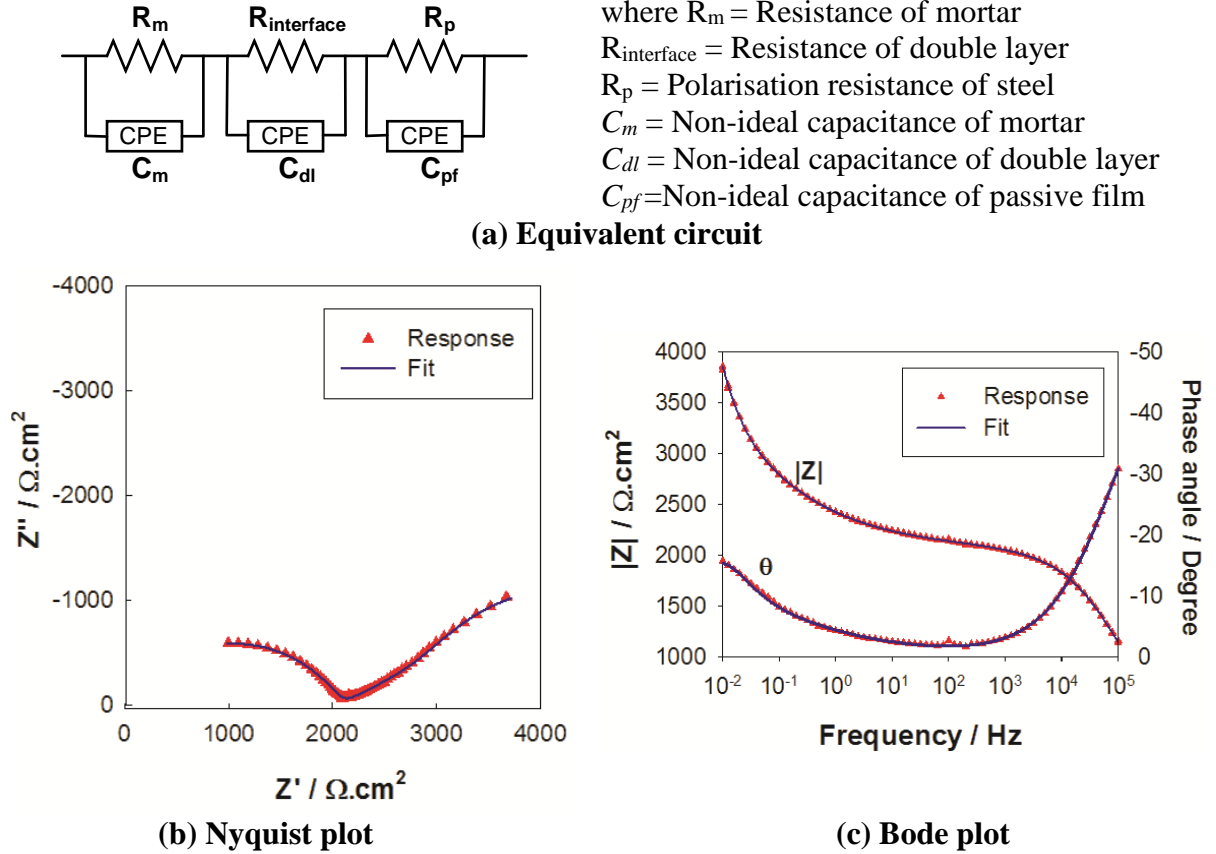
Figure 6.2 Chosen equivalent circuit and typical circuit fits in LC3

In Figure 6.2(a), the resistance (R_m) and constant phase element-CPE (C_m) represent the mortar cover, the $R_{interface}$ and C_{dl} (non-ideal capacitive nature of double layer represented as CPE) represent the S-B interface, and the R_p and C_{pf} represent the porous electrode (non-ideal passive film on the steel surface, represented as CPE). With the circuit analysis, keeping the chi-squared value less than 0.001 and error of the individual components less than 20%, the R_p of steel can be obtained separately.

The frequency spectra obtained from PFA and LC3 systems deviate from the conventional spectra revealing a diffusion process (negative slope of the 45° phase - conforming to Warburg type elements) obtained in OPC systems. This is mainly due to the difference in the geometry of the pore structure and tortuosity between these systems (Cooper et al., 2017). The PFA and LC3 systems have very small refined pores, which lead to greater tortuosity than the OPC systems with straight and bigger open pores (Dhandapani et al., 2017). Since there is a deviation in the low-frequency region from 45°, the conventional Randles circuit cannot be used to model the equivalent circuit for highly resistive S-B systems. In this study, the response from all the S-B systems is modelled as a porous electrode, as shown in Figure 6.2 (a), irrespective of the difference in resistivity in the specimens.

6.2.3 Detection of corrosion initiation

Determination of Cl_{th} is essential for the estimation of service life, for which repeated measurements of R_p of steel embedded in the hardened cementitious system are required until the corrosion initiation criteria is met. Figure 6.3 shows the difference in R_p obtained from LPR and EIS in lollipop specimens from OPC, PFA and LC3 specimens along with the visual observation of the corrosion spots in the specimens.

In this study, a statistically based initiation criteria was adopted as explained in Subsection 3.5.5. First a stable data was identified, where the $1/R_p$ readings of five consecutive measurements were within $\mu \pm 1.5\sigma$. The stable data is represented as filled markers in Figure 6.3. Corrosion initiation is detected when the $1/R_p$ reaches a value higher than $\mu + 3\sigma$ and is represented by big hollow square on the marker in Figure 6.3. In LC3 systems, due to the high R_m, the LPR technique could not detect the corrosion as soon as it was initiated. The earlier corrosion initiation was justified with the observation of a deep pit, which would take several days to form, under the given experimental conditions.

126

Corroded region
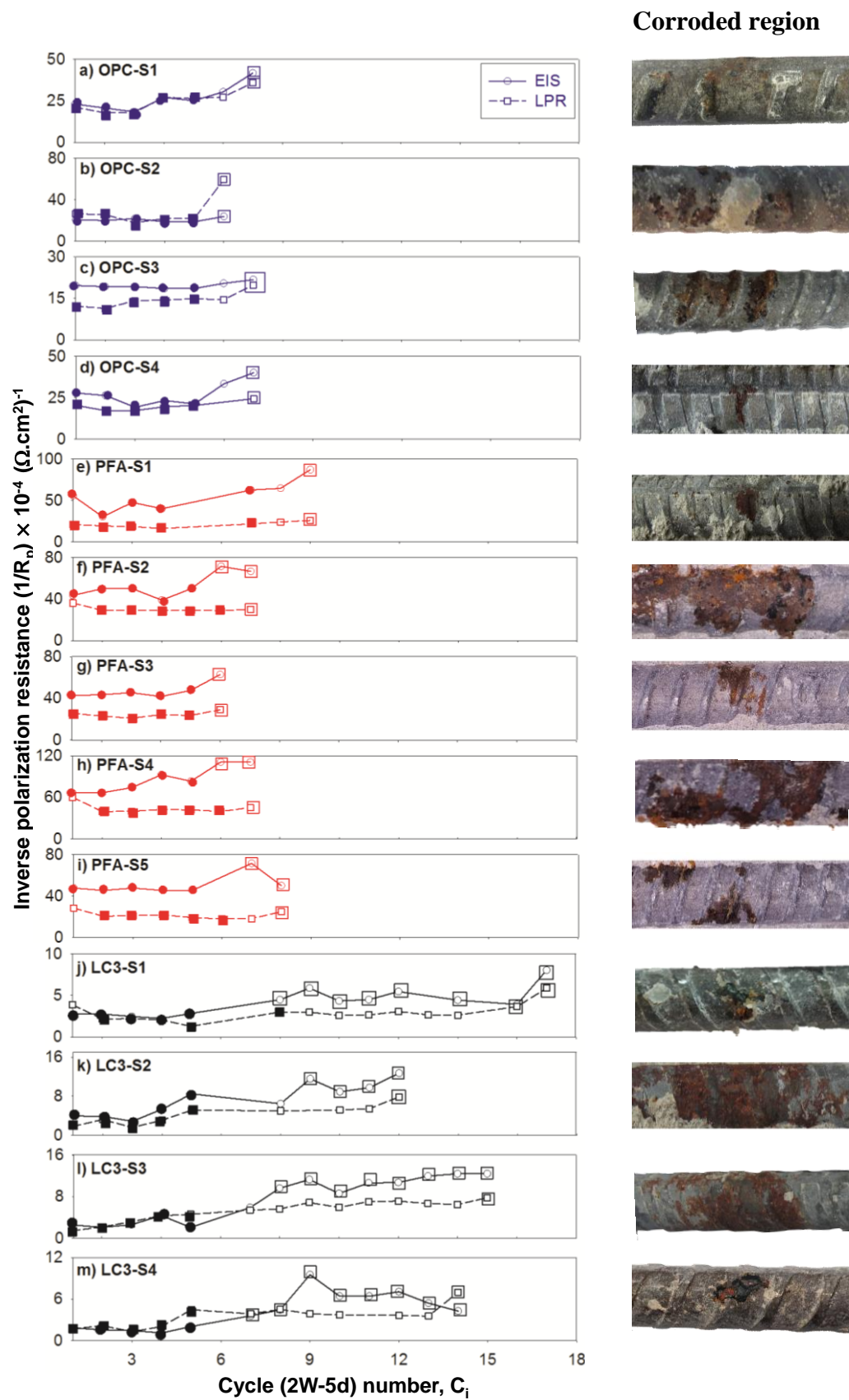
Figure 6.3 Electrochemical response from EIS and LPR techniques and visual observation from OPC, PFA, and LC3 specimens

Figure 6.4(a) shows the photograph of the corrosion pit and Figure 6.4(b) and (c) show longitudinal and cross-sectional tomographic image of the corrosion pit observed when autopsied. The analysis of the pit dimensions indicated a cross sectional loss of about 4% at that section of the rebar. This kind of deep pit cannot form in a single exposure cycle indicating that the LPR data could not detect the ongoing corrosion as soon as it was initiated. The LPR technique can detect corrosion only when the resistivity of the mortar cover is low.

| (a) | (b) | (c) Section A-A |
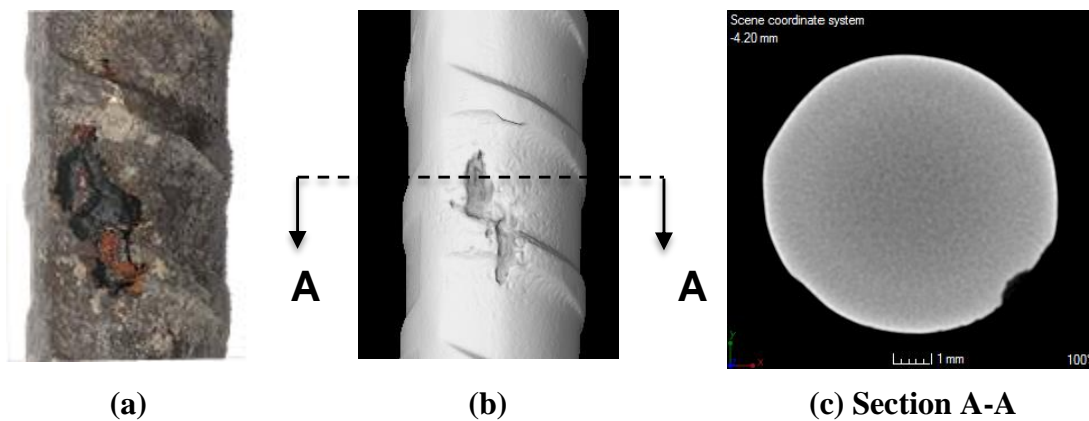
Figure 6.4 (a) Photograph, (b) and (c) tomographic image showing deep pit in LC3.

In OPC and PFA specimens, due to lower resistivity of cover in the early ages of testing, LPR and EIS techniques did not have a significant variation in the corrosion initiation time. In OPC specimens, both LPR and EIS techniques detected corrosion initiation in the same number of cycles for all the specimens. In PFA specimens, some of the specimens (S2, S4, and S5) had one cycle delay in the detection of corrosion initiation using LPR when compared to EIS. However, this is not the case with highly resistive LC3 systems. Table 6.1 gives the number of testing cycles taken to detect the corrosion initiation when LPR and EIS techniques were used in LC3 specimens. The EIS technique detects corrosion at early stages itself, which is not the case with LPR in highly resistive systems. LPR technique is able to detect corrosion only at later stages when the R_m reduces to 'low'

value, probably due to the significant increase in chloride concentration. Thus, in highly

resistive cementitious systems (say, $\rho > 37$ kΩ.cm), for the adopted test parameters and cell

geometry, the EIS technique suits better for early detection of corrosion initiation.

Table 6.1 Number of cycles to detect corrosion initiation in LC3 using LPR and EIS tests

Specimen Number	Number of cycles to detect corrosion initiation		
	LPR	**EIS**	**Difference**
S1	17	7	10
S2	12	9	3
S3	15	8	7
S4	14	7	7

6.2.4 Determination of chloride threshold

Figure 6.5 shows the Cl_{th} -values obtained for the OPC, PFA and LC3 binders. The lollipop

specimens were autopsied and the mortar powder was collected from the S-B interface. The

acid soluble chloride content was found using SHRP 330 method. As in the earlier test, the

highest mean value of Cl_{th} is obtained for OPC (i.e., 0.4% by weight of binder) followed

by PFA and LC3 systems are less, which is in agreement with the literature (Bentur et al.,

1997; Dhandapani and Santhanam, 2018). The pozzolanic reactions appear to decrease the

Cl_{th} while they increase the ionic resistance and decrease chloride transport. It is to be noted

that the mean value for LC3 is smaller than that for OPC and PFA, and hence, it creates an

illusion that scatter for LC3 is insignificant.
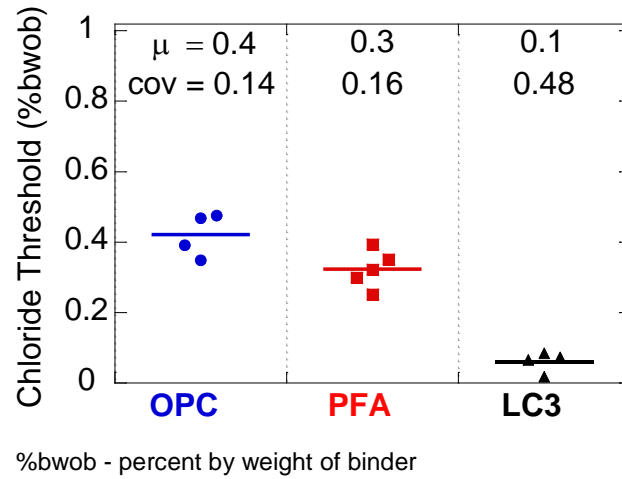
Figure 6.5 Cl_{th} for corrosion initiation of the rebar in OPC, PFA, and LC3 mortar

Figure 6.6 shows the initial pH found after 28 days (Dhandapani and Santhanam, 2018) and the final pH after the specimen is autopsied for determining the Cl_{th}. The mortar powder (1 gm) was collected at the interfacial region and was diluted with mortar to distilled water as 1:5. The pH meter was directly immersed in the solution to get the pH values. There is a decrease in the pH, which could be due to the buffering action of $Ca(OH)_2$ at the interface. The chloride-induced corrosion produces hydrochloric acid as an intermediate product, which reduces alkalinity. To compensate the alkalinity at the interface, $Ca(OH)_2$ dissolution takes place and OH^- ions moves towards the sites of reduced alkalinity. This buffering action will take place depending on the availability of $Ca(OH)_2$. In the blended systems, the buffering action will be less as they consume $Ca(OH)_2$ during the early age of the hydration for pozzolanic reaction. This could be the reason for reduction of pH at the interface after the chloride attack.
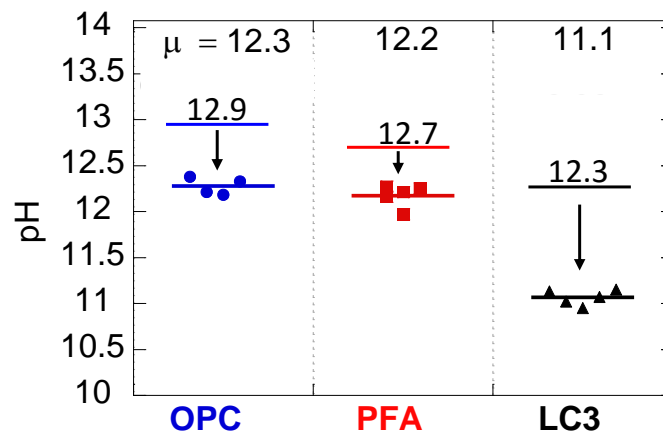
Figure 6.6 pH before and after corrosion initiation in OPC, PFA, and LC3 mortar

6.2.5 Finalized procedure for "hr-ACT" test method

The procedure to be followed for determination of Cl_{th} of steel embedded in highly resistive binders is explained in detail as follows.

6.2.5.1 Specimen preparation

1. Cut the steel specimen (8 mm diameter) each of length 100 mm using a coolant to ensure that the edges of the rebar are not affected.

2. A 4 mm thread is done at the center of the 8 mm steel rebar by means of drilling and threading.

3. The rebar is cleaned using an ultrasonic cleaner with the help of mild reagent ethanol until no visible rust products are seen.

4. A stainless steel fully threaded rod is connected to the 8 mm rebar.

5. Neoprene tube of sufficient thickness is used to seal the junction of stainless steel and steel rebar to prevent galvanic corrosion. Neoprene tube should extend up to 10 mm inside covering the steel rebar

6. Epoxy is used to fill the gap between the neoprene tubing and the stainless steel rod to prevent moisture and oxygen.

7. The steel specimen is allowed to cure until the epoxy coating is set and tack-free.

8. Mortar (0.5:1:2.75) is prepared and lollipop specimen is cast as shown in Figure 6.7.
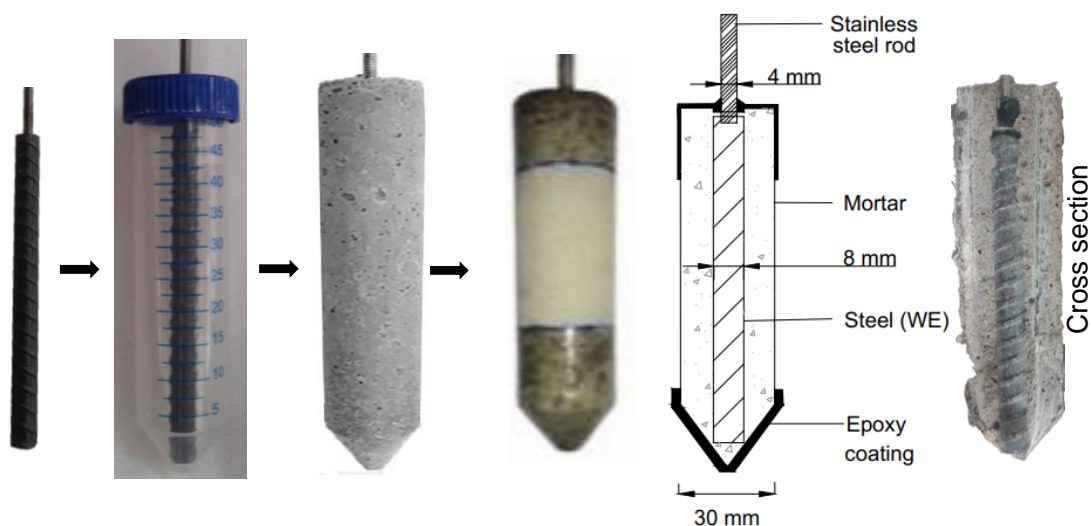
Figure 6.7 Lollipop casting – step-by-step procedure and cross section

9. The specimen is demoulded using the hot air blower and cured for 28 days in mist room.

10. After 28 days of curing, the external surface of the specimen is epoxy coated leaving 50 mm at the middle as shown in Figure 6.7. The bottom conical portion is dipped in epoxy to ensure thicker coating to avoid corrosion due to smaller cover thickness. The specimen is left for three days to dry completely.

11. The specimens are subjected to the cyclic wet-dry regime (2 days wet and 5 days dry) in simulated pore solution with 3.5% NaCl.

6.2.5.2 Monitoring of electrochemical response

The EIS response is recorded by over siding a perturbation signal of ±10 mV (peak-to-peak) amplitude at OCP and by sweeping the frequency from 100 kHz to 0.01 Hz. The data should be collected at 10 points per decade. Once the EIS response is collected, the R_p of steel is calculated by fitting the equivalent circuit. The equivalent circuit should be chosen

according to the system in testing. The procedure for fitting the equivalent circuit is explained in the Appendix E.

6.2.5.3 Failure criteria

The $1/R_p$ is treated for the statistical procedure as described next. Once five consecutive repeated readings are taken, mean (μ) and standard deviation (σ) of the five readings are calculated. Each of the five readings ($1/R_p$) is checked whether it is less than $\mu + 1.5\sigma$. If this criteria is satisfied, then the data are considered as stable data. If this criteria is not satisfied, then the testing is continued and ($1/R_p$) reading of the next cycle is taken. Once this reading is taken, the latest five readings (6th, 5th, 4th, 3rd and 2nd $1/R_p$) are tested for stable data. Repeated readings are taken and tested till stable data are generated. Once stable data are generated, the values μ_{st} and σ_{st} of the stable data are calculated. The measurement of $1/R_p$ is repeated till $1/R_p$ exceeds $\mu_{st}+3\sigma_{st}$. Figure 6.8 shows the flowchart of the test procedure for determination of Cl_{th}.

6.2.5.4 Determination of chloride content

The specimens which attained the failure criteria are autopsied into two pieces through the center. Then, the steel specimen is taken out and the mortar powder is collected from the S-B interface by Dremel tool. Then, the powder sample of 1.5 g is digested using 10 ml of digestion solution, (a mixture of 60 g of acetic acid, 50 g of isopropyl alcohol, and 940 g of distilled water) and stabilized by the addition of 40 ml of stabilizing solution. The stabilizing solution is prepared by the combination of 40 ml of the mixture containing 0.1545 grams of NaCl and 1 liter of distilled water with 960 ml of distilled water. The chloride specific ion probe is calibrated for millivolt readings with known chloride concentrations. Then, the millivolt readings for the final solution are converted mathematically into equivalent total percent chloride content. The acid soluble chloride as

found by chloride ion (ion selective) probe is reported as the chloride threshold (%by weight of binder).

Cast and cure the hr-ACT specimens for 28 days

Epoxy coat the specimens to restrict the exposure region and allow it to cure for 3 days

$t = 1$, $i = 0$, $n = 5$, sum=0, temp=0, μ=0, σ=0

Put the specimens in simulated pore solution containing 3.5% NaCl for 2 days

Connect the specimen to electrochemical workstation

Record the OCP and EIS response

Choose equivalent circuit

Calculate R_p by fitting the Equivalent circuit

Dry the specimen for 5 days

Is μ!=0 && σ!=0? — No — Is $t >= n$? — No — $t = t + 1$

Yes

Yes

$i = (t-n)+1$

$$Sum = Sum + \frac{1}{R_p^i}$$

i++

Is $i > t$? — No

Yes

$\mu = \frac{Sum}{n}$

$i = (t-n)+1$

$$temp = temp + \left(\frac{1}{R_p^i} - \mu\right)^2$$

i++

Is $i > t$? — No

Yes

$$\sigma = \sqrt{\frac{temp}{n}}$$

$i = (t-n)+1$

Is $(1/R_p)^i < (\mu + 1.5 \times \sigma)$? — No — μ=0; σ=0; i=0, sum=0, temp=0

i++

Yes

Is $i > t$? — Yes

No

Is $(1/R_p)^t > (\mu + 3\sigma)$? — No

Yes

Autopsy the specimen and collect the mortar near steel-cementitious interface

Determine the chloride and defined as Cl_{th}

Figure 6.8 Flowchart explaining the procedure for hr-ACT test method

6.3 SUMMARY

This chapter presented the results of the chloride threshold testing. The challenges in the data interpretation using LPR technique due to high resistivity of S-B systems were reported. The difference between LPR and EIS readings and the level of pitting occurred due to the delayed detection of corrosion was highlighted. The chloride threshold was then presented as the percentage by weight of binder for the three binders, namely OPC, PFA and LC3. Finally, the hr-ACT test method was provided in the form of a flowchart for easy understanding.

CHAPTER 7

SERVICE LIFE ESTIMATION TOOLS AND SYNERGISTIC EFFECTS

7.1 INTRODUCTION

This chapter presents the service life of structures estimated with the help of MATLAB® program (named as "SL-Chlor") for a different type of binders. Further, the comparison of Life-365[TM] with the "SL-Chlor" for features and estimated service life are presented. Then, two hypothetical case studies are studied, which demonstrated the dependency of many influencing parameters on the service life. In addition, a set of nomograms for various exposure conditions are presented, which can help the engineers to choose the materials effectively for the desired design life with optimum cost.

7.2 ESTIMATION OF PROBABILISTIC SERVICE LIFE USING SL-CHLOR

A MATLAB® program was written to estimate the service life using the solution of Fick's 2nd law of diffusion as shown in the flowchart in Figure 7.1. Here, the chloride ingress is considered as one-dimensional. The parameters, clear cover depth (d), chloride diffusion coefficient at 28 days ($D_{Cl,28d}$), ageing coefficient (m), exposure condition, maximum surface chloride concentration $Cl_{s,max}$ and Cl_{th} are taken from the user as input. The parameters, the time for complete hydration, chloride build up rate (depending on the exposure condition), number of simulations, and maximum number of estimated years of service life (t_{max}) are assumed in the code as constant. Then random numbers are generated for d, $D_{Cl,28d}$ and Cl_{th}. Then, surface chloride concentration Cl_s is calculated for each year depending on the chloride build up rate. The detailed calculation of surface chloride concentration is given in Figure 7.2.
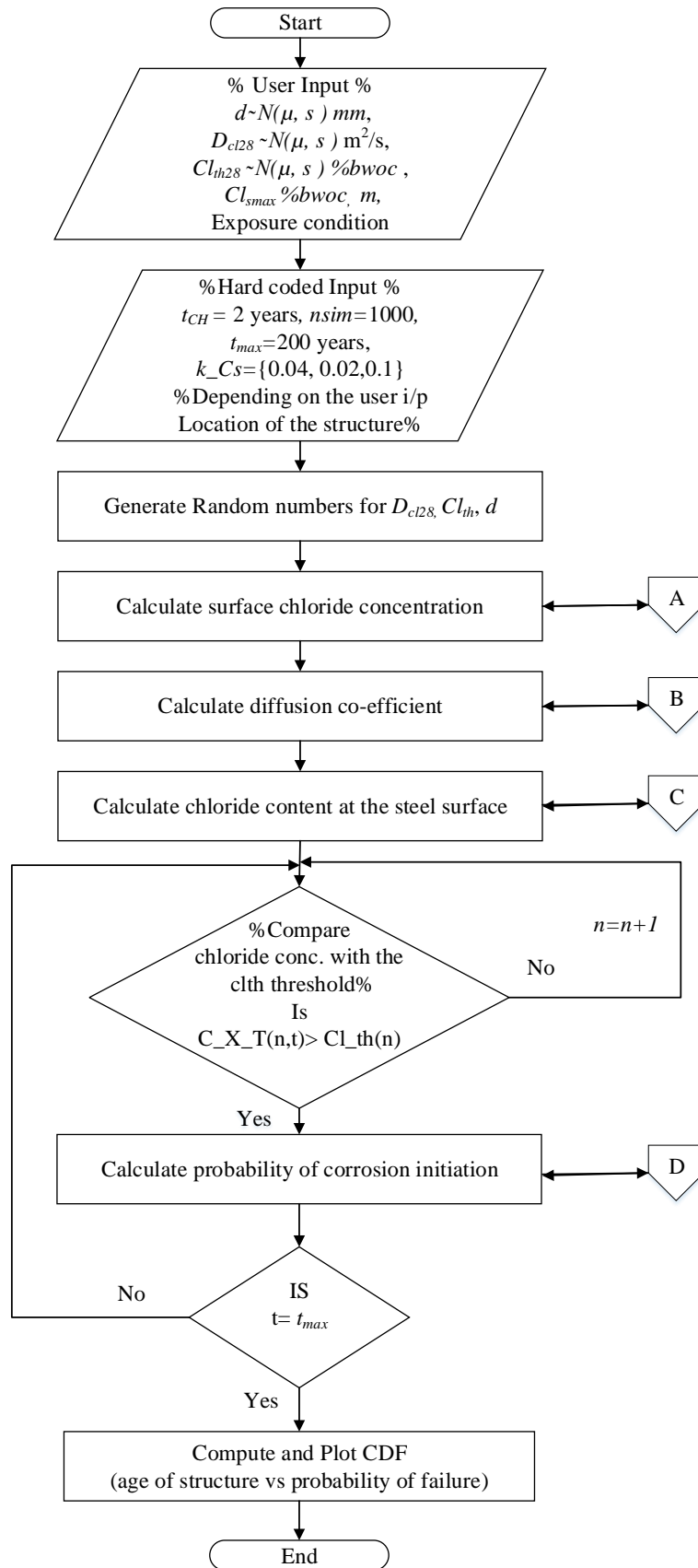
Figure 7.1 Flowchart for estimating service life of structure

Then, time-dependent D_{cl} is calculated as shown in Figure 7.3. Here, D_{cl} is considered to be decreasing as a function of time alone. Hence, the ageing factor m is considered. Then, chloride content is calculated using Crank's solution of Fick's law as shown in Figure 7.4, which is compared with the Cl_{th} for the t_{max}. Figure 7.5 gives the calculation of probability of corrosion, P_f. With the P_f, CDF is generated.

A

%Calculate surface chloride concentration%
$Cs\_t(t) = k\_Cs \times t$

$t=t+1$

Is $Cs\_t(t) >= C_{smax}$?   No

Yes

$Cs\_t(t) = C_{smax;}$

$t=t+1$

Is $t = t_{max}$?   No

Yes   t=1; $n=1$

Return
Cs_t(t)
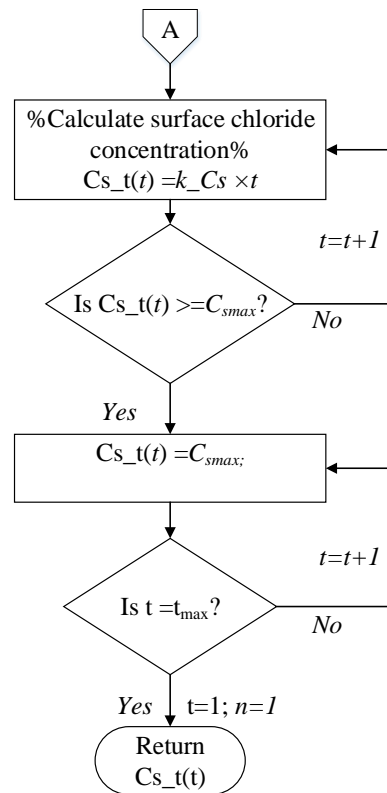
Figure 7.2: Sub-function to calculate surface chloride concentration
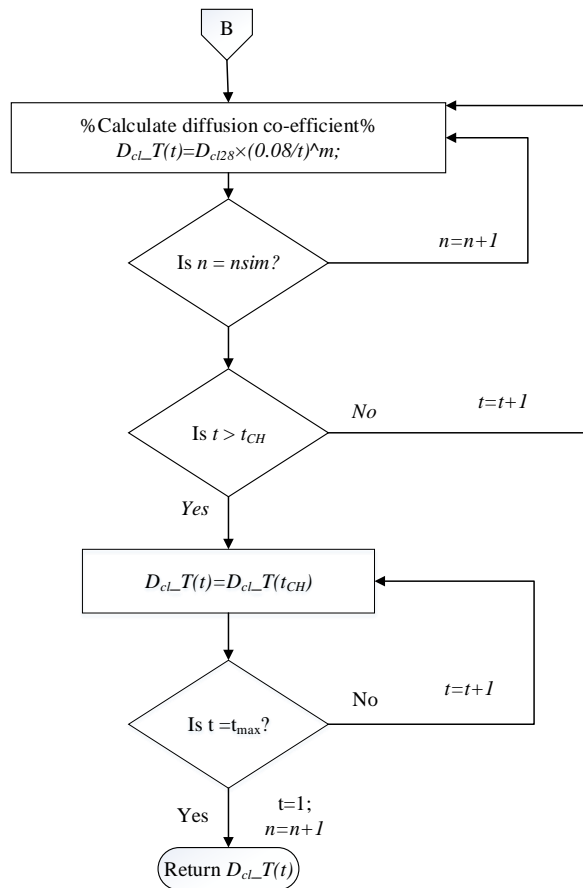
Figure 7.3 Sub-function to calculate time dependent chloride diffusion coefficient

C

$t=t+1$ && $n=1$

```
% calculation of error function%
time_S(t) = t × 365×24×60×60;
Denom(n,t)= 2×(sqrt(D_cl_T(t)× time_S(t)
Erfc_Calc(n,t) = erfc(cd/Denom(n,t));
C_X_T(n,t) = C_S_t(t) × Erfc_Calc(n,t);
```

Is n=nsim?

$n=n+1$

No

Yes

Is t =t_max?

Yes

$t=1;$
$n=1$

Return
C_X_T(n,t)
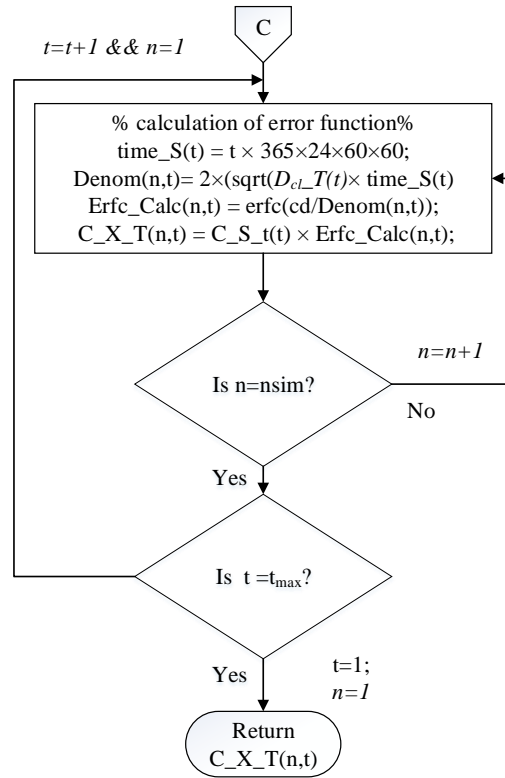
Figure 7.4 Sub-function to calculate chloride content on the steel surface

D

```
%Counting the no of
failures%
G(t) = G(t)+1
```

$i=2$

```
G_total(1)=G(1);
G_total(i) = G(i)+G_total(i-1)
```

Is
$i> t$

$i=i+1$

No

Yes

Pf(i)=G_total(i)/(nsim × i)

Return Pf(i)
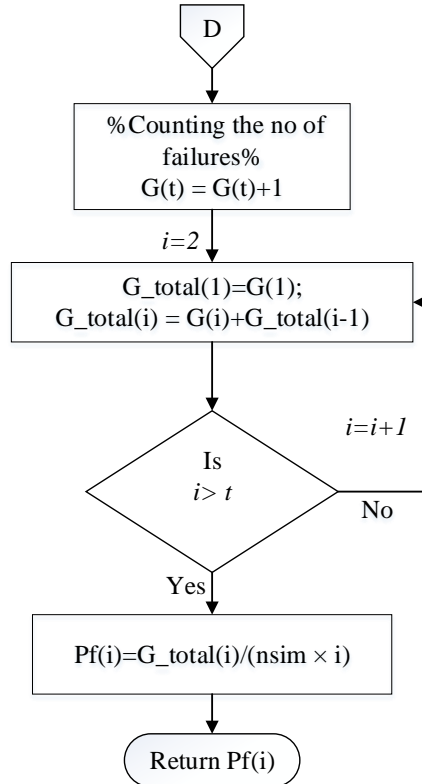
Figure 7.5: Sub-function to calculate probability for corrosion initiation

140

7.3 COMPARISION OF LIFE-365^{TM} AND 'SL-CHLOR' PROGRAMS

Life-365^{TM} is a user-friendly, popular tool for service life estimation. However, there are some difficulties in the service life estimation when using SCMs with ageing coefficient "m" of greater than 0.6. The effect of binders in decreasing the D_{cl} is underestimated in Life-365^{TM}. Nowadays, binders with ternary blends are widely used. These type of binders match the early-age strength of OPC with highly reactive SCM and evolve over time due to prolonged hydration with slowly reactive at the same time high performance SCM. Hence, a new tool has to be developed to account the ageing coefficient. Also, the coefficient of variation (cov) is taken as 25% by default for all the input parameters. Due to the variation in the material characteristics and site practices, cov can vary to a large extent. Due to these issues, SL-Chlor was developed. Table 7.1 gives the comparison of Life-365^{TM} and SL-Chlor.

Table 7.1 Comparison of Life-365^{TM} and SL-Chlor

S.No.	Life-365^{TM}	SL-Chlor
1.	Value of ageing coefficient "m" cannot be greater than 0.6	Any value of "m" can be input by the user
2.	The cov is predefined	The cov can be user-defined
3.	D_{cl} is considered as a function of time and temperature	D_{cl} is considered as a function of time alone
4.	The chloride ingress is considered as one-dimensional for slab and two dimensional for other RC elements, which is calculated by finite difference approach	The chloride ingress is considered one-dimensional for all the RC elements

Figure 7.6 shows the comparison of service life estimated using Life-365^{TM} and SL-Chlor. The service life calculated by Life-365^{TM} and SL-Chlor are comparable and follows the same trend, when the input parameters are same, if one-dimensional ingress is considered for a bridge pier.
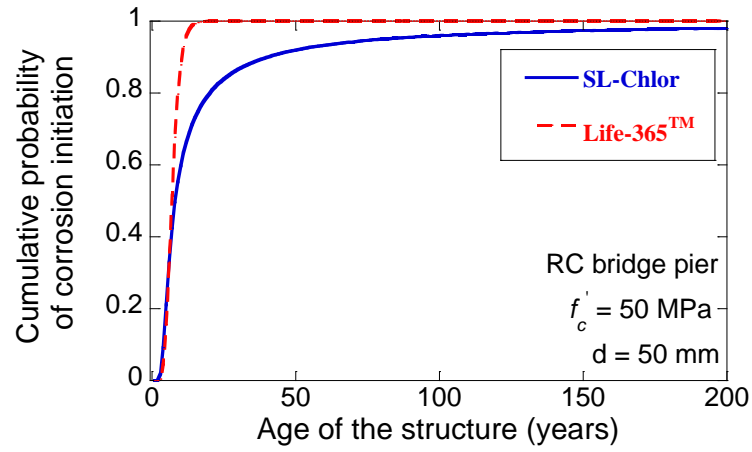
(a)
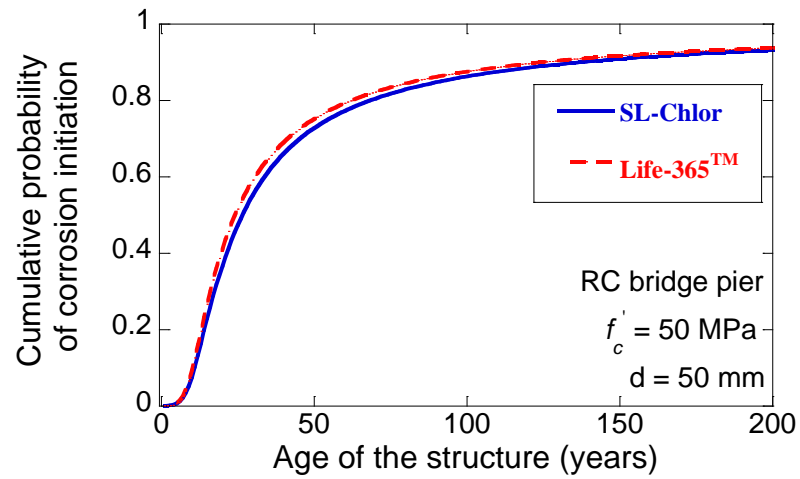
(b)
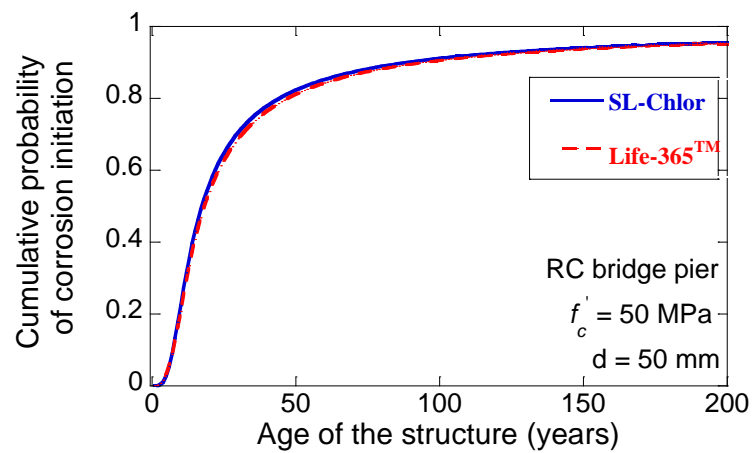
(c)

Figure 7.6 (a), (b) and (c) Comparison of service life estimated using Life 365™ and SL-Chlor in OPC, PFA, and LC3 respectively

7.4 CASE STUDIES

Two case studies related to typical RC bridges were performed to assess the effect of binder type and concrete proportions on the service life (defined as time to corrosion initiation). The surface chloride concentration (Cl_s) is related to the rate of build-up of chlorides on the concrete surface and the exposure conditions; here, the initial and maximum values of Cl_s were considered as 0 and 0.6 %bwoc; and the chloride build-up rate was assumed to be 0.04 %bwoc per year (considering the location of the bridge to be 800 m away from the ocean, on the Indian coast).

7.4.1 Case study 1 (Bridge pier)

Figure 7.7(a) shows the cross-section of a bridge pier. The pier is taken to be designed for a characteristic strength of 35 MPa, and consequently any of the M35 category concrete could be considered. When the service life is estimated for the concrete mentioned in Table 7.2 using the parameters given in Table 7.3 with the standard deviation of 25%, it yields the CDFs shown in Figure 7.7(c) for the four M35 concrete. If we consider a failure probability of 0.5 for comparison, it is seen that the bridge pier with 30 % fly ash concrete (PFA-1) can have a service life of approximately 30 years, which is 3 times longer than that of OPC (say, ≈ 10 years). When the same strength category mixes are compared (OPC- 1, PFA-1, LC3-1S), the concrete is able to deliver longer service life in the order (PFA-1 > LC3-1S > OPC-1). Here, LC3-1S and OPC-1 are having the same w/b (0.5) and PFA-1 is having lower w/b (0.45). It is to be noted that LC3-1P (same proportion as that of PFA) gives longer service life than its counterparts. The data of LC3-1P and LC3-1S indicate that it is possible to design LC3 concretes that can provide similar performance as that of concrete with PFA, despite the Cl_{th} being lower than that of OPC and PFA concretes.

All dimensions are in mm
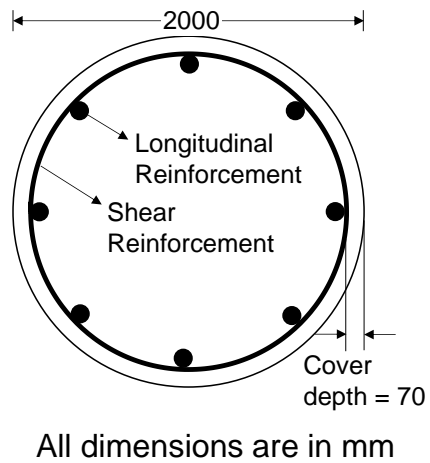
(a) Cross section of a typical bridge pier
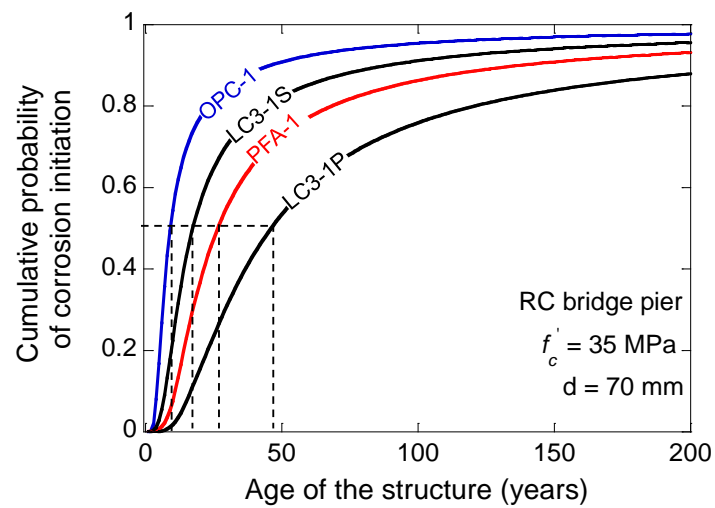
(b) Cumulative probability of corrosion initiation in bridge pier

Figure 7.7 Illustration of estimated service life of a bridge pier

Table 7.2 Mix design taken for case study (Pillai et al., 2018)

Ingredients of the concrete		M35				M50		
		OPC-1	PFA-1	LC3-1S	LC3-1P	OPC-2	PFA-2	LC3-2
Binder type		OPC	70%OPC + 30%PFA	LC3	LC3	OPC	70%OPC + 30%PFA	LC3
Binder content (kg/m^3)		310	360	310	360	360	380	340
Water content (kg/m^3)		155	162	155	162	144	133	136
Water-binder ratio		0.5	0.45	0.5	0.45	0.4	0.35	0.4
Fine aggregate content (kg/m^3)		695	721	708	687	703	699	704
Coarse aggregate content (kg/m^3)	10 mm	496	463	491	476	477	475	488
	20 mm	744	694	736	715	716	713	732

Table 7.3 Properties of the RC elements taken for case study (Pillai et al., 2018)

Input parameters	M35				M50		
	OPC-1	PFA-1	LC3-1S	LC3-1P	OPC-2	PFA-2	LC3-2
d (mm)	70	70	70	70	50	50	50
$D_{Cl,28d}$ ($\times 10^{-12}$ m^2/s)	36.5	21.1	11.9	5.1	24.1	7.8	6.8
m	0.26	0.7	0.5	0.53	0.17	0.55	0.54
$Cl_{th,}$ (% bwoc)	0.06	0.05	0.02	0.03	0.07	0.05	0.02

%bwoc - % by weight of concrete

7.4.2 Case study 2 (Bridge girder)

Figure 7.8(a) shows the cross-section of the RC bridge girder, with a cover depth of 50 mm. The M50 concrete considered in this case study are PFA-2, LC3-2, and OPC-2. Figure 7.8 (c) shows the CDFs of the corrosion initiation time, which indicates that the girder would have a service life of approximately 8, 25 and 19 years, for the OPC-2, LC3-2 and PFA-2 concrete, respectively, for P_f of 0.5.
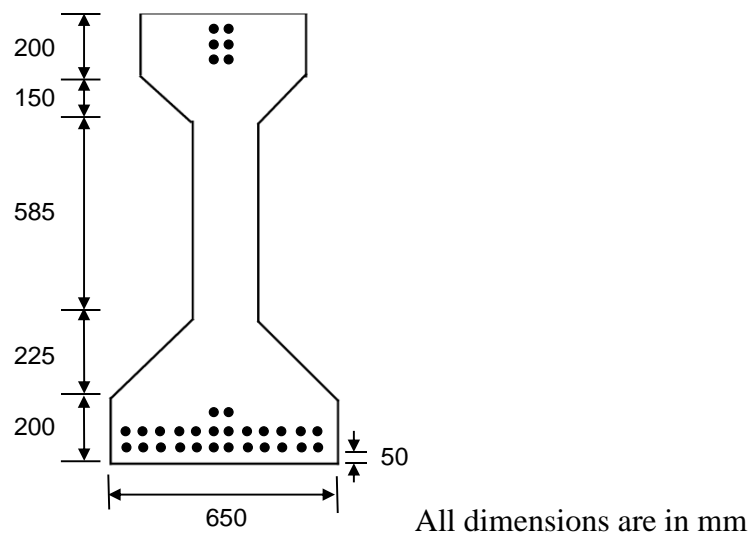
a) Cross-section of the AASHTO Type IV bridge girder
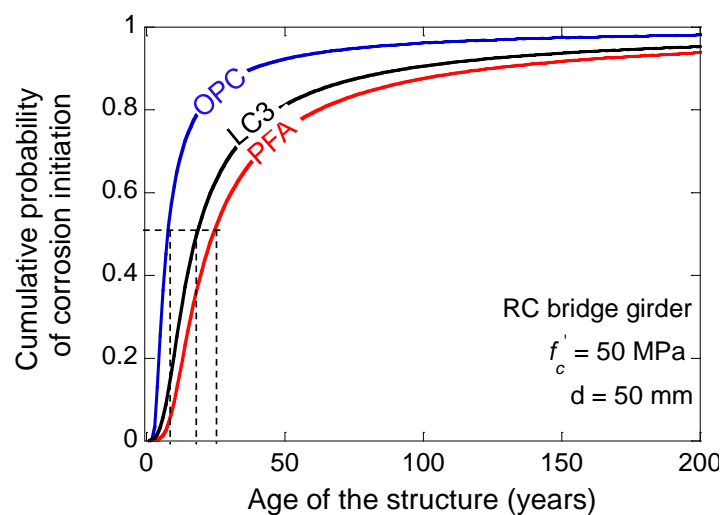
b) Cumulative probability of corrosion initiation in bridge girder

Figure 7.8 Illustration of estimated service life of a bridge girder.

It is to be noted that even though the Cl_{th} is higher for OPC, the service life with PFA and LC3 systems are longer than OPC. The potential of concrete made with LC3 in achieving longer service lives than concrete with OPC is substantiated by the results in Figure 7.8 (b). The difference in the service life estimates emphasizes the role of the binders, such as PFA and LC3, in enhancing the durability of concrete structures. The synergistic effect of various input parameters, namely D_{Cl}, m and Cl_{th} plays a crucial role in enhancing the service life. Lower D_{Cl} compensates the lower Cl_{th} in SCM based systems. The attainment of the Cl_{th} is delayed due to lower D_{Cl}. Thus, in estimating the service life, instead of emphasizing on one parameter, the synergistic effect should be considered.

7.5 NOMOGRAMS FOR PROBABILISTIC SERVICE LIFE

A set of nomograms were developed for the ease of the site engineers using the model explained earlier. Figure 7.9 shows the nomogram for estimating the service life of a structure, which is 800 m away from the seashore. Table 7.4 gives the value of m and Cl_{th} upon which the line numbers in the nomogram was developed. An example has been demonstrated to show the steps needed to arrive at the service life from the nomogram. For a given probability of failure and the chosen cover, concrete properties and type can be varied to a great extent to achieve the desired service life. Similar nomograms have been developed for other exposure locations, namely (i) 1500 m away from the sea (Figure 7.10), (ii) spray zone (Figure 7.11) and (iii) splash zone (Figure 7.12). This can help engineers to choose the materials effectively for the desired service life.

Table 7.4 Properties of various type of concrete

Line number to identify Point C.	Ingredients of concrete	m	Cl_{th} (%bwoc)
1	> 50% Slag/Fly ash + OPC + CIA	0.7	0.05
	< 20% Metakaolin/Fly ash +OPC + CIA	0.6	0.067
2	OPC + CIA	0.4	0.1
	> 50% Slag/Fly ash + OPC	0.7	0.02
	< 20% Metakaolin/Fly ash + OPC	0.6	0.05
3	(30-50%) Slag/Fly ash/ Metakaolin + OPC	0.6	0.02
	LC3 + CIA	0.5	0.05
	OPC; OPC+ Silica fume + CIA	0.4	0.067
4	LC3	0.5	0.02
	< 10% Silica fume + OPC	0.4	0.05
5	< 10% Silica fume + Metakaolin + OPC	0.4	0.02

CIA – Corrosion inhibiting admixture; OPC – Ordinary portland cement

d (mm)

10
20
30
40
50
60
70

B

A

C

Line Number - (Type of binder + CIA)

1 - > 50%Slag/FA + OPC + CIA;
< 20% MK/FA +OPC + CIA

2 - OPC + CIA;
> 50% Slag/FA + OPC;
< 20% MK/FA + OPC

3 - (30-50%) Slag/FA/ MK + OPC
LC3 + CIA; OPC + SF+ CIA

4 - LC3; < 10% SF + OPC

5 - < 10% SF + MK + OPC

0.6   0.5   0.4   0.3   0.2   0.1

Probability of corrosion initiation

Steps
1) Assume probability of corrosion initiation (A)
2) Choose cover and find the intercept (B)
3) Traverse right from B; choose binder property (C)
4) From C, move down and choose D_{Cl} (D)
5) Traverse left from D and navigate to y axis (E)
6) E is the corrosion-free service life for the chosen parameters

Assumptions
1) Chloride build-up rate = 0.04% bwoc
2) Max. surface Cl⁻ concentration = 0.6% bwoc
3) Duration of hydration = 2 years

CIA - Corrosion inhibiting admixture
d - Cover depth
D_{Cl} - Diffusion co-efficient
FA - Fly ash
LC3 - Limestone calcined clay cement
MK - Metakaolin
OPC - Ordinary portland cement
SF - Silica fume

Corrosion-free service life (years)

200
150
100
50
0

5   4   3   2   1

(i)   (ii)   (iii)   (iv)
(v)
(vi)
(vii)
(viii)(ix)
(x)
(xi)

E   D

(i) D_{cl}=1E-12m²/s   (v) D_{cl}=7E-12m²/s   (ix) D_{cl}=5E-11m²/s
(ii) D_{cl}=2E-12m²/s   (vi) D_{cl}=1E-11m²/s   (x) D_{cl}=1E-10m²/s
(iii) D_{cl}=3E-12m²/s   (vii) D_{cl}=2E-11m²/s   (xi) D_{cl}=5E-10m²/s
(iv) D_{cl}=5E-12m²/s   (viii) D_{cl}=3E-11m²/s

Figure 7.9 Nomogram for estimating service life of RC elements located 800 m away from the sea

Steps

1) Assume probability of corrosion initiation (A)
2) Choose cover and find the intercept (B)
3) Traverse right from B; choose m and Cl_{th} (C)
4) From C, move down and choose D_{Cl} (D)
5) Traverse left from D and navigate to y axis (E)
6) E is the corrosion-free service life for the chosen parameters

Assumptions

1) Chloride build-up rate = 0.04% bwoc
2) Max. surface Cl⁻ concentration = 0.6% bwoc
3) Duration of hydration = 2 years

CIA - Corrosion inhibiting admixture
d - Cover depth
D_{Cl} - Diffusion co-efficient
FA - Fly ash
LC3 - Limestone calcined clay cement
MK - Metakaolin
OPC - Ordinary portland cement
SF - Silica fume

Figure 7.10 Nomogram for estimating service life of RC elements located 1500 m away from the sea

150

Line Number - (Type of binder + CIA)
1 - > 50%Slag/FA + OPC + CIA; < 20% MK/FA +OPC + CIA
2 - OPC + CIA; > 50% Slag/FA + OPC; < 20% MK/FA + OPC
3 - (30-50%) Slag/FA/ MK + OPC; LC3 + CIA; OPC + SF+ CIA
4 - LC3; < 10% SF + OPC
5 - < 10% SF + MK + OPC

d (mm)

Probability of corrosion initiation

Corrosion-free service life (years)

Steps
1) Assume probability of corrosion initiation (A)
2) Choose cover and find the intercept (B)
3) Traverse right from B; choose m and Cl_{th} (C)
4) From C, move down and choose D_{Cl} (D)
5) Traverse left from D and navigate to y axis (E)
6) E is the corrosion-free service life for the chosen parameters

Assumptions
Chloride build-up rate = 0.04% bwoc
2) Max. surface Cl⁻ concentration = 0.6% bwoc
3) Duration of hydration = 2 years

CIA - Corrosion inhibiting admixture
d - Cover depth
D_{Cl} - Diffusion co-efficient
FA - Fly ash
LC3 - Limestone calcined clay cement
MK - Metakaolin
OPC - Ordinary portland cement
SF - Silica fume

(i) D_{cl}=1E-12m²/s   (v) D_{cl}=7E-12m²/s   (ix) D_{cl}=5E-11m²/s
(ii) D_{cl}=2E-12m²/s   (vi) D_{cl}=1E-11m²/s   (x) D_{cl}=1E-10m²/s
(iii) D_{cl}=3E-12m²/s (vii) D_{cl}=2E-11m²/s   (xi) D_{cl}=5E-10m²/s
(iv) D_{cl}=5E-12m²/s   (viii) D_{cl}=3E-11m²/s

Figure 7.11 Nomogram for estimating service life of structures located in the seawater spray zone

d (mm)

10
20
30
40
50
60
70

B

A

0.6   0.5   0.4   0.3   0.2   0.1

Probability of corrosion initiation

Line Number - (Type of binder + CIA)

1 - > 50%Slag/FA + OPC + CIA;
     < 20% MK/FA +OPC + CIA
2 - OPC + CIA;
     > 50% Slag/FA + OPC;
     < 20% MK/FA + OPC
3 - (30-50%) Slag/FA/ MK + OPC
     LC3 + CIA; OPC + SF+ CIA
4 - LC3; < 10% SF + OPC
5 - < 10% SF + MK + OPC

C

5   4   3   2   1

Corrosion-free service life (years)

200

150

100

50

0

E   D

(i) (ii) (iii)
(iv)
(v)
(vi)
(vii)
(viii)
(ix)
(x) (xi)

(i) D_{cl}=1E-12m^2/s   (v) D_{cl}=7E-12m^2/s   (ix) D_{cl}=5E-11m^2/s
(ii) D_{cl}=2E-12m^2/s   (vi) D_{cl}=1E-11m^2/s   (x) D_{cl}=1E-10m^2/s
(iii) D_{cl}=3E-12m^2/s (vii) D_{cl}=2E-11m^2/s (xi) D_{cl}=5E-10m^2/s
(iv) D_{cl}=5E-12m^2/s   (viii) D_{cl}=3E-11m^2/s

Steps
1) Assume probability of corrosion initiation (A)
2) Choose cover and find the intercept (B)
3) Traverse right from B; choose m and Cl_{th} (C)
4) From C, move down and choose D_{Cl} (D)
5) Traverse left from D and navigate to y axis (E)
6) E is the corrosion-free service life for the chosen parameters

Assumptions
Chloride build-up rate = 0.04% bwoc
2) Max. surface Cl$^-$ concentration = 0.6% bwoc
3) Duration of hydration = 2 years

CIA - Corrosion inhibiting admixture
d - Cover depth
D_{Cl} - Diffusion co-efficient
FA - Fly ash
LC3 - Limestone calcined clay cement
MK - Metakaolin
OPC - Ordinary portland cement
SF - Silica fume

Figure 7.12 Nomogram for estimating service life of structures located in the splash zone

7.6 LIMITATIONS

The 'SL-Chlor' model and nomograms do not consider the sophisticated equations for diffusion coefficient (say, effect of temperature, humidity, curing conditions, etc.). The model does not consider temperature and humidity variations. This model is based on the assumption that concrete is crack-free and the chloride ingress is one-dimensional. This model can be used for choosing the design parameters for the new structures being built and not for existing structures.

7.7 SUMMARY

The chapter presents the development of SL-Chlor computer program with a demonstration of case studies. The sensitivity of input parameters to understand the influencing parameters was done. Nomogram for easy estimation of service life in four different exposure conditions was developed.

CHAPTER 8

CONCLUSIONS AND RECOMMENDATIONS

8.1 INTRODUCTION

This thesis is based on a comprehensive experimental program on electrochemical response of steel embedded in OPC, PFA, and LC3 binder systems exhibiting low to high resistivity. First, the suitability of various existing techniques (namely, MCC test method, ICC test method, and LPR test method) in assessing corrosion characteristics was evaluated. Then, the effects of various electrochemical input parameters and electrode configuration on the electrochemical response were investigated, and suitable values for such parameters were defined - for testing of steel in highly resistive systems. Following this, the 'hr-ACT' test method was developed, and chloride threshold values of steel in OPC, PFA, and LC3 binder systems were estimated. Finally, a software program, named as 'SL-Chlor' was developed for estimating the corrosion-free service life of steel-binder systems. Using SL-Chlor, a set of nomograms were developed to facilitate relatively easy estimation of the corrosion-free service life of steel-binder systems exposed to various coastal exposure conditions.

8.2 CONCLUSIONS

The following are the major conclusions drawn from the experimental study carried out with three objectives.

8.2.1 Suitability of existing corrosion test methods for assessing highly resistive, steel-binder systems

The experimental program given in Subsection 3.4 evaluated the suitability of existing test methods and results are discussed in Subsection 4.2. The major conclusions include the following:

i) In systems with very high resistivity ($\rho > 37$ kΩ.cm), anodes and cathodes can form on same rebar (Circuit 2 type corrosion). Hence, macrocell corrosion measured in ASTM G109 type specimen will not reflect the ongoing Circuit 2 type corrosion. Specimen with single rebar is sufficient for testing corrosion in HR systems (unlike ASTM G109 specimen with three rebars).

ii) Impressed current corrosion (ICC) can lead to uniform corrosion, whereas natural chloride-induced corrosion can lead to localized/pitting corrosion.

iii) The corrosion products formed on the steel surface in OPC, PFA, and LC3 specimens due to impressed current corrosion are different from natural corrosion and exhibit different volumetric expansion characteristics. Hence, impressed current corrosion test is not recommended for studies evaluating the S-B interface characteristics such as corrosion rate and Cl_{th}.

iv) When the resistance of mortar cover (R_m) is negligible when compared to the polarization resistance of steel (R_p), the Linear polarization resistance (LPR) technique can detect corrosion initiation effectively. However, in highly resistive concrete systems (say, surface resistivity, $\rho > 37$ kΩ.cm), the LPR technique cannot detect corrosion initiation because the R_m and R_p in such cases are comparable.

8.2.2 Factors affecting the electrochemical response in S-B systems

The test program and results of factors affecting the electrochemical response in S-B systems are provided in Subsections 3.5 and 5.2, respectively. The following are the conclusions of the objective.

i) Scan rate and scan range do influence the electrochemical response from steel-binder systems and suitable values can vary as a function of the resistivity of binder system.

ii) A scan rate of 0.05 mVs^{-1} and a scan range of ±10 mV versus OCP can acquire good LPR curve (without current interruption technique) from low resistive steel-binder (S-B) systems (surface resistivity, ρ < 37 kΩ.cm).

iii) An AC amplitude of ±10 mV (peak-to-peak) and a frequency of 100 kHz to 0.01 Hz at OCP can acquire EIS spectra from highly resistive S-B systems (surface resistivity, ρ > 37 kΩ.cm).

iv) While testing steel-binder systems, EIS response is very sensitive to the positioning of the reference electrode and can get distorted (say, artefacts). The spacing between the luggin tip and mortar surface of the specimen should be at least twice the diameter of the tip of luggin probe. Also, the ohmic drop at the tip of the luggin probe must be low to avoid artefacts, irrespective of the resistivity of cementitious systems.

v) Randles' circuit for analyzing EIS response is not suitable for assessing R_p of steel embedded in highly resistive steel-binder systems. The suitable equivalent circuit should be chosen according to the S-B systems under study.

8.2.3 Determination of chloride threshold

The 'hr-ACT' test method was developed as described in Subsection 0, and the electrochemical response are discussed in detail in Subsection 6.2. The following conclusions are made.

i) The hr-ACT test using the lollipop test specimen and selected electrode configuration and the input parameters for EIS tests can be used for monitoring changes in the R_p of steel embedded in highly resistive cementitious systems and detecting corrosion initiation at early stages – and then determine chloride threshold in about 3 to 4 months.

156

ii) The Cl_{th} of OPC, PFA and LC3 are 0.4, 0.3 and 0.1 percent by weight of binder, respectively. This reflects the same order as that of pH of these three systems.

iii) The consumption of $Ca(OH)_2$ due to pozzolanic reactions in systems with SCMs can lead to reduction in pH and buffering capacity of pore solution at the interface. This can lead to reduced chloride threshold – as evident from the test results.

8.2.4 Effect of binders on the estimation of service life

A MATLAB® program has been developed (named as 'SL-Chlor') using Fick's second law of diffusion as described in Subsection 3.6. Based on the case studies using this program, the following conclusions are made.

i) The synergistic effects of ageing coefficient (m), diffusion coefficient (D_{Cl}), and Cl_{th} could result in enhanced corrosion-free service life.

ii) The corrosion-free service lives of structures with highly resistive concrete with PFA or LC3 binders can be significantly longer, despite their lower $Cl_{th,}$ than OPC in such systems.

8.3 MAJOR CONTRIBUTIONS

The following are the contributions from this research work

1. The suitability of ASTM G109 test method for assessing the corrosion performance in various resistivity ranges has been established.

2. The knowledge on the effect of test procedures on the form and nature of corrosion products is enhanced further.

3. A short term test method (named as 'hr-ACT') has been developed for estimating the chloride threshold of steel in highly resistive binders.

157

4. A computer program (named as 'SL-Chlor') has been developed to use user-defined statistical distributions of chloride threshold (Cl_{th}), chloride diffusion coefficient (D_{Cl}), cover depth (d), and ageing coefficient (m) and estimate probabilistic corrosion-free service life of S-B systems exposed to chloride environments.

5. Nomograms have been developed for estimating the service life of steel-binder systems with OPC and various SCMs and exposed to various coastal exposure conditions. These can be used during the design and planning stages.

8.4 RECOMMENDATIONS FOR FUTURE WORK

Recommendations for future work include the following

i) The study of passive film formed on steel in concrete with supplementary cementitious materials is recommended to understand the lower Cl_{th} of steel in such systems and to provide solutions to mitigate the same.

ii) Study the effect of corrosion inhibitors on the Cl_{th} of HR S-B systems.

iii) The microclimate at the time of repeated electrochemical testing is crucial in obtaining quality data for studies involving the monitoring of corrosion rate and chloride threshold assessment. The microclimate at the steel-binder interface depends on the type of binder and wet-dry exposure regime. Hence, suitable wet-dry exposure regime for various binder systems to achieve desired microclimate at particular test times need to be established.

iv) The investigation of Stern-Geary constant (B) in active and passive states and assessment of B-value for corrosion initiation studies are recommended.

v) A database of Cl_{th} with various steel-binder systems (stressed TMT, coated rebars, prestressing steel, inhibitors) need to be developed. Round robin tests and standardization of "hr-ACT" test is recommended.

vi) Field exposure with the new cementitious system (LC3) is recommended for understanding the performance in a more realistic condition. Long-term data on diffusion coefficient, ageing coefficient and time of hydration along with Cl_{th} for various exposure conditions can be considered for future studies.

vii) SL-Chlor program can be extended to consider two and three dimensional ingress of chlorides.

REFERENCES

AASHTO T 358 (2017). *Standard Method of Test for Surface Resistivity Indication of Concrete's Ability to Resist Chloride Ion Penetration*. American Association of State Highway and Transportation Officials, Washington, D.C., U.S.A.

Abosrra, L., Ashour, A. F., and Youseffi, M. (2011). "Corrosion of steel reinforcement in concrete of different compressive strengths." *Construction and Building Materials*, 25(10), 3915–3925.

ACI 222R-01. (2010). *Protection of metals in concrete against corrosion*, ACI Publication, USA.

Al-Alaily, H.S., and Hassan, A.A.A. (2016) "Time-dependence of chloride diffusion for concrete containing metakaolin." *Journal of Building Engineering*, 7, 159–169.

Alapati, P. (2014). "Accelerated corrosion test method and evaluation of steel − cementitious systems with corrosion inhibitors and blended cements", Dual degree Thesis, Indian Institute of Technology Madras, Chennai, India

Alexander, M. (2016). Personal communication.

Alexander, M.G., Beushausen, H., Otieno, M. B. (2013). "Corrosion of steel in reinforced concrete: Influence of cover cracking and concrete quality." *Research Monograph No.9 in: Guide to the Use of Durability Indexes for Achieving Durability in Concrete Structures*, 1– 77.

Alhozaimy, A., Hussain, R. R., Al-Zaid, R., and Al-Negheimish, A. (2012). "Coupled effect of ambient high relative humidity and varying temperature marine environment on corrosion of reinforced concrete." *Construction and Building Materials*, 28(1), 670–679.

Al-Khaja, W. A. (1997). "Influence of temperature, cement type and level of concrete consolidation on chloride ingress in conventional and high-strength concretes." *Construction and Building Materials*, 11(1), 9–13.

Alonso, C., Andrade, C., and González, J. (1988). "Relation between resistivity and corrosion rate of reinforcements in carbonated mortar made with several cement types." *Cement and Concrete Research*, 18(5), 687–698.

Alonso, C., Andrade, C., Castellote, M., Castro, P. (2000). "Chloride threshold values to depassivate reinforcing bars embedded in a standardized OPC mortar." *Cement and Concrete Research*, 30, 1047–1055.

Ameer, M. A., Khamis, E., and Al-Motlaq, M. (2004). "Electrochemical behaviour of recasting Ni-Cr and Co-Cr non-precious dental alloys." *Corrosion Science*, 46(11), 2825–2836.

Andrade, C. (2016). Future trends in research on reinforcement corrosion. Corrosion of Steel in Concrete Structures, Corrosion of steel in concrete structures, Woodhead Publishing, USA.

Andrade, C. and Alonso, C. (1996). "Corrosion rate monitoring and on-site." *Construction and Building Materials*, 10(5), 315–328.

Andrade, C., Castellote, M., D'Andrea R. (2011). "Measurement of ageing effect on chloride diffusion coefficients in cementitious matrices" *Journal of nuclear materials*, 412, 209-216

Andrade, C., Soler, L., Alonso, C., Novoa, X. R., and Keddamt, M. (1995). "The importance of geometrical consideration in the measurement of steel corrosion in concrete by means of AC impedance." *Corrosion Science*, 37(12), 2013–2023.

Andrade, P. C., Alonso, C., Polder, R., Cigna, R., Vennesland, O., Salta, M., Raharinaivo, A., and Elsener, B. (2005). *RILEM TC 154-EMC : - Electrochemical Techniques for Measuring Metallic Corrosion Test methods for on-site corrosion rate measurement of steel reinforcement in concrete by means of the polarization resistance method.* 37(November 2004), 623–643.

Angst, U. (2019). "Predicting the time to corrosion initiation in reinforced concrete structuresexposed to chlorides." *Cement and Concrete Research*, 115(2019), 559–567.

Angst, U., Elsener, B., Larsen, C. K., and Vennesland, O. (2009). "Critical chloride content in reinforced concrete — A review." *Cement and Concrete Research*, 39(12), 1122–1138.

Angst, U., Ronnquist, A., Elsener, B., Larsen, C. K., and Vennesland, O. (2011). "Probabilistic considerations on the effect of specimen size on the critical chloride content in reinforced concrete." *Corrosion Science*, 53(1), 177–187.

Arya, C., and Vassie, P. R. (1995). "Influence of cathode-to-anode area ratio and separation distance on galvanic corrosion currents of steel in concrete containing chlorides." *Cement and Concrete Research*, 25(5), 989–998.

ASTM G109-07 (2013) *Standard test method for determining effects of chemical admixtures on corrosion of embedded steel reinforcement in concrete exposed to chlorides.* ASTM International, West Conshohocken, PA, USA.

ASTM C876-15 (2015) *Standard test method for corrosion potentials of uncoated reinforcing in concrete.* ASTM International, West Conshohocken, PA, USA

ASTM C109 (2002). *Standard test method for compressive strength of hydraulic cement mortars (Using 2-in. or cube specimens).* ASTM International, West Conshohocken, PA, USA

ASTM C1556 – 04 (2010) *Standard Test Method for Determining the Apparent Chloride Diffusion Coefficient of Cementitious Mixtures by Bulk Diffusion.* American Society of Testing and Materials, Conshohocken, PA, USA.

ASTM G102 - 89 Reapproved (2010). *Standard Practice for Calculation of Corrosion Rates and Related Information from Electrochemical Measurements.* ASTM International, West Conshohocken, PA, USA.

ASTM G1-11 (2011). *Standard practice for preparing, cleaning and evaluating corrosion test specimens, American Society of Testing and Materials*, Conshohocken, PA, USA.

ASTM G180-13 (2014). *Standard Test Method for Corrosion Inhibiting Admixtures for Steel in Concrete by Polarization Resistance in Cementations Slurries.* American Society of Testing and Materials, Conshohocken, PA, USA.

ASTM G5 (2014). *Standard Reference Test Method for Making Potentiodynamic Anodic Polarization Measurements.* ASTM International, West Conshohocken, PA, USA

ASTM G59-97. (2014). *Standard test method for conducting potentiodynamic polarization resistance measurements*. ASTM International, West Conshohocken, PA, USA.

ASTM G61-86 (Reapproved 2014). *Standard Test Method for Conducting Cyclic Potentiodynamic Polarization Measurements for Localised Corrosion Susceptibility of Iron, Nickel,or Cobalt-Based Alloys*. ASTM International, West Conshohocken, PA, USA

Austin, S. A., Lyons, R., and Ing, M. (2004). "Electrochemical behaviour of steel reinforced concrete during accelerated corrosion testing." *Corrosion*, 60(2), 203–212.

Barroca, N., Borges, L. M., Velez, F. J., Monteiro, F., Górski, M., and Castro-Gomes, J. (2013). "Wireless sensor networks for temperature and humidity monitoring within concrete structures." *Construction and Building Materials*, 40(3), 1156–1166.

Batic, O.R., Sota, J.D., Fernández, J.L., Bellotti, N. Romagnoli, R. (2013). "Rebar corrosion in mortars with high limestone filler content" *Anti-Corrosion Methods and Materials*. 60, 3–13.

Bentur, A., Diamond, S., and Berke, N. S. (1997). "Steel Corrosion in Concrete: Fundamentals and civil engineering practice", *E&FN Spon*, London.

Berke, N. S., and Hicks, M. C. (2004). "Predicting long-term durability of steel reinforced concrete with calcium nitrite corrosion inhibitor." *Cement and Concrete Composites*, 26(3), 191–198.

Berke, N. S., Shen, D. F., and Sundberg, K. M. (1990). "Comparison of the Polarization Resistance Technique to the Macrocell Corrosion Technique" *Corrosion Rates of Steel in Concrete*, ASTM STP 1065, N S Berke, V Chaker, and D Whiting, Eds, American Society for Testing and Materials, Philadelphia, 1990, pp 38-51.

Bockris, John O.M., Reddy, Amulya K.N., Gamboa-Aldeco, Maria E. (2000). *Modern Electrochemistry 2A Fundamentals of Electrodics*, 2nd Ed., Kluwer Acasdemic Publishers, New York.

Botter, W., Scares, D. M., and Teschke, O. (1989). "The influence of the Luggin capillary on the response time of a reference electrode." *Journal of Electroanalytical Chemistry*, 267(1–2), 279–286.

Boubitsas, D., and Tang, L. (2013). "An approach for measurement of chloride threshold values." *International Journal of Structural Engineering*, 4(1–2), 24–34.

Caré, S., and Raharinaivo, A. (2007). "Influence of impressed current on the initiation of damage in reinforced mortar due to corrosion of embedded steel." *Cement and Concrete Research*, 37, 1598–1612.

Care, S., Nguyen, Q. T., L'Hostis, V., and Berthaud, Y. (2008). "Mechanical properties of the rust layer induced by impressed current method in reinforced mortar." *Cement and Concrete Research*, 38(8–9), 1079–1091.

Chang, C. Y., and Hung, S. S. (2012). "Implementing RFIC and sensor technology to measure temperature and humidity inside concrete structures." *Construction and Building Materials*, 26(1), 628–637.

Chechirlian, S., Keddam, M., and Takenouti, H. (1993). "Specific Aspects of Impedance Measurements in Low Conductivity Media," *Electrochemical Impedance: Analysis and Interpretation*, ASTM STP 1188, J. R. Scully, D. C. Silverman, and M. W. Kendig, Eds., American Society for Testing and Materials, Philadelphia, 1993, pp. 23-36

Cooper, S. J., Bertei, A., Finegan, D. P., and Brandon, N. P. (2017). "Simulated impedance of diffusion in porous media." *Electrochimica Acta*, 251, 681–689.

Criado, M., Martínez-Ramirez, S., and Bastidas, J. M. (2015). "A Raman spectroscopy study of steel corrosion products in activated fly ash mortar containing chlorides." *Construction and Building Materials*, 96, 383–390.

de la Fuente, D., Alcántara, J., Chico, B., Díaz, I., Jiménez, J. A., and Morcillo, M. (2016). "Characterisation of rust surfaces formed on mild steel exposed to marine atmospheres using XRD and SEM/Micro-Raman techniques." *Corrosion Science*, 110, 253–264.

Deus, J. M., Freire, L., Montemor, M. F., and Nóvoa, X. R. (2012). "The corrosion potential of stainless steel rebars in concrete: Temperature effect." *Corrosion Science*, 65, 556–560.

Dhandapani, Y., and Santhanam, M. (2017). "Assessment of pore structure evolution in the limestone calcined clay cementitious system and its implications for performance." *Cement and Concrete Composites*, 84, 36–47.

Dhandapani, Y., Sakthivel, T., Santhanam, M., Gettu, R., and Pillai, R. G. (2018). "Mechanical properties and durability performance of concretes with Limestone Calcined Clay Cement (LC3)." *Cement and Concrete Research*, 107(March), 136–151.

Dhanya, B.S. (2015). *Study of the Influence of Supplementary Cementitious Materials on Selected Durability Parameters of Concrete*, Ph.D Thesis, Indian Institute of Technology Madras, Chennai, India

Dhouibi, L., Triki, E., and Raharinaivo, A. (2002). "The application of electrochemical impedance spectroscopy to determine the long-term effectiveness of corrosion inhibitors for steel in concrete." *Cement and Concrete Composites*, 24(1), 35–43.

Diamond, S. (1986). "Chloride concentrations in concrete pore solutions resulting from calcium and sodium chloride admixtures." *Cement concrete and aggregates*, 8, 97–102.

Dong, S., Zhao, B., Lin, C., Du, R., Hu, R., and Xiaoge, G. (2012). "Corrosion behavior of epoxy / zinc duplex coated rebar embedded in concrete in ocean environment." *Construction and Building Materials*, 28(1), 72–78.

Dotto J.M.R., de Abreu A.G., Dal Molin D.C.C., Müller I.L. (2004) "Influence of silica fume addition on concretes physical properties and on corrosion behaviour of reinforcement bars." *Cement and Concrete Composites* 26(1), 31–9.

Duffó, G. S., and Farina, S. B. (2009). "Development of an embeddable sensor to monitor the corrosion process of new and existing reinforced concrete structures." *Construction and Building Materials*, 23(8), 2746–2751.

Duggal, S. (2016) 'India loses up to $100 billion annually to corrosion: Hind Zinc CEO SunilDuggal', URL:http://economictimes.indiatimes.com/articleshow/54878379.cms? utm_source=contentofinterest&utm_medium=text&utm_campaign=cppst; Last accessed on October 16, 2016

DuraCrete. (2000). DuraCrete – Final technical report, Document BE95–1347/R17; Statistical Quantification of the Variables in the Limit State Functions, Document BE95– 1347/R9. URL: www.cur.nl/upload/documents/duracrete/BE1347R17.pdf; Last accessed on December 14, 2012.

Ehrhardt, W. C. (1990) "IR Drop in Electrochemical Corrosion Studies--Part I: Basic Concepts and Estimates of Possible Measurement Errors," *The Measurement and Correction of Electrolyte Resistance in Electrochemical Tests*, ASTM STP 1056, L. L. Scribner and S. R. Taylor, Eds., American Society for Testing and Materials, Philadelphia, 1990, pp. 27-58.

Elsener, B. (2001). "Half-cell potential mapping to assess repair work on RC structures." *Construction and Building Materials*, 15(2–3), 133–139.

Elsener, B. (2002). "Macrocell corrosion of steel in concrete - Implications for corrosion monitoring." *Cement and Concrete Composites*, 24(1), 65–72.

Enevoldsen, J. N., Hansson, C. M., Hope, B. B. (1994). "The influence of internal relative humidity on the rate of corrosion of steel embedded in concrete and mortar." *Cement and Concrete Research* 24(7), 1373–1382.

Erdogdu, S., Bremner, T.W., Kondratova, I.L. (2001) "Accelerated testing of plain and epoxy-coated reinforcement in simulated seawater and chloride solutions", *Cement and Concrete Research,* 31(6), 861-867.

Fajardo, G., Valdez, P., and Pacheco, J. (2009). "Corrosion of steel rebar embedded in natural pozzolan based mortars exposed to chlorides." *Construction and Building Materials*, 23(2), 768–774.

Feliu, V., González, J. a., Andrade, C., and Feliu, S. (1998). "Equivalent circuit for modelling the steel-concrete interface. I. Experimental evidence and theoretical predictions." *Corrosion Science*, 40(6), 975–993.

Ferreira, R. M. (2007). "Sensitivity analysis of model parameters for corrosion initiation and implications on design." Proceedings of International RILEM Workshop on Integral Service Life Modelling of Concrete Structures, 205–214.

Ferreira, R. M., Castro-Gomes, J. P., Costa, P., and Malheiro, R. (2016). "Effect of metakaolin on the chloride ingress properties of concrete." *KSCE Journal of Civil Engineering*, 20(4), 1375–1384.

Figueira, R. B., Sadovski, A., Melo, A. P., and Pereira, E. V. (2017). "Chloride threshold value to initiate reinforcement corrosion in simulated concrete pore solutions: The influence of surface finishing and pH." *Construction and Building Materials*, 141, 183–200.

Fontana, M.G. (1987) Corrosion Engineering, third ed., McGraw-Hill, Singapore,

Frederiksen, J. M. (2000) "Chloride threshold values for service life design." URL: http://www.germann.org/TestSystems/RCT%20&%20RCTW/rct_3.6.pdf;   Last accessed on September, 2000.

Frías M. and Cabrera J. (2000). "Pore size distribution and degree of hydration of metakaolin–cement pastes". *Cement and Concrete Research*, 30(4):561–9.

Göhr, H., Mirnik, M., and Schiller, C. A. (1984). "Distortions of high frequency electrode impedance.*" Journal of Electroanalytical Chemistry and Interfacial Electrochemistry*, 180(1–2), 273–285.

Gonzalez, J., Molina, A., Otero, E., and Lbpezt, W. (2010). "On the mechanism of steel corrosion in concrete: the role of oxygen diffusion." *Magazine of Concrete Research*, 42(150), 23–27.

Gulikers, J., Polder, R., and Raupach, M. (2003). "Half-cell potential measurements – Potential mapping on reinforced concrete structures." *Materials and Structures*, 36(September), 1–11.

Hack H.P., Moran P.J., Scully J.R. (1990). "Influence of electrolyte resistance on electrochemical measurements and procedures to minimize or compensate for resistance errors. In: Scribner LL, Talylor SR, editors. *The Measurement and Correction of Electrolyte Resistance in Electrochemical Tests*. ASTM STP 1056, L. L. Scribner and S. R. Taylor, Eds., American Society for Testing and Materials, Philadelphia, 1990, pp. 5–26.

Hansson, C. M. (1984). "Comments on electrochemical measurements of the rate of corrosion of steel in concrete." *Cement and Concrete Research*, 14(4), 574–584.

Hansson, C. M., Poursaee, A., and Jaffer, S. J. (2012). "Corrosion of Reinforcing Bars in Concrete." *The Masterbuilder*.

Hansson, C. M., Poursaee, A., and Laurent, A. (2006). "Macrocell and microcell corrosion of steel in ordinary Portland cement and high performance concretes." *Cement and Concrete Research*, 36(11), 2098–2102.

Hong, K., and Hooton, R. D. (1999). "Effects of cyclic chloride exposure on penetration of concrete cover." *Cement and Concrete Research*, 29(March 1998), 1379–1386.

Hornbostel, K., Larsen, C. K., and Geiker, M. R. (2013). "Relationship between concrete resistivity and corrosion rate - A literature review." *Cement and Concrete Composites*, 39, 60–72.

Hsieh, G., Mason, T. O., Garboczi, E. J., and Pederson, L. R. (1997). "Experimental limitations in impedance spectroscopy: Part III. Effect of Reference Electrode Geometry/Position." *Solid State Ionics*, 96, 153–172.

Hussain, R. R., and Ishida, T. (2011). "Investigation of volumetric effect of coarse aggregate on corroding steel reinforcement at the interfacial transition zone of concrete." *KSCE Journal of Civil Engineering*, 15(1), 153–160.

Hussain, R., Ishida, T., and Wasim, M. (2012). "Oxygen Transport and Corrosion of Steel in Concrete under Varying Concrete Cover, w / c, and Moisture." *ACI Materials Journal* 109(1), 3–10.

IS 383-1970 (2002), *Specification for coarse and fine aggregates from natural sources for concrete*, Bureau of Indian Standards (BIS), New Delhi, India.

IS 456:2000 (2005) *Code of practice for Plain and Reinforced Concrete*, Bureau of Indian Standards (BIS), New Delhi, India.

IS 650-1991 (R2008), *Specification for Standard Sand for Testing of Cement, Bureau of Indian Standards (BIS)*, New Delhi, India.

Izquierdo, D., Alonso, C., Andrade, C., and Castellote, M. (2004). "Potentiostatic determination of chloride threshold values for rebar depassivation - Experimental and statistical study." *Electrochimica Acta*, 49(17–18), 2731–2739.

Jaime P. V., Jordi C. F., and Pere L. M. (2013). Bioelectronics for Amperometric Biosensors, State of the Art in Biosensors - General Aspects, Toonika Rinken (Ed.), InTechOpen.com

Jain, J., and Neithalath, N. (2011). "Electrical impedance analysis based quantification of microstructural changes in concretes due to non-steady state chloride migration." *Materials Chemistry and Physics*, 129(1–2), 569–579.

Jamil, H. ., Shriri, a, Boulif, R., Bastos, C., Montemor, M., and Ferreira, M. G. (2004). "Electrochemical behaviour of amino alcohol-based inhibitors used to control corrosion of reinforcing steel." Electrochimica Acta, 49(17–18), 2753–2760.

Jaśniok, T., and Jaśniok, M. (2015). "Influence of Rapid Changes of Moisture Content in Concrete and Temperature on Corrosion Rate of Reinforcing Steel." *Procedia Engineering*, 108, 316–323.

JIS A6205. (2013). *Corrosion inhibitor for reinforcing steel in concrete, Japan Industrial standard, 4-1-24,* Akasaka, Minato-ku, Tokyo, 107-8440, Japan.

Karuppanasamy, J., and Pillai, R. G. (2017). "A short-term test method to determine the chloride threshold of steel–cementitious systems with corrosion inhibiting admixtures." *Materials and Structures*, 50(4), 1–17.

Karuppanasamy, J.,and Pillai R.G. (2015) "Issues with the application of potential gradient in evaluating the performance of corrosion inhibitors in steel-cementitious systems", *International Conference on Ecstasy in Concrete (ACECON 2015)*, Kolkata, India, October 08-10, 2015.

Kelly, R.G., Scully, J.R., Shoesmith, D.W., Bucheit, R.G. (2003). "*Electrochemical Techniques in Corrosion Science and Engineering*", Marcel Dekker, Inc., New York.

Kessler, R.J., Powers, R.G., Cerlanek, W.D., and Sagüés, A. A. (2003). "Corrosion inhibitors in concrete" *NACE International*, Houston, TX, USA, corrosion paper no. 03288, 1–17.

Khatri, R. P., and Sirivivatnanon, V. (2004). "Characteristic service life for concrete exposed to marine environments." Cement and Concrete Research, 34(5), 745–752.

Kim, J. J., and Young, Y. M. (2013). "Study on the passive film of type 316 stainless steel." *International Journal of Electrochemical Science*, 8(10), 11847–11859.

Kirkpatrick, T. J., Weyers, R. E., Anderson-Cook, C. M., and Sprinkel, M. M. (2002). "Probabilistic model for the chloride-induced corrosion service life of bridge decks." Cement and Concrete Research, 32(12), 1943–1960.

Koch, G. H., Brongers, M.P.H., Thompson, N.G., Virmani, Y.P., and Payer J.H. (2002) *Corrosion cost and preventive strategies in the United States*, Report No. FHWA-RD-01-156, R315-01, Federal Highway Administration, McLean, VA, USA

Koleva, D. A., Hu, J., Fraaij, A. L. A., Stroeven, P., Boshkov, N., and de Wit, J. H. W. (2006). "Quantitative characterisation of steel/cement paste interface microstructure and corrosion phenomena in mortars suffering from chloride attack." *Corrosion Science*, 48(12), 4001–4019.

Koleva, D. a., Hu, J., Fraaij, a. L. a., van Breugel, K., and de Wit, J. H. W. (2007). "Microstructural analysis of plain and reinforced mortars under chloride-induced deterioration." *Cement and Concrete Research*, 37(4), 604–617.

Law, D. W., Cairns, J., Millard, S. G., and Bungey, J. H. (2004). "Measurement of loss of steel from reinforcing bars in concrete using linear polarisation resistance measurements." *NDT and E International*, 37(5), 381–388.

Li, Z., Ma, B., Peng, J. and Qi, M. (2000). "Microstructure and sulfate resistance mechanism of high-performance concrete containing CNI". *Cement and Concrete Composites,* 22(5): 369–377

Li, F., Yuan, Y., and Li, C. Q. (2011). "Corrosion propagation of prestressing steel strands in concrete subject to chloride attack." *Construction and Building Materials*, 25(10), 3878–3885.

Li, L., and Sagues, A. A. (1999). "Effect of chloride concentration on the pitting and repassivation potentials of reinforcing steel in alkaline solutions." *Nace Corrosion*, (567), No. 567.

Li, L., and Sagüés, A. A. (2002). "Chloride Corrosion Threshold of Reinforcing Steel in Alkaline Solutions—Effect of Specimen Size." *Corrosion*, 58(4), 305–316.

Lieser M. J., Xu J. (2016) "Composites and the Future of Society: Preventing a legacy of costly corrosion with modern materials." URL: "http://www.ocvreinforcements .com/pdf/library/CSB_Corrosion_White_Paper_Sept_10_10_English.pdf" Last accessed on 25 July, 2016

Life–365. (2012). Service life prediction model and computer program for predicting the service life and life–cycle cost of reinforced concrete exposed to chlorides. URL: http://www.life–365.org/; Last accessed on December 14, 2012

Liu, G., Zhang, Y., Ni, Z., and Huang, R. (2016). "Corrosion behavior of steel submitted to chloride and sulphate ions in simulated concrete pore solution." *Construction and Building Materials*, 115, 1–5.

Liu, P., Yu, Z., Guo, F., Chen, Y., and Sun, P. (2015). "Temperature response in concrete under natural environment." *Construction and Building Materials*, 98, 713–721.

Lollini, F., Redaelli, E., and Bertolini, L. (2016). "Investigation on the effect of supplementary cementitious materials on the critical chloride threshold of steel in concrete." *Materials and Structures*, 49(10), 4147–4165.

Malakooti A. (2017). *Investigation of concrete electrical resistivity as a performance based test*, M.S. Thesis, Utah state university, Utah, USA.

Mammoliti, L., C, B. L., Hansson, C. M., and Hope, B. B. (1996). "The influence of surface finish of reinforcing steel and pH of the test solution on the chloride threshold concentration for corrosion initiation in synthetic pore solutions." *Cement and Concrete Research*, 26(4), 545–550.

Mammoliti, L., Hansson, C. M., and Hope, B. B. (1999). "Corrosion inhibitors in concrete Part II: Effect on chloride threshold values for corrosion of steel in synthetic pore solutions." *Cement and Concrete Research*, 29, 1583–1589.

Manning, D. G. (1996). "Corrosion performance of epoxy-coated reinforcing steel : North American experience." *Construction and Building Materials*, 10(5), 349–365.

Mansfeld, F. (1976). "The effect of uncompensated IR-drop on polarization resistance measurements", *Corrosion,* 32(4), 143-146.

Mansfeld, F. (1982). "Effect of uncompensated resistance on the true scan rate in potentiodynamic experiments." *Corrosion*, 38(10), 556–559.

Marchand, J., and Samson, E. (2009). "Predicting the service-life of concrete structures – Limitations of simplified models." *Cement and Concrete Research*, 31(8), 515-521.

Marcotte, T. D., and Hansson, C. M. (2007). "Corrosion products that form on steel within cement paste." *Materials and Structures*, 40(3), 325–340.

Marcotte, T. D., Hansson, C. M., and Hope, B. B. (1999). "The effect of the electrochemical chloride extraction treatment on steel-reinforced mortar Part II: Microstructural characterization." *Cement and Concrete Research*, 29(10), 1561–1568.

Markeset, G., and Skjolsvold, O. (2010). "Time Dependent Chloride Diffusion Coefficient – Field Studies of Concrete Exposed To Marine Environment in Norway." *Proceedings of the 2nd International Symposium on Service Life Design for Infrastructures*, 0(1), 83–90.

Martínez, I., and Andrade, C. (2009). "Examples of reinforcement corrosion monitoring by embedded sensors in concrete structures." *Cement and Concrete Composites*, 31(8), 545–554.

McCarter, W., Chrisp, T., Starrs, G., Holmes, N., Basheer, L., Basheer, M., and Nanukuttan, S. (2010). "Developments in monitoring techniques for durability assessment of cover-zone concrete." *2nd International Conference on Durability of Concrete Structures*, 137–146.

Metrohm. (2011). *Ohmic Drop Part 1 – Basic Principles*. Autolab Application Note EC03, 1–2.

Millard, S. G., Law, D., Bungey, J. H., and Cairns, J. (2001). "Environmental influences on linear polarisation corrosion rate measurement in reinforced concrete." *NDT and E International*, 34(6), 409–417.

Misawa, T., Hashimoto, K., and Shimodaira, S. (1974). "The mechanism of formation of iron oxide and oxyhydroxides in aqueous solutions at room temperature." *Corrosion Science*, 14(2), 131–149.

Moreno, M., Morris, W., Alvarez, M.G., Duffó, G.S. (2004). "Corrosion of reinforcing steel in simulated concrete pore solutions: effect of carbonation and chloride content", *Corrosion Science*, 46, 2681–2699.

Myland, J. C., and Oldham, K. B. (2000). "Uncompensated resistance. 1. The effect of cell geometry." *Analytical Chemistry*, 72(17), 3972–3980.

NACE Impact Report, Material Performance (2016), *Mitigating corrosion to extend the life of concrete structures*.

Nagata, M., Itoh, Y., and Iwahara, H. (1994). "Dependence of observed overvoltages on the positioning of the reference electrode on the solid electrolyte." *Solid State Ionics* 67, 215–224.

Nair, S.A.O. (2017). Corrosion and mechanical characteristics of Quenched and Self-Tempered (QST) steel reinforcing bars used in concrete structures, M.S. Thesis, Indian Institute of Technology Madras, Chennai, India

Narasimhulu, K., Gettu, R., and Babu, K. G. (2014). "Beneficiation of Natural Zeolite through Flash Calcination for Its Use as a Mineral Admixture in Concrete." *Journal of Materials in Civil Engineering*, 26(1), 24–33.

Neff, D., Harnisch, J., Beck, M., L'Hostis, V., Goebbels, J., and Meinel, D. (2011). "Morphology of corrosion products of steel in concrete under macro-cell and self-corrosion conditions." *Materials and Corrosion*, 62(9), 861–871.

Nilsson, L-O. (2001). Prediction models for chloride ingress and corrosion initiation in concrete structures. In L- O. Nilsson (Ed.), P-01:6 Chalmers University of Technology.

Nmai, C. K. (2004). "Multi-functional organic corrosion inhibitor." *Cement and Concrete Composites*, 26(3), 199–207.

Norris, A., Saafi, M., and Romine, P. (2008). "Temperature and moisture monitoring in concrete structures using embedded nanotechnology/microelectromechanical systems (MEMS) sensors." *Construction and Building Materials*, 22(2), 111–120.

NT Build 443 (1995). Concrete, Hardened: Accelerated chloride penetration, Nordtest Method, ESPOO, Finland.

NT Build 492 (1999). Concrete, mortar and cement-based repair materials: chloride migration coefficient from non-steady-state migration experiments. Nordic Council of ministers, Finland. UDC 691.32/691.53/691.54

Ogunsanya, I. G., and Hansson, C. M. (2019). "Detection of the critical chloride threshold of carbon steel rebar in synthetic concrete pore solutions." *RILEM Technical Letters, 3(2018)*, 75–83.

Oh, S. J., Cook, D. C., and Townsend, H. E. (1998). "Characterization of iron oxides commonly formed as corrosion products on steel." *Hyperfine Interactions,* 112 (1-4), 59-66.

Ohtsu, M., and Yamamoto, T. (1997). "Compensation procedure for half-cell potential measurement." *Construction and Building Materials*, 11(7–8), 395–402.

Oldham, K. B., and Stevens, N. P. C. (2000). "Uncompensated resistance. 2. The effect of reference electrode nonideality." *Analytical Chemistry*, 72(17), 3981–3988.

Oslakovic, I. S., Bjegovic, D., and Mikulic, D. (2010a). "Evaluation of service life design models on concrete structures exposed to marine environment." *Materials and structures,* 43(10), 1397–1412.

Oslaković, I. S., Bjegović, D., Mikulić, D., and Krstić, V. (2010b). "Development of service life model CHLODIF++." *Computational modelling of concrete structures,* EURO–C, 573–578.

Pacheco, J., and Polder, R. B. (2016). "Critical chloride concentrations in reinforced concrete specimens with ordinary Portland and blast furnace slag cement." *Heron*, 61(2), 99–119.

Paredes, M.A., Carvallo, A.A., Kessler, R.J., and Sagüés, A.A. (2010). "Corrosion Inhibitors in Concrete – Second Interim Report." *Florida Department of Transportation and Federal Highway Administration, Gainesville*, FL, USA, FL/DOT/SMO/10-531.

Park, J.-I., Lee, K.-M., Kwon, S.-O., Bae, S.-H., Jung, S.-H., and Yoo, S.-W. (2016). "Diffusion Decay Coefficient for Chloride Ions of Concrete Containing Mineral Admixtures." *Advances in Materials Science and Engineering*, 2016, 1–11.

Pech-Canul M.A., Sagüés, A. A., and Castro, P. (1998). "Influence of Counter Electrode Positioning on Solution Resistance in Impedance Measurements of Reinforced Concrete." *CORROSION*, 54(8), 663–667.

Pettersson, K. (1996). "Service life of concrete structures - in a chloride environment." *Swedish Cement & Concrete Research Institute*, CBI Report 3:96.

Pettersson, K., and Norberg, J. (2000). "Service life with regard to chloride induced corrosion. A probabilistic approach." *Proceedings of PRO 14: International RILEM/CIB/ISO Symposium on Integrated Life-Cycle Design of Materials and Structures ILCDES 2000*, 491–496.

Pillai, R.G. (2009) "Electrochemical characterization and Time-variant structural reliability assessment of Post-tensioned, segmental concrete bridges", Ph.D Thesis, Texas A&M, Texas, USA

Pillai, R.G., Santhanam, M., Gettu, R., Rengaraju, S., Dhandapani, Y., Rathnarajan, S., and Basavaraj, A.S. (2019). "Service life and life cycle assessment of reinforced concrete systems with fly ash and limestone calcined clay cement (LC3*)", Cement and Concrete Research,* 118, 111-119.

Polder, R. B., and De Rooij, M. R. (2005). "Durability of marine concrete structures - Field investigations and modelling." Heron, 50(3), 133–154.

Poulsen, S.L., and Sorensen, H. E. (2014). "RILEM TC 235-CTC : Corrosion Initiating Chloride Threshold Concentrations in Concrete." *Final test report on DTI's participation in round robin test*, (March), 1–34.

Pour-Ghaz, M., Isgor, O. B., and Ghods, P. (2010). "Quantitative Interpretation of Half-Cell Potential." *Journal of Materials in Civil Engineering,* 21(9), 467–475.

Poursaee, A. (2010). "Determining the appropriate scan rate to perform cyclic polarization test on the steel bars in concrete", *Electrochemica Acta*, 55 (2010) 1200–1206.

Poursaee, A., and Hansson, C. M. (2007). "Reinforcing steel passivation in mortar and pore solution." *Cement and Concrete Research*, 37(7), 1127–1133.

Poursaee, A., and Hansson, C. M. (2009). "Potential pitfalls in assessing chloride-induced corrosion of steel in concrete." *Cement and Concrete Research*, 39(5), 391–400.

Prezzi, M., Geyskens, P., and Monteiro, P. J. M. (1996). "Reliability approach to service life prediction of concrete exposed to marine environments." ACI Materials Journal, 93(6), 544–552.

Rengaraju, S., Rathnarajan, S., Velayudhan, A., Pugal O., and Pillai R.G. (2015) "Effect of Corrosion Inhibitors on Durability Parameters of Cement Mortar", *CORCON 2015*, Chennai, India

Ribeiro, D. V., and Abrantes, J. C. C. (2016). "Application of electrochemical impedance spectroscopy (EIS) to monitor the corrosion of reinforced concrete: A new approach." *Construction and Building Materials*, 111, 98–104.

RILEM TC 235-CTC (2014), *Technical committee Corrosion initiating chloride threshold concentrations in concrete*, URL: https://www.rilem.net/groupe/235-ctc-corrosion-initiating-chloride-threshold-concentrations-in-concrete-237. Last accessed on May 19, 2019.

Rutman, J., and Riess, I. (2008). "Placement of reference electrode in solid state electrolyte cells." *Solid State Ionics*, 179(21–26), 913–918.

Ryu, D., Ko, J., and Noguchi, T. (2011). "Effects of simulated environmental conditions on the internal relative humidity and relative moisture content distribution of exposed concrete." *Cement and Concrete Composites*, 33(1), 142–153.

Sagoe-Cretsil, K. K., and Glasser, F. P. (1993). "Constitution of green rust and its significance to the corrosion of steel in portland cement." *Corrosion*, 49(6), 457–463

Sagues, A. (2001). "Corrosion performance of epoxy-coated rebar in Florida Keys Bridges." *Corrosion (01642),* NACE International, Houston, USA.

Saleem, M., Shameem, M., Hussain, S. E., and Maslehuddin, M. (1996). "Effect of moisture, chloride and sulphate contamination on the electrical resistivity of Portland cement concrete." *Construction and Building Materials*, 10(3), 209–214.

San Nicolas, R., Cyr, M., and Escadeillas, G. (2014). "Performance-based approach to durability of concrete containing flash-calcined metakaolin as cement replacement." *Construction and Building Materials*, 55, 313–322.

Sangoju, B., Gettu, R., Bharatkumar, B. H., and Neelamegam, M. (2011). "Chloride-Induced Corrosion of Steel in Cracked OPC and PPC Concretes: Experimental Study." *Journal of Materials in Civil Engineering*, 23(7), 1057–1066

Saremi, M., and Mahallati, E. (2002). "A study on chloride-induced depassivation of mild steel in simulated concrete pore solution." *Cement and Concrete Research*, 32(12), 1915–1921.

Saricimen, H., Mohammad, M., Quddus, A., Shameem, M., and Barry, M. (2002). "Effectiveness of concrete inhibitors in retarding rebar corrosion." Cement and *Concrete Composites*, 24(1), 89–100.

Sharkawi A.M. and Seyam A.M. (2018). "Efficiency of accelerated techniques for assessing corrosion protection of blended cements." *Magazine of Concrete Research*, Ahead of print.

Shekarchi, M., Ghods, P., Alizadeh, R., Chini, M., and Hoseini, M. (2008). "Durapgulf, a Local Service Life Model for the Durability of Concrete Structures in the South of Iran." *The Arabian Journal for Science and Engineering*, 33(1), 77–88.

SHRP-330 (1993). *Standard Test Method for Chloride Content in Concrete Using the Specific Ion Probe, In Condition Evaluation of Concrete Bridges Relative to Reinforcement Corrosion-Volume 8: Procedure Manual*, SHRP-S/FR-92-110, Strategic Highway Research Program, Washington, DC, USA, pp. 85-105

Soleymani, H.R. and Ismail, M.E. (2004). "Comparing corrosion measurement methods to assess the corrosion activity of laboratory OPC and HPC concrete specimens." *Cement and Concrete Research,* 34 (2004) 2037–2044.

Song, G. (2000). "Equivalent circuit model for AC electrochemical impedance spectroscopy of concrete." *Cement and Concrete Research* 30, 1723–1730.

Song, H. W., Saraswathy, V., Muralidharan, S., and Thangavel, K. (2008). "Tolerance limit of chloride for steel in blended cement mortar using the cyclic polarisation technique." *Journal of Applied Electrochemistry*, 38(4), 445–450.

Soylev, T. A., and Richardson, M. G. (2008). "Corrosion inhibitors for steel in concrete: State-of-the-art report*." Construction and Building Materials*, 22(4), 609–622.

Stanish, K. and Thomas, M. (2003). "The use of bulk diffusion tests to establish time-dependent concrete chloride diffusion coefficients". *Cement and Concrete Research*, 33(1), 55-62.

Suda, K., Misra, S., and Motohashi, K. (1993). "Corrosion products of reinforcing bars embedded in concrete." *Corrosion Science*, 35, 1543–1549.

Sun, Y.M., Chang, T.P., and Ming, T, L. (2010). "Service Life Prediction for Concrete Structures by Time-Depth Dependent Chloride Diffusion Coefficient." *Journal of Materials in Civil Engineering*, 22(11), 1187–1190.

Szymczewska, D., Karczewski, J., Chrzan, A., and Jasinski, P. (2015). "Three electrode configuration measurements of electrolyte-diffusion barrier-cathode interface." *Journal of the Ceramic Society of Japan*, 123(1436), 268–273.

Takeyama, T., and Shibata, T. (1977). "Stochastic theory of pitting corrosion." *Corrosion*.

Talero, R. (2012). "Synergic effect of Friedel's salt from pozzolan and from OPC co-precipitating in a chloride solution." Construction and Building Materials, 33, 164–180.

Tang, L. (1996). Chloride transport in concrete–measurement and prediction. *Ph.D. Thesis*, Department of Building Materials, Chalmes University of Technology, Gothenburg, Sweden.

Tang, L. (2007). "Service life modelling. In Report 38: Durability of Self-Compacting Concrete-State-of-the-Art." *Report of RILEM Technical Committee 205,* 163–174.

Tang, L. (2008). "Engineering expression of the ClinConc model for prediction of free and total chloride ingress in submerged marine concrete." *Cement and Concrete Research*, 38(8), 1092–1097.

Tang, L. and Gulikers, J. (2007). "On the mathematics of time- dependent apparent chloride diffusion coefficient in concrete." *Cement and Concrete Research* 37, 589–595

Thomas, M. (1996). "Chloride Threshold in marine concrete." *Cement and Concrete Research,* 26(4), 513–519.

Trejo, D. and Pillai, R.G. (2003). "Accelerated Chloride Threshold Testing : Part I — ASTM A 615 and A 706 Reinforcement." *ACI Materials Journal*, 519–527.

Trejo, D., and Reinschmidt, K. (2007). "Justifying materials selection for reinforced concrete structures. I: Sensitivity analysis." *Journal of Bridge Engineering*, 12(1), 31–37.

Victoria, S. N., and Ramanathan, S. (2011). "Effect of potential drifts and ac amplitude on the electrochemical impedance spectra." *Electrochimica Acta*, 56(5), 2606–2615.

Walter, G. W., and Centre, T. (1977). "Problems arising in the determination of accurate corrosion rates from polarization resistance measurements." *Corrosion Science*, 17(November 1976), 983–993

Yu, H., Chiang, K. T. K., and Yang, L. (2012). "Threshold chloride level and characteristics of reinforcement corrosion initiation in simulated concrete pore solutions." *Construction and Building Materials*, 26(1), 723–729.

Yuan, Q., Shi, C., Schutter, G. De, and Audenaert, K. (2009). "Effect of temperature on transport of chloride ions in concrete." *Concrete Repair, Rehabilitation and Retrofitting II*, 1(1), 345–352.

Zhang, F., Liu, J., Ivanov, I., Hatzell, M. C., Yang, W., Ahn, Y., and Logan, B. E. (2014). "Reference and counter electrode positions affect electrochemical characterization of bioanodes in different bioelectrochemical systems." *Biotechnology and Bioengineering*, 111(10), 1931–1939.

Zhang, J., Gao, Y., and Han, Y. (2012). "Interior Humidity of Concrete under Dry-Wet Cycles." *Journal of Materials in Civil Engineering*, 24(3), 289–298.

Zhang, X., Zhao, Y., and Lu, Z. (2011). "Probabilistic assessment of reinforcing steel depassivation in concrete under aggressive chloride environments based on natural exposure data." *Journal Wuhan University of Technology, Materials Science Edition*, 26(1), 126–131.

References from which the 100 data points for the diffusion coefficient plot (Figure 2.16) was sourced

Andrade, C., Sanjuán, M. A., Recuero, A., & Río, O. (1994). "Calculation of chloride diffusivity in concrete from migration experiments, in non steady-state conditions". *Cement and Concrete Research*, 24(7), 1214–1228.

Attari, A., McNally, C., & Richardson, M. G. (2016). "A probabilistic assessment of the influence of age factor on the service life of concretes with limestone cement/GGBS binders". *Construction and Building Materials*, 111, 488–494.

Azari, M. M., Mangat, P. S., & Tu, S. C. (1993). "Chloride ingress in microsilica concrete". *Cement and Concrete Composites*, 15(4), 215–221.

Ben Fraj, A., Bonnet, S., & Khelidj, A. (2012). "New approach for coupled chloride/moisture transport in non-saturated concrete with and without slag". *Construction and Building Materials*, 35, 761–771.

Bernal, S. A., Mejía de Gutiérrez, R., & Provis, J. L. (2012). "Engineering and durability properties of concretes based on alkali-activated granulated blast furnace slag/metakaolin blends". *Construction and Building Materials*, 33, 99–108.

Berndt, M. L. (2009). "Properties of sustainable concrete containing fly ash, slag and recycled concrete aggregate". *Construction and Building Materials*, 23(7), 2606–2613.

Buenfeld, N., & Zhang, J.-Z. (1998). "Chloride Diffusion through Surface-Treated Mortar Specimens". *Cement and Concrete Research*, 28(5), 665–674.

Byfors, K. (1987). "Influence of silica fume and fly ash on chloride diffusion and pH values in cement paste". *Cement and Concrete Research*, 17(1), 115–130.

Caré, S. (2008). "Effect of temperature on porosity and on chloride diffusion in cement pastes". *Construction and Building Materials*, 22(7), 1560–1573.

Castellote, M., Alonso, C., Andrade, C., Chadbourn, G., and Page, C. L. (2001). "Oxygen and chloride diffusion in cement pastes as a validation of chloride diffusion coefficients obtained by steady-state migration tests". *Cement and Concrete Research*, 31(4), 621–625.

Cheng, S., Shui, Z., Sun, T., Gao, X., and Guo, C. (2019). "Effects of sulfate and magnesium ion on the chloride transportation behavior and binding capacity of Portland cement mortar". *Construction and Building Materials*, 204, 265–275.

Chung, C.-W., Shon, C.-S., and Kim, Y.S. (2010). "Chloride ion diffusivity of fly ash and silica fume concretes exposed to freeze–thaw cycles". *Construction and Building Materials*, 24(9), 1739–1745.

Collepardi, M., Marcialis, A., and Turriziani, R. (1972). "Penetration of Chloride Ions into Cement Pastes and Concretes". *Journal of the American Ceramic Society*, 55(10), 534–535.

de Vera, G., Climent, M. A., Viqueira, E., Antón, C., and Andrade, C. (2007). "A test method for measuring chloride diffusion coefficients through partially saturated concrete. Part II: The instantaneous plane source diffusion case with chloride binding consideration". *Cement and Concrete Research*, 37(5), 714–724.

Dehghan, A., Peterson, K., Riehm, G., and Herzog Bromerchenkel, L. (2017). "Application of X-ray microfluorescence for the determination of chloride diffusion coefficients in concrete chloride penetration experiments". *Construction and Building Materials*, 148, 85–95.

Dehwah, H. A. F. (2012). "Corrosion resistance of self-compacting concrete incorporating quarry dust powder, silica fume and fly ash". *Construction and Building Materials*, 37, 277–282.

Dhir, R. K., Jones, M. R., and Elghaly, A. E. (1993). "PFA concrete: Exposure temperature effects on chloride diffusion". *Cement and Concrete Research*, 23(5), 1105–1114.

Djerbi, A., Bonnet, S., Khelidj, A., and Baroghel-bouny, V. (2008). "Influence of traversing crack on chloride diffusion into concrete". *Cement and Concrete Research*, 38(6), 877–883.

Erdoğdu, Ş., Kondratova, I. L., and Bremner, T. W. (2004). "Determination of chloride diffusion coefficient of concrete using open-circuit potential measurements". *Cement and Concrete Research*, 34(4), 603–609.

Fenaux, M., Reyes, E., Gálvez, J. C., and Moragues, A. (2019). "Modelling the transport of chloride and other ions in cement-based materials". *Cement and Concrete Composites*, 97, 33–42.

Ganesan, K., Rajagopal, K., and Thangavel, K. (2008). "Rice husk ash blended cement: Assessment of optimal level of replacement for strength and permeability properties of concrete". *Construction and Building Materials*, 22(8), 1675–1683.

Gao, Y., Zhang, J., Zhang, S., and Zhang, Y. (2017). "Probability distribution of convection zone depth of chloride in concrete in a marine tidal environment". *Construction and Building Materials*, 140, 485–495.

Gau, Y., and Cornet, I. (1985). "Penetration of Hardened Concrete by Seawater Chlorides with and without Impressed Current". *Corrosion*, 41(2), 93–100.

Goto, S., and Roy, D. M. (1981). "Diffusion of ions through hardened cement pastes". *Cement and Concrete Research*, 11(5-6), 751–757.

Gowripalan, N., Sirivivatnanon, V., and Lim, C. C. (2000). "Chloride diffusivity of concrete cracked in flexure". *Cement and Concrete Research*, 30(5), 725–730.

Gruber, K., Ramlochan, T., Boddy, A., Hooton, R., and Thomas, M. D. (2001). "Increasing concrete durability with high-reactivity metakaolin". *Cement and Concrete Composites*, 23(6), 479–484.

Gunasekara, C., Law, D. W., and Setunge, S. (2016). "Long term permeation properties of different fly ash geopolymer concretes". *Construction and Building Materials*, 124, 352–362.

Halamickova, P., Detwiler, R. J., Bentz, D. P., and Garboczi, E. J. (1995). "Water permeability and chloride ion diffusion in portland cement mortars: Relationship to sand content and critical pore diameter". *Cement and Concrete Research*, 25(4), 790–802.

Jiang, J., Zheng, X., Wu, S., Liu, Z., and Zheng, Q. (2019). "Nondestructive experimental characterization and numerical simulation on self-healing and chloride ion transport in cracked ultra-high performance concrete". *Construction and Building Materials*, 198, 696–709.

Jung, M. S., Kim, K. B., Lee, S. A., and Ann, K. Y. (2018). "Risk of chloride-induced corrosion of steel in SF concrete exposed to a chloride-bearing environment". *Construction and Building Materials*, 166, 413–422.

Kassir, M. K., and Ghosn, M. (2002). "Chloride-induced corrosion of reinforced concrete bridge decks". *Cement and Concrete Research*, 32(1), 139–143.

Kim, K., Shin, M., and Cha, S. (2013). "Combined effects of recycled aggregate and fly ash towards concrete sustainability". *Construction and Building Materials*, 48, 499–507.

Kim, M.-Y., Yang, E.-I., and Yi, S.-T. (2013). "Application of the colorimetric method to chloride diffusion evaluation in concrete structures". *Construction and Building Materials*, 41, 239–245.

Leng, F., Feng, N., and Lu, X. (2000). "An experimental study on the properties of resistance to diffusion of chloride ions of fly ash and blast furnace slag concrete". *Cement and Concrete Research*, 30(6), 989–992.

Liang, M. T., Wang, K. L., and Liang, C. H. (1999). "Service life prediction of reinforced concrete structures". *Cement and Concrete Research*, 29(9), 1411–1418.

Liu, J., Ou, G., Qiu, Q., Chen, X., Hong, J., and Xing, F. (2017). "Chloride transport and microstructure of concrete with/without fly ash under atmospheric chloride condition". *Construction and Building Materials*, 146, 493–501.

Liu, J., Qiu, Q., Chen, X., Xing, F., Han, N., He, Y., and Ma, Y. (2017). "Understanding the interacted mechanism between carbonation and chloride aerosol attack in ordinary Portland cement concrete". *Cement and Concrete Research*, 95, 217–225.

Liu, Y. W., and Cho, S. W. (2018). "Study on application of fiber-reinforced concrete in sluice gates". *Construction and Building Materials*, 176, 737–746.

Lu, X. (1997). "Application of the Nernst-Einstein equation to concrete". *Cement and Concrete Research*, 27(2), 293–302.

Luo, R., Cai, Y., Wang, C., and Huang, X. (2003). "Study of chloride binding and diffusion in GGBS concrete". *Cement and Concrete Research*, 33(1), 1–7.

Ma, Z., Li, W., Wu, H., and Cao, C. (2019). "Chloride permeability of concrete mixed with activity recycled powder obtained from C&D waste". *Construction and Building Materials*, 199, 652–663.

Mangat, P. S., and Gurusamy, K. (1987). "Chloride diffusion in steel fibre reinforced marine concrete". *Cement and Concrete Research*, 17(3), 385–396

McGrath, P. F., and Hooton, R. D. (1996). "Influence of voltage on chloride diffusion coefficients from chloride migration tests". *Cement and Concrete Research*, 26(8), 1239–1244.

Mustafa, M. A., and Yusof, K. M. (1994). "Atmospheric chloride penetration into concrete in semitropical marine environment". *Cement and Concrete Research*, 24(4), 661–670.

Nguyen, T. S., Lorente, S., and Carcasses, M. (2009). "Effect of the environment temperature on the chloride diffusion through CEM-I and CEM-V mortars: An experimental study". *Construction and Building Materials*, 23(2), 795–803.

Nokken, M., Boddy, A., Hooton, R. D., and Thomas, M. D. A. (2006). "Time dependent diffusion in concrete—three laboratory studies". *Cement and Concrete Research*, 36(1), 200–207.

Ozawa, M., Sakoi, Y., Fujimoto, K., Tetsura, K., and Parajuli, S. S. (2017). "Estimation of chloride diffusion coefficients of high-strength concrete with synthetic fibres after fire exposure". *Construction and Building Materials*, 143, 322–329.

Page, C. L., Short, N. R., and El Tarras, A. (1981). "Diffusion of chloride ions in hardened cement pastes". *Cement and Concrete Research*, 11(3), 395–406.

Page, C. L., Short, N. R., and Holden, W. R. (1986). "The influence of different cements on chloride-induced corrosion of reinforcing steel". *Cement and Concrete Research*, 16(1), 79–86.

Pang, L., and Li, Q. (2016). "Service life prediction of RC structures in marine environment using long term chloride ingress data: Comparison between exposure trials and real structure surveys". *Construction and Building Materials*, 113, 979–987.

Park, B., Jang, S. Y., Cho, J.-Y., and Kim, J. Y. (2014). "A novel short-term immersion test to determine the chloride ion diffusion coefficient of cementitious materials". *Construction and Building Materials*, 57, 169–178.

Qi, B., Gao, J., Chen, F., and Shen, D. (2018). "Chloride penetration into recycled aggregate concrete subjected to wetting–drying cycles and flexural loading". *Construction and Building Materials*, 174, 130–137.

Roy, S. K., Liam Kok Chye, and Northwood, D. O. (1993). "Chloride ingress in concrete as measured by field exposure tests in the atmospheric, tidal and submerged zones of a tropical marine environment". *Cement and Concrete Research*, 23(6), 1289–1306.

Shi, M., Chen, Z., and Sun, J. (1999). "Determination of chloride diffusivity in concrete by AC impedance spectroscopy". *Cement and Concrete Research*, 29(7), 1111–1115.doi:10.1016/s0008-8846(99)00079-4

Song, Z., Jiang, L., Liu, J., and Liu, J. (2015). "Influence of cation type on diffusion behavior of chloride ions in concrete". *Construction and Building Materials*, 99, 150–158.

Tadayon, M. H., Shekarchi, M., and Tadayon, M. (2016). "Long-term field study of chloride ingress in concretes containing pozzolans exposed to severe marine tidal zone". *Construction and Building Materials*, 123, 611–616.

Thomas, M. D., and Matthews, J. (2004). "Performance of PFA concrete in a marine environment—10-year results". *Cement and Concrete Composites*, 26(1), 5–20.

Truc, O., Ollivier, J. P., and Carcassès, M. (2000). "A new way for determining the chloride diffusion coefficient in concrete from steady state migration test". *Cement and Concrete Research*, 30(2), 217–226.

Truc, O., Ollivier, J.-P., and Nilsson, L.-O. (2000). "Numerical simulation of multi-species transport through saturated concrete during a migration test — MsDiff code". *Cement and Concrete Research*, 30(10), 1581–1592.

Van den Heede, P., De Keersmaecker, M., Elia, A., Adriaens, A., and De Belie, N. (2017). "Service life and global warming potential of chloride exposed concrete with high volumes of fly ash". *Cement and Concrete Composites*, 80, 210–223.

Wang, Y., Wu, L., Wang, Y., Liu, C., and Li, Q. (2018). "Effects of coarse aggregates on chloride diffusion coefficients of concrete and interfacial transition zone under experimental drying-wetting cycles". *Construction and Building Materials*, 185, 230–245.

Wood, J. G. M., and Crerar, J. (1997). "Tay road bridge: Analysis of chloride ingress variability & prediction of long term deterioration". *Construction and Building Materials*, 11(4), 249–254.

Xu, J., Li, F., Zhao, J., and Huang, L. (2018). "Model of time-dependent and stress-dependent chloride penetration of concrete under sustained axial pressure in the marine environment". *Construction and Building Materials*, 170, 207–216.

Yeau, K. Y., and Kim, E. K. (2005). "An experimental study on corrosion resistance of concrete with ground granulate blast-furnace slag". *Cement and Concrete Research*, 35(7), 1391–1399.

Yu, S. W., and Page, C. L. (1991). "Diffusion in cementitious materials: 1. Comparative study of chloride and oxygen diffusion in hydrated cement pastes". *Cement and Concrete Research*, 21(4), 581–588.

Yu, Z., Chen, Y., Liu, P., and Wang, W. (2015). "Accelerated simulation of chloride ingress into concrete under drying–wetting alternation condition chloride environment". *Construction and Building Materials*, 93, 205–213.

Zhang, J., Bian, F., Zhang, Y., Fang, Z., Fu, C., and Guo, J. (2018). "Effect of pore structures on gas permeability and chloride diffusivity of concrete". *Construction and Building Materials*, 163, 402–413.

Zhang, P., Cong, Y., Vogel, M., Liu, Z., Müller, H. S., Zhu, Y., and Zhao, T. (2017). "Steel reinforcement corrosion in concrete under combined actions: The role of freeze-thaw cycles, chloride ingress, and surface impregnation". *Construction and Building Materials*, 148, 113–121.

Zhang, W., Ba, H., and Chen, S. (2011). "Effect of fly ash and repeated loading on diffusion coefficient in chloride migration test". *Construction and Building Materials*, 25(5), 2269–2274.

Zhang, Y., Wan, X., Hou, D., Zhao, T., and Cui, Y. (2018). "The effect of mechanical load on transport property and pore structure of alkali-activated slag concrete". *Construction and Building Materials*, 189, 397–40

APPENDIX A

DESIGN OF IMPRESSED CURRENT CORROSION (ICC) SPECIMEN

INTRODUCTION

This section covers the various trials made on the specimen design during the impressed current corrosion (ICC) test. The outcomes of these test results and improvement made on the specimen are discussed in detail.

SPECIMEN DESIGN

Figure A.1 shows the schematic of ICC test specimen. Each ICC test specimen consisted of concrete cylinder (200 long x 100 mm diameter) with a 16 mm rebar embedded at the center. Two grades of concrete M35 and M50 were taken for the study.

(a) No Cover   (b) 20 mm Cover   (c) 50 mm cover
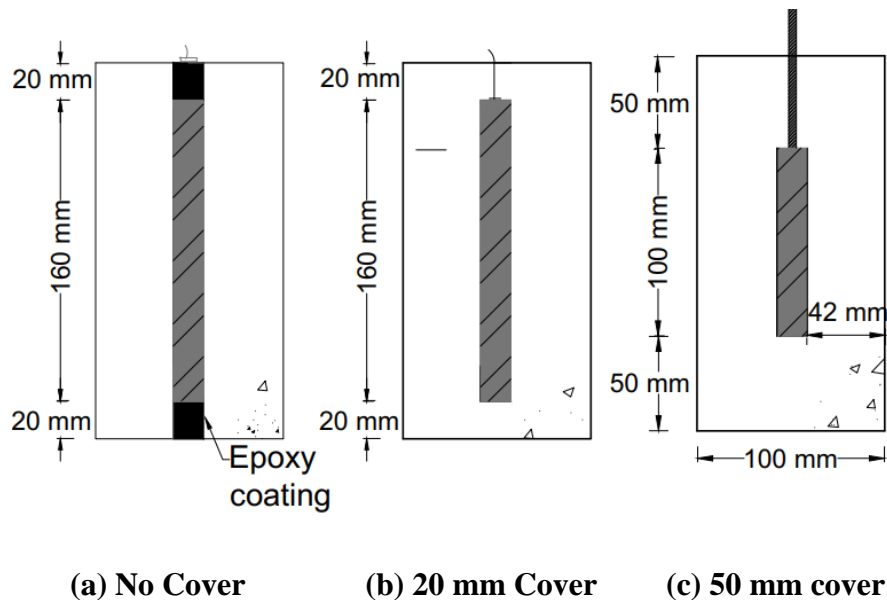
Figure A.1 Specimen design of ICC test

Case I No cover

An external potential gradient of 60 V was applied until failure occurred. The failure is defined as the time at which a current spike was observed. During this time, the corrosion current was measured (across a shunt) every hour after the application of potential gradient. The application of potential gradient and corrosion current measurement was continued until 10% mass loss was observed for OPC and visible crack was observed in other specimens. A total of 18 specimens were cast for this case (See Figure A.1 (a).

Case II Low cover (20 mm)

The specimens were cast as shown in Figure A.1 (b) with 20 mm cover. Here, no epoxy was coated on the rebar. Case II was formulated to test the effect of varying impressed current on corrosion-induced cracking in comparison with case I. The specimens with honey combs and other defects were discarded and hence each set had a different number of specimens contributing to a total of 26 specimens.

Case III Large cover (50 mm)

A total of 30 specimens were cast as shown in Figure A.1(c) with 50 mm cover. For case II and III, the effect of cover on cracking of concrete was studied under the application of the same potential. For both case, II and III, an external potential gradient of 15 Volts was applied for 12 hours a day until failure occurred. During this time, the corrosion current was measured (across a shunt) every 4 hours after the application of a potential gradient. The failure is defined as the time at which visible (using naked eyes) crack was observed. The testing was continued till the specimen cracked or 500 hours of potential application whichever was earlier.

RESULTS AND DISCUSSION

Figure A.2(a) and (b) show the typical graph showing the cumulative current obtained over the exposure time in M35 and M50 concrete respectively. The LC3 system did not crack even after 500 hours of application irrespective of the grade of concrete.

Note: Specimens marked C were cracked and testing discontinued

(a) M35 concrete

Note: Specimens marked with 'C' were cracked and testing discontinued
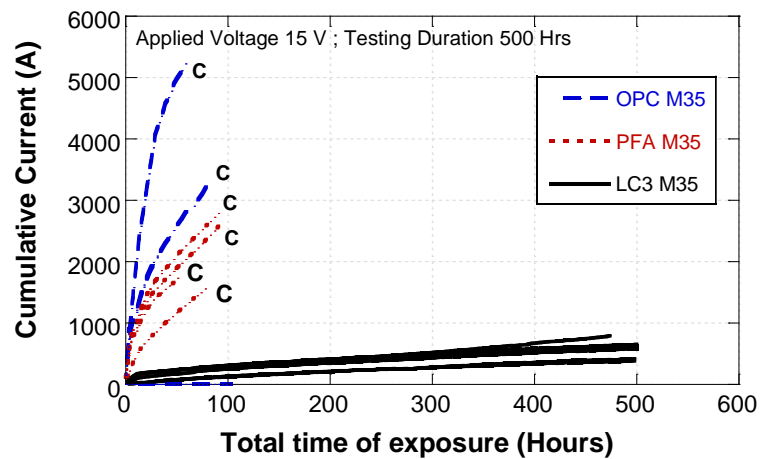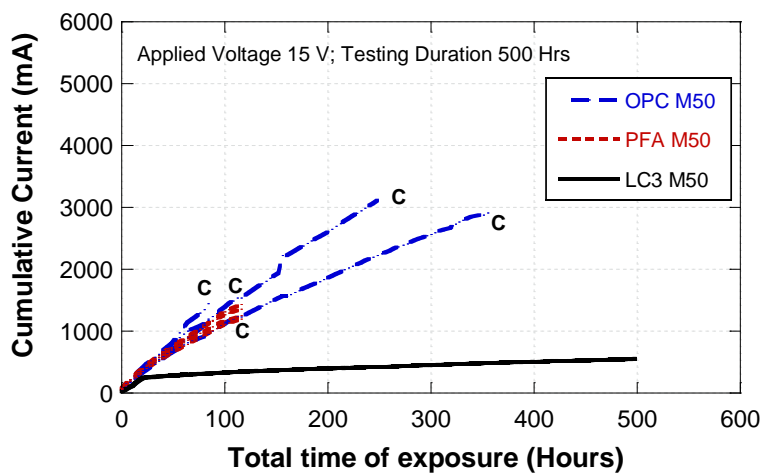
(b) M50 concrete

Figure A.2 Typical curve showing cumulative current as a function of time

The concrete cover cracking depends on many factors such as cover to diameter ratio, nature of S-B interface and quality of cover concrete. The high resistivity of LC3 system resists the current flow through the cover. When compared to OPC and PFA, LC3 has superior performance in restricting corrosion crack propagation in severe corrosive environment at any given instant. Figure A.3 shows the typical result of the three sets, which indicate rate of mass loss in specimens with three different binders and two different concrete grades. It shows that rate of mass loss is very low in LC3 system compared to OPC and PFA systems irrespective of concrete grades.
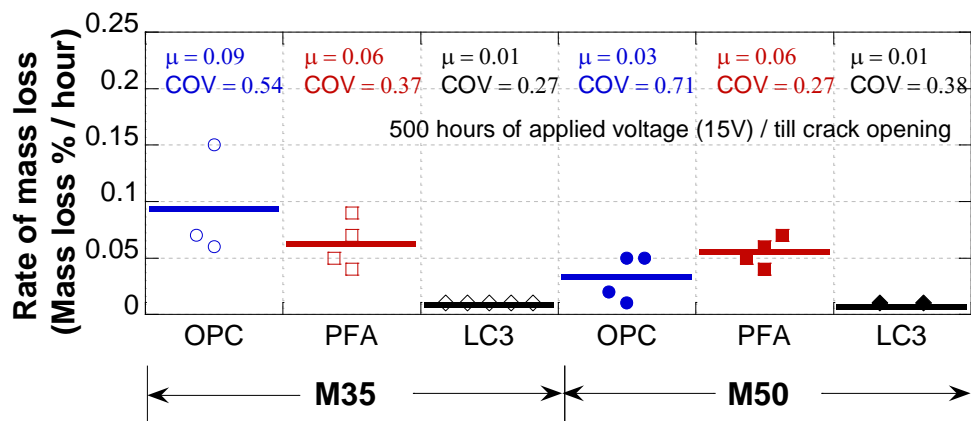
Figure A.3 Mass loss rate in various binders and grades of concrete

Figure A.4 shows the oozing out of corrosion products in LC3 specimen in Case I, Case II and Case III respectively. LC3 systems did not crack. However, rust products started oozing out due to longer application of potential. This could be due to changes in the microstructure of concrete. Also, the stainless steel used for connection got severe corrosion and the connection was lost in some of the LC3 specimens due to higher resistivity of concrete. Hence, the appliction of potential was restricted to 10 hours per day and the specimen design was slightly modified as mentioned in Chapter 4 to avoid the formation of rust in the stainless steel used for connection.
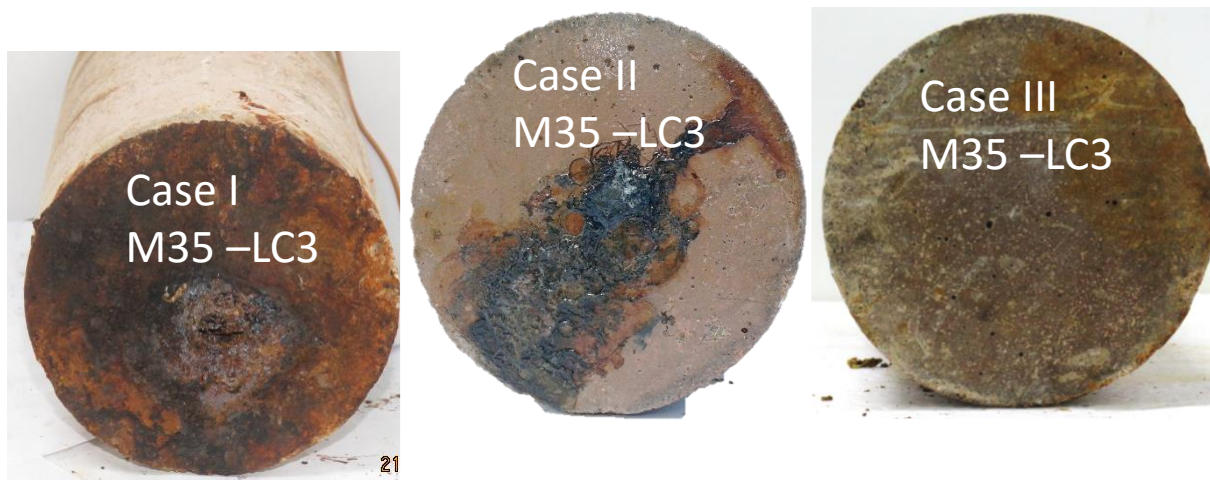
Figure A.4 Visual observation in LC3 specimen (a) Case I, (b) Case II and (c) Case III

Figure A.5 shows the typical corrosion pattern of OPC, PFA, and LC3 systems. OPC and PFA specimens cracked at early at around 100 and 120 hours of testing, whereas LC3 specimens had corrosion products oozing out at the surface at around 300 hours of testing. The rust which came out of the specimens was green in color, which later turned into brown. The rust formed at the steel surface, oozed out through the interconnected pores, which could have formed due to microstructural changes in LC3 as mentioned earlier. This prevented the radial pressure, which causes cracking.

Figure A.5 Specimens showing crack and corrosion products in M35 concrete (Case III)

SUMMARY

This section presented the various specimen designs adopted to conduct the impressed current corrosion test. The outcome of these trails led to the modification of the specimen design and restriction of the duration of the potential application every day.

APPENDIX B

ADMIXED CHLORIDES - PRELIMINARY STUDY

INTRODUCTION

This section describes trial made for the corrosion rate assessment with premixed chlorides. The outcomes of these test results are discussed in detail which led to the improvement on the specimen design.

EXPERIMENTAL PROGRAM

A comprehensive experimental program was conducted to obtain the corrosion current density, i_{corr} data for thermo-mechanically treated (TMT) bar. Three levels of chloride (0%, 5% and 10% NaCl) were added in the mixing water.

Specimen design and preparation

Figure B. shows a schematic diagram of the corrosion test specimen used in this study. Each specimen was prepared using 8mm diameter and 250mm long TMT bar. The bars were cleaned using isopropanol to remove any rust on the surface. The bars were exposed 50mm near the bottom and the rest were coated with two thin layers of low viscosity epoxy (Sikadur-52 UF). The prepared steel pieces were embedded in 100 mm long cylindrical mortar (water: cement: sand ratio - 0.5:1:2.75) and 10 mm cover.
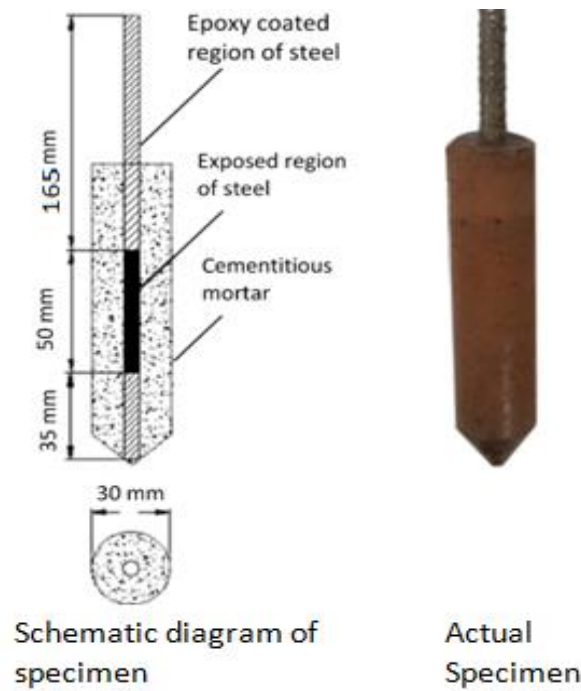
Figure B.1 Lollipop specimen

Curing and exposure condition

The test specimens were cured in laboratory environment (25°C and 65% RH approximately) for 24±1 hours. After this, the specimens were immersed / cured in simulated pore solution (SPS) and testing was started after 7 days.

RESULTS AND DISCUSSION

Figure B.2 shows the $1/R_p$ of the specimens with three different levels of chloride in OPC, PFA and LC3 systems for a period of about 550 days. The $1/R_p$ was very high during the beginning of the test and started to decrease continuously as testing continued, especially in premixed chloride specimens. This behaviour is attributed to the insufficient availability of moisture or oxygen. In the present case, sufficient moisture is available as all the specimens are continuously immersed. Low corrosion rate might be due to non-availability of oxygen. Hence, after 126 days of continuous immersion, the specimens were subjected to alternate wet-dry cycle with 7 days of wetting and 7 days of drying and polarization

resistance was measured by linear polarization resistance (LPR) technique at the end of wetting cycle till 180 days. The samples were then immersed in SPS with chlorides and tested after 365 days. The testing continued till 450 days following the wet-dry cycle. The alternate wet dry cycle exposure of the specimen increased the corrosion rate when compared to continuous immersion. All the binder systems perform very close to each other in corrosion rate and a definite conclusion could not be drawn in the superiority of one system over the other in chloride rich environments. The premixing of chlorides does not give enough time for passive layer formation (Poursaee and Hansson, 2009). The Cl_{th} of SCM based cementitious system will be usually lower than OPC system and SCM based system exhibit higher corrosion resistance due to its resistivity to the chloride ingress. In the premixed chlorides specimen, this resistivity is compromised and hence could not realize the beneficiary effect of SCMs. Hence, to evaluate the corrosion performance of SCMs, premixed chlorides were not adopted. Also, the epoxy coated region of the steel, which was outside of mortar started degrading and severe corrosion was found. Even after cleaning the specimens and recoating of epoxy, the LPR readings were very noisy. So, the specimen design had to be modified to avoid such corrosion on the steel outside of mortar.
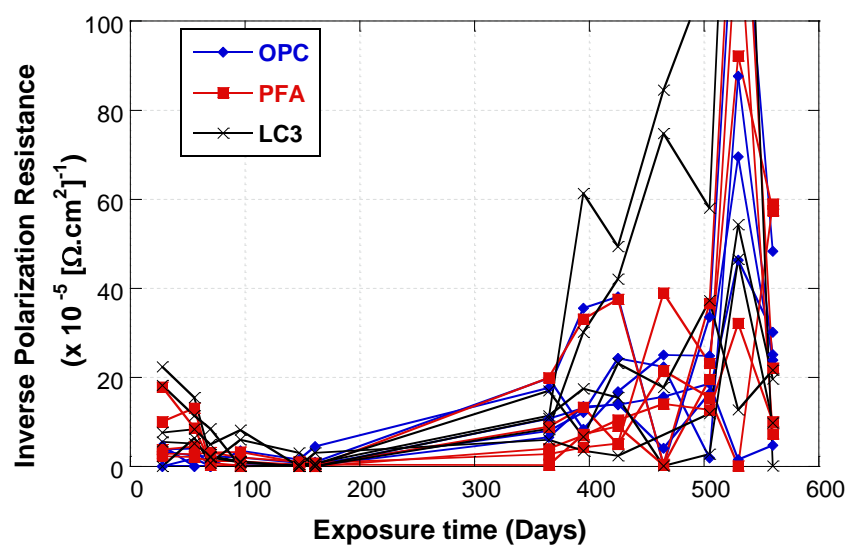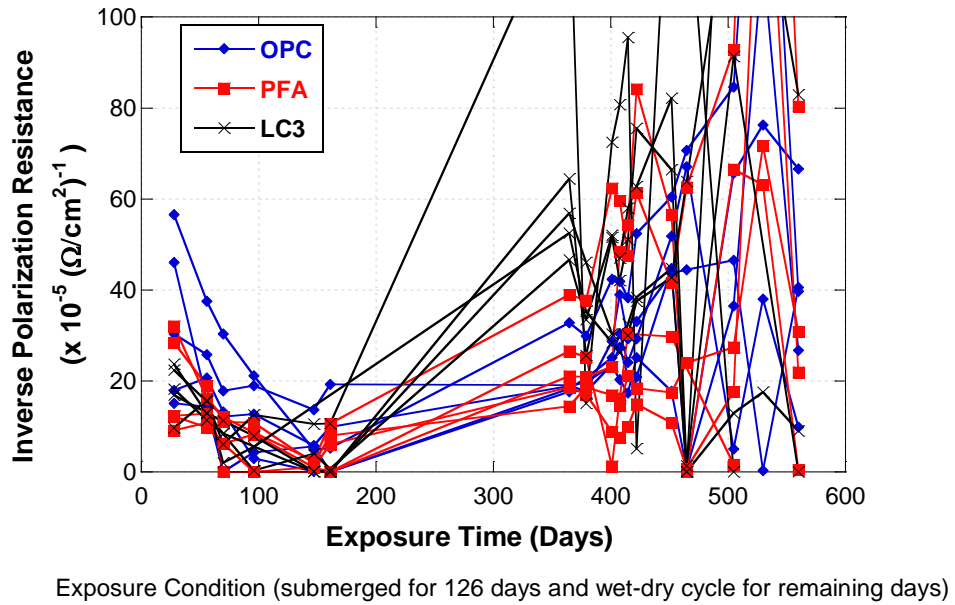

Exposure Condition (submerged for 126 days and wet-dry cycle for remaining days)

(a) Specimens with 0% NaCl

186

Exposure Condition (submerged for 126 days and wet-dry cycle for remaining days)

(b) Specimens with 5% NaCl

Exposure Condition (submerged for 126 days and wet-dry cycle for remaining days)
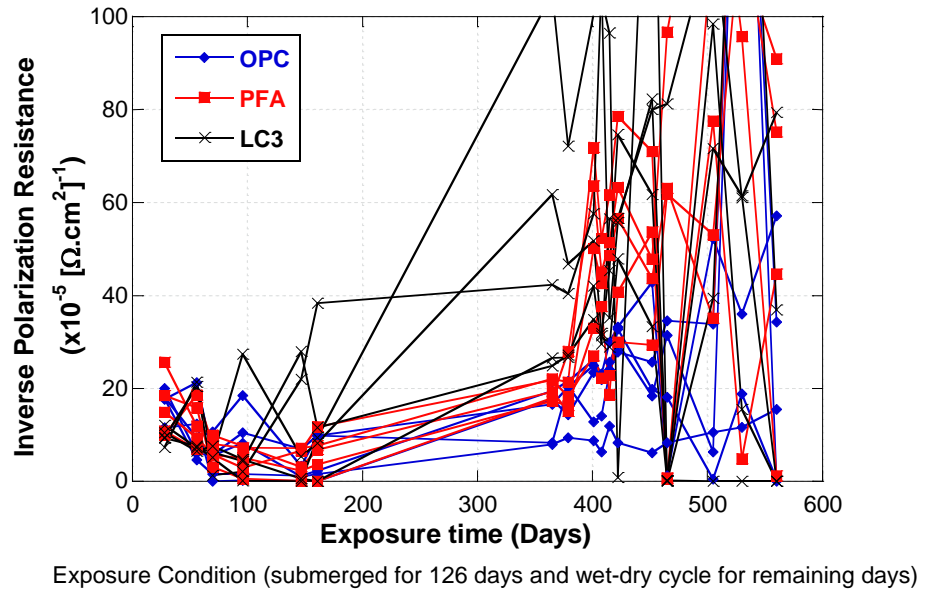
(c) Specimens with 10% NaCl

Figure B.2 $1/R_p$ of lollipop specimens with and without premixed chlorides

187

SUMMARY

This section presented the results of electrochemical testing of specimens with the premixed chlorides. For sustaining the corrosion rate, wet-dry cycle exposure is needed for sufficient availability of moisture and oxygen. Also, it was clear that the specimen design need to be revisited to restrict the exposure region and avoid unnecessary interference from the non-exposure regions due to degradation of epoxy and corrosion.in the experimental results.

APPENDIX C

SENSOR DETAILS AND ITS INSTALLATION

INTRODUCTION

Non-intrusive methods to measure humidity and temperature at the S-B interface is rare due the factors of alkalinity of the cementitious system impacting negatively on the sensor's durability and its accuracy. Also the case gets complex when the specimen undergoes alternate wet-dry cycle. This section details the factors considered to choose, an I_2C (Inter-integrated circuit) digital sensor SHT21 with SF2 filter cap.

SENSOR-SYSTEM SETUP

The sensor-system comprises of the following interconnected hardware and software components.

Hardware

- Sensirion SHT 21
- Sensirion SF2
- Breakout boards 1
- Breakout board 2
- DHT22
- Raspberry Pi version 3
- Internet router

Software

- Python programming code
- Postgresql database
- Thingspeak, cloud platform

Sensirion SHT21 and Sensirion SF2

Figure C.1 shows the sensor and the filter cap used in this study. SHT21 is an industrial sensor, which is pre-calibrated and commercially available. This sensor is capable of sending the data as programmed in the controller (Master-slave concept). Since the sensor is cast in-situ, to protect it from dust and alkalinity, filter cap with water proofing rank IPV67 was used along with the sensor. Both sensor and filter cap were mounted on a PCB with a breakout board and the connection wires were taken out to another PCB. This minimized the size of the sensor so that the space occupied is less.

(a)   (b)
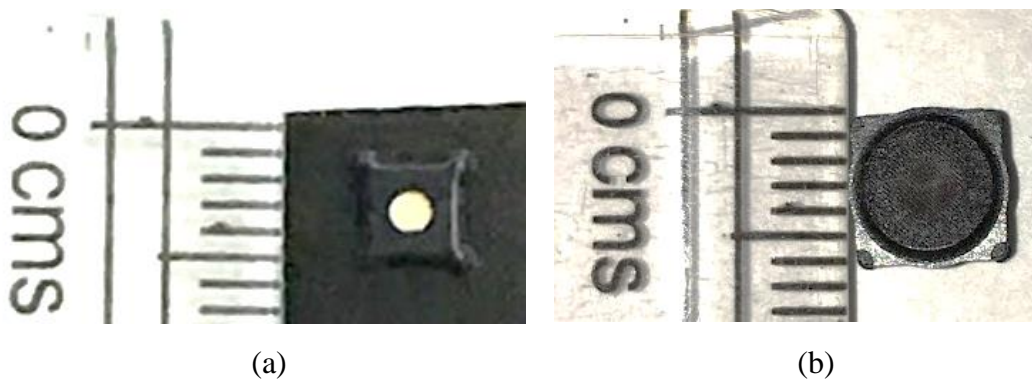
Figure C.1 (a) SHT21 sensor with the cover and (b) filter cap

Details of the Printed board circuit (PCB)

The sensor was mounted on a Printed circuit boards termed as surface mount device (SMD) by means of micro-soldering. The circuit board was designed in such a way to hold the sensor and the filter cap. The other components needed for sending the signals were designed in an outer PCB to reduce the size of the SMD and keep only the minimum required components. The design of the inner SMD and photo of the sensor mounted on the PCB with filter cap is shown in the Figure C.2.

Break-Out Board I

(a)

(b)
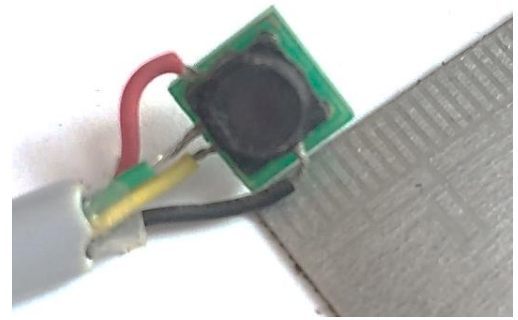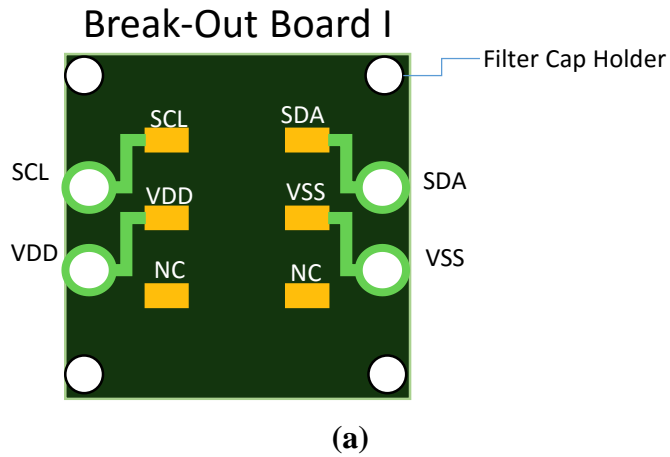
Figure C.2 (a) Design of the break-out board 1 and (b) photo showing its size

The connections were taken out by means of a wire and the other end of the wire was connected to other break-out board as shown in Figure C.3.
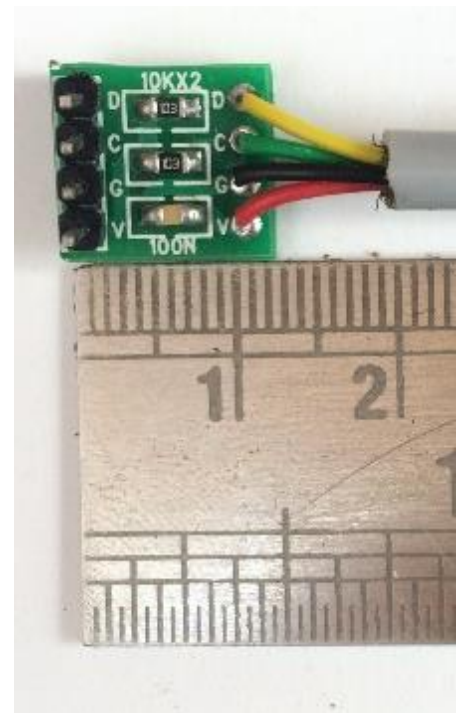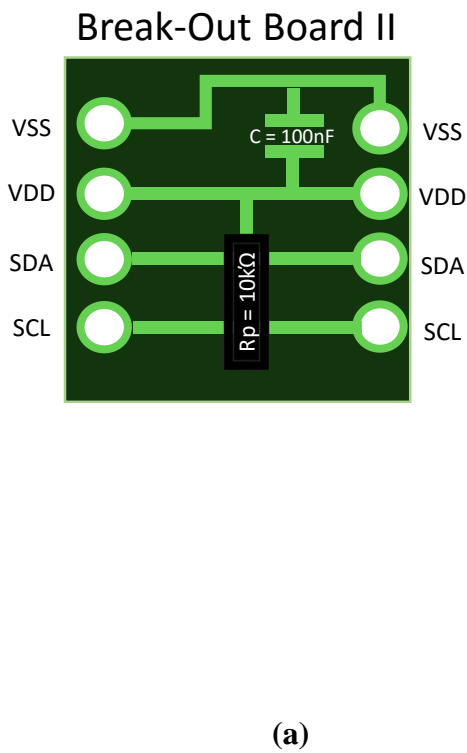

Break-Out Board II

(a)

(b)

Figure C.3 (a) Design of the break-out board 2 and (b) photo showing its size

Figure C.4 shows the entire sensor assembly fabricated at one end with break-out board 1 (with sensor and filter cap) and other end with pins required for the connection with Raspberry Pi.

Figure C.4 Fabricated sensor

Processor

 Raspberry Pi was chosen as the interface between the sensor and cloud, as it is capable of computing and storing the sensor information. Pi is the controller of the sensor, which sends out the command to execute and return the sensing signal. The database in the Pi stored the sensor data and sent it to the cloud (http:// www.thingspeak.com), which enabled the data to be seen online.

SENSOR WORKING PRINCIPLE

Figure C.5 shows the working principle showing the interconnectivity of various components. The Raspberry Pi3 triggers the sensor to read the data of its surrounding through the set of commands in python code. The SMD sends the data back to the Pi through the Break-out board II. An external sensor, DHT22 records the information on the ambient temperature and humidity in the laboratory. From these two data, the variation in temperature and humidity inside and outside the specimen can be obtained. For online monitoring of the data, the Pi is connected to cloud platform through internet.
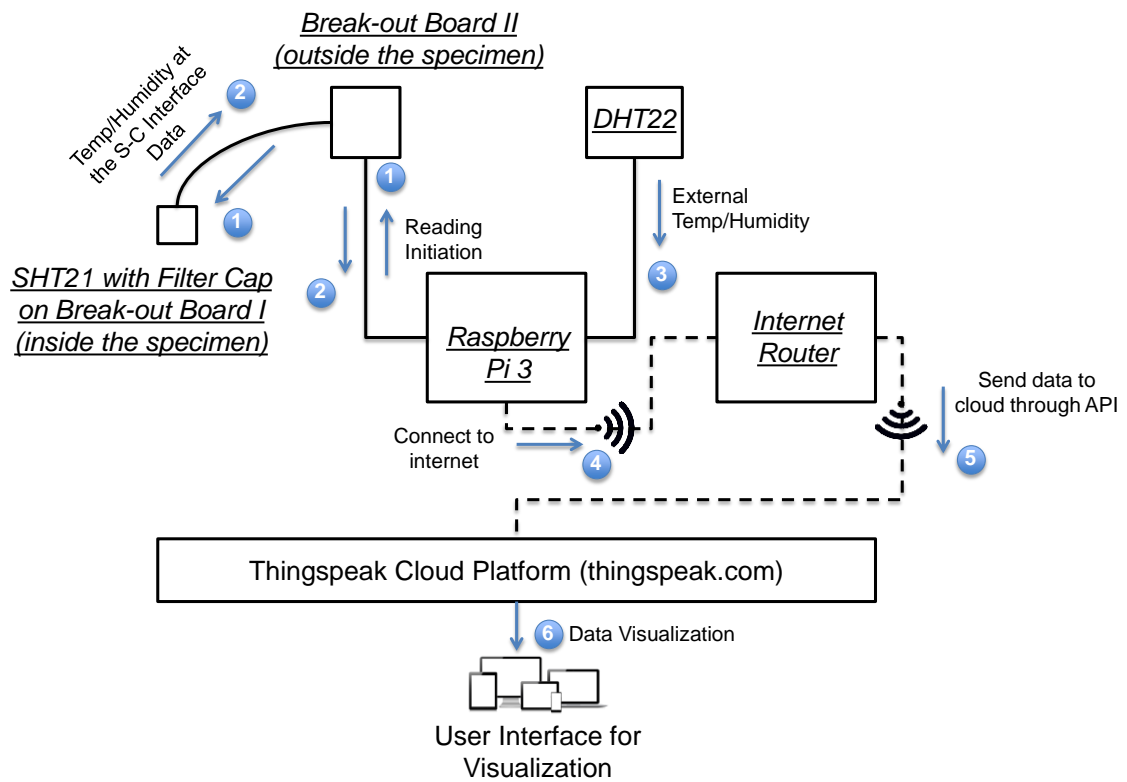
(a) Working principle of the sensor system
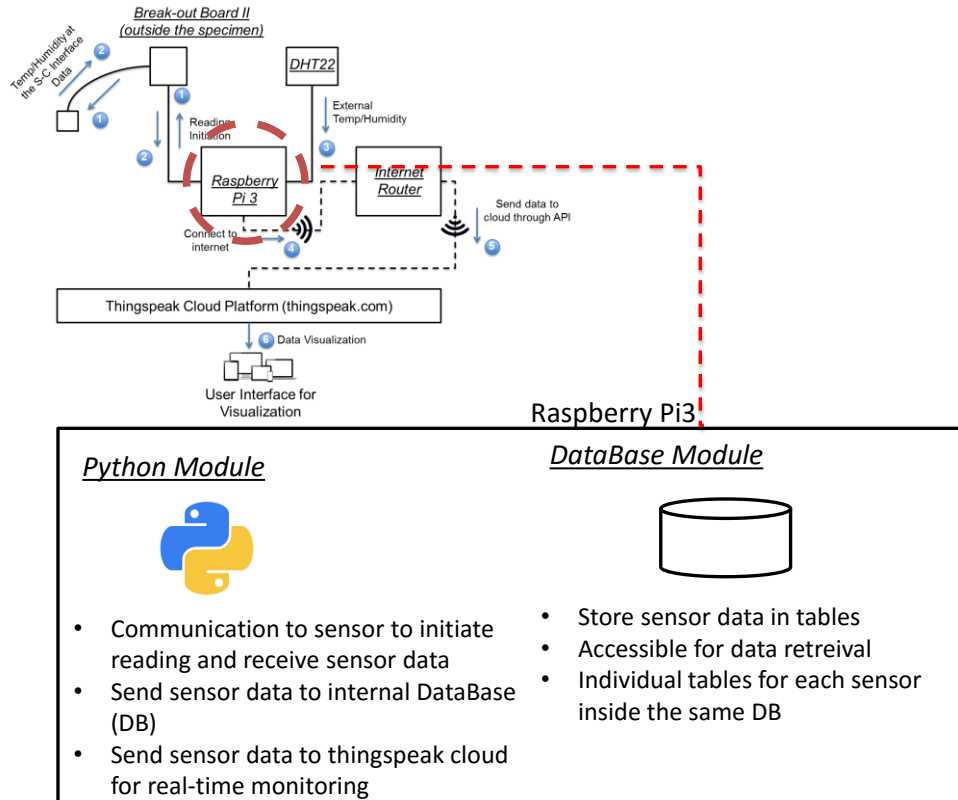
(b) Role of Raspberry Pi3

Figure C.5 Schematic of the Sensor system

METHODOLOGY

Before casting, the sensor system was tested for its accuracy in capturing the temperature and relative humidity. Table C.1 shows the results taken from the sensor-system at two varied environments. The sensor is very sensitive and measure very precisely the temperature and humidity of the ambient conditions of the room.

Table C.1 Results showing the accuracy of the fabricated sensor

| Location	Reading taken after exposure (minutes)	Measured Temperature (°C)	Expected Temperature (°C)	Measured Humidity (%)	Expected Humidity (%)
Fog room	30	26.3	26	95.5	95
	60	26.5	26	95.8	95
	90	26.5	26	96.1	95
	120	26.2	26	96.3	95
	150	26.4	26	96.5	95
	180	26.4	26	95.8	95
	210	26.4	26	95.0	95
Air conditioned laboratory	30	24.9	25	68.7	70
	60	24.7	25	67.8	70
	90	24.3	25	67.8	70
	120	24.7	25	68.8	70
	150	24.6	25	70.4	70
	180	24.4	25	68.3	70
	210	24.3	25	67.2	70

Casting procedure

Figure C.6 shows the step-by step procedure adopted for casting the specimens with sensors for obtaining the relative humidity and temperature at various depths.

(a) Groove made at the centre of a 100 mm wooden log to hold the sensor
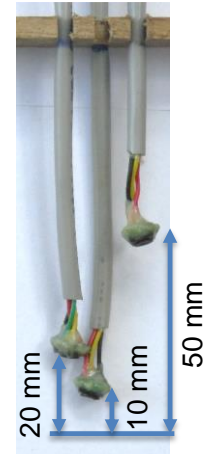
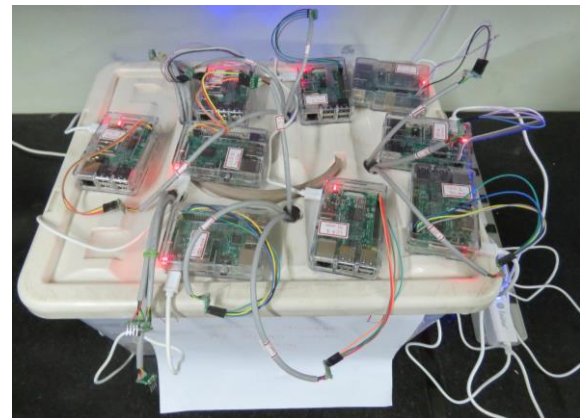**(b) Sensor mounted at different cover depths**
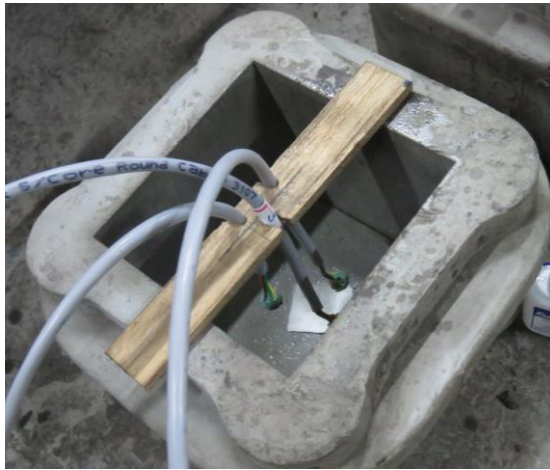
(c) 100 mm cube mould with sensors

(d) Surface finished specimen

(e) Specimens kept in wet cycle

(f) Monitoring of temperature and RH

Figure C.6 step-by-step procedure adopted for monitoring the temperature and humidity

A 100 mm cube was taken for the study. To place the sensors at various depths, a wooden plank with groves was used (Figure C.6(a)). Figure C.6(b) shows the prepared sensors to be kept in the mould, which was filled with mortar (0.5:1:2.75). Three different types of binders, namely OPC, PFA and LC3 was poured. Three replicas were made for each binder making it to a total of 9 specimens. One sensor for each cover depth 10 mm, 20 mm and 50 mm from the bottom was placed in one specimen. Then, the specimens were cured for 28 days and subjected to alternate wet-dry cycle of 2 days wet and 5 days dry in SPS solution. The sensors continuously recorded the temperature and humidity data as programmed.

RESULTS

Figure C.7 (a), (b) and (c) show the temperature and humidity data of OPC specimens at 10 mm, 20 mm and 50 mm cover depth respectively. When the specimen is subjected to curing, the relative humidity was within the range of 95% to 100%. The temperature at any depth follows closely the ambient temperature irrespective of the cover depth. Similar observations were found in PFA (Figure C.8) and LC3 (Figure C.9) specimens. From the results, it is clear that the temperature inside the mortar follows the ambient temperature with a very minimal time gap irrespective of the type of the binder used and depth of the cover. However, there is significant lag in the RH when different cover and binder are used. The lag could not be stablished clearly due to the failure of the sensor due to insufficient water proofing. The filtercap used for protecting the sensor is of the standard IPV67, which can withstand moisture to some extent. However, the 50 mm sensors were unable to give data for a longer period due to 100% saturation prevailing there all the time. The sensor assembly was capable of giving data for a longer duration when the specimen was dry. When the specimen was subjected to alternate wet-dry cycle, 100% saturation for prolonged period made the sensors to fail. Hence, a proper water proofing system is

necessary for continuous monitoring of the data. From this study, it was found that 2 days wet is sufficient for obtaining the 100% saturation at the interface when 10 mm cover was used. Hence, 2 days wet and 5 days dry cycle was adopted for hr-ACT method.
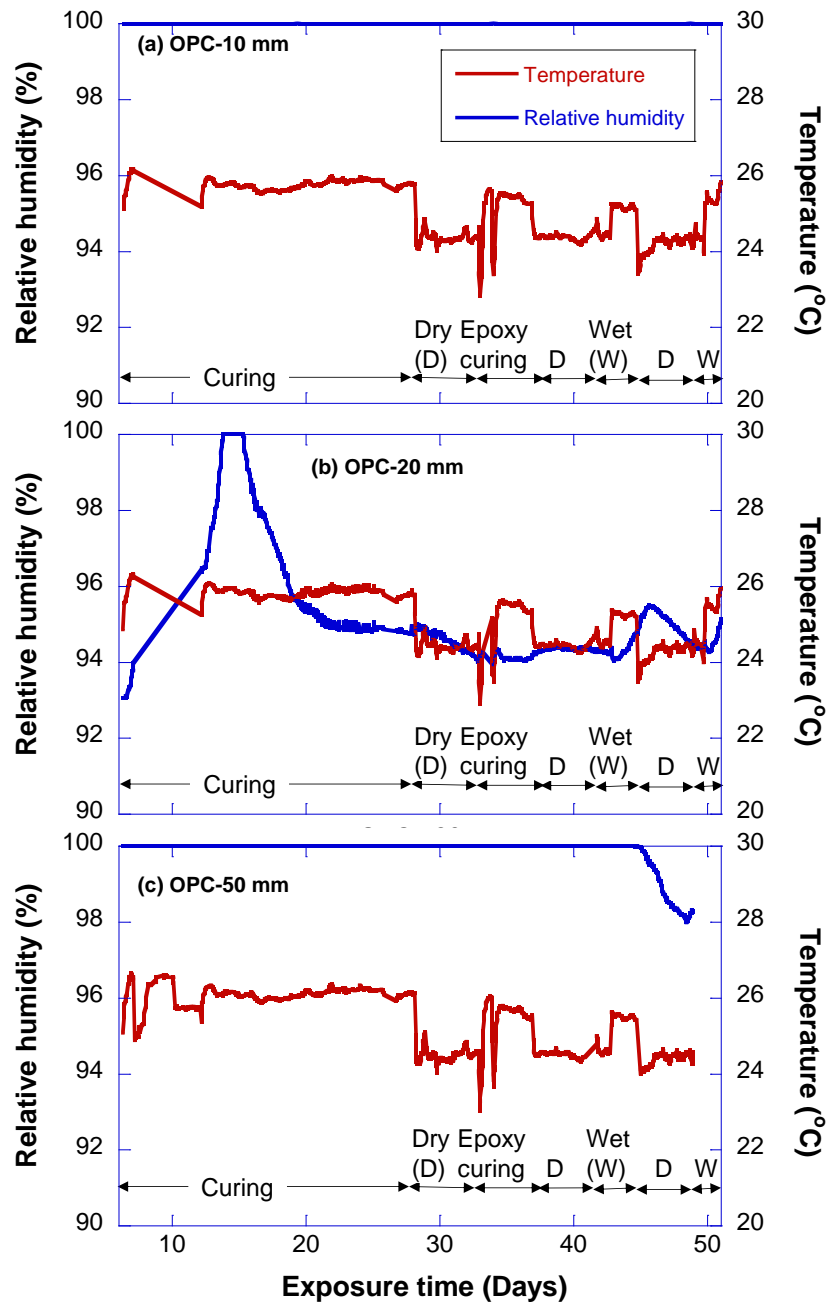

Figure C.7 Temperature and relative humidity data from OPC specimens
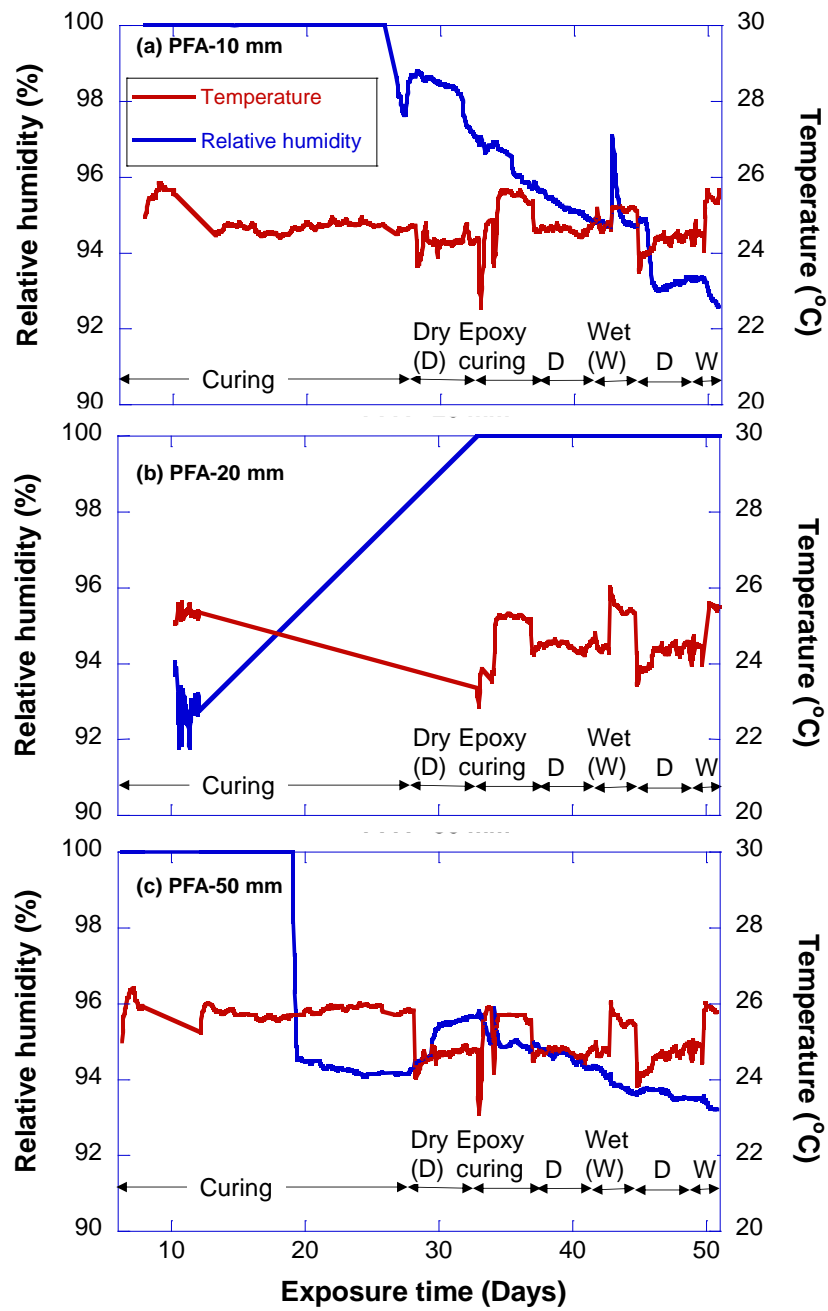
Figure C.8 Temperature and relative humidity data from PFA specimens
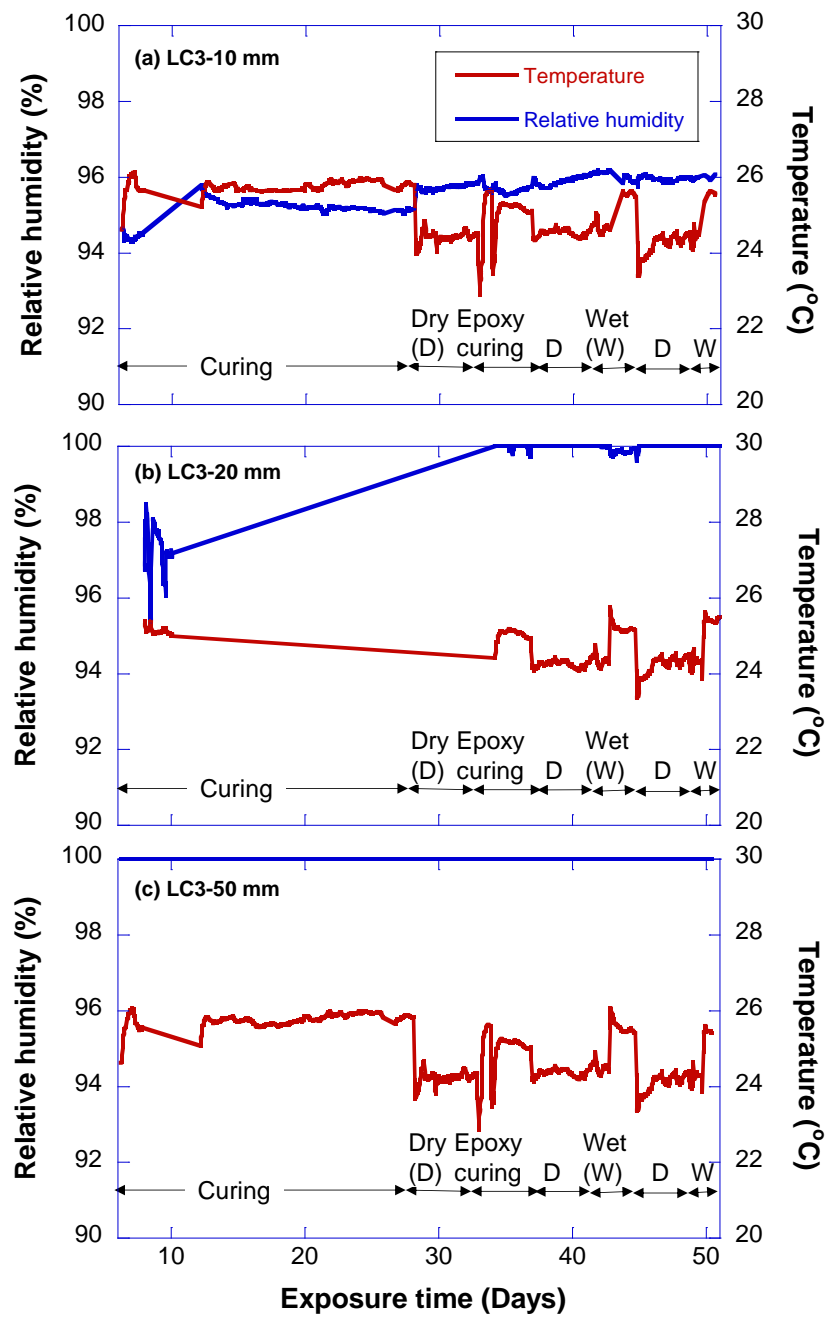
Figure C.9 Temperature and relative humidity data from LC3 specimens

PRECAUTIONS

The following are the precautions that need to be taken while handling the sensor specimens

(i) The connections from the break-out board1 are very sensitive to moisture resulting in corrosion and disconnection. Hence, proper water proofing needs to be done.

(ii) A protection mechanism for the sensor under 100% saturation need to found for continuous data for a longer period.

SUMMARY

This section presented the detailed experimental procedure and the results from the sensor specimens. The ability of the sensor for continuous monitoring in the dry period is established. However, a methodology for monitoring the data in 100% saturation need to be investigated further.

APPENDIX D

MACROCELL CORROSION - PRELIMINARY STUDY

INTRODUCTION

Nowadays, supplementary cementitious materials (SCMs) and corrosion inhibiting admixtures (CIAs) are used to delay the onset of corrosion in reinforced concrete structures. The use of SCMs and/or CIAs could result in 'moderate', 'high', and 'very high' resistive concrete, which pose significant challenges in their performance assessment. Using ASTM G109 (2013) test procedure, the present study monitored the corrosion of TMT steel in concretes with various resistivity levels and identified the possible corrosion mechanisms.

EXPERIMENTAL PROGRAM

The experimental program adopts ASTM G109 test method where three types of cement (namely Ordinary Portland Cement (OPC), Portland Pozzolana Cement (PPC), and Portland Slag Cement (PSC) –details are provided in Table D.1) and three CIAs (two anodic and one bi-polar type) were used to prepare various concretes (see Table D.2 for mixture proportions). The cement content, aggregate content and w/b were kept constant for all the concrete mixes. The CIAs were added as per the dosages recommended by the manufacturer (see Table D.3). Three ASTM G109 specimens were cast for each variable combination.

Table D.1 Chemical composition of Ordinary Portland Cement (OPC) and two blended cements used in this test program

Ingredient	Concentration (%)		
	OPC	PPC	PSC
Al_2O_3	4.51	9.04	12.64
CaO	66.67	53.51	46.09
Fe_2O_3	4.94	2.89	4.58
K_2O	0.43	0.50	0.70
MgO	0.87	3.77	0.74
Na_2O	0.12	0.13	0.13
SiO_2	18.91	26.00	30.98
SO_3	2.50	2.88	2.61

Table D.2 Mix design for concrete used

Ingredients	Quantity (kg/m³ of concrete)
Cement	400
water/binder	0.42
Fine aggregate	630
Coarse aggregate	1170
Corrosion inhibitors	As per Table C.3

Table D.3 Properties of corrosion inhibitors used

Type of inhibitor (chemical families)	Solid content (%)	Dosage (kg/m³)
R2: Amino alcohol	3	5
CN: Calcium nitrate and Calcium nitrite	45	25
RC: Calcium nitrate, Nitrous acid, and Calcium salt	32	20

Specimen preparation

As shown in Figure D.1, QST/TMT steel pieces of 16 mm diameter was used for this study. The steel pieces of 400 mm length were cut using a chop saw with an abrasive cutting blade. The surface of the steel was cleaned using acetone and wiped clean using a cloth. The 200 mm long portion at the centre of the steel rebar piece was exposed and the rest were coated with two thin layers of low viscosity epoxy (Sikadur 52 UF). The epoxy coating was left to cure for two days. The ASTM G109 specimens were cast using the prepared steel rebar pieces and cured for 28 days after casting. Then, a 15 mm thick slice was removed from the cover concrete – reducing the cover depth to 10 mm. A typical concrete cutter with a circular blade (diamond tipped) was used for the purpose. This reduction in cover depth helped in reducing the time required for chlorides to reach the steel rebar (anode) and eliminated the surface edge effects. After 28 days of curing, the specimens were kept in an environment of 70 ± 5 % relative humidity and 30 ± 5 °C for two weeks. Then, the epoxy coating was applied on the surfaces of the concrete prism specimen (except the area inside the chloride reservoir and bottom surface). The bottom surface was left uncoated to ensure oxygen availability for cathodic reaction and the top surface (inside the reservoir) was left uncoated to allow the one-dimensional chloride penetration. After the curing of epoxy, the top and the two bottom rebars were electrically connected using a 100 Ω resistor, as shown in Figure D.1. In QST/TMT solid rebars, a 4 mm diameter screw was used to fasten the lead wires to the resistor. The 2 mm thick acrylic sheets were cut and joined using chloroform to make the chloride reservoir. Then, the acrylic sheets were glued (using silicone sealant) to the clean and dry concrete surface.
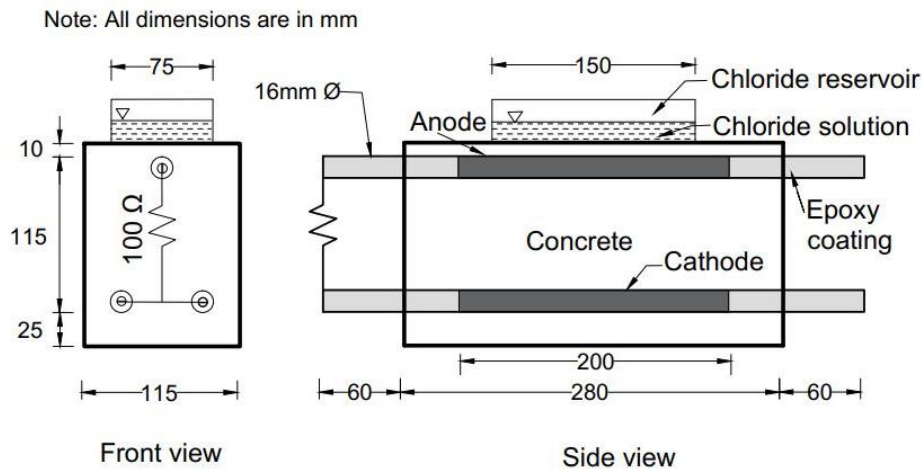
Figure D.1 Schematic diagram of ASTM G109 specimen with 10 mm cover

Chloride exposure and corrosion monitoring

The specimens were subjected to cyclic wet dry exposure (14 days of ponding followed by 14 days of drying) using 3% sodium chloride solution. The voltage across the 100 Ω resistor (i.e., in Circuit 1 - between the top and bottom rebars) was measured using a 5.5 digit precision multimeter at the 7th day of wetting in each cycle. This was used to calculate the $I_{corr, average}$ in Circuit 1. The End of Testing (EoT) was defined as the time when $I_{corr, average}$ attains 150 Coulombs (as per the ASTM G109) or 365 days of exposure, whichever was earlier. At EoT, all the specimens were autopsied and the anode steel was visually observed for corrosion.

Bulk resistivity measurements

As shown in Figure D.2, at the EoT, 70 mm cylindrical specimens were cored from the center of the prismatic specimens. The cored cylindrical specimens were cut to 150 mm length and bulk resistance was measured using Electrochemical Impedance Spectroscopy (EIS) in the surface wet condition (not saturated). Figure D.2(b) shows the schematic and photo of the EIS test setup with two stainless steel plates attached to the ends (acted as electrodes) of the cored specimen. The specimen was tested using a two-electrode

configuration using Solartron 1260 coupled with 1287. The EIS test parameters included a frequency range of 1 MHz to 2.5 kHz, AC amplitude of 10 mV, and 7 points per decade (per unit change of magnitude). Because of the high dielectric constant of concrete specimens, the EIS plots obtained at lower frequencies (say, less than 2.5 kHz to 1 Hz) exhibited significant noise; and hence, were not used in the calculations as shown in Figure D.3. The bulk resistance of concrete is determined as the distance from the origin to the projection of 'the point of intersection of the bulk and electrode arcs' on the abscissa of the Nyquist plots obtained. The bulk resistance of air-dry concrete is then converted to bulk resistivity of air-dry concrete by considering the dimensions of the specimen (70 mm dia. and 150 mm length). Further, it is converted to that of a saturated-surface dry specimen by using a factor of 0.1 for air-dry conditions.
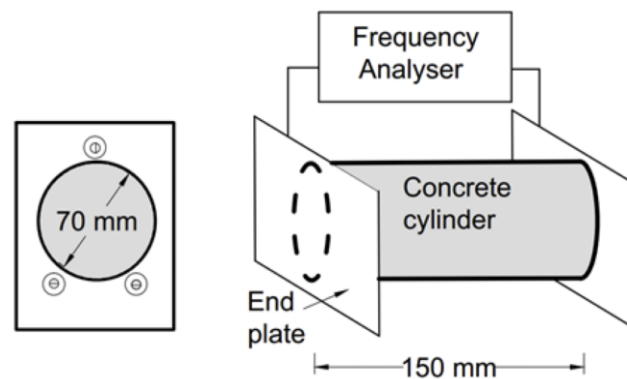

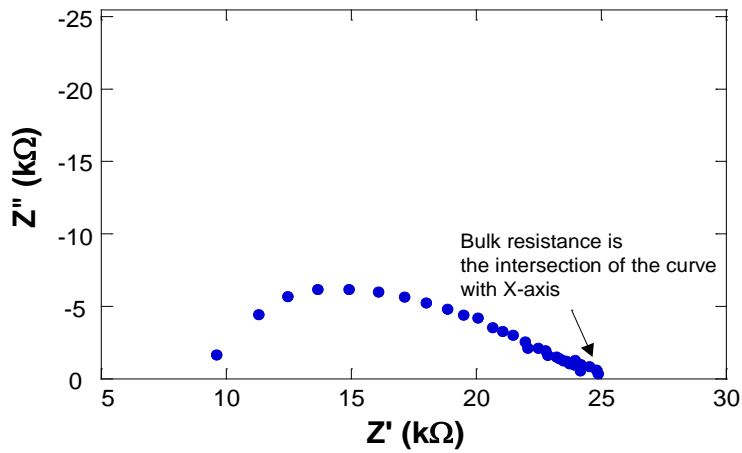**Figure D.2 (a) Core location (b) Bulk resistance test set-up**

Figure D.3 (a) Core location (b) Bulk resistance test set-up

RESULTS AND DISCUSSIONS

In this section, discussions on (i) Bulk resistance, (ii) Effect of cement type and CIAs on macrocell current, (iii) calculation of total average corrosion current, and (iv) Calculation of total average corrosion current ($I_{corr, average}$) are presented.

Bulk resistance

The type and quantity/dosage of binder and corrosion inhibiting admixtures (CIAs) can influence the resistance of concrete. This can affect the type of governing macrocell corrosion circuits. Figure D.4 shows the box plot on the bulk resistance exhibited by the 12 types of concretes (i.e., OPC, PPC, and PSC concretes with and without CIAs; see Table D.4) used. The bulk resistivity of saturated-surface dry concrete is categorized as follows: (i) low (< 25 kΩ.cm), (ii) moderate (25 to 50 kΩ.cm) (iii) high (50 to 100 kΩ.cm), and (iv) very high (> 100 kΩ.cm). In Figure D.4(a), (b), and (c), these regions are demarcated using the dashed, horizontal lines.

In the case of specimens without CIAs [1st box in Figure D.4 (a), (b), and (c)], the OPC concrete exhibited low resistivity (≈ 25 kΩ.cm); the PPC and PSC concretes exhibited ≈ 50 to 100 kΩ.cm (i.e., lower and upper regions of high resistance category). In general,

CIAs did not induce significant effects on resistivity, except in the case of R2 type CIA in PPC and PSC concretes. The 'very high' resistivity with significant scatter was observed only when the R2 type CIA was used. This is probably due to the additional pore blocking mechanism of R2, which significantly reduced the moisture ingress and enhanced the resistivity. It is evident that, even in the presence of CIAs, the PPC and PSC cement can enhance the microstructure and increase the resistivity of concrete. This effect is more prominent in PSC systems than in PPC systems. For example, a comparison of the box plots in the third columns in Figure D.4(a), (b), and (c) indicates that the resistance increased by about two and four times when OPC was replaced by PPC and PSC, respectively. In such levels of resistivity, monitoring of Circuit 1 macrocell current may not be sufficient.
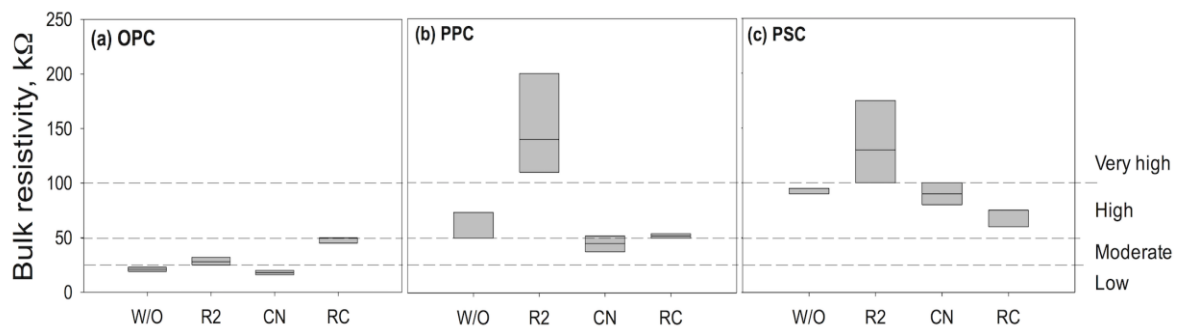

Figure D.4 Bulk resistivity of different concretes

Table D.4 Experimental design and key results

Type of cement	Type of steel	Number of Specimens [a]	Resistivity level	Results		
				Remarks on observed macrocell corrosion current	Could Circuit 2 exist?	Could the test detect Circuit 2?
OPC	TMT/ QST	12	Low to Moderate	High initial value	No	No
PPC	TMT/ QST	12	Moderate to High	Low in some cases	Yes [c]	No
PSC	TMT/ QST	12	Moderate to High	Low in some cases	Yes [c]	No
[a] 3 × 4 = 12; 3 replicas each of W/O, R2, CN, and RC type specimens (see Table C.3 for details). [b] When the resistance level is high.						

Effect of cement type and CIAs on macrocell current

Figure D.5 shows the macrocell current (Circuit 1) exhibited by the ASTM G109 type specimens with solid rebars. The subplots a-d, e-h, and i-l in Figure D.5 exhibit the behaviour of specimens with OPC, PPC, and PSC concrete, respectively (without and with three CIAs).
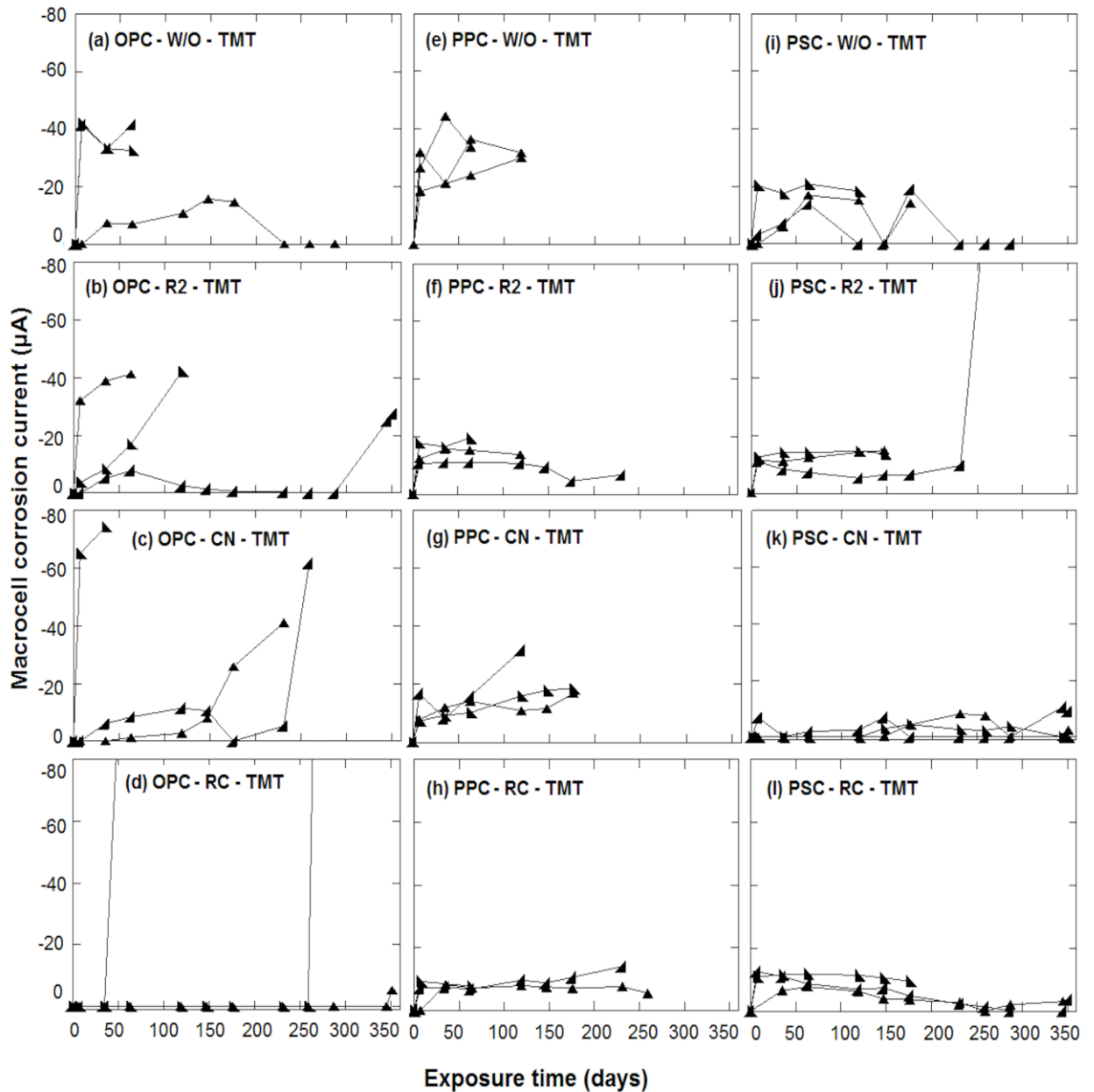
Figure D.5 Macrocell current Vs Exposure Time for QST/TMT specimens

In general, higher macrocell current was observed in OPC specimens when compared to the corresponding PPC and PSC specimens with higher resistivity. The resistivity of cover plays a significant role and is evident in the form of low macrocell current readings. The refined pore structure and high ionic resistance due to the pozzolanic reaction and the chloride binding due to the presence of aluminates enhance the corrosion resistance in the PPC and PSC specimens. In this case, PSC specimens performed better than PPC specimens. This shows that in case of solid rebars, resistivity determines the type of

macrocell corrosion circuit. In solid rebar specimens with CIAs, calcium nitrite based commercial inhibitors (CN and RC) were effective and the corrosion initiation time was enhanced by nearly 50% for all the three cases namely, OPC, PPC and PSC. From the results, it can be inferred that the decrease in resistivity due to CIAs did not significantly affect the corrosion performance and was compensated by the action of the inhibitors on the steel surface to prevent corrosion.

Possibility of Circuit 2 type corrosion

The resistivity of concrete can influence the type of macrocell circuit. In general, OPC specimens with low resistivity indicated high Circuit 1 current when the top rebar exhibited corrosion initiation. On the other hand, the PPC and PSC specimens with highly resistive concrete exhibited low current in Circuit 1 even when visible corrosion stains were observed on the concrete surface. Then, the specimens were autopsied and the top rebars were found to be significantly corroded. This indicates the presence of high current in Circuit 2 - completed by the movement of hydroxyl ions through the steel-concrete interface, as shown in Figure D.6. [Note: Figure D.6 is the reproduction of Figure 3.6(a) for the ease of the user]
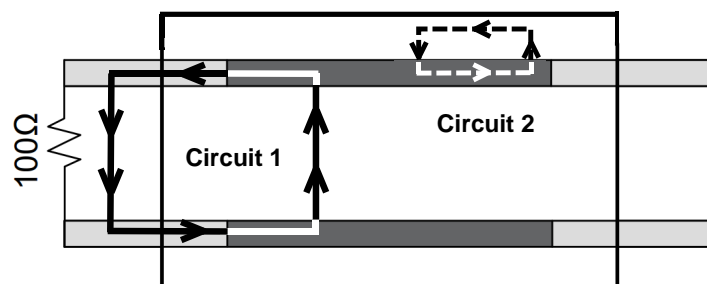

Figure D.6 Circuit 2 corrosion mechanism in highly resistive concrete

Calculation of total average corrosion current ($I_{corr, average}$)

The ASTM G109 standard defines the failure point as the time taken for $I_{corr, average}$ to reach 150 C. However, there were difficulties in correctly calculating $I_{corr, average}$ for many specimens in this study. This was due to the change/reversal in the sign of macrocell current (Circuit 1) observed at multiple times during the exposure period. Figure D.7 shows the raw macrocell corrosion current of specimens exhibiting this change in sign (negative current indicates that the top bar is anodic and vice versa). For brevity, data from only 9 QST/TMT (among 36 specimens each) are shown in Figure D.7. It is believed that this change in the sign of current could be due to one or more of the following situations: (i) passive state of the top steel (ii) dry S-B interface of top steel, (iii) saturated concrete adjacent to the top steel, which cathodically polarizes the top steel (i.e., the potential shifts to a value below the equilibrium potential in the cathodic region). Also, this current reversal was found more often for OPC and PSC specimens. The current reversals, it's reasoning, and how to incorporate it during the calculation of $I_{corr, average}$ is not well-reported. However, as the dissolution of metal is an irreversible process (i.e., Fe^{2+} ions cannot re-adhere to the steel rebar once it is dissolved in solution), the positive current values cannot be considered as such to calculate $I_{corr, average}$. Hence, in this study, all the positive values were changed to zero while calculating $I_{corr, average}$ as per Equation (D.1) given in ASTM G109 (2013).

$$TC_j = TC_{j-1} + [(t_j - t_{j-1}) \times \frac{i_j + i_{j-1}}{2}] \qquad \text{D.1}$$

where, TC = Total corrosion (Coulombs); t_j = Time (seconds) at which the measurement of the macrocell current is carried out; and i_j = Macrocell current (Amps) at time, t_j. If $i_j >$ zero, then i_j is considered as zero. Note that the parameter TC_j in ASTM G109 is same as $I_{corr, average}$.
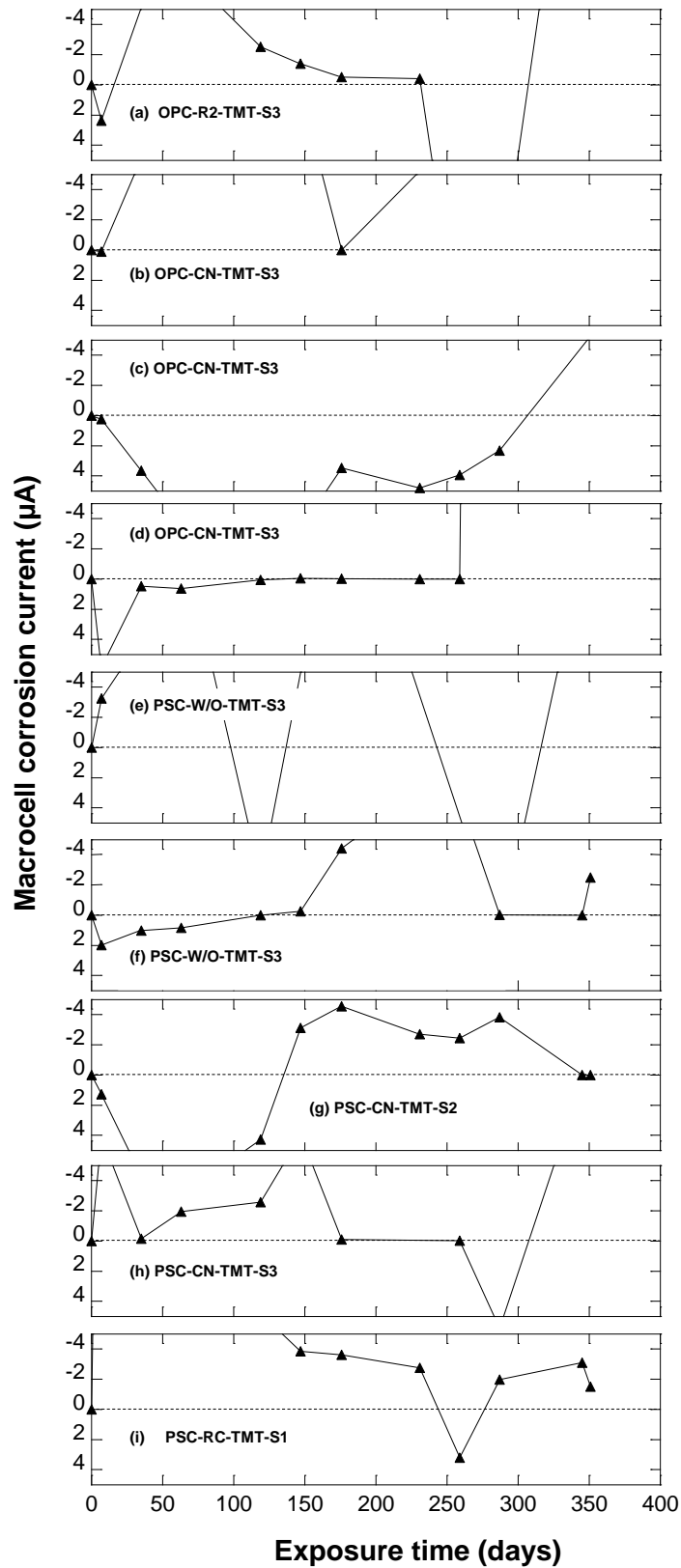
Figure D.7 Raw macrocell current showing change of sign in QST/TMT specimens

The current discrepancy, $I_{discrepancy}$, between the $I_{corr, average}$ calculated using the raw data and modified data are provided in Figure D.8 using the Equation (D.2).

$$I_{discrepancy} = \frac{I_{corr,average,raw} - I_{corr,average,corrected}}{I_{corr,average,raw}} \times 100 \qquad \text{D.2}$$

where, $I_{corr, average, raw}$ and $I_{corr, average, corrected}$ are the $I_{corr, average}$ calculated using the raw and modified data. It shows that 14 among the 36 QST/TMT rebar specimens showed discrepancies, which necessitates the measurement of Circuit 2, as it is the governing phenomenon in these cases.
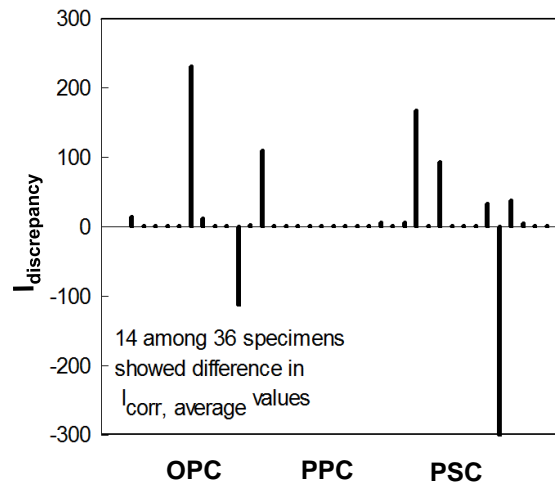

Figure D.8 Discrepancy in $I_{corr, average}$ calculation in QST/TMT

SUMMARY

In systems with solid rebars, anodes and cathodes forming on same rebar (Circuit 2a type corrosion) happens when the concrete is of very high resistivity. Also, the equation to calculate the total current, TC_j given in ASTM G109 cannot be used directly as there are challenges in the case of reversal of macrocell current and positive macrocell current. Hence, it is proposed to use the modified Equation D.1 for the calculation of total current.

APPENDIX E

FITTING EIS-CURVE WITH AN EQUIVALENT CIRCUIT

SELECTION OF EQUIVALENT CIRCUIT

Choose an equivalent circuit, which can define the physical elements in the S-B system. For e.g., Figure E.1 (a) and (b) show the EIS response and the Randles circuit. The physical meaning of a simple S-B system can be interpreted in the form of the equivalent circuit. R_{sol} represents the resistance of the cover material, C_{dl} the capacitance of the double layer, R_{ct} the charge transfer resistance and W_o the Warburg impedance. Warburg impedance represents the diffusional behavior, which has a unique 45° tail in the EIS spectra.
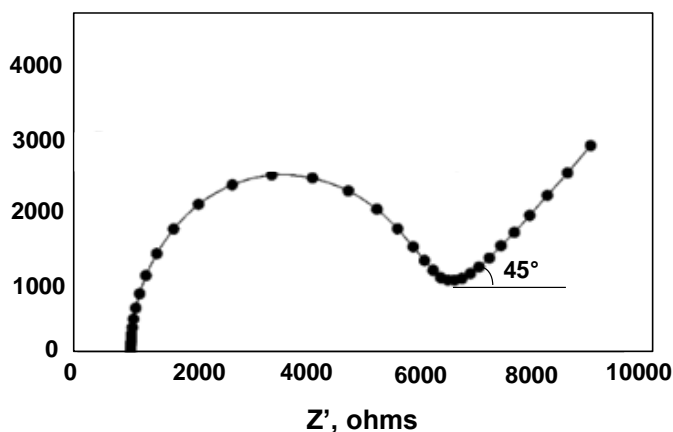
(a)
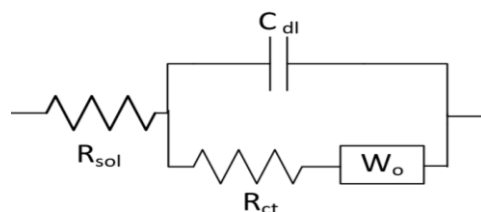
(b)

**Figure E.1 (a) EIS response and (b) Randles circuit**

If the steel has a coating, one more RC element can be added to the equivalent circuit to represent the coating behavior. Similarly, if the cover is saturated, the cover will have capacitance effect in addition to $R_{sol.}$ Hence, the equivalent circuit has to be chosen according to the S-B system under analysis.

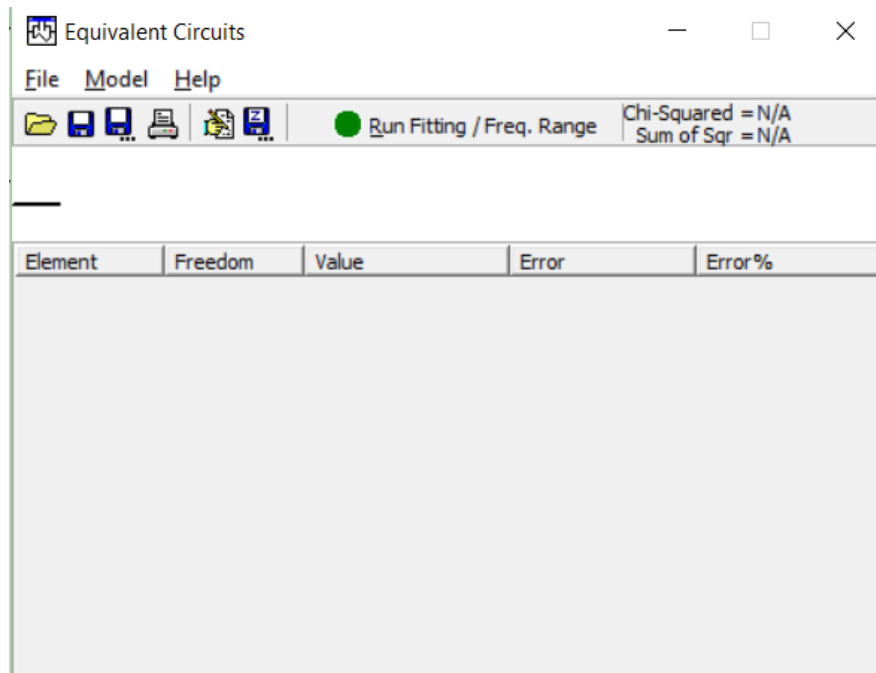**FITTING OF THE EQUIVALENT CIRCUIT**.

For the fitting purpose, any fitting software's such as Zplot, ZSwimpwin etc. can be used. For demonstration purpose, Zview is used in this study.

    i)   Open the EIS file to be fitted in the main menu
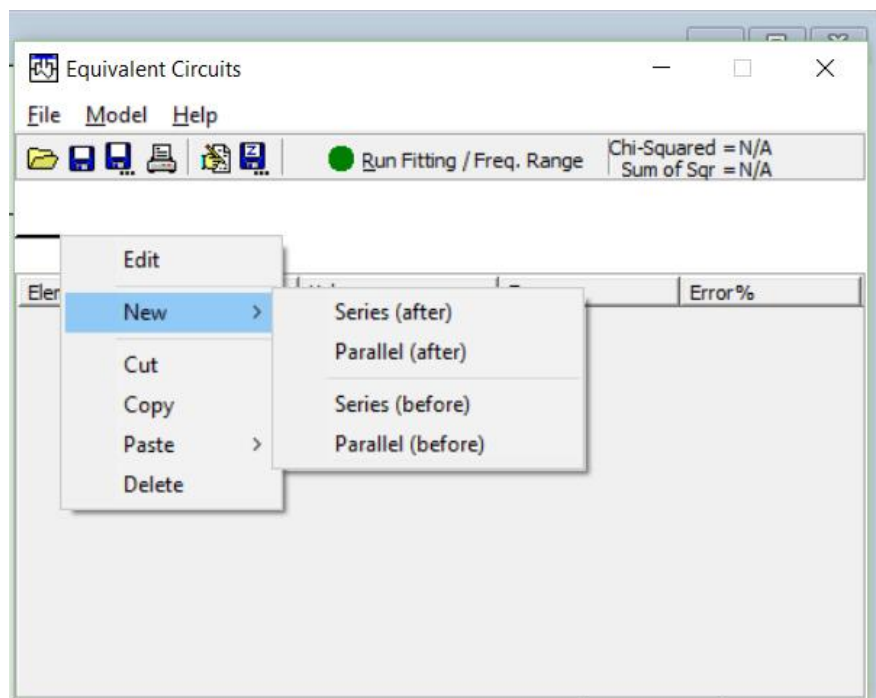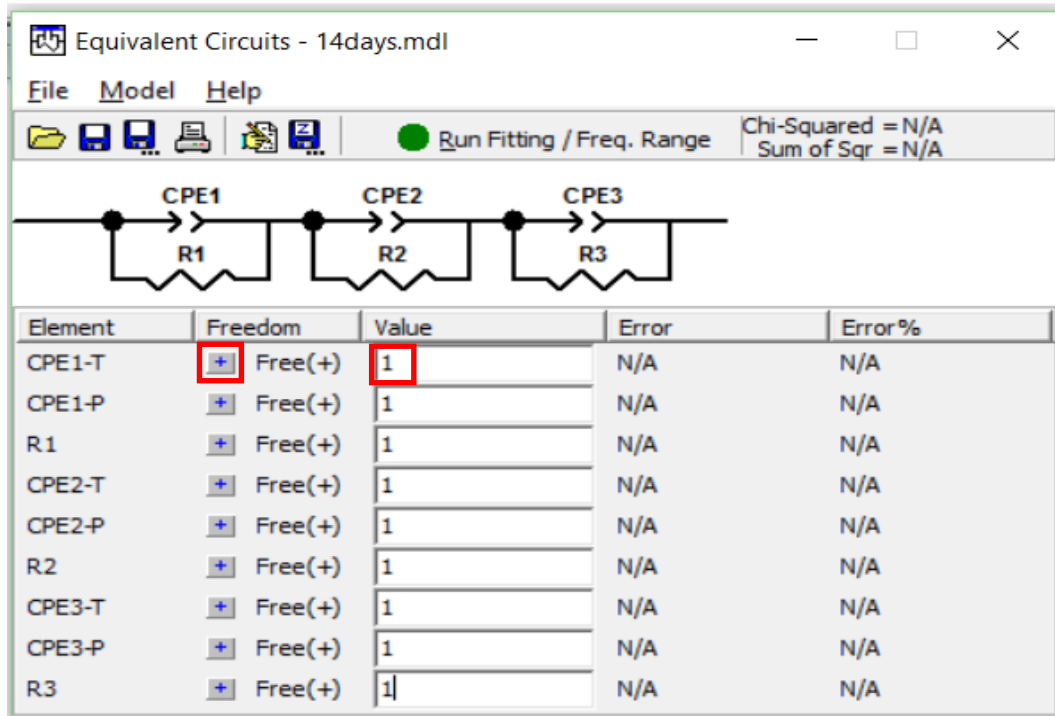
    ii) In Zview, click the equivalent circuit tool
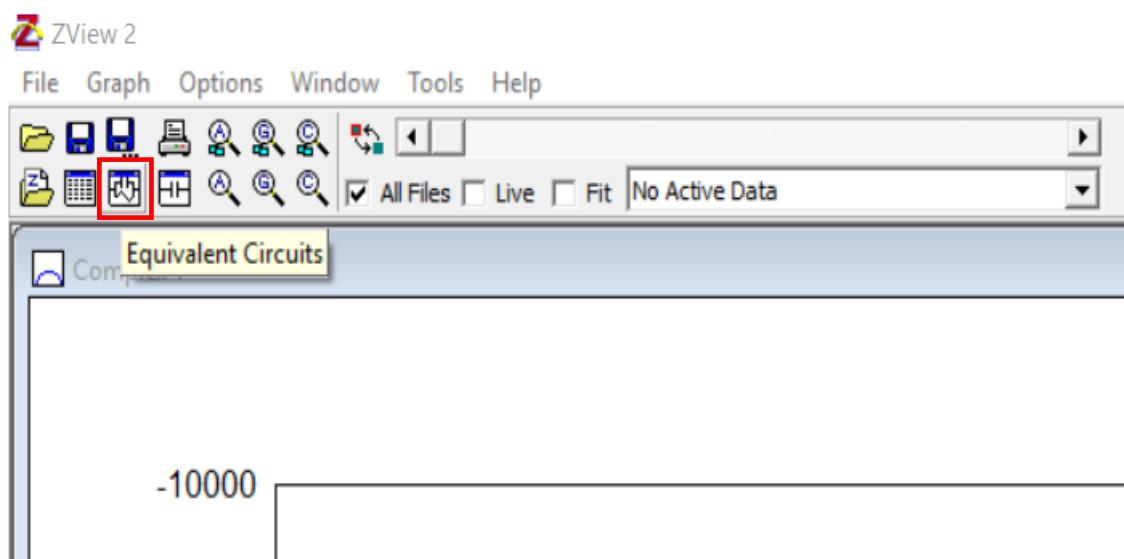
iii) A blank screen will be displayed

iv) Construct the chosen equivalent circuit from step 1.
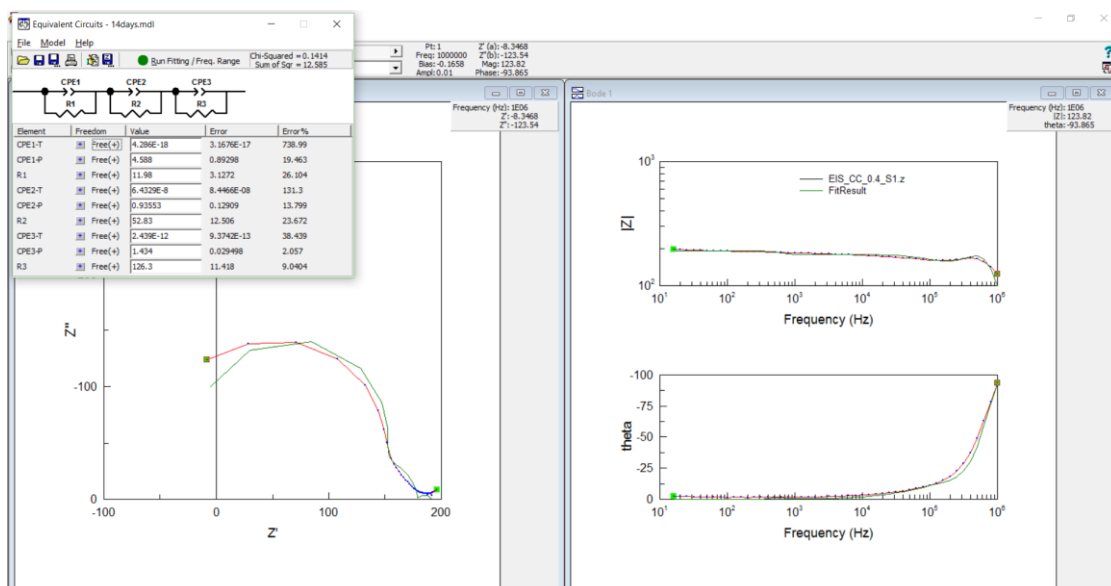
v) After construction of the equivalent circuit, make all the elements as free and give value as 1.

vi) Choose the EIS file in the main menu

   a) Click "Run Fitting/Freq. range"

   b) The fit will generate some numbers

vii) With trial and error, the values of the individual elements can be optimized. For optimization, certain elements can be fixed.

If an initial value closer to the circuit elements is given, the system can fit the circuit in lesser number of iterations. For e.g., R1 represents $R_{sol.}$ From the curve represented in step viii, it can be inferred that it will be approximately near 180. So, if R1 is fixed to that value, other elements can be optimised.

viii) Validation of the fit can be confirmed as follows

a) The chi-squared value should be ≤ 0.001 and sum of squares < 1.

b) The error percentage of individual elements should be less than 20%

c) (Ideally, in other aqueous systems, the error% $< 5\%$. In S-B systems, the error is high due to inhomogeneity)

LIST OF PUBLICATIONS BASED ON THIS THESIS

Refereed Journals

1. **Sripriya Rengaraju**, Lakshman Neelakantan, and Radhakrishna G. Pillai (2019) "Investigation on the polarization resistance of steel embedded in highly resistive cementitious systems – An attempt and challenges", Electrochimica Acta, 308, 131-141. [Journal Impact Factor (JIF): 5.116]
2. Radhakrishna G. Pillai, Manu Santhanam, Ravindra Gettu, **Sripriya Rengaraju**, Yuvaraj Dhandapani, Sundar Rathnarajan, and Anusha Basavaraj (2019) "Service life estimation and life cycle assessment for portland cement, fly ash, and LC3 systems", Cement and Concrete Research 118, 111-119. [JIF: 5.43]
3. **Sripriya Rengaraju**, Anand Godara, Prasanth Alapati and Radhakrishna G. Pillai (2018) "Macrocell corrosion mechanisms of prestressing strands in various concretes", Magazine of Concrete research, https://doi.org/10.1680/jmacr.18.00284. [JIF: 1.488]

International Conference Papers

* Indicates presenter

1. Ravindra Gettu*, Manu Santhanam, Radhakrishna G. Pillai, Yuvaraj Dhandapani, T. Sakthivel, **Sripriya Rengaraju**, Sundar Rathnarajan, Fathima Suma M., Anusha S. Basavaraja, Sanoop Prakasan and Nithya Nair V.G. "Summary of 4-years of research at IIT Madras on concrete with Limestone Calcined Clay Cement (LC3)", RILEM spring convention and Sustainable Materials, Systems And Structures (SMSS) Conference 2019, Rovinj, Croatia
2. **Sripriya Rengaraju***, Radhakrishna G. Pillai and Lakshman Neelakantan "Acquisition and interpretation of electrochemical response from highly resistive (HR), steel-binder (S-B) systems", 3rd R.N.Raikar Memorial International Conference & Gettu-Kodur International Symposium on Advances in Science & Technology of Concrete 2018, India.
3. Ravindra Gettu*, Manu Santhanam, Radhakrishna G. Pillai, Yuvaraj Dhandapani, Sakthivel T., **Sripriya Rengaraju**, Fathima Suma, Sanoop Prakasan, Sundar Rathnarajan, Anusha S. Basavaraja, (2018) "Recent research on Limestone Calcined Clay Cement (LC3) at IIT Madras", Centennial of LMC and Karen Scrivener's 60th birthday conference, Forum Rolex, Lausanne, Switzerland, August 2018.
4. Ravindra Gettu*, Radhakrishna G. Pillai, Manu Santhanam, Sundar Rathnarajan, Anusha Basavaraja, **Sripriya Rengaraju**, and Yuvaraj Dhandapani "Service Life and Life-Cycle Assessment of Reinforced Concrete with Fly ash and Limestone Calcined Clay Cement", International Conference on the Durability of Concrete Structures (ICDCS) 2018, UK
5. Dyana Joseline, Deepak Kamde, **Sripriya Rengaraju***, and Radhakrishna G. Pillai "Residual Service Life Estimation and its Importance for Pretensioned Concrete (PTC) Bridges in Coastal Cities", International Conference on the Durability of Concrete Structures (ICDCS) 2018, UK

6. **Sripriya Rengaraju***, Kokubo Wataru, Radhakrishna G. Pillai and Lakshman Neelakantan "Effect of cell geometry on electrochemical measurements of steel cementitious systems", CORSYM 2018, India

7. Ravindra Gettu*, Manu Santhanam, Radhakrishna G. Pillai, Yuvaraj Dhandapani, Sakthivel T., **Sripriya Rengaraju**, Fathima Suma M., Sanoop Prakasan, Sundar Rathnarajan, Nithya Nair V.G. and Anusha Basavaraja "Properties and prospectus of Limestone Calcined Clay Cements (LC 3) – An overview of three years of research studies in India", Calcined Clay for Sustainable Concrete Conference, 2017, Cuba.

8. **Sripriya Rengaraju*** and Radhakrishna G. Pillai "Challenges in Determining the chloride threshold of Steel Embedded in Cementitious Systems", International conference on Advances in Construction Materials and Systems 2017, India **(RILEM Best Student Poster award)**

9. **Sripriya Rengaraju*** and Radhakrishna G. Pillai "Electrochemical testing in highly resistive steel-cementitious systems", CORCON 2017, India

10. Radhakrishna G. Pillai, Manu Santhanam, Ravindra Gettu*, Yuvaraj Dhandapani, **Sripriya Rengaraju**, Sundar Rathnarajan, and Anusha Basavaraja "Service life estimation and life cycle assessment for portland cement, fly ash, and LC3 systems", Service-life prediction of concrete: The Corvallis Workshops, 2017, USA

11. **Sripriya Rengaraju***, Sundar Rathnarajan, Anupama Velayudhan, Oviya Pugal and Radhakrishna G. Pillai "Effect of Corrosion Inhibitors on Durability Parameters of Cement Mortar", CORCON 2015, India **(Best Student Paper Award in the "Young Scientist Forum" Category)**

International Conference Posters/Presentations

1. **Sripriya Rengaraju***, Radhakrishna G. Pillai, Lakshman Neelakantan, Manu Santhanam, and Ravindra Gettu "Electrochemical response from steel in highly resistive binder systems and estimation of chloride threhsold and service life", American Concrete Institute (ACI) Spring 2019 Convention, Quebec, Canada (Poster presentation) **(ACI Best Poster Award)**

2. **Sripriya Rengaraju***, Radhakrishna G. Pillai and Lakshman Neelakantan "Acquisition and Interpretation of Electrochemical Response from Advanced Steel-cementitious (S-C) Systems Exposed to Chlorides", Electrochemical Methods in Corrosion Research 2018, UK (Poster presentation)

3. **Sripriya Rengaraju***, Radhakrishna G. Pillai and Lakshman Neelakantan "Acquisition and Interpretation of Electrochemical Response from Advanced Steel-cementitious (S-C) Systems Exposed to Chlorides", CORROSION 2018, USA (Poster presentation)

4. **Sripriya Rengaraju*** and Radhakrishna G. Pillai "Chloride-Induced Corrosion Rates of Steel Embedded in Mortar with Ordinary Portland and Limestone Calcined Clay Cements (OPC and LC3)", 1st International Conference on Calcined Clays for Sustainable Concrete 2015, Switzerland. (oral presentation)

DOCTORAL COMMITTEE

CHAIRPERSON   Dr. K. Ramamurthy

Professor and Head

Department of Civil Engineering

GUIDE   Dr. Radhakrishna G. Pillai

Associate Professor

Department of Civil Engineering

MEMBERS   Dr. Manu Santhanam

Professor

Department of Civil Engineering

Dr. Ravindra Gettu

Professor

Department of Civil Engineering

Dr. Lakshman Neelakantan

Associate Professor

Department of Metallurgical and Materials Engineering

CURRICULUM VITAE

Name   Ms. Sripriya Rengaraju

Date of birth   June 5, 1984

Educational qualifications

2005   **Bachelor of Engineering (B.E.)**

Institution   Visvesvaraya National Institute of Technology

                                          Nagpur, Maharashtra, India

Specialization   Civil Engineering

2013   **Master of Engineering (M.E.)**

Institution   College of Engineering, Guindy

                                          Anna University, Chennai, Tamil Nadu, India

Specialization   Construction Engineering and Management